PROCEEDING & ABSTRACT

AAT47

The 47th International Conference of the Anatomy Association of Thailand

May 7th - 9th, 2025

Bangsaen Heritage Hotel, Chonburi, Thailand

THE 47th INTERNATIONAL CONFERENCE OF THE ANATOMY ASSOCIATION OF THAILAND (AAT47)

May 7th-9th, 2025

Venue: Bangsaen Heritage Hotel, Chon Buri, Thailand

Organized by
Faculty of Allied Health Sciences, Burapha University
Faculty of Medicine, Thammasat University
Chulabhorn International College of Medicine, Thammasat University
Faculty of Science, Rangsit University, and
The Anatomy Association of Thailand

THE 47th INTERNATIONAL CONFERENCE OF THE ANATOMY ASSOCIATION OF THAILAND (AAT47)

The proceeding of the Anatomy Association of Thailand is officially published annually by the Anatomy Association of Thailand, Bangkok 10700, Thailand

Organized by
Faculty of Allied Health Sciences, Burapha University
Faculty of Medicine, Thammasat University,
Chulabhorn International College of Medicine, Thammasat University,
Faculty of Science, Rangsit University, and
The Anatomy Association of Thailand

ISBN: 978-616-622-019-3

May 2025 -50 copies

Message from the President of Burapha University

Watcharin Kasalak, Ph.D.
Associate Professor

Esteemed delegates, guests and colleagues,

It is with great pleasure and extent a warm welcome to all participants to the 47th Annual International Conference of the Anatomy Association of Thailand. This academic gathering is here in Bangsean city, Chonburi Province, a beautiful city with long stunning beaches and a variety of huge seafood trading centers.

Burapha University has been committed as an academic research agency to raise health science research literacy, including anatomy segment, which is a foundation of the others research area. Anatomy is also recognized as the important branch of health sciences to be a core component in the academic mission of Burapha University. Therefore, integrative anatomical research and teaching are essential for the development of anatomical field. We are particularly willing to be a co-host of this global international conference. These sessions hopefully to be admired as a global collaboration opportunity for all participants to develop advanced research and teaching skills.

I would like to extend my sincere thanks to all organizers, sponsors and participants for working hard with the collaborative spirit to bring this conference to be successful.

Thank you and welcome

Message from the Dean of the Faculty of Medicine, Thammasat University

Auchara Tangsathapornpong, M.D.
Associate Professor

Distinguished guests, keynote speakers, fellow researchers, and all participants,

On behalf of the Faculty of Medicine, Thammasat University, it is my great honor and sincere pleasure to welcome you to the 47th International Conference of the Anatomical Association of Thailand (AAT47), taking place from May 7th – 9th, 2025, at the Bangsaen Heritage Hotel in Chonburi.

We are pleased to co-host this year's conference in collaboration with the Anatomical Association of Thailand, Burapha University, and Rangsit University. This conference provides a significant academic platform for the exchange of knowledge, the presentation of innovative research, and the exploration of new perspectives in anatomical sciences—bringing together scholars and students from across Thailand and around the world.

We are confident that this event will not only inspire intellectual growth but also cultivate meaningful collaborations that will drive the advancement of anatomy education and research in the years to come.

Thank you for being a part of AAT47. I wish you all a productive, insightful, and memorable conference.

Message from the Dean of Chulabhorn International College of Medicine, Thammasat University

Peerapong Kittipawong, M.D.
Assistant Professor

Dear attendees, respected colleagues, and honored guests,

I am delighted to extend a warm welcome to the 47th International Conference of the Anatomy Association of Thailand (AAT47) on behalf of Chulabhorn International College of Medicine, Thammasat University.

This year's theme, "Advancing Anatomical Sciences and Innovative Clinical Anatomy," places us at the forefront of a new era in biomedical research and education. The rapid advancement of computational modeling, digital imaging, and artificial intelligence is revolutionizing the way we study the human body, not only in the classroom but also in the research laboratory and clinical setting.

Anatomical science is no longer restricted to static structures. It has evolved into a dynamic, data-driven field, where AI enables us to generate predictive models with unparalleled precision, simulate physiological processes, and map complexity. These advancements necessitate that we reconsider our pedagogical strategies, redefine our research questions, and reimagine clinical applications.

AAT is an organization that encourages visionary thinking, international collaboration, and innovative ideas. I urge all of us, including instructors, investigators, and clinicians, to innovate, question, and explore in order to prepare the next generation of anatomical scientists.

I am grateful to all organizers, instructors, and participants. May this conference serve as an incubator for a future that is marked by transformative discovery, wiser technology, and deeper insight.

Welcome to AAT47, and thank you.

Message from the Dean of the Faculty of Science, Rangsit University

Vorachai Sirikulchayanonta, M.D.
Professor Emeritus

Dear Distinguished Guests, Esteemed Speakers, and Valued Participants,

On behalf of the Faculty of Science, Rangsit University, it is with great pleasure and honor that I extend a warm welcome to all of you **to the 47th International Conference of the Anatomy Association of Thailand (AAT47)** under the inspiring theme, **"Advancing Anatomical Sciences and Innovative Clinical Anatomy"**. It is our privilege to serve as a co-host for this significant academic gathering, which brings together researchers, educators, and practitioners in the field of anatomy from across the nation and around the world. The conference theme reflects our shared commitment to driving progress in anatomical education and research, while embracing innovation that bridges basic science and clinical application.

Rangsit University takes pride in fostering academic excellence, scientific inquiry, and interdisciplinary collaboration. We are confident that this conference will serve as a platform for fruitful discussions, knowledge exchange, and professional networking that will inspire future directions in anatomical sciences and clinical anatomy.

We are delighted to welcome you to this vibrant academic community, and we hope your participation will be both intellectually enriching and personally rewarding. Thank you for joining us, and we wish you a successful and memorable conference.

With warmest regards

Message from the President of the Anatomy Association of Thailand

Sutisa Thanoi, Ph.D.
Professor

On behalf of the Anatomy Association of Thailand (AAT), it is our great honor and pleasure to extend a heartfelt welcome to all distinguished guests, esteemed speakers, and participants at the 47th Annual Conference of the AAT (AAT47). This year's conference is proudly co-hosted in collaboration with the Faculty of Allied Health Sciences, Burapha University; the Faculty of Science, Rangsit University; and the Faculty of Medicine, along with Chulabhorn International College of Medicine, Thammasat University. We are deeply grateful for the invaluable contributions of our partner institutions in making this event possible.

The conference will highlight recent advancements and future directions in various fields of anatomical sciences, including gross and microscopic anatomy, clinical anatomy, neuroscience, cell and molecular biology, and anatomical education. Through keynote and plenary lectures, panel discussions, technical seminars, as well as oral and poster presentations, we aim to foster insightful discussion and enrich collective knowledge. With such an exceptional gathering of experts, we are confident this conference will inspire meaningful discussions and facilitate the exchange of cutting-edge research in anatomy.

As President of AAT, I would like to express my deepest gratitude to all our distinguished speakers, dedicated participants, and delegates whose presence is essential to the success of this event. I also extend my sincere appreciation to the organizing committee members for their tireless efforts in planing and arranging the details necessary to make this conference with meticulous care.

I am delighted to welcome you to Chonburi, home to the breathtaking Bangsaen Beach, one of Thailand's most beloved destinations. I hope you will find time to explore its charm and create unforgettable memories during your stay.

Once again, thank you for being part of AAT47. May this conference be both intellectually rewarding and an enjoyable experience for all.

Message from the Chair of the Scientific Committee

Krai Meemon, Ph.D.
Associate Professor

On behalf of the Scientific Committee of the 47th International Conference of the Anatomy Association of Thailand (AAT47), it is my great honor and pleasure to extend a warm welcome to all participants joining us for this distinguished academic gathering. This year, AAT47 conference is held from May 7th – 9th, 2025, in Chonburi province, Thailand, under the theme of "Advancing Anatomical Sciences and Innovative Clinical Anatomy." The conference features an engaging and well-rounded scientific program, including 9 invited speakers, 5 expert panelists in a panel discussion, and a total of 62 research presentations - 18 oral and 44 poster presentations. These contributions reflect the vibrant academic activity and diverse interests in anatomical sciences.

The scientific program encompasses a wide range of disciplines, including gross and clinical anatomy, tissue and cell biology, neuroscience, developmental biology, and innovations in anatomical education. We are delighted to provide this platform for the exchange of knowledge, the cultivation of academic collaboration, and the strengthening of professional networks. Additionally, participants will have the opportunity to explore exhibits from leading companies showcasing the latest innovations and technologies in scientific and anatomical equipment.

As chair of the Scientific Committee, I would like to express my sincere gratitude to all invited speakers, panelists, presenters, delegates, and supporting staffs. Your participation and dedication are vital to the success of this conference and the continued progress of our field.

I trust that you will find the conference intellectually stimulating, and that your time in Chonburi, one of Thailand's most iconic and welcoming destinations, will be enjoyable and memorable.

Thank you for being a part of this significant academic event.

Message from the Chair Organizing Committee

Witoon Khawsuk, Ph.D.
Lecturer

Dear Honored Guests and Colleagues

On behalf of a part of organizing committee, it is my pleasure to extend a warm welcome to the 47th AAT international Conference in Bangsean, Chonburi Province, Thailand. This conference is a great opportunity for anatomists from around the world to exchange their knowledge and making a participation in the research and teaching fields. Together with Faculty of Medicine and Chulabhorn International College of Medicine, Thammasat University and Faculty of Science, Rangsit University, our shared commitment to drive the up-to-date anatomical knowledge through the honorary lecturers and speakers. This conference will extend to the young anatomists, graduate and undergraduate students, to develop their research and teaching ideas through the plenary lecture, special lecture, oral presentation and poster presentation of honor guests and participants from around the world. Moreover, this platform might be a good opportunity for young anatomists to make valuable national or international collaboration in the coming future.

I would like to extend my gratitude to all participants for joining and getting valuable experience at this conference, including immersing in the inestimable Thai culture. Please enjoy yourself with the academic and non-academic activities provided and perhaps consider joining us again in the future.

Thank you, and welcome to the 47th AAT International Conference

Organizing Committee

Chair
Witoon Khawsuk

Co-chair
Peerapong Kittipawong
Pathanin Chantree
Gun Anantasomboon

Secretariat
Tanapan Siangcham

Committee
Amornpun Sereemaspun
Chitraporn Kuanpradit
Jirasuda Nakkiem
Jirawat Saetan
Kanokporn Chayaburakul
Kanta Pranweerapaiboon
Krai Meemon
Manussabhorn Phatsara
Naovarat Tarasub
Napamanee Kornthong
Nattpawit Kaewnoonual
Nopporn Jongkamonwiwat
Paweena Kaewman
Phetcharat Phanthong
Porncharn Saitongdee
Sani Baimai
Siriporn Chamniansawat
Sutisa Thanoi
Thewarid Berkban
Worawit Suphamungmee
Yuttapong Thongpob

Scientific Committee

Chair
Krai Meemon

Co-chair
Pathanin Chantee

Secretariat
Kant Sangpairoj

International Scientific Committee
Boon Huat Bay (Singapore)
Chin Kin-Fah (Malaysia)
Eiji Sugiyama (Japan)
Gavin P Reynolds (UK)
Ming-Der Lin (Taiwan)
Mitsutoshi Setou (Japan)
Robert Mann (USA)
Tracey Wilkinson (UK)
Wai Chen (Australia)

Local Scientific Committee
Amornnat Thuppia
Anongnad Ngamjariyawat
Bumpenporn Sanannam
Decha Buranajitpirom
Dhave Setabutr
Jirawat Saetan
Kajorn Lakchayapakorn
Kamontip Rasri Klosen
Nadthaganya Suwanlikhid
Nantawan Soonklang
Phetcharat Phanthong
Pornpun Vivithanaporn
Pornrut Rabintossaporn
Sani Baimai
Sumon Thitiorul
Suphaket Saenthaweesuk
Sutisa Thanoi
Thanitsara Songtavisin
Viriya Pankao
Thewarid Berkban

CONTENTS

PLENARY LECTURE

Plenary Lecture - I

Professor Dr. Mitsutoshi Setou
Department of Cellular & Molecular Anatomy, Hamamatsu University School of Medicine, Japan
e-mail: setou@hama-med.ac.jp

Spatial Omics Analysis by Mass Microscopy for Drug Discovery in Neuropsychiatric Disorders

Mass microscopy, a spatial omics technique, enables label-free molecular imaging by performing a two-dimensional mass spectrometry scan of the sample surface. We have developed a mass microscopy system and have been advancing its technological development and medical applications at the International Mass Imaging Center. Using model animal tissues, human surgical specimens, and postmortem brains, we have reported significant findings on disease mechanisms through molecular imaging of lipids and small-molecule metabolites. Currently, with the support of AMED's Drug Discovery Support Program, we are working on the development of pharmacokinetics technologies and human resource training. To expand the analytical capabilities of mass microscopy, we are integrating molecular imaging of antidepressants and their metabolites, endogenous cannabinoids, oxytocin, and neuropeptides with spatial transcriptomics. Looking ahead, we aim to engage in our own drug discovery efforts. Specifically, we are focusing on UBL3, a novel post-translational modification factor we identified as a key regulator of intercellular communication. By targeting UBL3, we aim to develop therapeutics for neurodegenerative diseases, particularly synucleinopathies such as Parkinson's disease, dementia with Lewy bodies, and multiple system atrophy, with the goal of eliminating pathological protein aggregates.

Professor Setou is currently a Professor at Hamamatsu University School of Medicine and the Director of the Spatial Omics Research Division at the International Mass Imaging Center. His research focuses on developing mass spectrometry-based molecular imaging (mass microscopy) and its medical applications, with a particular emphasis on drug discovery for neuropsychiatric disorders. After graduating from the University of Tokyo, Faculty of Medicine, he studied at Harvard Medical School and completed my clinical training at the University of Tokyo Hospital. He served as an Assistant Professor at the University of Tokyo in 1998 and later became an Associate Professor at the National Institute for Physiological Sciences (NIPS) in Okazaki in 2002. Since 2008, he have been a Professor at Hamamatsu University School of Medicine and also served as Director of the International Mass Imaging Center (2016–2023) and have been the Director of the Institute for Promoting Photon Medicine since 2021, assuming my current role in 2024. He have led the development of mass microscopy technology, utilizing label-free molecular imaging of lipids and small-molecule metabolites to elucidate disease mechanisms. Currently, with support from AMED, he was advancing pharmacokinetics technology, integrating spatial transcriptomics with molecular imaging, and developing UBL3-targeted therapeutics for neurodegenerative diseases. Moving forward, he remain committed to advancing spatial omics and drug discovery research, contributing to the progress of medical science.

Plenary Lecture - II

Professor Dr. Boon Huat BAY
Department of Anatomy, Yong Loo Lin School of Medicine,
National University of Singapore, Singapore
e-mail: antbaybh@nus.edu.ag

Peroxiredoxin 3 Mediates Breast Cancer Progression

Peroxiredoxin 3 (PRDX3) which belongs to the thiol-specific antioxidant family, has been implicated in the tumorigenesis and progression of several cancers. Breast cancer ranks as the most prevalent female cancer worldwide with tumor recurrence and metastatic spread as the leading cause of cancer-related mortality. Among the breast cancer subtypes, triple negative breast cancer which is characterized by the absence of hormonal and HER-2 receptors is known to be an aggressive tumor with limited treatment options. In this study, the functional roles of PRDX3 in triple negative breast cancer were explored using *in vitro* and *in vivo* experimental models, and also tissue microarrays from breast cancer patients. Expression of the PRDX3 protein in triple negative MDA-MB-231 breast cancer cell line was manipulated by insertion of an expression plasmid into the host cells for PRDX3 overexpression, and down-regulated by using either small interfering RNA (siRNA) for transient knock down of the *PRDX3* gene or short hairpin RNA (shRNA) for stable knockdown. Cell proliferation, cell cycle, migration and invasion *in vitro* assays were performed. To provide mechanistic insights into the effect of PRDX3 on cancer spread, Matrix Metalloproteinase-1 (MMP-1) expression and activity (which has been reported to be associated with invasive behavior and tumor progression), together with pathway analysis using the Human phospho-MAPK proteome profiler array were investigated. For the *in vivo* experimental protocol, control and shPRDX3 MDA-MB-231 breast cancer cells were injected into the mammary fat pads of female nude mice and the size of tumors monitored. Breast tissue microarrays were immunostained with PRDX3, MMP-1 and Proliferating Cell Nuclear Antigen (PCNA) antibodies. Overall, the findings show that PRDX3 could mediate breast cancer proliferation and also cancer spread, thus verifying that PRDX3 plays an essential role in breast cancer growth and progression.

Dr Boon Huat Bay is the Kwan Im Thong Hood Cho Temple Professor of Anatomy at the Yong Loo Lin School of Medicine, National University of Singapore. He was Head of the Department of Anatomy at NUS Medicine from 2008-2016. He graduated with a medical degree from the National University of Singapore and obtained his PhD in Cancer Biology from his alma mater. He was subsequently awarded a Commonwealth Medical Fellowship for his postdoctoral training at the University of Oxford, His research interests have focused on the utility of biological markers of malignancy, drug design based on tumor biology and molecular targeted therapy in breast cancer. He has also an interest in nanomaterials research, especially on the biomedical applications and toxicology of gold, silver and ultra small ferrite nanoparticles.

Plenary Lecture - III

Professor Dr. Gavin P Reynolds
Sheffield Hallam University, Sheffield UK
e-mail: gavin.reynolds@shu.ac.uk

Why is there more cardiac and metabolic disease in psychiatric patients?

Psychiatric illness is associated with reduced life expectancy, with increased incidence of suicide but also of non-suicidal mortality. This mortality is particularly associated with cardiac factors, which in turn may be influenced in part by an increase in metabolic disease. Thus excessive cardiac morbidity and mortality are important features of psychiatric disease and its treatment, but are multifactorial in both aetiology and pathogenic mechanisms. Focusing particularly on schizophrenia, perhaps best researched are the metabolic contributors to cardiovascular disease, likely mediated by several factors: behaviours associated with schizophrenia (e.g. poor diet, smoking), pathogenic factors common to both psychiatric illness and metabolic risk (e.g. chronic inflammation), and antipsychotic drug treatment. The contribution of some antipsychotic drugs to obesity and metabolic syndrome as a mediator of cardiovascular risk involves antagonism at 5-HT2C and other neurotransmitter receptors that influence weight gain by affecting hormonal control of food intake.

More direct effects on cardiac pathology and an increased risk of sudden cardiac death are a less-clearly understood feature of antipsychotic drug treatment. The potentially fatal arrhythmia toursade de pointes (TdP) is considered to result from drug inhibition at the hERG potassium channel causing a QT prolongation. Other drug effects influencing QT prolongation including action at sodium channels (attenuating effects at the hERG channel), possibly with contributions from antagonism of some neurotransmitter receptors. However, cardiac arrhythmias have multiple markers of risk including late potentials and diminished heart rate variability, both observed in schizophrenia independent of drug treatment. It seems likely that some developmental influences (e.g. early life trauma) elevate risk both to schizophrenia and to cardiac dysfunction. Evidence for this comes from inflammatory and epigenetic indicators: for example DNA methylation of BDNF – which is closely linked to inflammatory markers – is abnormal following childhood trauma and may be associated with developmental effects on both the brain and the heart.

Smoking is a further factor contributing directly to cardiac risk in schizophrenia. This too may relate to childhood trauma - we find in patients that the severity of child abuse reported in early life correlates with the numbers of cigarettes/day. Not only is smoking more prevalent, the intensity of smoking is greater than in an otherwise healthy smoker, with greater cardiotoxic consequences. The mechanisms underlying smoking-related cardiac risk are many and varied; here again chronic inflammation may play a role. This emphasises the importance of inflammation in several of the pathogenic pathways contributing to cardiac risk in psychiatric disease.

Gavin Reynolds is Honorary Professor in the Biomolecular Sciences Research Centre at Sheffield Hallam University and Professor Emeritus, previously Chair of Neuroscience, at Queen's University Belfast. He also has an honorary research position at Rotherham, Doncaster and South Humber NHS Trust. After a biochemistry PhD, he undertook postdoctoral work in London, Vienna and Cambridge, following which he held university posts in Nottingham, Sheffield and Belfast. He has international

collaborations with Visiting Professor appointments at universities in Thailand and China, and has been President of the British Association for Psychopharmacology (2008-10). His main research interests are: the neurotransmitter pathology of schizophrenia, with a recent focus on the epigenetic effects of environmental risk factors, and the mechanisms underlying beneficial and adverse effects of antipsychotics and other psychoactive drugs, particularly pharmacogenetic influences and cardiometabolic consequences. Additional interests include mechanisms of neurodegenerative disease and the biological effects of substance abuse. He has over 340 research publications, including papers in Nature and The Lancet, with an h-index of 86 and 28000 citations (Google Scholar).

Plenary Lecture - IV

Professor Dr. Wai Chen
Curtin Medical School, Curtin University, Bentley, WA 6102, AUSTRALIA.
Fiona Stanley Hospital, 11 Robin Warren Dr, Murdoch WA 6150, AUSTRALIA
e-mail: wai.chen@curtin.edu.au; wai.chen@health.wa.gov.au

The Relevance of Neuroactive Hormones in Premenstrual Dysphoric Disorder, Peri-menopause and Neurodivergence

Premenstrual Dysphoric Disorder (PMDD) represents a significant yet frequently under-recognized psychiatric condition with substantial clinical and functional implications. Unlike the more common Premenstrual Syndrome (PMS) which affects up to 80% of females of reproductive age, PMDD is characterized by severe cyclical depressive, cognitive, and anxiety symptoms resulting from central nervous system (CNS) responses to gonadal hormone fluctuations during the menstrual cycle. With a prevalence of 2-8% among reproductive-age females, PMDD warrants greater clinical attention. The DSM-5-TR diagnostic criteria clearly distinguish PMDD from PMS through the presence of more severe manifestations: affective lability, irritability leading to interpersonal conflicts, depressed mood, marked anxiety, decreased interest in activities, concentration difficulties, lethargy, appetite or sleep disturbances, feeling overwhelmed, and physical symptoms. Crucially, these symptoms follow a cyclical pattern with abrupt onset and resolution typically associated with menstruation. PMDD should be understood as a brain disorder rather than a reproductive system dysfunction. Its consequences can be profound, negatively impacting relationships, work performance, and emotional well-being. In severe cases, PMDD has been associated with suicidality and aggressive behaviors. Strong correlations exist between PMDD and post-traumatic stress disorder (PTSD), complex PTSD (cPTSD), and histories of early life or recent trauma. For some cases, psychological or physical trauma in an adult woman (such as, experiencing a difficult childbirth) can trigger the onset of PMDD.

The neurobiological underpinnings of PMDD involve several key mechanisms. Estrogen modulates serotonin, norepinephrine, brain-derived neurotrophic factor (BDNF), and dopamine functions, influencing both emotional regulation and cognitive processes including attention, memory, and executive functioning. Progesterone and its metabolite (allopregnanolone) interact with GABA receptors, potentially reducing anxiety. Allopregnanolone is sometimes considered an ‘anti-anxiety’ hormone. These complex hormonal interactions help explain the diverse symptom presentation in PMDD. Evidence suggests that individuals with PMDD history are more vulnerable to severe perimenopausal symptoms, indicating a continuum of hormone sensitivity across reproductive transitions. Effective management approaches include hormonal interventions, selective serotonin reuptake inhibitors (SSRIs), cognitive-behavioral therapy, and lifestyle modifications. Early identification through validated screening tools can significantly improve outcomes. This presentation will explore current advances in PMDD understanding, highlight practical approaches to assessment using standardized measures, and discuss evidence-based treatment strategies. Special attention will be given to managing PMDD across reproductive transitions including perimenopause. The goals are to equip clinicians with knowledge to better recognize, assess, and effectively treat this debilitating condition; and inform researchers novel research opportunities.

Professor Wai Chen is a clinician-scientist specializing in developmental neuropsychiatry at Fiona Stanley Hospital. He serves as psychiatry discipline lead at Curtin Medical School and holds concurrent professorships at Curtin enAble Institute, University of Western Australia, Murdoch University.He served as an external reviewer for the DSM-5 Clinical and Public Health Committee; and one of his publications on neurodevelopmental disorders was cited by DSM-5-TR to inform text revision. More recently, his research also includes on neuroendocrine influences on brain function and mental health. His work bridges neuroscience with clinical psychiatry, emphasizing translational research that improves outcomes across the developmental lifespan.

SPECIAL LECTURE

Special Lecture - I

Professor Dr. Ming-Der Lin
Department of Molecular Biology and Human Genetics, Tzu Chi University, Taiwan
e-mail: mingder@gms.tcu.edu.tw

Osteoblastogenesis Enhancement by *Clematis montana*, the Source of Chuan-Mu-Tong, in a Zebrafish Model of Glucocorticoid-Induced Osteoporosis

Clematis montana, known as Chuan-Mu-Tong (CMT), has been traditionally used in Chinese medicine to promote urination, reduce inflammation, and treat conditions associated with kidney essence deficiency—a concept closely linked to osteoporosis in traditional Chinese medicine. Given the need for novel bone-anabolic drugs, this study aims to evaluate the osteogenic effects of CMT, identify its bioactive compounds that promote osteoblastogenesis, and elucidate the molecular mechanisms underlying its bone-anabolic properties. To assess the osteoprotective effects of CMT, we used a dexamethasone (Dex)-induced zebrafish osteoporosis model. The results showed that CMT effectively counteracts Dex-induced calcification reduction. Additionally, CMT enhances vertebral calcification in zebrafish under normal conditions, further demonstrating its bone-protective effects. Through network pharmacology analysis, we found that the combined effects of CMT's chemical constituents ultimately converge on the process of osteoblastogenesis. Using transgenic zebrafish *Tg*(*Ola.sp7:EGFP*), where GFP expression serves as a marker for osteoblast formation, we confirmed that CMT promotes osteoblastogenesis. Furthermore, syringaresinol (SYR) was identified as a key bioactive compound in CMT, which effectively counteracts Dex-induced osteoblast reduction. Network analysis further revealed that SYR, along with other CMT-derived compounds, acts synergistically on multiple osteoblast-associated targets and pathways essential for osteoblastogenesis and bone homeostasis. These findings suggest that CMT exerts its osteogenic effects through a multi-target, multi-pathway mechanism. By integrating *in vivo* zebrafish models with network pharmacology, this study provides scientific evidence supporting the traditional use of CMT in bone health and highlights its bioactive compounds contributing to osteogenic properties.

Keywords: *Clematis montana*, Chuan-Mu-Tong, osteoporosis, osteoblastogenesis, zebrafish model

Dr. Ming-Der Lin is a Professor in the Department of Molecular Biology and Human Genetics at Tzu Chi University, Hualien, Taiwan. He earned his Ph.D. from National Taiwan University, Taipei, Taiwan. His research focuses on using zebrafish models to investigate the therapeutic effects of herbal medicine on osteoporosis and performing functional analyses of disease-causing genes in both Drosophila and zebrafish. Additionally, he has a strong interest in insect germline development and entomology.

Special Lecture - II

Associate Professor Dr. Pornpun Vivithanaporn
Chakri Naruebodindra Medical Institute (CNMI), Faculty of Medicine Ramathibodi Hospital, Mahidol University, Thailand
e-mail: pornpun.viv@mahidol.edu

Game On! Transforming Traditional Learning into Playful Innovation

With the availability of online learning, lots of students prefer not to come into the classroom and there is less student engagement. Preclinical science is a branch of medical science that focuses mainly on cognitive domain by remembering a large volume of content, leading to lack of interest. Playing the game is one of the most primitive human learning behaviour due to its competitive nature of human. Game-based learning that integrates game elements into the learning process has been evolving the pedagogy of medical education. This method has gained considerable interest because it makes learning enjoyable and engaging for students. The proposed games range from simple formats that require minimal preparation, such as trivia, crossword puzzles, and case-based scenarios to identify appropriate treatments, to more specialized games like board games, online games, series of problem-solving activities in the form of escape rooms, and virtual reality games. In this session, I will share my experiences in game creation and the adaptation into classroom setting. The game-based approach motivates students and boosts learner' confidence in their knowledge. Playing games as a team promotes student's teamwork, communication, and negotiation skills. Therefore, the implementation of game-based learning in preclinical education should be encouraged and developed.

With the rise of online learning, many students now prefer to avoid traditional classrooms, resulting in reduced engagement. Preclinical sciences primarily focused on the cognitive domain, often require students to memorize vast amounts of content, leading to waning interest and motivation. One of the most fundamental human learning behaviors is play, driven by our competitive nature. Game-based learning, which integrates game elements into the educational process, has significantly evolved the pedagogy of medical education. This method has gained widespread attention for its ability to make learning enjoyable and engaging. The spectrum of game formats varies widely—from simple activities like trivia and crossword puzzles to more intricate designs such as board games, online games, escape room challenges, and virtual reality experiences. In this session, I will share my experiences in developing and adapting games for the classroom. Game-based learning not only motivates students but also enhances their confidence in their knowledge. Collaborative play fosters teamwork, communication, and negotiation skills. As such, the integration of game-based learning into preclinical education is a promising approach that should be further embraced and developed.

Dr. Pornpun Vivithanaporn is an Associate Professor in Pharmacology at Chakri Naruebodindra Medical Institute (CNMI), Faculty of Medicine Ramathibodi Hospital, Mahidol University, Thailand. She was honored with the Innovative Teaching Award at the Mahidol University Quality Fair in 2023 for the creation of PharMatch, an online card game designed to enhance student engagement and improve their ability to memorize drug-related information. In 2024, she received the same award for her successful adaptation of game-based learning within the classroom. Her dedication to excellence in teaching was further recognized in 2025, when she was awarded the Mahidol University Teaching Excellence Award.

Special Lecture - III

Professor Dr. Chin Kin-Fah
Professor of Surgery, Faculty of Medicine and Health Sciences, Universiti Tunku Abdul Rahman. Malaysia & Founding Chairman and Executive Director, Academy for Silent Mentor:
e-mail:

Impact of Silent Mentor Anatomical Teaching on 32-body Parts Meditation Practice on Monastic Practitioners and Laity

Abstract:

Introduction: The 32-body parts Buddhist meditation practice enhances mindfulness and suppressing worldly desires through contemplation of bodily elements.

Aims: This study assesses the effects of Silent Mentor Anatomical Teaching on mental wellbeing, compassion, and sensual desires in monastic and lay practitioners.

Methodology: A prospective interventional study (2023 to 2024) involved 53 monastic and 26 lay practitioners. Lay practitioners first completed a mandatory pre-workshop meditation retreat to ensure psychological readiness. The study participants were assessed pre- and postworkshop using validated scales; the Warwick-Edinburgh Mental Wellbeing Scale, Self compassion Scale-Short Form, Compassionate Love for Humanity Scale and Fears of Compassion Scale, and a custom 32-body parts meditation questionnaire. Data were analyzed using ANOVA; questionnaire reliability was confirmed (Cronbach's alpha = 0.836).

Results: The mental wellbeing in lay practitioners improved significantly post-retreat ($P<0.005$) with no significant decline post-anatomical teaching. Laity showed reduced attraction to opposite sex and general sense desire ($P<0.005$) for pre-retreat. Post-anatomical teachings, results demonstrated a significant increase in impermanence ($P=0.031$), and demonstrated a progressive increased attraction to opposite sex. The workshop significantly influenced desires for food ($P=0.031$), general sense desire ($P=0.013$) and concern about health ($p=0.026$) across both groups. Significant differences between monastics and laity were noted in impermanence ($p=0.004$), inner peace ($P=0.023$), desires for food ($P=0.016$), identification with one's body ($P=0.020$) and identification with the mind ($P=0.032$).

Conclusions: The pre-retreat is essential for the lay practitioners' mental well-being. The 32-body parts anatomical meditation teaching had a significant impact on certain domains of sensual desires but not the compassion scales, with notable differences in these domains between monastics and lay practitioners. The measurement scale of sensual desires domain warrants further development.

Professor Dr. Chin Kin Fah is one of few foremost laparoscopic surgeons in Malaysia currently serving as Consultant Surgeon with special interest in Minimally Invasive Laparo-Endoscopic Surgery, surgical oncology, gastrointestinal surgery (Upper & Lower), bariatric and metabolic surgery and clinical nutrition at Gleneagles Hospital Kuala Lumpur, Assunta Hospital, Tung Shin Hospital and Sungai Long Medical Hospital. Prof. Dr Chin is the pioneer of 'SILENT MENTOR' Program in

Malaysia, a humanity program that encourages people to come forward, donate their bodies after their demise for betterment and benefit of Medical Education, Training & Research. Many specialists, intern doctors & medical students will use the donated remains as cadaver. He founded the Silent Mentor program in 2012 while he was a professor in the University of Malaya. In 2017, he formed the Academy For Silent Mentor, an independent not-for-profit Education and Research institution, which promotes the i·Silent Mentor program to whole Malaysia, collaborating with various Public and Private Universities, and oversea institutions (Royal College of Surgeons of Edinburgh, Royal College of Physicians and Surgeons of Glasgow, UNESCO Bioethics Chair (Haifa University), Tzu Chi University, Nan Hua University and National Taipei University of Nursing and Health Sciences), and benefiting to more medical students in Malaysia and abroad. He also founded the Rapid Tissue Donation Program for Cancer Research and Development in 2021.Prof. Dr Chin has published research papers in both local and international medical journals. He has been elected to many committees & positions for various local and international medical bodies, such as Governor of Endoscopic and Laparoscopic Surgeons of Asia, Council Member of College of Surgeons of Malaysia, Governor of Asia Pacific Metabolic and Bariatric Surgery Society, Vice President of Asian Society of Cryosurgery, Board Member of Asia Endosurgery Task Force, Vice President of PENSMA and committee member of MUGIS, SELSMA and MyMBS.

Special Lecture - IV

Associate Professor Dr. Eiji Sugiyama
Faculty of Pharmacy, Meijo University, Japan
e-mail: esugi@meijo-u.ac.jp

Method Development for Histological Analysis of Monoamine Dynamics and Chiral Metabolites Using Mass Spectrometry

Metabolic processes in tissues or cells are highly compartmentalized and their dysregulation is closely linked to pathology. However, histological analysis of small molecules by immunohistochemistry or autoradiography is challenging due to the requirement for an antibody, radioisotope, or chemical fixation. Mass spectrometry imaging (MSI) is an alternative method that enables label-free molecular detection. Although basic sample preparation protocols have been established and used for large-scale spatial omics studies [1], further technical improvements are expected to extend the capability of MSI. We previously developed various MSI-related techniques, such as one that improves the ionization efficacy of cationic metabolites [2] and another that visualizes lipids in isolated distal neurites of cultured neurons [3]. In this lecture, after introducing our representative applications of MSI, two topics will be presented. The first topic is about the analysis of monoamine neurotransmitters in the brain. We optimized the conditions for internal standard-based quantitative imaging of serotonin, dopamine, and norepinephrine. The optimized conditions were applied to discover monoamine co-localized nuclei and visualize rapid monoamine turnover [4,5]. The localized dynamic changes of monoamine content strongly support the importance of direct histological analysis of metabolites. The second topic focuses on the challenge of enantioselective imaging of minor chiral metabolites, which are associated with various human diseases. We recently developed a new method that involves charged chiral derivatization and ion mobility spectrometry to visualize the distribution of a pair of enantiomers (D, L-2-hydroxyglutaric acid) in the mouse testis [6]. The chiral derivatization reagent used in this study is now being optimized to expand the range of target molecules. Our preliminary data support the potential of this approach for visualizing enantioselective metabolic processes in tissues.

References

[1] HuBMAP Consortium, *Nature*, 574, 187–192 (2019).
[2] Sugiyama E., Setou M. *et al.*, *Anal. Chem.* 87, 11176–11181 (2015).
[3] Sugiyama E, Setou M. *et al.*, *Biochem. Biophys. Res. Commun.*, 495, 1048–1054 (2018).
[4] Sugiyama E., Setou M. *et al.*, *iScience*, 20, 359–372 (2019).
[5] Sugiyama E., Sugiura Y. *et al.*, *Pharm. Ther.*, 208, 107478–107478 (2020).
[6] Sugiyama E., Todoroki K. *et al.*, *Chem. Commun.*, 59, 10916–10919 (2023).

Dr. Eiji Sugiyama is an Associate Professor in Analytical Chemistry at the Department of Pharmacy, Faculty of Pharmacy, Meijo University. His research interests have been focused on visualizing compartmentalized metabolism and dynamics of small molecules in tissues or cells by new techniques for mass spectrometry imaging, which provides broad new insights on histology or pathology.

Currently, Eiji has been appointed as associate editor for Analytical Sciences, an international journal by the Japan Society of Analytical Chemistry (JSAC).

Special Lecture - V

Assistant Professor Dr. Dhave Setabutr
- Department of Otolaryngology Head and Neck Surgery, Thammasat University Hospital
- Chulabhorn International College of Medicine, Thammasat University, Pathum Thani, Thailand
e-mail: dhave.cicm@gmail.com

Anatomy Lab to Hospital Ward: Bridging the Gap to Clinical Correlates in the Head & Neck

The plethora of information in anatomy can be intimidating to the medical student. Many times, the massive amounts of information can be difficult to decipher in the preclinical years. Moreover, once these same students reach their clinical years; often what they've learned is incongruent to what they see on hospital rounds.

We highlight key clinically relevant scenarios that we full students should be exposed to during their preclinical years. It is important for the anatomist and practicing physicians collaborate to achieve a curriculum that both benefits the student and their future patients. This lecture may encourage other educators to integrate a specialist's clinical practice to a student's anatomy curriculum early on.

Dr. Setabutr is an assistant professor in otolaryngology and currently Vice Dean for International & Student Affairs at Chulabhorn International College of Medicine, Thammasat University. He received Thai Board of Otolaryngology – Head & Neck Surgery, Diplomat of the American Board of Otolaryngology and Complex Pediatric Otolaryngology Board Certified. He has published 33 Thai and international research articles and 6 of international book chapters.

PANEL DISCUSSION

Panel Discussion - I

Innovations in Anatomy

Dr. Muthukrishnan Chandrika
Address: 4 Medical drive, MD10, Lower Kent Ridge Road, National University of Singapore
e-mail: antmc@nus.edu.sg

Abstract:

Adopting new pedagogical tools paves the way for a deeper understanding of Anatomy. As a fundamental discipline—particularly crucial for surgeons—Anatomy cannot be effectively taught through a single method alone. Given the intricate organization of the human body, a blended learning approach proves highly beneficial.

Relying solely on factual recall is inadequate. Incorporating clinical reasoning and highlighting the functional significance of each organ enhances students' comprehension significantly. Anatomy education can span a wide range of approaches—from traditional cadaveric dissection to modern innovations such as AI-powered chatbots, 3D models, and mixed reality platforms. Furthermore, integrating Anatomy with related subjects like Physiology and Clinical Medicine allows students to develop a more cohesive and meaningful understanding of the human body. Self-directed learning, flipped classrooms, gamification, collaborative case-based learning, and radiological tools such as ultrasound have a significant impact on student learning. These approaches not only enhance engagement but also consistently receive positive feedback from students. Ultimately, user-friendly technology for educators and teaching methods that resonate with today's "beta-age" students are always welcomed and widely appreciated.

Keywords: *Blended learning, feedback, Dissection, Clinical Reasoning*

Panel Discussion - II

Optimizing Embryology Teaching with Digital and Printed Models

Asst. Prof. Nutmethee Kruepunga, Ph.D.
Address: Department of Anatomy, Faculty of Medicine, Kasetsart University
e-mail: nutmethee.kr@ku.th

Abstract:

Human embryology, or human developmental anatomy, involves 3D mapping of the developing body, essential for understanding congenital abnormalities. Unlike adult anatomy, embryonic structures are microscopic and constantly changing, making them challenging to study. Traditionally, serial sectioning and whole mounting were used in education—serial sections provide internal detail but lose external shape, while whole mounting preserves morphology but lacks resolution. Both require imagination to grasp developmental processes. Moreover, wax models were later introduced. They improved visualization but were rigid and limited in adaptability.

With technological advancements, 3D morphology is now digitally reconstructed, enhancing visualization. Computational analysis allows for exporting models into formats like 3D PDFs and 3D-printed models. 3D PDFs act as interactive electronic atlases, easily accessible and adjustable, while 3D printing offers scalable, adaptable, and reproducible physical models.

Due to time constraints in medical curricula, embryology classes are often shortened, yet core concepts remain essential. In personal implementation, 3D PDFs and 3D-printed models have been integrated into teaching, improving accessibility and comprehension. These tools enable students to visualize developmental anatomy from presentations, interact with 3D-printed models (similar images in presentations), and explore materials independently through 3D PDFs. By incorporating modern technology, these methods could make embryology education more effective within limited class time.

Panel Discussion - III

Integrated Educational Technology in Teaching Anatomy: A Case Study from VinUniversity

Hoang Mai Duy
Address: College of Health Sciences, VinUniversity, Hanoi, Vietnam
e-mail: duy.hm@vinuni.edu.vn

Abstract:

The curriculum in teaching anatomy is under increasing pressure to transform from traditional to interdisciplinary integration, from cadaver-based to multimodal instruction with a system-based approach. Educational technologies are becoming critical and urged to be integrated into teaching medicine. At the College of Health Sciences, VinUniversity, the block of Human Body Structure and Function (HBSF) within the undergraduate medical training program was designed to teach anatomy with relevant basic medical sciences based on the principles of the system-based integrated structure. To support students in achieving the intended learning outcomes, multiple innovative technological platforms have been introduced into the curriculum using the moderation of the Adaptation - Standardization - Integration - Compliance (ASIC) framework over four key terms: adaptation, standardization, integration, and compliance. In this paper, the process for curriculum development is presented with an illustration of the selected technological platforms and the lessons learned using the ASIC model.

Panel Discussion - IV

Extended Reality (XR) Clinical Anatomy for Ramathibodi Integrated Anatomy Classroom

Bernita Jitaree, Ph.D.
Address: Ramathibodi Medical School, Faculty of Medicine Ramathibodi Hospital, Mahidol University, Thailand
e-mail: benrita.jit@mahidol.ac.th

Abstract:

The Innovation and Educational Technology Unit of Chakri Naruebodindra Medical Institute, Faculty of Medicine Ramathibodi Hospital, recognizes the importance of modernizing teaching materials to enhance educational efficiency. As the number of medical students continues to rise while the availability of cadavers remains limited and costly, the unit has developed XR Clinical Anatomy—a digital learning tool utilizing XR technology. This allows students to study anatomy using high-resolution scans of real cadavers through VR headsets, providing an immersive and accessible learning experience.

Objectives

1. Enhance interactive learning among students.
2. Enable students to review anatomical content before and after classes.
3. Improve clarity in anatomical structures, especially considering that students with limited dissection experience may not achieve optimal visibility in traditional cadaveric studies.
4. Provide an experience akin to studying a formalin-preserved cadaver while offering a highly realistic view comparable to a soft cadaver.
5. Address the shortage of cadavers, which are also needed for specialist training.
6. Reduce exposure to hazardous chemicals used in cadaver preservation.

Key Features of the Innovation

- XR images are generated from actual cadaver scans, ensuring high realism.
- Anatomical structures can be segmented for detailed study of individual organs.
- Compatible with both VR/XR headsets and standard application screens.

Accessible anytime for continuous learning.

Panel Discussion - V

A General Exploration of the Process of the Development and Application of 3D Media, Material and Innovations in the Instruction of Anatomy for Students in the Medical Field

Atthaboon Watthammawut, Ph.D.
Address: Department of Anatomy, Faculty of Medicine, Srinakharinwirot University, Sukhumvit 23, Bangkok 10110, Thailand
e-mail: atthaboon@g.swu.ac.th

Abstract:

The post-Covid-19 pandemic world and the massive societal and technological shifts have profoundly disrupted higher education systems worldwide, prompting an abrupt shift from traditional pedagogical methods to remote and digital learning solutions. In the field of anatomical sciences, this transition posed significant challenges due to the essential need for hands-on, on-site practical instruction, crucial for developing proficiency in dissections and anatomical orientation. As a response to these challenges, anatomical instructors have had to swiftly adapt to the present demands by leveraging digital media, creating videos featuring real dissection footage from experienced instructors at laboratories. However, this adaptation received mixed feedback from learners. Two primary concerns emerged: firstly, digital dissections, confined to a 2D format, lacked the engagement and tactile feedback of 3D interaction, turning learning into a passive activity with potential reductions in student interest and attention span. Secondly, video formats using zooming to clarify structures were criticized for abstracting from a genuine laboratory experience, causing a disconnection that impeded immediate comprehension by students. These challenges underscored the imperative for educational innovation beyond the surface-level transition to digital media. The pursuit of alternative solutions led to the proliferation of 3D learning tools designed to address the limitations of 2D experiences. Research suggests that virtual and augmented reality (VR/AR) technologies offer promising avenues for creating immersive and interactive learning environments, simulating the tactile aspects of dissection without the associated costs or restrictions of physical specimens.

In response to this social and technological evolution, our present work and research explore the various media, interactive material and psychosomatic implementations to address these challenges. Firstly, we discuss the implementation of a Virtual Anatomical Dissection Room grounded in 3D modeling, enhanced with AR/VR, and holographic display technologies. This innovation aims to mimic the spatial and tactile feedback of an actual dissection lab, transcending the limitations imposed by the current climate. Furthermore, we discussed the development and produced multimodal instructional media for gross anatomy and neuroanatomy, in which specimens that normally were prepared for practical sessions converted into 3D instruction media that could cater to the differing learning styles of prospective students. The instructional media included high-fidelity 3D models of brains created with the latest 3D scanning technologies which highly resemble their fresh counterparts, and the creation of a repository where students can view all the 3D models with their educative annotations anywhere for free. Furthermore, the high-fidelity scans of the anatomical specimens were also converted into 3D models for 3D printing, from which we were able to print out brain models from the original scans with the highest fidelity and resolution possible (Moreover, the 3D models were incorporated into the virtual-/augmented-reality functions of the repository; through which students can use Google Cardboard/VR headsets/smartphones trackers to observe the models in 3D space. Lastly, we discuss the further modifications of the 3D scanned models to be shown for the first time on a cutting-edge 3D holographic display, where the viewer can observe the models to be 3D with

depth in real-time. These innovations aim to transcend the limitations imposed by the current climate and provide a paradigm shift in anatomical education. As we continue to grapple with the repercussions of the Covid-19 outbreak and future educational disruptions, the need for dynamic, interactive, and student-centered teaching mediums becomes increasingly paramount

Keywords: *Virtual Anatomical Dissection Room (VADR), 3D modeling and printing, augmented reality (AR)/virtual reality (VR), anatomy instructional media, holographic display technology*

ORAL PRESENTATION

O-01

Spatial Genome Organization in Neural Circuit Formation

Yuki Fujita[1*]
[1] Department of Anatomy and Developmental Biology, Graduate School of Medical Research, Shimane University, 89-1 Enya-cho Izumo-shi, Shimane, 693-8501 JAPAN
*Corresponding author, e-mail: yuki.fujita@med.shimane-u.ac.jp

Abstract

Gene expression regulated by spatial chromatin organization and nuclear architecture plays crucial roles in the development of the brain. We have focused on the role of the cohesin complex, which is chromosome-associated multi-subunit proteins, in embryonic and adult neurogenesis. Cohesin is a highly conserved nuclear protein complex composed of four subunits, Smc1, Smc3, Scc3, and Scc1 (Rad21), which form a ring structure. The cohesin complex is well known for its role in sister chromatid cohesion to maintain the proper cell cycle process, through its inclusion of the sister chromatid into its ring-like structure. However, the cohesin subunit proteins continue to be expressed in postmitotic cells, including NeuN-positive neurons. Cohesin mediates chromatin loop formation, which has a role in regulating gene expression. Loss of cohesin function causes disruptions in chromatin loops, with subsequent effects on transcriptional regulation. Mutations that perturb the function of cohesin or the proteins that regulate cohesin function cause Cornelia de Lange syndrome (CdLS), a rare malformation syndrome characterized by mental retardation, limb abnormalities, and distinctive facial features. Most of these mutations do not cause overt defects in cohesion or chromosomal segregation. To investigate the potential role of cohesin in terminally differentiated cells in vivo, we generated conditional Smc3-knockout mice. We observed craniofacial abnormality and decreased spine density in cortical neurons of heterozygous Smc3-knockout mice. Heterozygous Smc3-knockout mice exhibited increased anxiety-related behavior, which is consistent with a symptom of Cornelia de Lange syndrome. Thus, neuronal cohesin contributes to neural network formation, and cohesin deficiency leads to higher brain dysfunction.

Keywords *Brain, Development, Neuron, Chromatin, 3D Genome*

O-02

DNA Methylation Patterns in Keloid Fibroblasts

Piyawan Prabsattru[1,2*] Tanchanok Nakbua[2], Nakarin Kitkumthorn [5,] Jiraroch Meevassana [2,3,4]
[1] Program of Medical Science, Faculty of Medicine, Chulalongkorn University, Bangkok, Thailand.
[2] Center of Excellence in Burn and Wound Care, Faculty of Medicine, Chulalongkorn University, Bangkok, Thailand.
[3] Division of Plastic and Reconstructive Surgery, Department of Surgery, Faculty of Medicine, Chulalongkorn University, Bangkok, Thailand.
[4] Department of Anatomy, Faculty of Medicine, Chulalongkorn University, Bangkok, Thailand.
[5] Department of Oral Biology, Faculty of Dentistry, Mahidol University, Bangkok, Thailand.
*Corresponding author, e-mail: piyawan.fern96@gmail.com

Abstract
Keloids are fibroproliferative disorders characterized by abnormal wound healing and excessive extracellular matrix deposition. Despite their clinical significance, the molecular mechanisms driving keloid formation remain poorly understood. Recent studies highlight the effectiveness of comprehensive treatment strategies, Surgical excision remains a primary treatment for keloids, but recurrence rates can be high without additional therapies, reaching 45–100%. Sequential comprehensive treatment, which combines surgery with subsequent therapies, reported a recurrence rate of 15%. However, despite the promise shown by surgical and adjuvant therapies, the complex nature of keloid pathology means that recurrence remains a significant challenge. This underscores the need for ongoing research to establish optimal treatment protocols. This study aimed to investigate the role of DNA methylation in keloid pathogenesis by performing genome-wide methylation profiling of keloid fibroblasts compared to control fibroblasts. We identified 745 differentially methylated regions (DMRs), with hypermethylation (74.90%) being more prevalent than hypomethylation (25.10%). Functional enrichment analysis revealed that hypomethylated genes were associated with developmental processes, immune response, and transcriptional regulation, while hypermethylated genes were linked to metabolic and cellular regulatory pathways. Key pathways included the mesodermal commitment pathway, NOD-like receptor signaling pathway, and mitochondrial complex IV assembly. These findings highlight the critical role of epigenetic dysregulation in keloid formation, with methylation patterns influencing gene expression and cellular processes. This study provides novel insights into the epigenetic mechanisms underlying keloid pathogenesis and identifies potential targets for future therapeutic interventions aimed at modulating DNA methylation to treat or prevent keloids.

Keywords *Keloid, DNA methylation, Epigenetics, Differentially methylated regions (DMRs), Fibroblast*

Background

Keloids are fibroproliferative disorders resulting from abnormal wound healing, characterized by excessive deposition of extracellular matrix (ECM) components, particularly collagen. Unlike hypertrophic scars, keloids extend beyond the original wound boundaries and often recur after treatment [1]. Current therapeutic strategies, including surgical excision, corticosteroid injections, and radiation, are often ineffective, highlighting the need for a deeper understanding of the molecular mechanisms driving keloid formation [2]. Recent studies have implicated epigenetic modifications, such as DNA methylation, in the regulation of fibrotic processes [3]. DNA methylation, a key epigenetic mechanism, involves the addition of a methyl group to cytosine residues in CpG dinucleotides, typically leading to gene silencing. Aberrant methylation patterns have been observed in various fibrotic diseases, but their role in keloid pathogenesis remains underexplored [4].

While epigenetic modifications are implicated in fibrosis, their precise role in keloid pathogenesis remains unclear. Moreover, critical knowledge gaps by correlating DNA methylation patterns with keloid formation, offering potential biomarkers for clinical management. Notably, few studies have explored correlations between DNA methylation patterns and clinical outcomes such as keloid recurrence or severity.

This study aims to characterize the genome-wide DNA methylation profiles in keloid tissues compared to normal skin and adjacent scar tissues. By identifying differentially methylated regions

(DMRs) and their associated genes, we seek to elucidate the epigenetic mechanisms underlying keloid formation. Understanding these mechanisms may improve diagnostic capabilities, for instance through the identification of early detection biomarkers or recurrence predictors. Furthermore, the findings may have translational potential by guiding the development of targeted therapies, including the exploration of DNA methylation inhibitors for keloid management.

Materials and Methods

Sample Collection

Tissue samples were collected from patients at the Plastic Surgery Department in Chulalongkorn Memorial Hospital under Institutional Review Board (IRB) approval (IRB No. 0743/67). All participants provided informed consent before sample collection. A total of 18 samples were obtained, including 12 keloid tissues and 6 normal tissues from unaffected skin areas for comparative analysis. Which, Keloid tissues (<2 years old) and normal skin (from surgical sites without scarring/trauma) were excised from plastic surgery patients. Before DNA extraction, samples were stored at -80°C in Tissue-Tek® O.C.T. Compound (Sakura Finetek, USA).

DNA Extraction

Fibroblast were separated from tissues sample (approximately 20–30 mg) and homogenized in 500 µL of lysis buffer (10 mM Tris-HCl, pH 8.0, 100 mM EDTA, 0.5% SDS) and Proteinase K (20 mg/mL) was added to a final concentration of 100 µg/mL, and the mixture was incubated at 50°C in a water bath for 2–4 hours or overnight with gentle agitation to ensure complete tissue digestion. DNA was then extracted with phenol:chloroform:isoamyl alcohol (25:24:1) according to standard procedures.

Methylation Microarray Assay

Genome-wide DNA methylation profiling was performed using the Illumina Infinium MethylationEPIC BeadChip v2.0 (Illumina, San Diago, CA, USA), which interrogates over 930,000 CpG sites across the genome (GPL33022). Approximately 500 ng of genomic DNA was subjected to bisulfite conversion using the EZ DNA Methylation Kit (Zymo Research). Bisulfite-converted DNA was amplified, fragmented, and hybridized to the Illumina Infinium MethylationEPIC BeadChip v2 according to the manufacturer's protocol (Illumina 2023).

Bioinformatics Analysis

Differentially methylated regions (DMRs) were identified using statistical t-tests with adjustments for multiple testing with the Benjamini-Hochberg correction, controlling the false discovery rate (FDR) at 5%. For each CpG site, DM was assessed using three metrics: the difference in mean methylation beta values between keloid tissues and normal tissues, the log2-transformed ratio of methylation levels, and the p-value derived from the Linear Models for Microarray Data (Limma) analysis [5].

Functional enrichment analysis was conducted to identify pathways and biological processes associated with DMRs using the DAVID (Database for Annotation, Visualization, and Integrated Discovery) web tool. This analysis focused on annotating differentially methylated genes with Gene Ontology (GO) terms, categorized into Cellular Component (CC), Molecular Function (MF), and Biological Process (BP). The enriched GO terms provided insights into the biological roles of these genes, revealing their involvement in specific cellular structures, molecular activities, and pathways relevant to keloid pathogenesis.

Results and Discussion

Identification of Differentially Methylated Regions (DMRs)

The DMRs revealed significant changes in methylation patterns in keloid fibroblasts compared to control fibroblasts. To enhance the reliability of our analysis, we removed CpG sites with low information content by applying an interquartile range (IQR) threshold of 0.02. This reduced the number of CpG sites from an initial total of 850,000 to **570,098**. As shown in Table 1, a total of **745 DMRs** were identified with a significance threshold of **p-value ≤ 0.02**, of which **187 (25.10%)** were hypomethylated and **558 (74.90%)** were hypermethylated, indicating a predominant trend of hypermethylation.

These DMRs were further categorized based on their genomic location, with **148 (19.87%)** located in promoter regions and **597 (80.13%)** in non-promoter regions. Within the promoter regions, **34 DMRs (22.97%)** were hypomethylated, while **114 (77.03%)** were hypermethylated, underscoring the prevalence of hypermethylation in gene regulatory regions. Hypomethylated DMRs in promoter regions were predominantly located in the **TSS1500 region (64.70%)**, followed by the **TSS200 region (35.30%)**. Similarly, hypermethylated DMRs in promoter regions were primarily distributed in the **TSS1500 region (70.18%)**, with the remainder in the **TSS200 region (29.82%)**. The majority of hypermethylated differentially methylated regions (DMRs) were found within CpG islands, which are

crucial regulatory areas often associated with gene silencing. The hypomethylated and hypermethylated DMRs were linked to **131 genes** and **508 genes**, respectively. The extensive methylation changes observed in keloid fibroblasts, particularly in promoter regions, offer insights into the epigenetic mechanisms involved in keloid formation.

Table 1 Distribution of Differentially Methylated Regions (DMRs)

A: Methylation status of 745 DMRs (p-value ≤ 0.02)	
Hypomethylation	187 (25.10 %)
Hypermethylation	558 (74.90 %)
B: 745 DMRs distribution in promoter versus non-promoter	
Promoter	148 (19.87 %)
Non- Promoter	597 (80.13 %)
C: Methylation status of 148 DMRs in promoter regions	
Hypomethylation	34 (22.97 %)
Hypermethylation	114 (70.03 %)
B: Hypomethylated distribution regions	
TSS1500*	22 (64.70 %)
TSS200**	12 (35.30 %)
E: Hypermethylated distribution regions	
TSS1500*	80 (70.18 %)
TSS200**	34 (29.82 %)

* TSS1500: 1500 base pairs upstream of the transcription start site
** TSS200: 200 base pairs upstream of the transcription start site

Functional Enrichment Analysis

The GO enrichment analysis of genes associated with the top 100 differentially methylated regions (DMRs) revealed distinct functional roles for hypomethylated and hypermethylated genes in keloid pathogenesis. For hypomethylated DMRs, the most enriched GO terms included positive regulation of DNA-binding transcription factor activity (GO:0051071, p = 0.0011), platelet-derived growth factor receptor signaling pathway (GO:0048008, p = 0.0025), and DNA binding (GO:0003677, p = 0.0050). These findings align with previous studies demonstrating that hypomethylation in keloids is associated with the activation of genes involved in transcriptional regulation and growth factor signaling. For instance, hypomethylation of transcription factor binding sites has been linked to the upregulation of genes driving fibroblast proliferation and extracellular matrix (ECM) deposition, key features of keloid formation [6]. Additionally, the enrichment of platelet-derived growth factor receptor signaling supports the role of growth factor pathways in promoting fibrotic responses, consistent with findings in other fibrotic disorders [7].

The enrichment of terms such as visual learning (GO:0008542, p = 0.0062) and nucleoplasm localization (GO:0005654, p = 0.0231) further highlights the involvement of hypomethylated genes in cellular localization and neural-related processes. While the connection to visual learning may seem unexpected, recent studies suggest that epigenetic modifications in keloids may influence genes with pleiotropic functions, including those involved in neural signaling [8]. This underscores the complexity of epigenetic regulation in keloid pathogenesis.

For hypermethylated DMRs, the enriched GO terms included metal ion binding (GO:0046872, p = 0.001), cytosol localization (GO:0005829, p = 0.008), and negative regulation of transcription by RNA polymerase II (GO:0000122, p = 0.010). These findings are consistent with the role of hypermethylation in gene silencing, particularly in pathways related to metabolic regulation and transcriptional repression. For example, hypermethylation of genes involved in metal ion binding has been associated with disrupted cellular homeostasis and impaired wound healing, which may contribute to keloid formation [9]. The enrichment of cytoskeleton organization (GO:0007010, p = 0.021) further supports the involvement of hypermethylated genes in regulating cellular structure and motility, processes critical to fibroblast function in keloids [10].

The enrichment of nucleoplasm localization (GO:0005654, p = 0.018) in both hypomethylated and hypermethylated DMRs suggests that epigenetic modifications may differentially regulate genes localized to the nucleoplasm, a key site for transcriptional and post-transcriptional regulation.

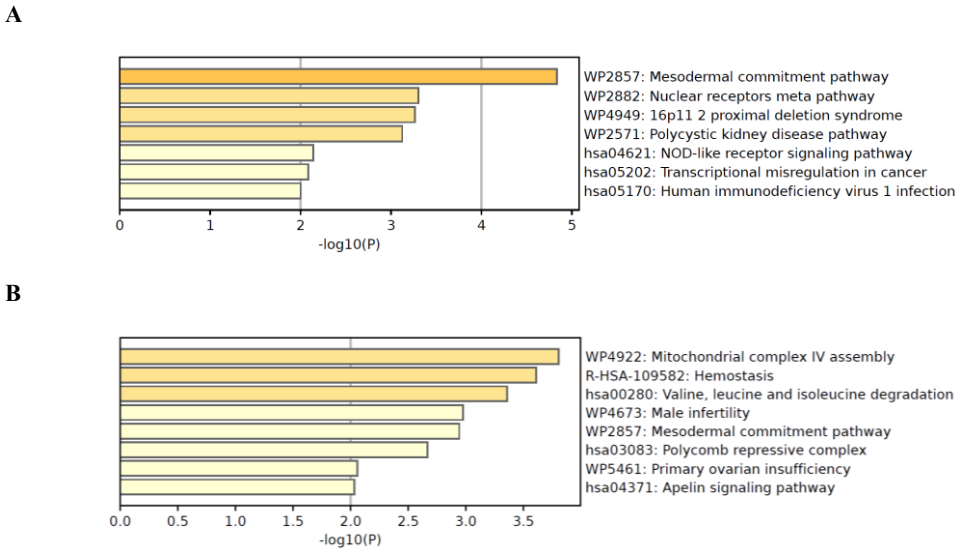

Fig.1 Pathway and process enrichment analysis of gene lists from KEGG, Reactome, Canonical Pathways, and WikiPathways. Pathways were ranked by (-log10(P)), where P-values were calculated using the cumulative hypergeometric distribution and adjusted for multiple testing using the Benjamini-Hochberg procedure (-log10(q)). Only pathways with $P < 0.01$, a minimum count of 3, and an enrichment factor > 1.5 were considered. (A) Top enriched pathways from hypo gene lists. (B) Top enriched pathways from hyper gene lists.

This dual role of methylation in activating or repressing nucleoplasm-localized genes highlights the nuanced regulation of gene expression in keloids.

Pathway Analysis

The pathway analysis of genes associated with hypomethylated and hypermethylated differentially methylated regions (DMRs) revealed distinct biological pathways implicated in keloid pathogenesis, providing insights into the molecular mechanisms underlying this fibroproliferative disorder. For hypomethylated DMRs, the most significantly enriched pathways included the Mesodermal commitment pathway (WP2857, p = 1.45e-05), Nuclear receptors meta pathway (WP2882, p = 5.01e-04), and 16p11.2 proximal deletion syndrome (WP4949, p = 5.37e-04)(Fig 1A). These findings align with previous studies demonstrating that hypomethylation in keloids is associated with the activation of genes involved in developmental processes and transcriptional regulation. The mesodermal commitment pathway has been linked to fibroblast differentiation and extracellular matrix (ECM) remodeling, key processes in keloid formation [10]. Similarly, the enrichment of the nuclear receptors meta pathway suggests a role for nuclear hormone receptors in modulating fibrotic responses, consistent with findings in other fibrotic diseases [11].

In contrast, genes associated with hypermethylated DMRs were significantly enriched in pathways related to metabolic and cellular processes, including mitochondrial complex IV assembly (WP4922, p = 1.55e-04), hemostasis (R-HSA-109582, p = 2.45e-04), and valine, leucine, and isoleucine degradation (hsa00280, p = 4.37e-04) (Fig 1B). These findings suggest that hypermethylation may suppress genes critical for metabolic homeostasis and cellular function, contributing to keloid pathogenesis. For example, the mitochondrial complex IV assembly pathway is essential for cellular energy production, and its dysregulation has been linked to impaired wound healing and fibrosis [12]. These findings suggest that hypermethylation may contribute to keloid formation by silencing genes involved in cellular regulation and homeostasis.

Conclusion

This study reveals significant DNA methylation dysregulation in keloid fibroblasts, with hypermethylation dominating hypomethylation. Key pathways linked to immune response, metabolism, and cellular regulation were identified. These findings highlight epigenetic roles in keloid formation, suggesting methylation-targeted

therapies and advancing research into epigenetic treatments.

Acknowledgments

This research was conducted with support from the Faculty of Medicine at Chulalongkorn University.

References

1. Qi, W., X. Xiao, J. Tong, and N. Guo, *Progress in the clinical treatment of keloids.* Frontiers in Medicine, 2023. **10**.
2. Xia, G., et al., *The effects of systemic diseases, genetic disorders and lifestyle on keloids.* International Wound Journal, 2024. **21**(4): p. e14865.
3. He, Y., et al., *From genetics to epigenetics: new insights into keloid scarring.* Cell Proliferation, 2017. **50**(2): p. e12326.
4. Russell, S.B., et al., *Epigenetically Altered Wound Healing in Keloid Fibroblasts.* Journal of Investigative Dermatology, 2010. **130**(10): p. 2489-2496.
5. Ritchie, M.E., et al., *limma powers differential expression analyses for RNA-sequencing and microarray studies.* Nucleic Acids Res, 2015. **43**(7): p. e47.
6. Liu, C.-S., et al., *Epigenetic Modulation of Radiation-Induced Diacylglycerol Kinase Alpha Expression Prevents Pro-Fibrotic Fibroblast Response.* Cancers, 2021. **13**(10): p. 2455.
7. Jung, S.-C., D. Kang, and E.-A. Ko, *Roles of PDGF/PDGFR signaling in various organs.* The Korean Journal of Physiology & Pharmacology, 2025. **29**(2): p. 139-155.
8. Lin, C.-X., et al., *The m6A-methylated mRNA pattern and the activation of the Wnt signaling pathway under the hyper-m6A-modifying condition in the keloid.* Frontiers in Cell and Developmental Biology, 2022. **10**.
9. Jones, L.R., et al., *Biological significance of genome-wide DNA methylation profiles in keloids.* The Laryngoscope, 2017. **127**(1): p. 70-78.
10. Tekkela, S., et al., *P12 Transcriptional and epigenetic changes drive increased cellular plasticity in keloid fibroblasts.* British Journal of Dermatology, 2024. **190**(6): p. e84-e84.
11. Shi, X., C.D. Young, H. Zhou, and X. Wang, *Transforming Growth Factor-β Signaling in Fibrotic Diseases and Cancer-Associated Fibroblasts.* Biomolecules, 2020. **10**(12).
12. Hunt, M., M. Torres, E. Bachar-Wikström, and J.D. Wikström, *Multifaceted roles of mitochondria in wound healing and chronic wound pathogenesis.* Front Cell Dev Biol, 2023. **11**: p. 1252318.

O-03

Alterations of Seminal Histology and Essential Protein Expressions in Rats Induced by Tramadol

Yutthaphong Patjorn[1], Nawaphon Koedbua[1], Pornpan Kerdsang[1], Chadaporn Chaimontri[1], Chayakorn Taoto[1], Sararat Innoi[1], Natthapol Lapyuneyong[1], Tarinee Sawatpanich[1], Nichapa Phunchago[1], Nareelak Tangsrisakda[1*], Sitthichai Iamsaard[1*]
[1] Department of Anatomy, Faculty of Medicine, Khon Kaen University, Khon Kaen, Thailand
*Corresponding author, e-mail: nareelak@kku.ac.th and sittia@kku.ac.th

Abstract

Tramadol is a centrally acting opioid analgesic that is widely used for managing moderate to severe pain. While prolonged use of this drug has been reported to have adverse effects on male reproductive system such as testis and sperm qualities, its impact on seminal vesicles, which are responsible for major seminal fluid production, remains unexplored. This study aimed to investigate histological changes and alterations of essential protein expressions in the seminal vesicles of male rats administered with tramadol. The adult Wistar male rats (12 weeks) were divided into control (distilled water; DW) and tramadol (50 mg/kg B.W.) groups for treatment for 45 consecutive days. Then, seminal vesicle tissue (SVT) was collected to investigate the histomorphometry (H&E staining) and protein expressions like phosphotyrosine (TyrPho) and seminal vesicle secreting protein 4 (SVS4) by immunoblotting analysis. Moreover, the seminal vesicle fluid (SVF) was examined for its secretion volume percentage. The results showed no significant differences in the relative seminal vesicle weight and SVF secretion between groups. However, it showed the shorter epithelial cell height in the tramadol-treated group compared to control but its thickness of smooth muscle cells surrounding the seminal vesicle wall was thicker. Additionally, SVS4 and Hsp-70 expressions were higher in the tramadol rats. In contrast, a 38-kDa TyrPho protein expression was decreased in the tramadol seminal vesicle as compared to that of control. In conclusion, tramadol did not affect the seminal vesicle secretion volume, but it caused histological changes and increased SVS4 and Hsp-70 expressions with alteration of the 38-kDa TyrPho protein in seminal vesicle tissue.

Keywords *Tramadol, Seminal vesicle, Svs4 protein*

Background

Tramadol, a centrally acting opioid analgesic, is widely used for managing moderate to severe pain. While effective, prolonged use or misuse of tramadol has been associated with adverse effects on various organ systems, including the male reproductive system (5). Recent studies have reported that chronic tramadol exposure disrupts testicular function, reduces sperm quality, and alters the hormonal balance necessary for male fertility (7). However, the impact of tramadol on the seminal vesicles, a crucial accessory gland responsible for seminal fluid production, remains largely unexplored.

The seminal vesicles contribute significantly to semen composition by secreting a fluid rich in fructose, proteins, and bioactive molecules essential for sperm motility, capacitation, and fertilization (2). Structural or functional impairments of the seminal vesicles can negatively affect male reproductive capacity. Opioid-induced oxidative stress and apoptosis have been implicated in reproductive tissue damage, suggesting that tramadol may similarly impact seminal vesicle histology and protein expression (4).

Despite growing concerns about tramadol abuse and its impact on reproduction, there is limited research exploring its effects on the morphology of the seminal vesicles and the expression of key proteins associated with oxidative stress, apoptosis, and seminal secretion. Therefore, this study aims to investigate histological changes and alterations of essential protein expressions in the seminal vesicles of male rats that were administered with tramadol. This will help improve

the understanding of tramadol's effects on reproduction.

Materials and Methods

Tramadol preparation

Tramadol was used to induce damage to the rat seminal vesicle structure and function. The drug, purchased from Srinagarind Hospital, was dissolved in distilled water to prepare a 20 mg/ml stock solution and was diluted to a 50 mg/kg BW. dose for oral administration.

Animal and experimental design

Eleven-week-old male Wistar rats (n=16) were used in the study. After one week of acclimatization, rats were divided into control (distilled water; DW) and tramadol (50 mg/kg B.W.) groups. Rats were orally administered DW or tramadol for 45 days. Rat weights were recorded daily. At the end of the experiment, rats were anesthetized and euthanized for sample collection.

Collections of seminal vesicle tissue and its fluid

At the end of the experiment, the seminal vesicles (SV) were dissected, washed, and weighed. The left SV was cut to collect seminal vesicle fluid (SVF) and kept it in an Eppendorf tube for secretion percentage calculation. The left SV tissue (SVT) without its fluid was collected, weighed, and stored at -20°C for protein expression analysis. The right SV was washed, weighed, fixed in 10% formalin, and processed for histological examination.

Calculation of seminal vesicle fluid secretion percentage

After collecting SVF, the percentage of SVF secretion was calculated by dividing the weight of SVF by the total weight of the SV and multiplying by one hundred. This calculation was based on a formula previously described by Tian et al., 2015 (8).

Histological investigation

The right SVT sections were deparaffinized with xylene and rehydrated (descending ethanol series). Then, the tissue sections were stained with hematoxylin and eosin, dehydrated through an ascending ethanol series, cleared with xylene, and mounted with DPX before being covered with coverslip. The stained sections were examined under a light microscope and photographed for morphometric analysis.

Measurement of SVT epithelial height and thickness of its smooth muscle wall

Histomorphological metrics of SVT sections were measured by selecting ten random fields using ZEN 2 lite (ZEISS). The epithelial height and smooth muscle thickness were measured using the point-counting method with 25 squares drawn on the section (9). Images were captured with an AxioCam ICc 5 camera (ZEISS), and measurements were taken under 40X and 20X.

Immuno-Western blot analysis

Total SVT protein lysates were mixed with 2X loading buffer, boiled, and loaded onto an SDS-PAGE gel. Proteins were separated, transferred to nitrocellulose membranes, and blocked with 5% BSA. The membranes were incubated with primary antibodies (SVS4, Hsp70, β-actin, and TyrPho), washed, and probed with HRP-conjugated secondary antibodies. EGF and BSA were used as positive and negative controls for TyrPho antibodies, respectively, while other antibodies used β-actin as internal control. Immunoreactivity was detected by using an ECL substrate and visualized with Gel Documentation 4.

Statistical analysis

All data were subjected to the independent t-test (for normally distributed data) to compare the differences between the control and tramadol-treated groups. The statistical analyses were carried out using GraphPad Prism 10 (GraphPad Software, USA). A statistically significant difference was considered when the *p*-value was less than 0.05.

Results

Effect of tramadol on SV weight and SVF secretion

The relative weight of the SV in tramadol group seemed to be higher than non-treated group. The percentage of SVF secretions were not significantly different between the control and tramadol-treated groups (Fig. 1).

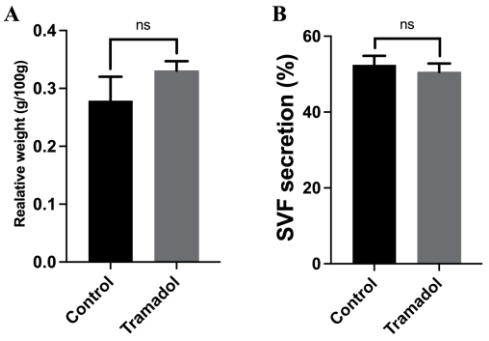

Fig. 1 The relative weight (A) and SVF secretion (B) of the seminal vesicle compared between the control and tramadol-treated groups.

Effect of tramadol on histomorphometry of SVT

It was found that the height of the seminal epithelial cells in tramadol-treated group was significantly shorter than the control group (Fig. 2B). Furthermore, the smooth muscle cells surrounding the seminal vesicle wall were significantly increased in tramadol-treated group (Fig. 2C).

Expression of Svs4, Hsp-70, β-actin, and phosphotyrosine

SVS4 and Hsp-70 exhibited stronger expression in the tramadol-treated group compared to the control group. In contrast, β-actin showed equal expression in both groups, serving as a loading control. Tyrpho expression was stronger in the control group than in the tramadol-treated group (Fig. 3).

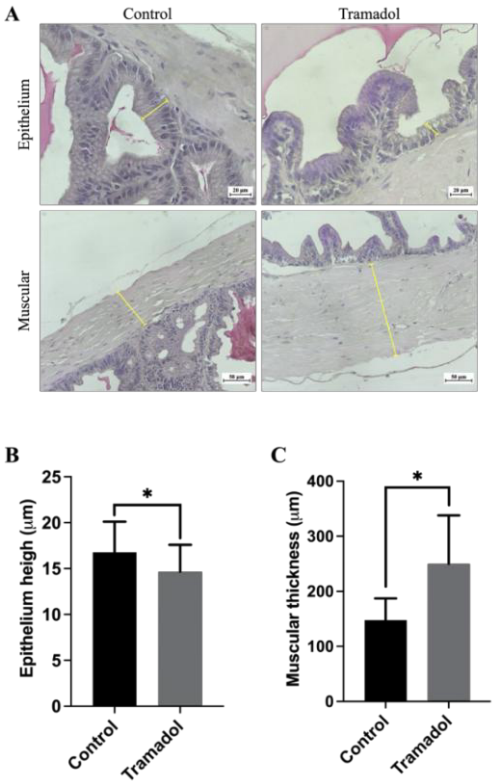

Fig. 2 Micrographs show the measurement of epithelium height and muscular thickness (A), and histograms show the comparison of epithelium height (B) and muscular thickness (C) between the control and tramadol-treated groups. Significant differences between the groups are indicated by $*p < 0.05$.

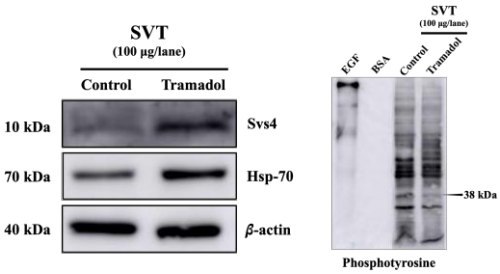

Fig. 3 Immunoblot analysis shows Svs4, Hsp-70, β-actin, and Tyrpho protein expressions in the seminal vesicle tissue.

Discussion

The present study aimed to investigate the effects of tramadol on the seminal vesicle (SV) histology and protein expression in rats. The results revealed no significant differences in the relative

weight of the seminal vesicle or the percentage of seminal fluid secretion between the tramadol-treated and control groups, suggesting that tramadol may not immediately impact these functions. However, histological analysis showed that the epithelial height in the tramadol group was significantly shorter compared to the control group, while the smooth muscle thickness around the SV was significantly thicker in the tramadol-treated group. These structural changes could indicate adaptive responses to tramadol exposure (3). Additionally, the expression of key proteins such as SVS4 and Hsp-70 was significantly higher in the tramadol-treated group, suggesting that these proteins may play a role in the cellular response to tramadol, potentially linked to stress or protective mechanisms (1, 10). On the other hand, β-actin expression, which served as a loading control, was consistent across both groups. Notably, phosphotyrosine (tyrpho) expression was higher in the control group, indicating that tramadol may interfere with certain signaling pathways (6). These findings highlight the complex effects of tramadol on the seminal vesicle, including potential alterations in its histological structure and protein expression, which may have implications for its function. Further studies are needed to better understand the underlying mechanisms of these changes and their long-term consequences on male reproductive health.

Conclusion

Tramadol did not significantly affect the weight or secretion of the seminal vesicle, but histological changes such as reduced epithelial height and increased muscular thickness were observed. Higher expression of SVS4 and Hsp-70 suggests a potential stress response.

Acknowledgements

This study was funded by Postgraduate Study Support Grant of the Faculty of Medicine, Khon Kaen University, Thailand to Mr. Yutthaphong Patjorn.

References

1. Araki N, Kawano N, Kang W, Miyado K, Yoshida K, Yoshida M. Seminal vesicle proteins SVS3 and SVS4 facilitate SVS2 effect on sperm capacitation. Reproduction. 2016;152(4):313-321.
2. Drabovich AP, Saraon P, Jarvi K, Diamandis EP. Seminal plasma as a diagnostic fluid for male reproductive system disorders. Nat Rev Urol. 2014;11(5):278-288.
3. Elghait ATA, Mostafa TM, Gameaa FK, Mohammed GK, Meligy FY, Sayed MM. Comparative Histological Study on the Effect of Tramadol Abuse on the Testis of Juvenile and Adult Male Albino Mice. Anat Cell Biol. 2022;55(3):341-355.
4. Ghosh A, Rabbani SI, Asdaq SMB, Mohzari Y, Alrashed A, Najib AH, et al. Morus alba Prevented the Cyclophosphamide Induced Somatic and Germinal Cell Damage in Male Rats by Ameliorating the Antioxidant Enzyme Levels. Molecules. 2021;26(5):1266.
5. Hamed MA, Ekundina VO, Akhigbe RE. Psychoactive drugs and male fertility: impacts and mechanisms. Reprod Biol Endocrinol. 2023;21(1):69.
6. Nunes CE, Mingo J, López JI, Pulido R. The role of protein tyrosine phosphatases in prostate cancer biology. Biochim Biophys Acta Mol Cell Res. 2019;1866(1):102-113.
7. Soliman T, Shaher H, Mohey A, El-Shaer W, Sebaey A. Gonadotoxic effect of tramadol administration: A prospective controlled study. Arab J Urol. 2021;20(1):54-60.
8. Tian JC, Xia JY, Jiang J, Jiang R, He YZ, Lin H. Effect of androgen deprivation on the expression of aquaporins in rat prostate and seminal vesicles. Andrologia. 2016;48(3):268-76.
9. Taoto C, Tangsrisakda N, Thukhammee W, Phetcharaburanin J, Iamsaard S, Tanphaichitr N. Rats Orally Administered with Ethyl Alcohol for a Prolonged Time Show Histopathology of the Epididymis and Seminal Vesicle Together with Changes in the Luminal Metabolite Composition. Biomedicines. 2024;12(5):1010.
10. Walker VR, Jefferson WN, Couse JF, Korach KS. Estrogen receptor-α mediates diethylstilbestrol-induced feminization of the seminal vesicle in male mice. Environ Health Perspect. 2012;120(4):560-56

O-04

Tramadol Changes Histomorphometry and the Expression of a 50 kDa Tyrosine-phosphorylated Protein and Caspase-3

Nawaphon Koedbua[1], Pornpan Kerdsang[1], Yutthaphong Patjorn[1], Chayakorn Taoto[1], Chadaporn Chaimontri[1], Sararat Innoi[1], Natthapol Lapyuneyong[1], Tarinee Sawatpanich[1], Supatcharee Arun[1], Sitthichai Iamsaard[1*]
[1] Department of Anatomy, Faculty of Medicine, Khon Kaen University, Mittraphap Road, Khon Kaen, Thailand
*Corresponding author, e-mail: sittia@kku.ac.th

Abstract

Tramadol, a centrally acting pain reliever drug, is known to inhibit serotonin secretion and norepinephrine reuptake to reduce the pain. However, prolonged use of this drug has adverse effects on many organ systems including the male reproductive system. Tramadol can reduce the levels of testosterone, LH, and FSH and sperm motility but its effects on epididymis have never been reported. This study aimed to examine the effects of tramadol on morphometric changes and expressions of caspase-3 and tyrosine-phosphorylated (TyrPho) proteins in rat cauda epididymis. Wistar rats were divided into control and tramadol (50 mg/kg BW) treated groups with administration for 45 consecutive days. Histomorphometry of ductus epididymis was observed from H&E slide staining. Expressions of TyrPho proteins and caspase-3 in the epididymis tissue were investigated using immunoblotting. Results showed no significant difference in ductus epididymal duct diameter between the tramadol and control groups. However, tramadol significantly decreased epithelial cell height. The expression of a 50 kDa TyrPho protein was decreased in tramadol epididymis, but caspase-3 expression was obviously increased as compared to control. In conclusion, tramadol alters reduced epididymal epithelial height and tyrosine phosphorylation via caspase-3 activation. This effect may lead to affect the sperm maturation in men with long-term use of tramadol.

Keywords *Tramadol, Epididymis, Caspase-3, TyrPho protein*

Background

Tramadol is a centrally acting pain reliever used to manage various types of pain, including post-surgical recovery, and chronic cancer pain [5]. It is primarily metabolized by CYP3A4 and CYP2D6 and exerts its effects by binding to the μ-opioid receptor (MOR) while inhibiting serotonin and norepinephrine reuptake, enhancing their levels to reduce pain [12,14]. Despite its medical benefits, tramadol is frequently misused, leading to concerns regarding addiction and dependency. Its side effects include euphoria, which increases the risk of overdose [9]. Furthermore, combining tramadol with other substances, such as those used for erectile dysfunction, can result in severe side effects, including cardiovascular complications and dangerously low blood pressure. Long-term or excessive use can cause toxicity in vital organs such as the brain, heart, and lungs [4,15].

Several studies have reported the adverse effects of tramadol on different organ systems, as well as the reproductive system. Research indicates that prolonged tramadol use reduces testosterone, luteinizing hormone (LH), and follicle-stimulating hormone (FSH) levels. Tramadol was demonstrated to decrease count and motility of epididymal sperm. A morphometric study found that tramadol reduced the diameter and epithelial height of the ductus epididymis while increasing epididymal cell necrosis, potentially impairing sperm maturation and leading to male infertility [3]. This increase in epididymal cell necrosis may be mediated by the activation of caspase-3, a key protein of apoptosis, along with alterations in tyrosine-phosphorylated proteins (TyrPho), which play a crucial role in sperm maturation.

Therefore, this study aimed to determine the association between these morphometric changes and caspase-3 expression, as well as the expression of TyrPho, which play a crucial role in sperm maturation, in epididymal damage induced by tramadol in adult male rats.

Materials and Methods

Experimental design

The male Wistar rats were used and were randomly divided into two group: control group received distilled water (DW), and tramadol group received 50 mg/kg BW of tramadol HCl. Each group were administered once daily via oral gavage for 45 consecutive days. At the end administration, all

animals were anesthetized and euthanized by cervical dislocation. This study was already approved by Institutional Animal Care and Use Committee of Khon Kaen University, based on the Ethic of Animal Experimentation of National Research Council of Thailand. (Rec. No. IACUC-KKU-92/67).

Morphometric study

The right epididymis of rats in both the control and tramadol groups was dissected and fixed in 10% formalin, dehydrated in alcohol, embedded in paraffin, and sectioned at a thickness of 5 µm. The sections were stained with hematoxylin and eosin (H&E) staining and subsequently examined under a light microscope. Five non-overlapping fields from six H&E-stained sections of the sperm duct of each rat were evaluated an image analyzer (Image J-analysing system software).

To examine epididymal duct diameter, transversely sectioned epididymal ducts with a rounded shape were selected. Two perpendicular diameters of each duct were measured, and the average value was calculated [13].

To evaluate epididymal epithelial height, measurements were taken from the basement membrane to the apical surface, excluding stereocilia [7].

Immuno-Western blot

The left cauda epididymal tissue of each rat was minced and homogenized with plastic tissue grinder with RIPA buffer containing cocktail protease inhibitors. After centrifugation, the total protein concentrations of the epididymal lysate were determined using a NanoDrop Spectrophotometers. The proteins were separated with 10% sodium dodecyl sulphate polyacrylamide gel electrophoresis (SDS-PAGE) and transferred to nitrocellulose membranes. The protein membrane was incubated with 5% BSA in 0.1% TBST, and washed with 0.1% TBST. After that, the protein membrane was probed with primary antibodies diluted in 0.1% TBST including anti-caspase 3 and anti-phosphotyrosine antibodies at 4°C overnight, followed by incubation with the secondary antibody (goat anti-mouse IgG-HRP) for 1 hour at room temperature. The protein expressions in epididymal tissue were visualized with enhanced chemiluminescence (ECL) by using the Gel Documentation System (ImageQuant 600, GE Healthcare, USA)

Statistical analysis

The data were analyzed statistically using GraphPad Prism version 10. The independent t-test was used to compare the significant differences in the data between the control and tramadol groups. All significance levels were inferred at $p < 0.05$.

Results

The epididymal duct diameter in the tramadol group showed no significant difference compared to the control group, as shown in Figure 1B. In contrast, the epididymal epithelial height in the tramadol group was significantly decreased compared to the control group ($p < 0.05$), as shown in Figure 1D**.**

For caspase-3 expression, the tramadol group exhibited an intense band (17 kDa), indicating

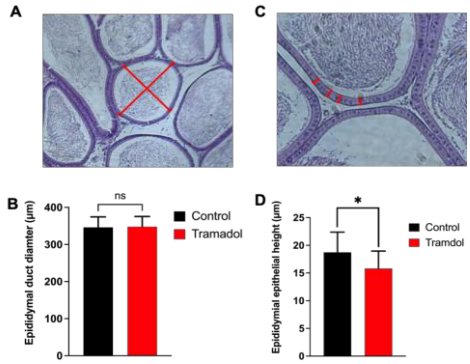

Fig.1 (A) The measurement of epididymal duct diameter (B) The mean epididymal duct diameter of the control and tramadol groups. (C) The measurement of epididymal epithelial height. (D) The mean epididymal epithelial height of the control and tramadol groups.
ns; no significant
*; statistically significant difference compared with the control

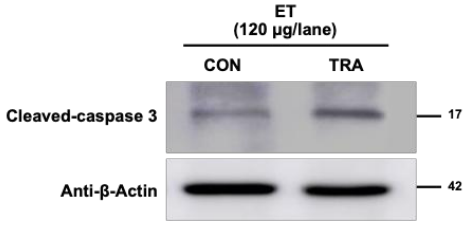

Fig.2 Cleaved-caspase 3 expression in epididymal tissue (ET).

higher caspase-3 expression compared to the control group, as shown in Figure 2.

The expression of TyrPho protein of epididymal tissue (50 kDa) was lower in the tramadol group, as shown in Figure 3.

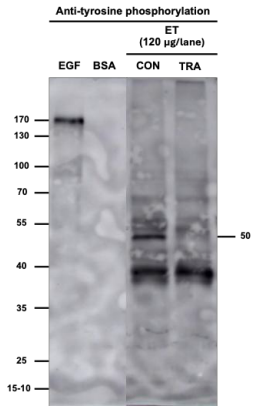

Fig.3 TyrPho protein expression in epididymal tissue (ET).

Discussion

In this study, we found that the tramadol group showed a reduction in epididymal epithelial height and a decrease in the expression of tyrosine phosphorylation at a 50 kDa band in epididymal tissue. Additionally, the tramadol group increased expression of caspase-3.

Tramadol-induced epididymal abnormalities occur indirectly through testosterone deprivation, caused by reduced LH secretion and degeneration of Leydig cells. The epididymis has LH receptors, and both androgens and LH are essential for its normal structure and function. Decreased testosterone and LH levels affect epididymal cell metabolism, leading to changes in cell character and tubule diameter [10,11]. On the other hand, the increased expression of caspase-3 in the tramadol group, which is one of the proteins involved in apoptosis, is consistent with the findings of Ahmed and Kurkar [1]. They reported that tramadol administration increased nitric oxide synthase and ROS production in testicular tissue, leading to apoptosis, which affected changes in epididymal epithelial height and the expression of Tyrpho in both testicular and epididymal tissues [1].

The decreased expression of TyrPho, a protein crucial for spermatogenesis, testosterone production in the testis, sperm maturation, acrosome reaction, fertilization, and sperm motility in the tramadol-treated group [2,8], may be related to semen parameters. Further studies are needed to explore this relationship.

Conclusion

Long-term administration of tramadol can affect the structure of the epididymis and decrease the expression of TyrPho proteins, which are related to sperm maturation via caspase-3 activation. This may lead to impaired or decreased function, resulting in reduced sperm quality and an increased risk of male infertility.

Acknowledgements

This study was funded by the Postgraduate Study Support Grant from the Faculty of Medicine, Khon Kaen University, Thailand to Mr. Nawaphon Koedbua for master's degree studying in Anatomy program

References

Ahmed MA, Kurkar A. Effects of opioid (tramadol) treatment on testicular functions in adult male rats: The role of nitric oxide and oxidative stress. Clin Exp Pharma Physio. 2014;41(4):317–23.

Arun S, Chaiyamoon A, Lapyuneyong N, Bunsueb S, Wu AT, Iamsaard S. Chronic stress affects tyrosine phosphorylated protein expression and secretion of male rat epididymis. Andrologia. 2021;53(3).

Attia AM, Bakry OA, Yassin H, Sarhan N, Samaka R, Gamal N. Morphometric and ultrastructural analysis of tramadol effects on epididymis: an experimental study. Ultrastructural Pathology. 2018;42(3):295–303.

Faria J, Barbosa J, Leal S, Afonso LP, Lobo J, Moreira R, et al. Effective analgesic doses of tramadol or tapentadol induce brain, lung and heart toxicity in Wistar rats. Toxicology. 2017;385:38–47.

Faria, J., Barbosa, J., Leal, S., Afonso, L. P., Lobo, J., Moreira, R., Queirós, O., Carvalho, F., &

Dinis-Oliveira, R. J. Effective analgesic doses of tramadol or tapentadol induce brain, lung and heart toxicity in Wistar rats. Toxicology. 2017; 385, 38–47.

Grond, S., & Sablotzki, A. Clinical Pharmacology of Tramadol. Clinical Pharmacokinetics. 2004; 43(13), 879–923.

Hamzeh M, Robaire B. Effect of Testosterone on Epithelial Cell Proliferation in the Regressed Rat Epididymis. Journal of Andrology. 2009;30(2):200–12.

Iamsaard S, Welbat JU, Sukhorum W, Krutsri S, Arun S, Sawatpanich T. Methotrexate Changes the Testicular Tyrosine Phosphorylated Protein Expression and Seminal Vesicle Epithelia of Adult Rats. Int J Morphol. 2018;36(2):737–42.

Kubola J and Siriamornpun S. Phenolic contents and antioxidant activities of bitter gourd (Momordica charantia L.) leaf, stem and fruit fraction extracts in vitro. Food Chemistry. 2008;10: 881–890.

Lei ZM, Zou W, Mishra S, Li X, Rao ChV. Epididymal Phenotype in Luteinizing Hormone Receptor Knockout Animals and Its Response to Testosterone Replacement Therapy1. Biology of Reproduction. 2003;68(3):888–95.

Londonkar RL, Sharangouda S, Patil SB. Morphine induced inhibition of the activities of accessory reproductive ducts in male rats. Oriental Pharmacy and Experimental Medicine. 2008;8(1):67–72.

Miotto K, Cho AK, Khalil MA, Blanco K, Sasaki JD, Rawson R. Trends in Tramadol: Pharmacology, Metabolism, and Misuse. Anesthesia & Analgesia. 2017;124(1):44–51.

Narayana K, Prashanthi N, Nayanatara A, Bairy LK, Dõsouza UJA.An organophosphate insecticide methyl parathion (O-O-dimethyl O-4-nitrophenyl phosphorothioate) induces cytotoxic damage and tubular atrophy in the testis despite elevated testosterone level in the rat. J Toxicol Sci. 2006;31(3):177–89.

Saiz-Rodríguez M, Ochoa D, Román M, Zubiaur P, Koller D, Mejía G, et al. Involvement of CYP2D6 and CYP2B6 on Tramadol Pharmacokinetics. Pharmacogenomics. 2020; (10):663–75.

Youssef S, H. Histopathological and Biochemical Effects of Acute & Chronic Tramadol drug Toxicity on Liver, Kidney and Testicular Function in Adult Male Albino Rats. Foresic Research & Criminology International Journal. 2016; 2(4).

O-05

Histopathology and Decrease of Pro-caspase Markers in Adult Rat Testis Treated with an Opioid Analgesic

Pornpan Kerdsang[1], Nawaphon Koedbua[1], Yutthaphong Patjorn[1], Chadaporn Chaimontri[1], Sararat Innoi[1], Chayakorn Taoto[1], Natthapol Lapyuneyong[1], Nongnut Uabundit[1], Arada Chaiyamoon[1], Rarinthorn Samrid[1*], Sitthichai Iamsaard[1*]
[1] Department of Aantomy, Faculty of Medicine, Khon Kaen University, Mittraphap Road, Khon Kaen, Thailand
*Corresponding author, e-mail: rarisa@kku.ac.th and sittia@kku.ac.th

Abstract

An opioid analgesic drug especially "Tramadol" is commonly used to relieve moderate to severe pain. However, both overdose and long-term uses of tramadol are reported to have adverse effects on reproductive system, particularly damaging testis. Since the actual mechanism of such damage caused by tramadol is still not fully understood, the aim of recent study was to additionally investigate more histopathology and expressions of apoptotic and tyrosine-phosphorylated (TyrPho) proteins in rat testis. Male Wistar rats (270–300 g) were divided into two groups: the control group (received distilled water) and the tramadol group (received tramadol at a dose of 50 mg/kgBW per day) for 45 consecutive days. The histopathological features and seminiferous tubule morphometrics were observed. The expressions of pro-caspase (3,9) and TyrPho protein profiles in testicular lysate were examined by using Western blot analysis. Results showed that the relative weight of the testis was significantly increased in tramadol group. It was observed that the shrunken seminiferous tubules, degenerated interstitial tissue, and basement membrane damage were present in some testicular tissues of tramadol-treated rats. Moreover, the expressions of pro-caspases (3 & 9) and a 57 kDa TyrPho protein were obviously decreased as compared to control rats. However, no difference in HSP70 expression between the groups was observed. In conclusion, tramadol induced some testicular histopathology by activating caspase 3 and 9 expressions. Taken together, it is possible to interfere tyrosine phosphorylation especially function of a 57 kDa TyrPho protein, resulting in testicular dysfunctions like interrupted spermatogenesis and androgen production.

Keywords *Tramadol, Testis, Apoptosis, Pro-caspase*

Background

The pain is a symptom that occurs when noxious stimuli activate nociceptors in various parts of the body. One of the effective pain medications is opioid analgesics, such as tramadol. Tramadol is an opioid analgesic that generally acts directly on the central nervous system [9]. This drug is used to relieve moderate to severe pain. Its action includes being an agonist of μ-opioid receptors and also inhibiting serotonin and norepinephrine reuptake [8], which is potent in reducing pain perception.

Although tramadol is an effective and important medication for pain relief, some individuals misuse its effects inappropriately. In many countries, as well as in Thailand, tramadol has been classified as a controlled drug that requires a prescription and categorized as a dangerous drug. The adverse effects of this drug have been reported in many studies. Both overdose and long-term use of tramadol can cause adverse effects on several systems, such as the respiratory, cardiovascular, nervous, and gastrointestinal systems [3,8]. Especially, previous reports have shown that tramadol affects the reproductive system, leading to abnormalities in sex hormone levels and sexual dysfunction in humans [5]. In animal models, many studies have shown that tramadol can cause damage to the testis by increasing apoptotic markers [1], leading to the disruption of seminiferous tubule structure. Therefore, this study aims to investigate the adverse effects of tramadol on histological features and the expression of apoptotic and related proteins involved in the testicular tissue.

Materials and Methods

Animals, experimental design, and drug

In this study, adult male Wistar rats (11 weeks, 270–300 g) were purchased from the Northeast Laboratory Animal Center, Khon Kaen University, Thailand. The animals were divided into two groups: the control group (received 2 ml of distilled water) and the tramadol group (received tramadol solution at a dose of 50 mg/kgBW per day). This study was performed for 45 consecutive days.

Tramadol hydrochloride (tramadol HCl, 50 mg/capsule) was purchased from Srinagarind Hospital, Faculty of Medicine, Khon Kaen University, Thailand.

Hematoxylin & Eosin (H&E) staining

After the rats were sacrificed, the testes were removed and immediately fixed in 10% formalin solution for 48 hours, then they were processed routinely for paraffin sectioning. First, the fixed testes were dehydrated through an ethanol series (70% to 100%, respectively) and cleared by using xylene. After that, the samples were infiltrated with liquid paraffin and embedded. The tissue paraffin blocks were trimmed and sectioned to a thickness of 5 µm. The sections were placed on glass slides and dried at room temperature. Subsequently, the sections were deparaffinized by using xylene, rehydrated, and stained with Mayer's hematoxylin for 10 minutes. After that, the slides were counterstained with eosin Y for 5 minutes. After washing with tap water, the stained slides were dehydrated, cleared, and mounted with dibutylphthalate polystyrene xylene (DPX), covered with a coverslip, and observed under the light microscope.

Measurements of seminiferous tubule diameter

To evaluate the histomorphometric changes in the testicular tissue, the H&E-stained slides were observed under a light microscope, and their seminiferous tubule diameter was measured. The round seminiferous tubules were randomly measured along four transverse axes, approximately 60 tubules per animal [2]. The seminiferous tubule diameter was measured from one side of the basement membrane to the opposite basement membrane using the ImageJ program.

Immuno-Western blot

The testicular lysates (100 µg) were denatured, boiled, and run under sodium dodecyl sulfate-polyacrylamide gel electrophoresis (SDS-PAGE). After that, the separated proteins were transferred onto the nitrocellulose membrane. Subsequently, the transferred protein membrane was blocked with 5% BSA for 1 hour. The membrane was incubated with specific primary antibodies, including anti-tyrosine phosphorylation, anti-caspase 3, anti-caspase 9, and anti-Hsp70. The membrane was incubated at 4°C overnight on an automatic shaker. Then, the membrane was further incubated with specific secondary antibodies conjugated with horseradish peroxidase (HRP). For all primary antibodies above, goat anti-mouse IgG was used to probe and incubated at room temperature for 1 hour. After washing, the enhanced chemiluminescence (ECL) substrate reagent kit was used to detect the immunoreactivity of the antigen-antibody complex and visualized using a Gel Documentation system. To confirm the equal loading of total protein concentrations, anti-β-actin was used as an internal control.

Statistical analysis

All data will be expressed as mean ± standard deviation (SD). The statistical significance between groups was analyzed using an independent t-test with GraphPad Prism software version 10. A statistically significant difference was considered when the p-value was less than 0.05.

Results

Relative weight of testis

The relative weight of the testis was significantly different between the control group and the tramadol group (Fig. 1). It is possible that chronic exposure to tramadol may affect body weight and organ weight.

Histopathology of the testis

The histopathology of testicular tissue in the tramadol group is shown in Fig. 2C and 2D. In the tramadol-treated group, the seminiferous tubules

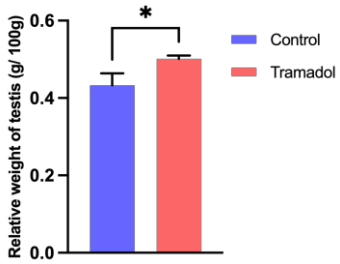

Fig.1 Relative weight of testis

were shrunken, and the interstitial tissue was degenerated. Additionally, basement membrane damage was observed in Fig. 2D. When compared to the control group (Fig. 2A and 2B), the seminiferous tubules were arranged tightly, and the interstitial tissue remained mostly intact.

Tramadol reduced seminiferous tubule diameter

The quantitative analysis of seminiferous tubule diameter compared between the control and tramadol groups (Fig. 3) found that the mean

diameter in the tramadol group was significantly lower ($p < 0.05$) than in the control group. This may be explained by the histopathological features, as the seminiferous tubules in the tramadol group appeared shrunken.

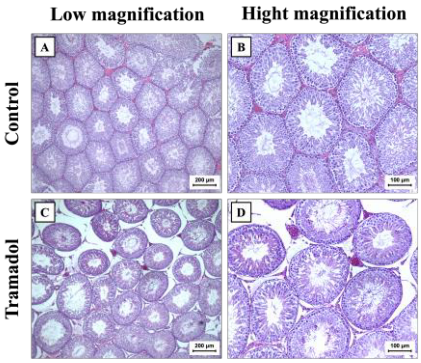

Fig.2 Showing testicular histopathology of control and tramadol group. The tramadol group shows testicular damage compared to control group. A and C; low magnification, B and D; Hight magnification

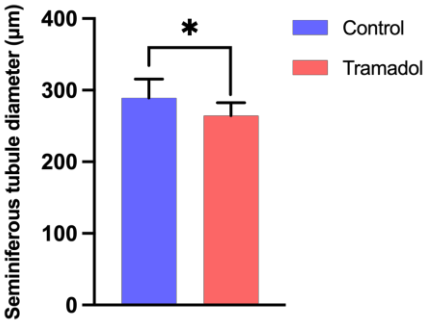

Fig.3 Quantitative analysis of seminiferous tubule diameter compared between control and tramadol group

Tramadol decreased pro-caspase 3 and 9 protein expression

The tramadol-treated group showed decreased pro-caspase 3 and 9 expression compared to the control group. While the expression of HSP70 appeared to show no difference between the two groups. However, the decreased expression of pro-caspase 3 and 9 may indicate that the cells were undergoing apoptosis (Fig.4).

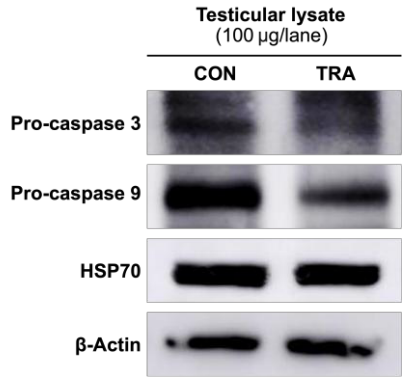

Fig.4 Showing the expressions of testicular pro-caspase 3, pro-caspase 9, and HSP70 proteins compared between control and tramadol groups. The β actin was used as an internal control.

Tramadol decreased TyrPho protein expression

The expression of TyrPho protein in testicular tissue at 57 kDa was different among the groups (Fig. 5). The control group showed a darker band than the tramadol group.

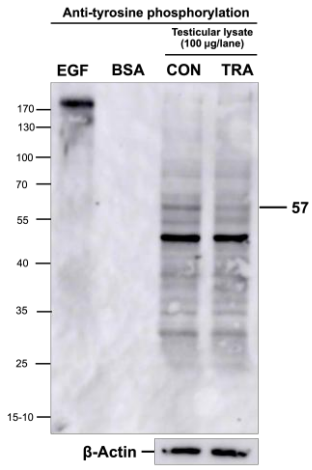

Fig.5 Showing the expressions of testicular TyrPho proteins compared between control and tramadol groups. The β actin was used as an internal control.

Discussion

Tramadol may affect body weight and organ weight. Previous studies have shown that tramadol decreased testicular weight [1]. However, this study showed that the relative weight of the testis in the

tramadol group was higher on average compared to the control group. This suggests that body weight and organ weight may not necessarily change in the same direction. In addition, some previous studies have shown that tramadol results in a reduction in body weight, which may indicate that the damage caused affects body weight but may not impact the weight of the testes [7]. When comparing the organ weight relative to body weight in both experimental groups, the relative weight of the testis in the tramadol group was significantly higher than in the control group. Furthermore, histopathological analysis has shown that the structure of the seminiferous tubule is damaged due to tramadol administration. Previous studies have indicated that tramadol causes damage to the seminiferous tubule, including intercellular spaces in the seminiferous tubule, interstitial vacuoles, germ cell exfoliation, congestion of blood vessels, and degeneration of spermatogenic cells [8]. Similarly, this study found that the seminiferous tubules in the tramadol-treated group were shrunken, the interstitial tissue was degenerated, and the basement membrane was damaged. These damages may be a result of apoptosis occurring in the cells.

Pro-caspase 9 is a protein involved in the initiation of apoptosis. When pro-caspase 9 is activated, it is converted into cleaved-caspase 9, which in turn activates pro-caspase 3. Pro-caspase 3 is involved in the final stages of apoptosis, and upon activation, it becomes cleaved-caspase 3, which functions to degrade cellular proteins, ultimately leading to apoptosis. A previous study reported that tramadol significantly increases p53 protein expression in the testes and enhances caspase-3 activity [1]. This finding aligns with the present study, which demonstrated that tramadol reduces the expression of pro-caspase 3 and pro-caspase 9. This may indicate that these proteins have already been activated into their active forms. However, further investigation of cleaved-caspase 3 and cleaved-caspase 9 expression would provide stronger confirmation of this hypothesis, and additional experiments are still required.

Tyrosine phosphorylation is a protein present in the testis that plays a crucial role in spermatogenesis and testosterone synthesis [4]. It is also involved in regulating cell survival and maintaining the tight junctions of Sertoli cells. This study demonstrated that the expression of TyrPho protein was reduced in the tramadol-treated group, which may suggest that tramadol affects the expression of this protein and could lead to testicular damage. However, this study also found that the expression of HSP70 protein did not differ significantly between the two groups.

Conclusion

In conclusion, tramadol induced testicular damage by activating caspase 3 and 9, which resulted in histopathological alterations and reduced seminiferous tubule diameter. These damages can impact spermatogenesis and may also contribute to male infertility.

Acknowledgements

This study was supported by Postgraduate Study Support Grant of the Faculty of Medicine, Khon Kaen University, Thailand.

References

Adelakun SA, Ukwenya VO, Akintunde OW. Vitamin B12 ameliorate Tramadol-induced oxidative stress, endocrine imbalance, apoptosis and NO/iNOS/NF-κB expression in Sprague Dawley rats through regulatory mechanism in the pituitary-gonadal axis. Tissue and Cell. 2022; 74:101697.

Altoé PM, Tatsuo ES, Paulo DN, Jarske R, Milagres M, Loureiro ID. Effects of human chorionic gonadotropin on the normal testicular tissue of rats. Acta Cir Bras. 2014;29(5):292-8.

Grond S, Sablotzki A. Clinical Pharmacology of Tramadol: Clinical Pharmacokinetics. 2004;43(13):879–923.

Iamsaard S, Welbat JU, Sukhorum W, Krutsri S, Arun S, Sawatpanich T. Methotrexate Changes the Testicular Tyrosine Phosphorylated Protein Expression and Seminal Vesicle Epithelia of Adult Rats. Int J Morphol. 2018 Jun;36(2):737–42.

Kabbash A, El Kelany R, Oreby M, El Gameel D. Effect of tramadol dependence on male sexual dysfunction. Interdisciplinary Toxicology. 2019; 12(4):157–62.

Minisy FM, Shawki HH, El Omri A, Massoud AA, Omara EA, Metwally FG, et al. Pomegranate Seeds Extract Possesses a Protective Effect against Tramadol-Induced Testicular Toxicity in Experimental Rats. Rahman MdA, editor. BioMed Research International. 2020 :2732958.

Oka VO, Udefa AL, Nna VU, Owu DU. Sildenafil Citrate and Tramadol Administered Separately

and in Combination Affects Basal Metabolic Rate, Triiodothyronine (T3) and Cortisol Levels in Albino Wistar Rats. Trends in Medical Research. 2015;10:51–62.

Subedi M, Bajaj S, Kumar MS, Yc M. An overview of tramadol and its usage in pain management and future perspective. Biomedicine & Pharmacotherapy. 2019; 111:443–51.

Vazzana M, Andreani T, Fangueiro J, Faggio C, Silva C, Santini A, et al. Tramadol hydrochloride: Pharmacokinetics, pharmacodynamics, adverse side effects, co-administration of drugs and new drug delivery systems. Biomedicine & Pharmacotherapy. 2015; 70:234–8.

O-06

Preventive Effects of Tri Garn Pis Recipe Extract on Testicular Apoptosis and Low Sperm Quality in Chronic Stress Mice Induced with Dexamethasone

Chadaporn Chaimontri[1], Tarinee Sawatpanich[1], Nongnut Uabundit[1], Arada Chaiyamoon[1], Rarinthorn Samrid[1], Sitthichai Iamsaard[1], Supatcharee Arun[1]*
[1] Department of Anatomy, Faculty of Medicine, Khon Kaen University, Mittraphap Road, Khon Kaen, Thailand
*Corresponding author, e-mail: supatar@kku.ac.th

Abstract

Chronic stress (CS) is a cause of male infertility, leading to a decline in testosterone and poor semen quality. The glucocorticoid-induced CS models have previously shown low sperm quality in animal studies. Moreover, a previous study reported that dexamethasone (DEX) induced testicular apoptosis. Herbal medicine or single plant extracts were used to decline its adverse effects from CS conditions, preventive effect of Tri Garn Pis (TGP) recipe extract on the male reproductive system and its protein function in DEX-induced CS mice has never been reported. Therefore, this study aimed to investigate the TGP extract properties on testicular function, sexual performances and sperm quality using CASA analysis in CS-induced mice treated with DEX. Seventy-two male ICR mice were randomly divided into 6 groups: control, DexCS, TGP50+DexCS, TGP100+DexCS, TGP200+DexCS, and TGP200 groups, respectively. For the co-treated group, mice were pretreated with TGP extract at doses of 50, 100, and 200 mg/kg BW for 14 consecutive days (preventive period) and then injected with DEX at 4 mg/kg BW for 28 days (co-treatment period). The experiment was performed for 42 consecutive days. The depression-like behavior tests (sucrose preference, tail suspension, and forced swimming) were used to estimate CS-related behaviors in mice. Sexual behaviors were evaluated. The epididymal sperm quality, testicular histopathology, functional reproductive proteins (AR, CYP11A1, and StAR), and apoptotic protein expressions (Hsp70, caspase3, and caspase9) were analyzed. Results showed that TGP containing phenolic, flavonoid contents, and antioxidant activities improved immobility, sexual disorder and testicular histopathology (loss of germ cell and sperm mass in the cauda epididymis). The percentage of motile sperm was significantly increased in TGP50+DexCS. Moreover, the TGP extract improved testicular StAR protein expressions and decreased the expressions of caspase3 and 9 in DexCS mice. In conclusion, the TGP extract has preventive effects against testicular apoptosis, sexual dysfunction, and poor sperm motility caused by chronic stress conditions.

Keywords *Tri Garn Pis recipe extract, Dexamethasone, Sexual behavior, Ssperm motility, Testis*

O-07

Mitragyna speciosa (Korth) Havil Extract Containing Anti-Oxidant Capacity Prevents Sperm and Testicular Damages Induced by Chronic Stress

Natthapol Lapyuneyong[1], Chadaporn Chaimontri[1], Chayakorn Taoto[1], Therachon Kamollerd[1], Nawaphon Koedbua[1], Pornpan Kerdsang[1], Yutthaphong Patjorn[1], Chetsadaporn Naksing[1], Sararat Innoi[1], Supatcharee Arun[1], Tarinee Sawatpanich[1], Sitthichai Iamsaard [1*]
1 Department of Anatomy, Faculty of Medicine, Khon Kaen University, Mittraprap road, Khon Kaen, Thailand
*Corresponding author, e-mail: sittia@kku.ac.th

Abstract

Previous studies demonstrated that chronic stress (CS) can decrease heat shock protein 70 (HSP70) and steroidogenic acute regulatory (StAR) expressions in testicular tissue, which can lead to decrease sperm production and motility. Interestingly, *Mitragyna speciosa* (Korth) Havil or MS leaf extract has been found to contain compounds with antioxidant properties and has the ability to increase testosterone levels. However, the mechanisms of this extract in improving the testicular damages caused by CS have not been studied. Therefore, the goal of this study was to investigate the protective effects of MS extract on testicular damages arising from CS. The MS water extract was analyzed for antioxidant compounds. Fifty male rats were divided into five groups (10 rats/group): control (I), DEX (II), DEX+MS100 (III), DEX+MS200 (IV), and DEX+MS400 (V). Control rats were injected with Na_3PO_4 whereas rats in groups (II-V) were injected with dexamethasone (DEX) for 21 consecutive days. For groups (I-II), rats received DW while the threated rats (groups III-V) were administered with MS extract (100, 200, and 400 mg/kg BW, respectively) after DEX injection on each day. At the end of study, rats were determined and confirmed for CS behaviors. Testes were collected for investigating the histomorphometrics and the expressions of HSP70 and StAR. Sperm qualities were evaluated by using CASA. This study found that MS extract contained flavonoid and phenolic contents with antioxidant capacities. The diameter and the epithelial height of seminiferous tubules had significantly increased in the treated groups compared to the DEX group. Although HSP70 expression was not different among groups, MS extract increased StAR expression and sperm qualities compared to DEX group. It was concluded that MS extract could improve CS-testicular damages.

Keywords *Dexamethasone, Mitragyna speciosa (Korth) Havil, HSP70, StAR, and testis*

O-08

A Bioelectrically Enabled Smart Bandage for Accelerated Wound Healing and Predictive Monitoring

Aziza Alrafiah[1] *, and Ahmad F Turki[2]
[1] Department of Medical Laboratory Sciences, Faculty of Applied Medical Sciences, King Abdulaziz University, Jeddah 21589, Saudi Arabia Electrical and Computer
[2] Engineering Department, Faculty of Engineering, King Abdulaziz University, Jeddah, Saudi Arabia; aftorke@kau.edu.sa
* Correspondence: aalrafiah@kau.edu.sa

Abstract
Background: Chronic wounds pose a significant healthcare burden due to slow healing and high infection risks. Smart bandages that combine therapeutic stimulation with real-time monitoring offer a novel approach to improve healing outcomes. **Objective:** This study aims to develop and evaluate a bioelectrically enabled smart bandage that enhances wound repair using electric field stimulation while continuously monitoring vital signs. **Methods**: 100 Sprague-Dawley rats were assigned to either an electric field (EF)-treated group or a control group. Full-thickness excisional wounds were induced, followed by applying a smart bandage delivering 2V electric stimulation (200 mV/mm) for five hours daily over 14 days. Healing progression was tracked using digital imaging and histological analysis. Physiological data—heart rate, oxygen saturation, and temperature—were continuously recorded. Machine learning models were trained to predict healing outcomes based on biometric inputs. **Results:** EF-treated wounds showed accelerated healing, achieving 82% closure by Day 7 versus 70.75% in controls. By Day 14, treated wounds were reduced to 0.01 cm^2, compared to 0.24 cm^2 in the control group. Histological analysis revealed increased neovascularization, organized collagen deposition, and enhanced epithelial regeneration. The smart bandage maintained stable vital signs with no signs of systemic inflammation. Machine learning models (XGBoost and Random Forest) exceeded 98% accuracy in predicting wound healing stages, with SHAP analysis highlighting EF exposure and treatment duration as primary contributors. **Conclusion:** Integrating electric field therapy with continuous monitoring through smart bandages significantly accelerates wound healing and enables accurate predictive modeling. These findings demonstrate strong potential for advanced, AI-enhanced wound care technologies in clinical settings.

Keywords *Wearable Technologies; Smart Bandage; Wound Healing; Electric Field Therapy; Advanced Wound Care; Machine Learning.*

O-09

The Effect of Melatonin on Tight Junctions Related to Cognitive Function in the Hippocampus of Diabetic Rats

Sunantha Yang-en[1], Chutikorn Nopparat[2], Pansiri Phansuwan[1], Ratchadaporn Pramong[1*]
[1] Department of Anatomy, Faculty of Medicine, Srinakharinwirot University, Sukhumvit 23, Bangkok, Thailand
[2] Innovative Learning Center, Srinakharinwirot University, Sukhumvit 23, Bangkok, Thailand
*Corresponding author, e-mail: ratchadapornpr@g.swu.ac.th

Abstract

Diabetes mellitus causes contributes to microvascular dysfunction in several organs, including hippocampus. Previous studies found that diabetes can lead to tight junction impairment in the hippocampus. Tight junction is structure of blood-brain barrier that connects endothelial cells to protect the pathogens in circulation through brain parenchyma. Diabetes can cause neuroinflammation, which leads to blood-brain barrier injury. Melatonin, a neurohormone secreted from pineal gland, is a neuroprotective effect and plays a vital role in learning and memory. The objective of this study is to investigate protective effect of melatonin on alteration of tight junction that leads to cognitive impairment in hippocampus of diabetic rats. Male Wistar rats were divided into four groups: control, diabetes, melatonin-treated diabetic, and melatonin groups. For diabetic induction, rats were induced by streptozotocin via intraperitoneal injection at 60 mg/kg single dose. Then the rats received 10 mg/kg melatonin injection via intraperitoneal injection or vehicle for eight weeks. During the seventh week, Morris Water Maze test was evaluated cognitive function, and hippocampus was collected. Tight junction genes, claudin-5 and zonula occludens-1, were performed by real-time PCR. Expression of tight junction proteins presented co-localization of endothelial cells and tight junction proteins by immunofluorescence. The results of the Morris Water Maze revealed that diabetic group spent less time in the target quadrant compared to control group. However, melatonin-treated diabetic rats spent more time in the target quadrant. For the results of mRNA levels of tight junction was found that claudin-5 and zonula occludens-1 genes were significantly decreased in the diabetic group compared with the control group. Melatonin administration significantly upregulated these tight junction genes expression. At the same time, the co-localization of these proteins was consistent with the mRNA. Our findings indicate that melatonin can protect against diabetes-associated tight junction injury and promote cognitive function in the hippocampus.

Acknowledgement: This research was financially supported by the research grant of Faculty of Medicine (No. 267/2565), and The Graduate School (GRAD-S-3-67) of Srinakharinwirot University.

Keywords *Diabetes, Tight junction, Blood-brain barrier, Melatonin, Hippocampus*

O-10

Sensory lineage Maturation of Neural Stem Cells Derived from Stem Cells from Apical Papilla Undergo 3D-neurosphere Formation by Using Co-culture of Chick Embryo Dorsal Root Ganglion

Tarinee Chodchavanchai[1], Thanawit Juntamongkon[2], Phubase Chadaratthiti[2], Pukit Limyothin[2], Peeratchai Seemuang[3], Amarin Thongsuk[1], Tatcha Balit[4], Nisarat Ruangsawasdi[3], Charoensri Thonabulsombut[1], Anupong Thongklam Songsaad[5*]
[1] Department of Anatomy, Faculty of Science, Mahidol University, Bangkok, Thailand
[2] Mahidol International Dental School, Faculty of Dentistry, Mahidol University, Bangkok, Thailand
[3] Department of Pharmacology, Faculty of Dentistry, Mahidol University, Bangkok, Thailand
[4] School of Medicine, Walailak University, Nakhon Si Thammarat, Thailand
[5] Department of Anatomy, Faculty of Dentistry, Mahidol University, Bangkok, Thailand
*Corresponding author, e-mail: Anupong.son@mahidol.ac.th

Abstract

Sensory neuropathies are a specific subtype of the peripheral nervous system disease, characterized by degenerated of dorsal root ganglion (DRG), which effect to DRG (sensory)-neurons. Human stem cells from apical papilla (hSCAPs) established from apical papilla tissue of human third-molar teeth and shared the similarity origin with DRG-neurons, resulting in superior neuronal differentiation ability. Recently, hSCAPs were successfully induced into neural stem cells (NSCs-hSCAPs) under 3D-neurosphere formation. These NSCs-hSCAPs could differentiate into multilineage of neural cells under appropriate neurogenic maturation. During developmental processes, DRG presents sensory neurogenic niche that could be a beneficial for sensory lineage maturation. Therefore, this study aims to demonstrate neurogenic maturation of NSCs-hSCAPs and highlight the potential of using co-culture of chick embryonic-DRG to commit sensory lineage maturation. Firstly, 3D-Neurosphere was performed to generate NSCs-hSCAPs and characterized their stemness by self-renewal test and immunofluorescence staining (Nestin/SOX2). Consequently, these characterized NSCs-hSCAPs were performed neurogenic maturation by using 3 different culture condition including control medium, neurogenic maturation medium and co-culture with chick embryonic-DRG (E9). At neurogenic maturation day 7, the differentiated cells were characterized by cresyl violet staining, functional neuronal activity and immunofluorescence staining. These findings demonstrated that the NSCs-hSCAPs presented self-renewal ability and positively expressed Nestin/SOX2 to determine their early neuronal stage. Interestingly, the highest percentage of pseudounipolar neurons which revealed Nissl substance by Cresyl violet staining was observed in co-culture group. Furthermore, these neurons presented the dynamic change of Ca^{2+} to indicate their functional neuronal activity and positively expressed neurogenic-associated markers especially, Brn3a (a hallmark of sensory neurons) that showed the similarities profiling to chick embryonic DRG-neurons. Taken together, these findings suggested the beneficial neurogenic niche of chick embryonic-DRG to generate functional sensory neurons derived from NSCs-hSCAPs as the stem cell-based therapy for further treatment of sensory neuropathies.

Keywords *Chick embryonic dorsal root ganglion, Human stem cell from apical papilla, Neural stem cells, Sensory neurons*

O-11

A Multicentre Study on Umbilical Cord Morphometry In Preeclamptic Cases

Ajay Ningaiah[1*], Tejaswi H Lokanathan[2],
[1] Department of Anatomy, Faculty of Medical and Allied Health Sciences, Adichunchanagiri University, B G Nagara, Mandya District, Karnataka State, India
[2] Department of Anatomy, Faculty of Medical and Allied Health Sciences, Adichunchanagiri University, B G Nagara, Mandya District, Karnataka State, India
*Corresponding author, e-mail: ajay.ganalu@gmail.com

Abstract
Background: Pregnancy related hypertensive disorders contribute significantly towards maternal and perinatal morbidity and mortality rates. Preeclampsia and eclampsia form about 70% of the cases of PIH. Preeclampsia complicates 2 – 8% of all pregnancies worldwide; 10% in developing countries. The aim of the present study is to study the morphological and histological changes in the umbilical cord of pre-eclamptic women. **Objectives:** To measure the vessel wall thickness and luminal area of umbilical arteries and vein and to measure the total cord and Wharton Jelly area. **Methods:** This is a multicenter, observational, cross-sectional study involving 30 preeclamptic cases with gestational ages between 37 to 40 weeks. Tissue samples have undergone paraffin embedding, H&E staining, and measurement using a whole slide scanner by Morphle Labs. Ethical clearance has been obtained, and data entered into Excel sheets for analysis using SPSS software, with results presented as Mean ± Standard deviation. **Results:** The mean thickness of umbilical arteries is 481.21±142.69 µm, while that of the umbilical vein is 418.55±119.34 µm. The luminal area of umbilical arteries measures 0.32±0.18 mm^2, compared to 1.50±0.36 mm^2 for the vein. The total area of the umbilical cord is 61.743±11.139 mm^2, with Wharton's jelly occupying an area of 41.324±2.4 mm^2. **Conclusion:** Combining umbilical histomorphometry data with Doppler FVW radiological indices will enhance the understanding of preeclampsia and facilitate more effective treatment planning. This integration will advance the assessment of neonatal outcomes, thereby expanding the existing body of knowledge in this field.

Keywords *Umbilical cord, Histomorphometry, Umbilical artery, Umbilical vein, Preeclampsia*

O-12

Revisiting the Normal Anatomy of the Axillary Artery: A Systematic Review and Meta-Analysis

Kavin Tangmanpakdeepong[1], R. Shane Tubbs[2], Joe Iwanaga[2], Worawit Suphamungmee[3], Athikhun Suwannakhan[3*]
[1] Mahidol University International College, Mahidol University, Salaya, Nakhon Pathom, Thailand
[2] Tulane University School of Medicine, Tulane University, New Orleans, LA, USA
[3] Department of Anatomy, Faculty of Science, Mahidol University, Rama VI Road, Bangkok, Thailand
*Corresponding author, e-mail: athikhun.suw@mahidol.ac.th

Abstract

The axillary artery is among the most anatomically variable arteries in the human body. While traditionally described as having three parts — each giving rise to one, two, and three branches, respectively — this classification does not accurately reflect the anatomical variations observed in the general population. Despite longstanding recognition of these variations among anatomists, standard anatomy textbooks have not yet incorporated them. It is therefore necessary to redefine what constitutes normal anatomy of the axillary artery to better align with its true presentation. To address this, a systematic review was conducted to identify original studies reporting variations of axillary artery. PRISMA 2020 guideline was followed, and a risk-of-bias assessment was also performed using AQUA tool. Our results indicated four most commonly reported variations of the axillary artery, in 19 out of 35 studies, including (1) the posterior circumflex humeral artery originating from the subscapular artery (12.4%, 95% CI: 7.5–17.3%), (2) a common trunk of the posterior circumflex humeral and subscapular arteries (11.4%, 95% CI: 6.5–16.3%), (3) a common trunk of the anterior and posterior circumflex humeral arteries (14.5%, 95% CI: 9.2–19.9%), and (4) a common trunk of the lateral thoracic and subscapular arteries (9.6%, 95% CI: 3.3–15.8%). Given their consistent occurrence in the general population, we propose that these variations should be incorporated into anatomical education. Knowing these variations is also crucial for vascular surgery in the axilla region to reduce risks of intraoperative complications and avoid misidentification during angiographic procedures.

Keywords *Axillary artery; Anatomical variations; Systematic review; Meta-analysis*

O-13

Morphometric and Histological Analysis of Circle of Willis: Cadaveric Study

Jessy J P[1*], Sarah S Sangma[2], Arthi G[1], Saroj Kaler Jhajhria[1]
[1]Department of Anatomy, All India Institute of Medical Sciences, New Delhi, India
[2]Department of Anatomy, All India Institute of Medical Sciences, Gorakhpur, India
*Corresponding author, email: jesjp07@gmail.com

Abstract
Background: The Circle of Willis (CW), a network of anastomotic arteries situated at the base of the brain in the interpeduncular fossa, plays a crucial role in maintaining cerebral circulation via collateral pathways, redistributing blood flow, and preventing ischemia. Variations in CW are often linked to cerebral hemodynamics and vessel-related diseases; however, the precise etiology remains unclear. The diameter of these arteries directly influences blood flow volume, with proper CW function reliant on its completeness and the absence of hypoplastic vessels. **Objectives:** The present study examined variations in the branching pattern of CW, with the presence of hypoplastic vessels, and their histological characteristics. **Methods:** The CW and its branches were dissected in 35 cadaveric brains (cadavers obtained through the Voluntary Donation Programme), the variations in branching patterns were recorded and photographed. Vessel diameters were measured using a digital vernier caliper. Sections of arteries were taken and subjected to histological examination using Masson's Trichrome staining to assess structural changes. **Results**: The present study found a significant proportion of CW specimens exhibited anomalies (48.57%). Hypoplasia was the most common anomaly, followed by duplication (28.57%) of vessels. Morphometric data for CW vessels were recorded and tabulated. Histological analysis revealed structural changes in the tunica media of hypoplastic vessels. **Conclusion:** Variations in CW are believed to develop during early embryonic stages and are likely influenced by genetic factors. These anomalies persist postnatally and can impact the occurrence, severity of symptoms, treatment, and recovery from cerebrovascular disorders. Variations in communicating arteries have been associated with a higher incidence of conditions like migraines, schizophrenia, and cerebrovascular disorders due to compromised collateral circulation and reduced blood redistribution. Understanding these variations is crucial for surgical planning and minimizing the risk of inadvertent vascular trauma during interventional procedures.

Keywords *Anterior Cerebral Artery, Anterior Communicating Artery, Circle of Willis, Posterior Cerebral Artery, Posterior Communicating Artery*

O-14

Enhancing Anatomical Education Through Digital Learning: A Pilot Study of Innovative Online Interactive Course (Anatomy No Secret—Introduction to Human Anatomy) and Student Feedbacks

Keerakarn Somsuan[1,2], Pakakrong Panthanan[3], Chanatip Premvichai[1,2], Nilubon Singto[4], Arunothai Wanta[1,2], Adchara Junyoo[1], Aida Moohammadaree[1], Benjamard Sukjai[1], Dusit Staworn[1]
[1] School of Medicine, Mae Fah Luang University, Chiang Rai, 57100, Thailand
[2] Cancer and Immunology Research Unit (CIRU), Mae Fah Luang University, Chiang Rai, 57100, Thailand
[3] MFU Learning Innovation Institute, Mae Fah Luang University, Thailand
[4] Ramathibodi Comprehensive Cancer Center, Faculty of Medicine Ramathibodi Hospital, Mahidol University, Bangkok 10400, Thailand.
*Corresponding author, e-mail: keerakarn.som@mfu.ac.th

Abstract

The rapid growth of educational technology has transformed how complex subjects like human anatomy are taught. Anatomy No Secret—Introduction to Human Anatomy is an interactive online course designed to enhance learning through multimedia content, hands-on activities, and self-paced modules. This pilot study assessed its effectiveness among second-year students before its official launch. Forty voluntary medical and paramedical students participated, exploring five chapters that incorporated interactive elements such as card-based games, multiple-choice quizzes, terminology lists, and a voice dictionary. Students connected with instructors via email or Line, and after two weeks, they completed a questionnaire evaluating nine aspects, including instructor performance, course structure, media quality, and overall satisfaction. Results showed high ratings in instructor performance, self-learning promotion, and communication mechanisms (Score = 5.00, excellence). Students particularly enjoyed the engaging visuals and the course's flexibility, which helped boost their understanding and motivation. However, they suggested improvements like diversifying assessments, providing additional study materials, and addressing technical issues such as data loss when refreshing the browser. Overall, Anatomy No Secret proved to be a highly effective learning tool. Students found it relevant, practical, and beneficial for their studies. These insights will help refine the course further to maximize its educational impact.

Keywords *Anatomy education, Interactive course, Educational technology, Student feedback*

O-15

Sex Estimation Using Acetabulum Digital Image Processing in Thai Population

Phasinee Winyawong[1], Tawachai Monum[2], Padchanee Sangthong[3], Sukon Prasitwattanaseree[4], Pagorn Navic[5], Pasuk Mahakkanukrauh[6]*
[1] Master's degree in forensic science Multidisciplinary and Interdisciplinary School, Chiang Mai University, Chiang Mai 50200 Thailand
[2] Department of Forensic Medicine, Faculty of Medicine, Chiang Mai University, Chiang Mai 50200 Thailand
[3] Department of Chemistry, Faculty of Science, Chiang Mai University, Chiang Mai 50200 Thailand
[4] Department of Statistics, Faculty of Science, Chiang Mai University, Chiang Mai 50200 Thailand
[5] Department of Anatomy, Faculty of Medicine, Chiang Mai University, Chiang Mai 50200 Thailand
[6] Department of Anatomy, Excellence center of osteology research and training, Cadaveric surgical and training center, Faculty of Medicine, Chiang Mai University, Chiang Mai 50200 Thailand
*Corresponding author, e-mail: pasuk034@gmail.com

Abstract

Forensic anthropologists play a vital role in human identification, with sex estimation being a key component of biological profile analysis. The acetabulum is widely recognized as a reliable skeletal indication due to its distinct sexual dimorphism. While studies have demonstrated its effectiveness in different populations, limited research has been conducted on the Thai population. This study aims to analyze acetabular size differences between sexes using digital image processing to improve accuracy and efficiency. A total of 240 skeletal samples (122 males, 118 females) were obtained from body donors at Chiang Mai University. Digital images of the acetabulum were captured using a DSLR camera under standardized conditions. The lunate surface area was measured using ImageJ software, and statistical analyses were conducted using SPSS to assess sex differences and classification accuracy. The analysis indicated a statistically significant difference in lunate surface between sexes ($p < 0.001$), with males exhibiting a larger surface. The logistic regression model achieved an 87.5% accuracy in sex classification. This study found that the lunate surface of the acetabulum demonstrates significant sexual dimorphism and can be effectively utilized for sex estimation. The high accuracy rate highlights the potential of digital image processing in forensic anthropology, providing a valuable tool for biological profile reconstruction and personal identification within Thailand's population.

Keywords *Forensic science, Acetabulum, Sex estimation, Digital Image Processing*

Background

Forensic anthropologists are faced with the important responsibility of identifying individuals, and determining sex is a crucial aspect of constructing a biological profile. analysis. The analysis consists of skeletal characteristics and dimensions that indicate sexual dimorphism. Additionally, sex estimation aids in narrowing the parameters and facilitating comparisons with antemortem records of missing persons (1). The pelvis (2), acetabulum (3), skull (4), and vertebrae (5) are the most widely used for sex estimation. The study by Phenice et al (2). examined the morphological characteristics of the pelvis at three specific locations, obtaining an accuracy rate of 96.00% in sex estimation. Subsequently, the study by Wangdee et al (6). analyzed the pelvis of a Thai population, including 11 morphological variables for sex estimation. The findings indicated an accuracy rate ranging from 72.5% to 98.7%. Sex estimation methods have been refined through metric analysis to enhance reliability and objectivity. A study by Bubalo et al (7). examined 200 pelvic samples from a Croatian population, measuring two acetabular variables. The results demonstrated that the acetabulum could be used for sex estimation with an accuracy of 87% to 88%. Only two dimensions to analyze acetabular size differences have shown high accuracy in sex estimation. Therefore, similar methodologies should be applied to study acetabular size variations in other populations. However, the acetabulum has not been extensively investigated for this purpose, even though using the pelvis for sex estimation has been applied to the Thai population. Sex estimation may be inaccurate due to variations in the

morphology of the acetabulum among individuals. Statistical analysis is frequently used as a reference to reduce these individual differences and improve the reliability of assessments (8). This study integrated image processing techniques into the analysis to improve accuracy, facilitate practical application, and reduce observer-related errors. One widely accessible and commonly used software for image analysis is ImageJ, which has been downloaded over 80,000 times and is available free of charge. ImageJ is designed to analyze object proportions and areas within images, measuring them in pixels or other standard units. Additionally, it can be used to measure lengths and image density, allowing for further statistical analysis and visualization through bar charts or other graphical representations. A study by Krudtong and Mahakkanukrauh (9). utilized the acetabular fossa for age estimation by applying image processing to analyze colour variations associated with bone porosity across different age groups. The findings indicated no correlation between bone porosity and age in females, while a weak correlation was observed in males (R^2 = 0.2442). The study suggested that two-dimensional imaging techniques might have contributed to discrepancies in colour values, leading to challenges in precise age estimation.

Previous studies focused on age range (9). Therefore, this study aims to analyze the differences in acetabular size between sexes using computational software to enhance the accuracy and efficiency of the analysis in Thais.

Materials and Methods

The skeletal samples used in this study were collected from body donors through the Department of Anatomy at the Osteology Research and Training Center (ORTC), Faculty of Medicine, Chiang Mai University. The selection process focused on acetabular bones from males and females aged between 26 and 95 years old. Data were collected from 240 skeletal samples (122 males and 118 females). The inclusion criteria for the study were as follows: the remaining skeletons belonged to individuals of Thai ethnicity, the actual age at the time of death was documented, the acetabulum exhibited no structural damage and remained intact, allowing for morphological assessment (e.g., no fractures or other bone deterioration and no pathological changes or disease-related alterations were observed in the acetabular region during the individual's lifetime). The acetabular were photographed using a digital single-lens reflex (DSLR) camera with the following settings: ISO auto, F 4.0, and shutter speed 1/80. The acetabulum was photographed using a digital camera, with the pelvic bone positioned on a box. The posterior superior iliac spine (PSIS) was oriented downward, while the acetabulum faced upward. The bone was adjusted so that the superior border of the greater sciatic notch extended beyond the upper edge of the supporting box, ensuring that the acetabulum was parallel to the camera lens. A levelling ruler was used as a reference to confirm that the acetabular fossa remained parallel to the camera lens. Measurement of the area was taken the ImageJ program by selecting the region of interest (ROI).

This study focuses on analyzing the size of the lunate surface (Fig.1), which is a peripheral, horseshoe-shaped region within the acetabulum between males and females. The obtained area measurements were analyzed using correlation analysis in SPSS software. The analysis involved statistical methods to assess the relationship between lunate surface area and sex, providing insights into any significant variations between the two groups.

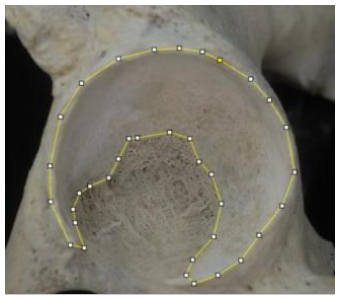

Fig.1 Selected area of lunate surface

Results and Discussion

Analysis of the lunate area revealed a normal distribution, as indicated by the Kolmogorov-Smirnov test, with a p-value > 0.05 for the female sample. Conversely, the male sample yeilded a p-value < 0.05. The analysis results indicated a non-normal distribution of the data. Therefore, the

Table 1 Descriptive and Mann-Whitney U test of lunate surface area

	Mean (cm^2)	Std.	Mann-Whitney U	Z	Sig
Female	13.15	1.82	1117.50	-11.308	<0.001
Male	16.91	1.99			

Mann-Whitney U test was used to assess the differences in the lunate surface between sexes. The descriptive statistical values showed that the mean acetabular area for females is 13.15 cm^2, while for males, it is 16.91 cm^2, as shown in Table 1.

Previous studies, such as that of Phenice et al (2), utilized the pelvis for sex estimation, showing significant differences in the morphological features of the pelvic bones between males and females. Additional studies have explored other characteristics. The acetabulum is a structurally robust and durable region, resistant to post-depositional processing (10). For instance, Bubalo et al (7) demonstrated that the size of the acetabulum is significantly greater in males relative to females. In the present study of the lunate surface, a component of the acetabulum, was examined and revealed significant area differences between males and females. Additionally, the mean rank values indicate that the acetabular area is larger in the male group compared to the female group. Furthermore, the acetabular area shows a statistically significant difference between females and males (p-value < 0.001). This finding suggests that acetabular area can be effectively used for sex classification.

As shown in Table 2, the equation for sex classification based on area of lunate surface is provided. The equation demonstrates.

Table 2 Logistic regression for sex estimation by using area of lunate surface

	Coefficient	Constant	Cut off
Area	1.083	-16.189	0.5

$$\text{Probability (P)} = \frac{1}{1+e^{-(1.083 \times \text{Area} - 16.189)}}$$

The probability value represents the likelihood of an event occurring, ranging from 0 to 1. In this study, a cutoff value of 0.5 was set for classification. By a cutoff threshold of 0.5, The probability of the individual being female is determined using the equation, where if the calculated P for the area is below 0.5, the sample is classified as female. In contrast, if the P is above 0.5, it is classified as male, and this study revealed accuracy 87.5% for sex estimation. Therefore, this equation can be effectively utilized for sex classification based on area of lunate surface. As illustrated in Table 3, the overall accuracy of the data is 87.5%, with female samples an accuracy of 85.6% and male samples an accuracy of 89.3%. These results indicate that the data can be reliably analyzed, demonstrating a high level of accuracy in the classification process. According to the study by Warrier (11), machine learning methods were used to estimate sex based on acetabular size, achieving an accuracy range of 83-89%. This study suggests that the acetabulum can be used for sex classification, whether using direct measurements or not, though some cases may not yield clear separation. Additionally, the study by Bubalo (7) on the acetabular size in the Croatian population demonstrated its effectiveness for sex differentiation, with an accuracy rate of up to 88%. These findings highlight that the acetabulum can be a reliable feature for sex estimation, providing high accuracy. In the study by Sangchay et al.,(12) digital images were utilized to analyze the pelvic bones, focusing on the anterior and posterior borders of the ilium at 28 parameters, for sex estimation within a Thai population. The accuracy of sex determination across all ten discriminant functions varied from 67.07% to 89.46%. Conversely, a study by Cao et al. (13). utilized AI or CNNs for sex classification and found that the ventral pubis (VP), dorsal pubis (DP), greater sciatic notch (GSN), and the pelvic inlet achieved an accuracy of over 90%. In contrast, the ischium and acetabulum regions demonstrated accuracy rates of 83% and 75%, respectively. Moreover, the study by Mahakkanukrauh et al (14). examined the coxal bone for estimating sex in the Thai population, yielding an accuracy between 89% and 95%. This high accuracy is attributed to the coxal bone's sexual dimorphism. Furthermore, a study by Intasuwan et al (15) assessed sex estimation using three techniques: dry bone morphology, 2D photographic morphometry, and deep learning artificial neural networks. The focus of the study was on the greater sciatic notch of the os coxae in a Thai population, with accuracy rates for each method being 80.65%, 90.3%, and 91.95%, respectively. It seems to highlight that photographs play a crucial role in assisting forensic identification across various forensic science contexts. High-quality images provide detailed visual records that can be reviewed, compared, and preserved for further analysis, ensuring that critical information is not lost. One of the practical tools in forensic disciplines is the DSLR camera. DSLR cameras

Table 3 Classification rate for sex estimation

Sex	Female	Male	Percentage Correct
Female	101	17	85.6
Male	13	109	89.3
Percentage Correct	87.5		

offer superior resolution, better control over lighting conditions, and reduced image distortion compared to smartphone cameras (16). Their adjustable settings, such as aperture, shutter speed, and ISO, allow practitioners to optimize image clarity and depth of field, ensuring that fine anatomical details of the acetabulum are preserved for accurate analysis. Therefore, this study chose a DSLR camera to ensure high-quality imaging for the analysis of the acetabulum. Moreover, these findings highlight that 2D morphometry and AI methods resulted in accuracy rates of around 90-92%. Based on the examined studies, the pelvic bones have been found to achieve up to 90% accuracy in sex estimation across various populations. Furthermore, assessments of the acetabulum, a part of the pelvis, have shown an accuracy of about 80% in sex determination. Due to its structural durability and common preservation in skeletal remains (17), the acetabulum can be considered a dependable anatomical feature for sex estimation in forensic science.

Conclusion

This research revealed that the lunate surface area of the pelvic bone shows significant variation between males and females. Additionally, the area of the lunate surface serves as a reliable metric for sex estimation, efficiently differentiating between the sexes. The present analysis yielded an accuracy rate of up to 87.5% in sex classification. Therefore, utilizing the lunate surface for sex estimation can serve as a valuable tool in forensic science, contributing to biological profile reconstruction and personal identification.

Acknowledgements

The authors express their gratitude to the Faculty of Medicine and the Excellence in Osteology Research and Training Center (ORTC) at Chiang Mai University for their support of this project.

References

1. Spradley MK. Metric Methods for the Biological Profile in Forensic Anthropology: Sex, Ancestry, and Stature. Acad Forensic Pathol. 2016;6(3):391-9.
2. Phenice TW. A Newly Developed Visual Method of Sexing The Os Pubis. American Journal of Physical Anthropology. 1969;30(2):297-301.
3. Bağcı Uzun G, Değermenci M, Uçar İ, Arslan A, Nisari M. Morphometrıc Evaluatıon of Acetabulum. Journal of Surgery and Medicine. 2020;4(7):555-7.
4. Ramsthaler F, Kreutz K, Verhoff MA. Accuracy of Metric Sex Analysis of Skeletal Remains Using Fordisc® Based on A Recent Skull Collection. International Journal of Legal Medicine. 2007;121(6):477-82.
5. Garoufi N, Bertsatos A, Chovalopoulou M-E, Villa C. Forensic Sex Estimation Using the Vertebrae: an Evaluation on Two European Populations. International Journal of Legal Medicine. 2020;134(6):2307-18.
6. Wangdee A, Thipdet W, Prasitwattanaseree S, Singsuwan P, Mahakkanukrauh P, editors. Efficiency of Sex Determination by Using External Morphology of the Pelvis in Thai Population2014.
7. Bubalo P Fau - Baković M, Baković M, Tkalčić M Fau - Petrovečki V, Petrovečki V Fau - Mayer D, Mayer D. Acetabular Osteometric Standards for Sex Estimation in Contemporary Croatian Population. 2019(1332-8166 (Electronic)).
8. Caliskan A. Artificial Intelligence, Bias, and Ethics2023. 7007-13 p.
9. Krudtong S. and Mahakkanukrauh P. , Age Estimation from Acetabulum Using Digital Image Processing Techniques in Thai Population, 2024 9th International STEM Education Conference (iSTEM-Ed), Cha-am, Hua Hin, Thailand, 2024, pp. 1-3.
10. San-Millán M, Rissech C, Turbón D. New Approach to Age Estimation of Male and Female Adult Skeletons Based on the Morphological Characteristics of the Acetabulum. International Journal of Legal Medicine. 2017;131(2):501-25.
11. Warrier V, San-Millán M. A Statistical Evaluation of the Sexual Dimorphism of the Acetabulum in An Iberian Population. International Journal of Legal Medicine. 2025;139(1):393-409.
12. Sangchay N, Dzetkuličová V, Zuppello M, Chetsawang J. Consideration of Accuracy and Observational Error Analysis in Pelvic Sex Assessment: A Study in a Thai Cadaveric Human Population. Siriraj Medical Journal. 2022;74(5):330-9.
13. Cao Y, Ma Y, Yang X, Xiong J, Wang Y, Zhang J, et al. Use of Deep Learning in Forensic Sex Estimation of Virtual Pelvic Models from the Han Population. Forensic Sciences Research. 2022;7(3):540-9.
14. Mahakkanukrauh P, Ruengdit S, Tun SM, Case DT, Sinthubua A. Osteometric Sex Estimation from the Os Coxa in a Thai Population. Forensic Science International. 2017;271:127.e1-.e7.
15. Intasuwan P, Palee P, Sinthubua A, Mahakkanukrauh P. Comparison of Sex Determination Using Three Methods Applied to the Greater Sciatic Notch of Os Coxae in a Thai Population: Dry Bone Morphology, 2-Dimensional Photograph Morphometry, and Deep Learning Artificial Neural Network. Medicine, Science and the Law. 2022;62(4):261-8.

16. Healy SS, Stephan CN. Focus Distance Estimation from Photographed Faces: a Test of PerspectiveX Using 1709 Frontal and Profile Photographs from DSLR and Smartphone Cameras. International Journal of Legal Medicine. 2023;137(6):1907-20.

17. Rissech C, Estabrook GF, Cunha E, Malgosa A. Using the Acetabulum to Estimate Age at Death of Adult Males. Journal of Forensic Sciences. 2006;51(2):213-29.

O-16

Schematics and Comics in a Regional Anatomy Book

Min Suk Chung*
Department of Anatomy, Ajou University School of Medicine, 164 World cup-ro, Suwon, 16499, Republic of Korea
*Corresponding author, e-mail: dissect@ajou.ac.kr

Abstract

The author has created the board lecture rather than the slide lecture; no artistic talent results in schematics, which makes it easy to explain the human body. The schematics motivated the author to draw comics containing mnemonics and humors of anatomy. A regional anatomy book was also elaborated with full of schematics and comics to make regional anatomy easy and more comfortable. Such application of schematics and comics is disclosed to suggest other anatomists to create their own schematics and comics. This book contained 374 schematics and 242 comics. As the schematics, the muscles are drawn as arrows; the cavernous sinus and tympanic cavity are drawn as opened boxes; the pericardium, pleura, peritoneum are drawn as simple balloons. The comics deal with mnemonics of anatomical issues including surface anatomy, meanings of anatomical structures, and humors of anatomy. To assess the book's learning effects, medical students in Korea were invited to volunteer after explanation. Students who read the regional anatomy book have remarked on the strong and weak points of schematics. A strong point is that students can redraw the schematics to enhance the memorization; a weak point is that two-dimensional figures are too simple for students to get the real morphology. For comics, a strong point is that intermittent humors relieve the boredom. The regional anatomy book (converted into PDF file) is obtainable (anatomy.co.kr) without any payment or registration. Every anatomist can draw one's own schematics and comics to create extraordinary learning materials, which will contribute to anatomy education.

Keywords *Artistic anatomy, Cartoons, Humor, Medical education, Questionnaires*

O-17

Transforming Anatomy Education: The 'Skull Master' Application in Teaching Head and Facial Bones to Dental Students

Aina Vaiyasilpa[1], Achiraya Khoonphithaksakun[1], On-anong Kawa[2], Punnapa Pramotekul[3], Atthaboon Watthammawut[1], Worakamol Kuanpradit[4], Sumon Jungudomjareon[1] and Chitraporn Kuanpradit[1]*
[1] Department of Anatomy, Faculty of Medicine, Srinakharinwirot University, Wattana, Bangkok, Thailand
[2] Faculty of Engineering Srinakharinwirot University, Bangkok Thailand
[3]Faculty of Engineering, Kasetsart University, Bangkok Thailand
[4]Faculty of Humanity, Srinakharinwirot University, Bangkok Thailand
*Corresponding author, e-mail: chitraporn@g.swu.ac.th

Abstract
Background: Understanding the anatomy of the head and face, particularly the oral cavity, is essential for dental students. Each academic year, 60 students had access to only 6 plastic skulls for group study, while real human bones in the museum provided an opportunity for self-directed learning. Challenges identified included: 1) Limited access to real skulls; 2) limited visualizing the realistic textures and anatomical detail; 3) Inadequate models for visualizing cranial nerves and blood vessels; 4) Unengaging traditional methods; and 5) Insufficient self-directed study tools. To address these issues, we developed a web-based game application with 3D models of the cranial fossa. ***Materials and Methods:*** Specimens such as plastic models of skull, facial bones, and brains were selected and mounted on a rotating support with a light studio. Multiple scans were taken in layers, followed by 3D model generation, texturization, and optimization of lighting and shadowing. The models were uploaded to Sketchfab for labeling. Interactive games were incorporated, including a brain image and name-matching game and a flashcard quiz. The application was developed using HTML, CSS, and JavaScript to ensure accessibility and interactivity.
Results: The 3D resources enhance visualization of the cranial fossae and cranial nerves (CNI–CNXII) utilization, shown to significantly improve students' anatomy comprehension, as evidenced by student's comments and suggestions in the regular course evaluation. ***Conclusion:*** In the future plan, this project will be developed by using real human specimens after the ethical certificate is obtained. This 3D content will serve not only dental students but also medical students, facilitating broader anatomy education. Furthermore, it can be integrated with other tools to advance 3D anatomy applications in the future.

Keywords *Web-based 3D model, 3D anatomy game, 3D cadaveric dissection, face bone, Base of skull*

O-18

The Use of Free Radical Polymerization in Plastination of Swine Organs: Poly (Butyl Methacrylate) and poly (2-Ethylhexyl Methacrylate)

Duy Hoang[1*], Ky Nguyen[1], Roshan Peiris[1,2], Duy Tran[1], Thuong Le[1,3], Chineney Susan Ekwebelem[1], Tu Ha[1], Chien Huynh[1]
[1] College of Health Sciences, VinUniversity, Hanoi, Vietnam
[2] Department of Basic Sciences, Faculty of Dental Sciences, University of Peradeniya, Peradeniya, Sri Lanka
[3] Department of Human Anatomy, Hanoi Medical University, Hanoi, Vietnam
*Corresponding author, e-mail: duy.hm@vinuni.edu.vn

Abstract
Introduction: Plastination is a superior method of preserving biological specimens for anatomy teaching and research developed by Dr. Gunther von Hagen in 1977. It offers durable and long-lasting plastinated specimens while keeping their natural appearances. This method works by removing the water and lipids of the specimens with a volatile, water-miscible solvent, followed by an exchange of the solvent with a curable prepolymer mixture. The resulting plastinates are highly durable, robust, odour-free, and non-toxic. **Objectives:** This research aims to develop plastination methods that employ commercially available chemicals and instruments yet could produce comparative results at lower costs to other plastination methods based on free radical polymerization. **Methods:** Swine organs including hearts, lungs, kidneys, and brains were attempted to plastinate. The fresh organs were fixed in 5% formalin at 4 ºC for 6 – 12 days, washed with tap water for 18 hours, dehydrated in three baths of acetone at -25 ºC for 3 – 5 days per bath, and degreased in cetone for 1 hour at room temperature. The forced impregnation step was performed by immersing the organs in prepolymer mixtures composed of either Butyl methacrylate or 2-Ethylhexyl methacrylate and Azobisisobutyronitrile at 4 ºC while decreasing pressure from 760 mmHg to 5 mmHg over 2 days. The organs were then cured under Argon at room temperature, 35 ºC, 45 ºC, and 50 ºC until completion. **Results:** All samples were successfully plastinated with minimal volume shrinkage and shape distortion while preserving their macroscopic anatomy. Their anatomical features, colours, and physical durability were satisfactory. **Conclusions:** These findings paved a more affordable route to plastination and allowed many institutions, especially those from low-income and lower-middle-income countries, to adopt the technique.

Keywords *Plastination, Free radical polymerization, Anatomy, Medical education*

POSTER PRESENTATION

P-01

Effect of Mulberry Fruit on Lung Histopathology in High-Fat Diet Induced Dyslipidemic Rats: Preliminary Data

Wittawat Tajai[1,2], Nutthakamon Seetim[1], Sujira Seesin[1], Chalisa Suwannasorn[1], Saowalak Rungruang[2],Chakriya Promsuban[1], Apichaya Niyomchan[3], Piyanee Sriya[4], Hiroki Nakata[5], Wai Chen[6,7], Kroekkiat Chinda[2,8,9], Kannika Adthapanyawanich[1,2,9], and Yutthapong Tongpob[1,2,9*]
[1]Department of Anatomy, Faculty of Medical Science, Naresuan University (NU), Thailand
[2] Integrative Cardiovascular Research Unit, Faculty of Medical Science, NU, Thailand
[3] Department of Anatomy, Faculty of Medicine Siriraj Hospital, Mahidol University, Thailand
[4] Phramongkutklao College of Medicine: Rachathevi, Bangkok, Thailand
[5] Department of Clinical Engineering, Faculty of Health Sciences, Komatsu University, Japan
[6] Fiona Stanley Hospital, Perth, Australia
[7] Curtin Medical School, and Curtin enable Institute, Curtin University, Perth, Australia
[8] Department of Physiology, Faculty of Medical Science, NU, Thailand
[9] Centre of Excellence in Medical Biotechnology (CEMB), Faculty of Medical Science, NU, Thailand
*Corresponding author, e-mail: yutthapongt@nu.ac.th

Abstract
Introduction: Dyslipidemia-induced systemic inflammation has been demonstrated to augment the risk of pulmonary complications. Mulberry fruit contains anthocyanins with known anti-inflammatory properties, but its effects on lung tissue in dyslipidemia remain unclear. **Objective**: To examine the impact of crude mulberry fruit extract on lung histopathology in high-fat diet-induced dyslipidemic rats. **Methods:** Twenty-four male Wistar rats were divided into 4 groups (n=6/group): (1) normal diet (ND); (2) high-fat diet (HFD); (3) HFD+crude extract of mulberry fruit (CEM) 100 mg/kg/day; and (4) HFD+atorvastatin (ATV) 10 mg/kg/day. After 90 days of treatment, body weight and lung weight were recorded, and blood lipid profiles were analyzed. Lung tissues were then examined histopathologically using hematoxylin and eosin and Masson's trichrome staining. All parameters were analyzed using one-way ANOVA with post-hoc Tukey test. $P<0.05$ was considered statistically significant. **Results:** Body weight and relative lung weight were comparable between groups. HFD significantly increased total cholesterol and LDL-C levels compared to ND ($P<0.001$). CEM treatment significantly reduced both total cholesterol ($P<0.001$) and LDL-C ($P<0.01$) compared to HFD, similar to atorvastatin's effects. Histopathological examination with H&E staining revealed infiltration of inflammatory cells in the HFD group, while both HFD+CEM and HFD+ATV groups showed reduced inflammatory cell infiltration. Masson's trichrome staining demonstrated increased collagen fiber thickness in all HFD-fed groups (HFD, HFD+CEM, and HFD+ATV) compared to the ND group. **Conclusion:** While crude mulberry fruit extract improves dyslipidemia and reduces lung inflammation similar to atorvastatin, it does not appear to prevent collagen deposition in lung tissue. These findings suggest that mulberry fruit may offer partial protective benefits against pulmonary complications of dyslipidemia through anti-inflammatory mechanisms, but further studies are needed to address fibrotic changes and investigate underlying molecular pathways.

Keywords *Dyslipidemia, Mulberry fruit, Anthocyanins, Lung histopathology*

P-02

The Influence of Follicular Fluid from Different-Sized Pig Oocytes on HepG2 Cell Line Viability

Nongnuch Gumlungpat[1*], Mayuva Youngsabanat [1*],Thanaporn Chuen-im[2], Maijukkee Areekijseree [3], Theerapat Santanaprasit[3], Sukjai Rattanayuvakorn [4]
[1] Department of Biology, Faculty of Science, Silpakorn University
[2] Department of Microbiology, Faculty of Science, Silpakorn University
[3] Department of Mechanical Engineering, Faculty of Engineering, King Mongkut's University of Technology Thonburi
[4] Department of Science and Mathematics, Faculty of Agriculture and Technology, Rajamangala University of Technology Isan, Surin Campus
*Corresponding author, e-mail: gumlungpat_n@su.ac.th, maijackee@hotmail.com

Abstract

This study used protein from porcine follicular fluid (pFF) to culture HepG2 cells to investigate its effects on cell viability. Because pFF contains components that may be beneficial to in vitro cell growth. The experiment study growth and development of HepG2 (support from Korean Cell Line Bank, Seoul Korea) by a pig follicular fluid protein (from a standard slaughterhouse at Nakorn-Pathom Province) supplement at concentrations of 2, 4, 20, 40, 200, 400, 500, and 600 µg protein/mL on HepG2 cell line. The results showed that all the fluid protein concentrations used to test the small and medium-sized follicles had a percentage of live HepG2 cells that were higher than the control group. The percentage of live cells in all concentrations of small-sized follicles (1-3 mm in diameter) were 108.871±4.484, 112.7±4.9, 122.421±1.838, 119.079±5.226, 113.247±4.144, 112.154±5.996, 117.005±7.207 and 104.343±3.696 respectively. Which were higher than the control group and non-statistic significant ($p>0.05$), except at concentrations 20, 40 and 500 protein/mL. All of fluid protein concentrations used to test in the medium-sized follicles had a percentage of live are lower than the positive control group (127.076±6.503) and non-statistic significant ($p<0.05$). While the percentage of live HepG2 cells used to test the medium-sized follicle (4-6 mm in diameter) in all concentrations were 104.621±6.936, 109.706±7.147, 116.384±9.486, 121.202±7.807, 123.54±9.678, 103.601±10.559, 102.861±6.247 and 106.249±6.894, respectively and non-significantly higher than the control group, except at concentrations 40 and 200 µg proteins/mL. All of fluid protein concentrations used to test had a percentage of live are lower than the positive control group and non-statistic significant. The cell morphology of those cultured in pFF from the 2-sized follicles remained normal in all concentration. From the results of this study, it was concluded that, small-sized pFF concentrations at 20, 40 and 500 µg proteins/mL and medium-sized pFF at concentrations 40 and 200 µg proteins/mL could promoting the growth of cell lines in the laboratory similar to the group supplemented with heat treated fetal calf serum (HTFBS). It can use this data results from research to be applied in various cancer cell cultures in the laboratory.

Keywords *HepG2, in vitro culture, porcine follicular fluid, MTT assay*

Background

The aims of this project were to study the benefits of pig follicular fluid (pFF) of pig follicular, This province has many pig farms and there are many pig slaughterhouses around the university. The researchers are interested in the sterile collection of fluid from the ovaries of dead pigs for application of biotechnology and innovations that promote cell line development for creating biotechnology work in new and innovative ways. The importance of pig follicular fluid contains cell coatings secreted from follicular cells. It was found that the protein band from SDS-PAGE analyzed influenced promoting the breakdown of the nucleus membranes of oocytes, which promoted oocyte maturation and played a role in ovulation stimulation (Ducolomb et. al., 2013; Youngsabanant-Areekijseree et. al., 2019; Youngsabanant et. al., 2019). Moreover, investigation of pig follicular fluid revealed various compositions (Youngsabanant and Mettasart, 2020.

These included 1) hormones e.g., FSH, LH, estrogen, progesterone 2) sugars, hyaluronan 3) growth factors of the Transforming Growth Factor-beta (TGF-beta) superfamily; 4) other growth factors and interleukins; 5) Reactive Oxygen Species (ROS); 6) anti-apoptotic factors; 7) proteins, peptides and amino-acids; 8) anti-apoptotic factors; 9) prostanoids. So,
the components of pFF such as FSH, LH, estrogen, progesterone, growth factors of the Transforming Growth Factor-beta (TGF-beta) superfamily, interleukins may affect HepG2 cell growth in culture media. For hyaluronan (HA), it formed extracellular matrix covering cumulus cells. Increasing of hyaluronic acid were observed when follicular cells were induced by FSH to support completion of oocyte development, leading into expansion of cumulus cell in cumulus cell-oocyte complexes (COCs). Detection of mRNA of hyaluronan synthase 2 (has2) and CD44 in cumulus cells, and hyaluronan synthase 3 (has3) in oocytes implied that these cells may function in synthesis and secrete the proteins into follicular fluid.

There are some studies reported that pig follicular fluid influenced the development of HeLa and Vero cell lines. It was found that to promote the development of cell lines and cancer cell lines (Youngsabanant., et. al., 2019; Youngsabanant and Rabiab, 2020). Therefore, in this research the researchers focused on testing the exudate from pig follicular of various sizes to determine the growth of HepG2, which was shown to be effective in the laboratory. On the selection of fluid secretions from two different follicle sizes of and efficacy with biotechnology applications. The research could provide knowledge useful for selecting the optimal concentration of pFF from follicles of different sizes for future use in cell culture. Porcine follicular fluid (unvaluable from slaughter house) can be applied instead of fetal bovine serum (which expensive and trade deficit). The responses to specific cells still vary and need to be further researched. This research can help in other relevant cell cultures in the laboratory in the future.

Materials and Methods

Culture Medium: Dulbecco's Modified Eagle Medium **(**DMEM) with 10% heat treated fetal calf serum (HTFBS) and culture for 12 h before use, at 37ºC, high humidity, with 5% CO_2 in 95% air atmosphere.

Animal: Pubertal pig ovaries from pigs (aged between 210 and 250 days) were collected from a standard slaughterhouse at Nakorn-Pathom Province using the method of Areekijseree (Areekijseree and Vejaratpimol, R. (2006). Pongsawat and Youngsabanant., 2019).

Pig follicular fluid collection: Pig ovaries were removed within 30 ms after being slaughtered and then transported to a laboratory in a thermos container at a temperature of 30-35°C. Pig follicular fluid was collected from n npubertal pig ovarian follicles of two sizes: small-size follicles (1-3 mm in diameter) and medium-size follicles (4-6 mm in diameter) by using a syringe connected to an 18-gauge needle. Then, fluid was collected in a conical tube and centrifuged for 5 ms at 1500 x *g* to remove oocytes and cells. Pig follicular fluid was stored at -80°C until use. Protein quantification was carried out using the Lowry method (Lowry et al., 1951) to calculate the protein concentrations of pig follicular fluid from three sizes of ovarian follicles to supplement the culture medium.

HepG2 cancer cell line culture: HepG2 cancer cell lines (support from Korean Cell Line Bank, Seoul Korea) were cultured in DMEM with 10% HTFBS, at 37°C, in high humidity, in a 5% carbon dioxide and 95% air atmosphere, at 37°C before experiments were performed. The separated cells were seeded in culture medium at 5×10^5 cells/mL at 37°C, in a 5% carbon dioxide and 95% air atmosphere, in high humidity, for 48 h.

Experimental design: Pig follicular fluids from small and medium-sized ovarian follicles were cultured in vitro with HepG2 cancer cell lines in an experimental design consisting of three groups, in six trials. Group 1: The control group consisted of HepG2 cancer cell lines cultured in DMEM. Group 2: The positive control group comprised HepG2 cancer cell lines cultured in DMEM and 10% HTBFS. Group 3: The treatment group consisted of 2, 4, 20, 40, 200, 400, 500, and 600 µg protein/mL of pFF extracted from small-, medium-, and large-sized ovarian follicles, all of which were in vitro cultured in HepG2 cancer cell lines for 24 hr. before using the MTT assay to determine the number of viable cells present.

MTT assay and cell morphological study: HepG2 cancer cell line lines were seeded in a 96-well plate at 20,000 cells/well for 48 h. before treatment with pFF from three sizes of ovarian follicles at concentrations of 2, 4, 20, 40, 200, 400, 500, and 600 µg proteins/mL for 24 h.. After incubation, they were incubated with tetrazolium salt for 4 h, and cell viability was quantified by detecting formazan dye crystal formation with a spectrophotometer at 570 nm. Meanwhile, cell morphology was observed during the culture period and after treatment with pFF under an inverted microscope.

Statistical analysis: Effects of pFF on HepG2 viability were determined using MTT assay. Then, differences of cell viability between pFF treatments, control, and positive control were analyzed by one-way ANOVA and post hoc Duncan. Significant differences of cell viability were considered when $P<0.05$.

Results and Discussion

The results showed the morphology of HepG2 cancer cell line from inverted microscopy before MTT assay at 0 h of culture, the cells were oval shaped. At 24 h of culture, the cells were a fusiform shape with approximately 50% adherence with the culture plate. After culture for 48 h, the HepG2 cancer cells were a fusiform shape, with approximately 90 percent adherence with the culture plate and oval shape about 10 percent before MTT assay (Fig. 1). The results from MTT assay in six trials showed that, all the fluid protein concentrations used to test the small and medium-sized follicles had a percentage of live HepG2 cells that were higher than the control group. The percentage of live cells in all concentrations of small-sized follicles were 108.871±4.484, 112.7±4.9, 122.421±1.838, 119.079±5.226, 113.247±4.144, 112.154±5.996, 117.005±7.207 and 104.343±3.696 respectively (Fig. 2). Which were higher than the control group and non-statistic significant ($p>0.05$), except at concentrations 20, 40 and 500 protein/mL. All of fluid protein concentrations used to test in the medium-sized follicles had a percentage of live are lower than the positive control group (127.076±6.503) and non-statistic significant ($p<0.05$). While the percentage of live HepG2 cells used to test the medium-sized pFF in all concentrations were 104.621±6.936, 109.706±7.147, 116.384±9.486, 121.202±7.807, 123.54±9.678, 103.601±10.559, 102.861±6.247 and 106.249±6.894, respectively and non-significantly higher than the control group, except at concentrations 40 and 200 µg proteins/mL (Fig. 3). All of fluid protein concentrations used to test had a percentage of live are lower than the positive control group and non-statistic significant. The cell morphology of those cultured in pFF from the 2-sized follicles remained normal in all concentration. Because of the protein components in pFF from small and medium-sized ovarian follicles could stimulate cell growth study on the SDS-PAGE and analyzed protein using mass spectrometry. The protein components of pFF from small-sized ovarian follicles indicated a molecular weight of a protein concentration at 100 kDa, a truncated receptor of the epidermal growth factor receptor (trEGF-R). It can promote cell growth and differentiation. Meanwhile, the molecular weight of protein concentration at 92 kDa, which is a heat shock protein that functions to promote cell growth (Ducolomb et al., 2013; Youngsabanant-

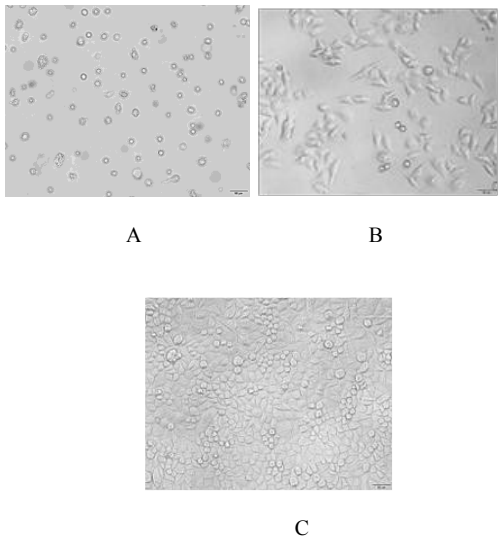

Fig. 1 The morphology of HepG2 cancer cell line from inverted microscopy (A) at 0 h of culture, the cells were oval shaped. (B) At 24 h of culture, the cells were a fusiform shape with approximately 50% of adherence with the culture plate. (C) At 48 h of culture, the cells were a fusiform shape, with approximately 90% adherence with the culture plate and oval shape about 10% (magnification of images at 200x, scale bar = 50 micrometer).

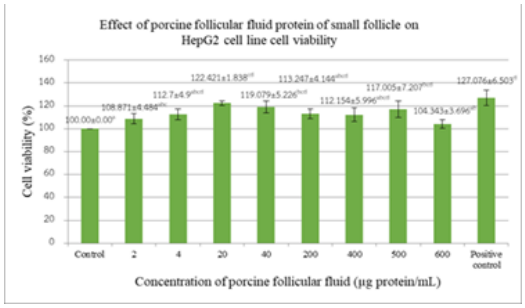

Fig. 2 Effect of porcine follicular fluid from small-sized follicles (1-3 mm in diameter) on HepG2 cell line viability on 2, 4, 20, 40, 200, 400, 500, and 600 µg protein/mL in 24 h. (mean±SE).

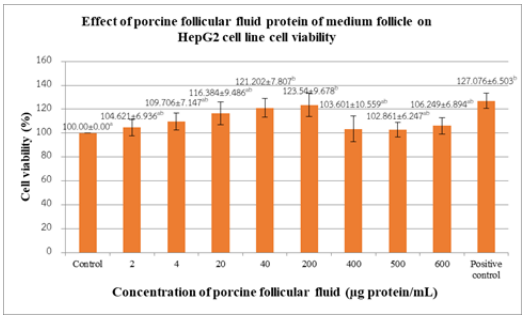

Fig. 3 Effect of porcine follicular fluid from medium-sized follicles (4-6 mm in diameter) on HepG2 cell line viability on 2, 4, 20, 40, 200, 400, 500, and 600 µg protein/mL in 24 h. (mean±SE).

Areekijseree et. al., 2019). This study also the same results with Hela and Vero cancer cell lines which promote cell culture by pFF in culture medium (Youngsabanant., et. al., 2019; Youngsabanant and Rabiab, 2020). From the results of this study, it was concluded that, small-sized pFF concentrations at 20, 40 and 500 µg proteins/mL and medium-sized pFF at concentrations 40 and 200 µg proteins/mL could promote the growth of cell lines in the laboratory similar to the group supplemented with HTFBS. It can use this data results from research to be applied in various cancer cell cultures in the laboratory. This result implies that pFF from porcine ovaries can be used as supplement instead of HTFBS in a culture medium to promote viability in other cancer cell lines which were use as cell model study in laboratory.

Conclusion

Pig follicular fluid at 20, 40 and 500 µg proteins/mL from small-sized ovarian follicles and 40 and 200 µg proteins/mL from medium-sized ovarian follicles, which supplemented DMEM culture medium groups, indicated the highest cell viability, which was significantly different from the percentage of cell viability in the control group but not higher than the positive control group (DMEM medium supplemented with 10% HTFBS). This result review that pFF from small and medium-sized ovarian pig ovaries can be used as supplement instead of a serum in a culture medium to promote viability HepG2 cancer cell line cultures in the laboratory.

Acknowledgements

This research is financially supported by Faculty of Science, Silpakorn University and Thailand Science Research and Innovation (TSRI) National Science, Research and Innovation Fund (NSRF) (Fiscal Year 2023 Project code 4232809).

The authors are grateful to The Korean Cell Line Bank (Seoul Korea) for their kind to support cell lines for this work. We are also grateful to Assistant Professor Dr. Thongchai Taechowisan (Department of Microbiology, Faculty of Science Silpakorn University, Thailand) for his kindness to render on cell line culture technique.

References

Areekijseree M, Vejaratpimol R. In vivo cells cumulus oocyte complexes and granulosa cells: A scanning electron microscopy and inverted microscopy study. Micron 2006; 37: 707-716.

Areekijseree M, Veerapraditsin T. Characterization of pig oviductal epithelial cells, cumulus cells and granulosa cells-conditioned media and their ability to induce acrosome reaction on frozen-thawed bovine spermatozoa. Micron 2008; 39 (2): 160-167.

Ducolomb Y, González-Márquez H, Fierro R, Jiménez I, Casas E, Flores D, Bonilla E, Salazar Z, Betancourt M. Effect of porcine follicular fluid proteins and peptides on oocyte maturation and their subsequent effect on in vitro fertilization. Theriogenology 2013; 79(6): 896-904.

Pongsawat W, Youngsabanant M. Porcine cumulus oocyte complexes (pCOCs) as biological model for determination on in vitro cytotoxic of cadmium and copper assessment. Songklanakarin Journal of Science and Technology (SJST) 2019; 41 (5):1029-1036.

Lowry OH, Rosebrough N J, Farr A L, Randall R J. Protein measurement with the Folin phenol reagent. Journal of biological chemistry 1951; 193(1): 265-275.

Youngsabanant M, Rabiab S. Potential Effect of porcine follicular fluid (pFF) from Small-, medium-, and large-sized ovarian follicles on HeLa cell line viability. Science, Engineering and Health Studies 2020;14 (1): 141-151.

Youngsabanant M, Mettasart M. Changes in secretory protein of pig ampulla and isthmus parts of oviduct on follicular and luteal phases. Songklanakarin Journal of Science and Technology (SJST) 2020; 42 (4): 941-947.

P-03

Exploring the Potential of Hemp Extract in Alleviating Lipopolysaccharide-Induced Kidney Inflammation

Manwika Singsuwan[1], Maythanil Kantavaree[1], Plaiyfah Janthueng[1], Wanfrutkon Waehama[1], Jureepon Roboon[1], Paweena Kaewman[1], Samur Thanoi[2], Sutisa Nudmamud-Thanoi[1,3], Ittipon Phoungpetchara[1,3*],
[1] Department of Anatomy, Faculty of Medical Science, Naresuan University, Phitsanulok, Thailand
[2] School of Medical Sciences, University of Phayao, Phayao, Thailand
[3] Center of Excellence in Medical Biotechnology (CEMB), Naresuan University, Phitsanulok, Thailand
*Corresponding author, e-mail: ittiponp@nu.ac.th

Abstract

The kidney plays a role in waste excretion and fluid balance. Kidney inflammation leads to tissue deterioration. In research, lipopolysaccharides (LPS) are used to induce inflammation and result in tissue damage. Dexamethasone (DEX) is commonly used to reduce inflammation. However, it has side effects. Hemp (*Cannabis sativa*) can be cultivated domestically. It contains cannabidiol (CBD) which has anti-inflammatory, analgesic, and antioxidant properties. These characteristics suggest that hemp extract, particularly its CBD component, may offer therapeutic potential in alleviating kidney inflammation and associated damage. This study aims to investigate pathology and examine the effect of hemp extract on rat's kidney inflammation induced by lipopolysaccharides. Male rats (Sprague-Dawley) took a week's rest and were reared in rat cages with appropriate light, temperature and relative humidity controls. Rats were divided into 4 groups of 6 each, the first group was controlled, the second group was LPS-induced (7.5 mg/kg BW), the third group was treated with LPS followed by hemp extract (15 mg/kg BW), and the fourth group was treated with LPS followed by DEX (5 mg/kg BW) for two weeks before euthanized. The kidneys were collected and fixed then processed and sectioned at 5 μm thick, then stained with H & E, Masson's trichrome. The results were examined under a microscope. LPS induces acute inflammation that stimulates neutrophils, macrophages and lymphocyte initiating the inflammatory response and tubular epithelial cells injury cause tissue fibrosis in the Bowman's capsule and around the renal vessels. When receiving hemp extract, it was found that the condition of inflammation tended to decrease and reduced the formation of tissue fibrosis, which gave the same results as the group receiving DEX. It has been shown that hemp extract has the effect of reducing inflammation of rat kidneys and reducing fibrosis as well as DEX.

Keywords *Hemp, CBD, Inflammation, Fibrosis, Masson's trichrome*

P-04

Therapeutic Potential of Hemp Extract in Lipopolysaccharide-induced Liver Inflammation in rats

Ittipon Phoungpetchara[1,3*], Maythanil Kantavaree[1], Thanaporn Prasertsuk[1], Manwika Singsuwan[1], Plaiyfah Janthueng[1], Wanfrutkon Waehama[1], Jureepon Roboon[1], Paweena Kaewman[1], Samur Thanoi[2], Sutisa Nudmamud-Thanoi[1,3]
[1]Department of Anatomy, Faculty of Medical Science, Naresuan University, Phitsanulok, Thailand
[2]School of Medical Sciences, University of Phayao, Phayao, Thailand
[3]Center of Excellent Medical Biotechnology (CEMB), Naresuan University, Phitsanulok, Thailand
*Corresponding author, e-mail: ittiponp@nu.ac.th

Abstract

The liver regulates blood chemical concentrations, facilitates waste excretion through the bile, and detoxifies substances. Liver inflammation can result from infections or chemical exposure. Lipopolysaccharide (LPS) induces inflammation, leading to liver histopathology and fibrosis. Dexamethasone (DEX) reduces inflammation but has adverse effects with prolonged use. Hemp (*Cannabis sativa*) contains cannabidiol (CBD) (analyzed using high-performance liquid chromatography for cannabinoids in hemp seed cold ethanol extract), which has shown potential in reducing inflammation, fibrosis, and macrophage infiltration while promoting hepatocyte proliferation. This study investigates the effects of hemp extract on histopathological improvement and inflammation reduction in LPS-induced liver injury in rats. Eight-week-old male Sprague-Dawley rats were divided into four groups (n=6): control, LPS-induced (7.5 mg/kg BW, single dose), LPS + hemp extract (CBD 15 mg/kg BW, 2 hours post-LPS) (EU GMP-certified Cannabis sativa, oral LD50 value of over 5000 mg/kg in rats), and LPS + DEX (5 mg/kg BW, 2 hours post-LPS). Treatments continued for two weeks before euthanasia. Liver tissues were fixed, processing, sectioned (5 µm), and stained with H&E and Masson's trichrome for histopathological analysis. LPS-induced rats exhibited increasing of hepatocyte vacuolation, collagen thickening around the central vein, expanded hepatic sinusoids, and white blood cell (WBC) infiltration (WBC determined by observation of shape of nucleus). Treatment with hemp extract decreases these abnormalities similar to the result of DEX. Hemp extracts alleviated LPS-induced liver inflammation and fibrosis, suggesting its potential as a therapeutic agent for liver injury. Further research is needed to confirm these findings and explore the underlying mechanisms.

Keywords *Hemp, CBD, Hematoxylin & Eosin, Masson's trichrome, Collagen fibers*

P-05

Chimeric MrNV-VLPs with CLEC17A's Fucose-Binding Domain: A Novel Strategy to Combat MrNV Infection in Sf9 Susceptible Cells

Rueangtip Chantunmapitak[1], Supawich Boonkua[1], Orawan Thongsum[1], Adrien Breiman[2], Wattana Weerachatyanukul[1], Somluk Asuvapongpatana[1], Atthaboon Watthammawut[3]* and Monsicha Somrit[1*],
[1]Department of Anatomy, Faculty of Science, Mahidol University, 272 Rama VI Road, Ratchathewi District, Bangkok 10400, Thailand
[2]Université de Nantes, Inserm, CRCINA, Nantes, France, CHU de Nantes, Nantes, France
[3]Department of Anatomy, Faculty of Medicine, Srinakharinwirot University, Wattana, Bangkok 10110, Thailand
*Corresponding authors, e-mail: monsicha.som@mahidol.ac.th

Abstract

Our previous studies showed that Macrobrachium rosenbergii nodavirus (MrNV), which causes white-tail disease (WTD), can infect and replicate in the Sf9 insect cell line. We found that specific fucosylated N- and O-glycans (HexNAc(Fuc)HexNAc-R or Fuc-LacdiNAc) play a crucial role in helping the virus attach to target tissues in the giant freshwater prawn, Macrobrachium rosenbergii**.** Additionally, we demonstrated that virus-like particles (MrNV-VLPs) can bind and enter Sf9 cells using the C-terminal region of the capsid's protruding (P) domains**,** highlighting the importance of this structure in host-cell interactions. In this study, we investigated the impact of modifications to the P-domain on virus-like particle formation and function of particles after replacing it with the fucose-binding carbohydrate-recognition domain (CRD) of the CLEC17A lectin (Prolectin) or CLEC17A/CRD. We found that even after truncating the P-domain near known calcium-binding domains (CBDs) in the capsid's S-shell**,** the virus-like particles could still form. However, these particles were smaller and lacked the usual protrusions. We named them V250-MrNV-VLPs**.** With their S-shells still intact**,** we were able to completely replace the P-domains with the CLEC17A/CRD, creating chimeric particles called CLEC17A/CRD-MrNV-VLPs. These chimeric VLPs remained stable and icosahedral**,** with distinct P-domains compared to V250-MrNV-VLPs and regular MrNV-VLPs**.** More importantly, the CLEC17A/CRD-MrNV-VLPs are specifically bound to fucosylated glycoconjugates and Sf9 cell protein lysates**.** Notably, CLEC17A/CRD-MrNV-VLPs were able to reduce MrNV binding and infection in Sf9 cells. This suggests that these chimeric particles have the potential to be developed into nanoparticles that can effectively target fucosylated glycans and reduce MrNV infection in susceptible cells.

Keywords *Nodavirus, Virus-like particles, Glycans, Fucosylated LacdiNAcs, Carbohydrate-recognition domains, Prolectin*

P-06

Thunbergia Laurifolia Improves Lung Pathology in PD Mice Induced by MPTP

Kewalee Seeharach[1], Chatchadaporn Jaiyen[1], Chanida Thongsopha[1], Sumitra Gomonchareonsiri[2], Salin Mingmalairak[2], Noppadol Phasukdee[1], Paiwan Sudwan[1], Ranida Quiggins[1,*]
[1] Department of Anatomy, Faculty of Medicine, Chiangmai University, 110 Intawaroros Road, Si Phum, Muang, Chiang Mai 50200, Thailand
[2] Department of Physiology, Faculty of Medicine, Chiangmai University, 110 Intawaroros Road, Si Phum, Muang, Chiang Mai 50200, Thailand
*Corresponding author, e-mail: ranida.quiggins@cmu.ac.th

Abstract

The compound 1-methyl-4-phenyl-1, 2, 3, 6-tetrahydropyridine (MPTP) is a toxin commonly used to induce a Parkinson's disease (PD) model in animals. This model exhibits various motor and non-motor defects, particularly affecting the respiratory system. Although *Thunbergia laurifolia* Lindl (*TL*) extract has been shown to improve lung pathology induced by Paraquat, there are currently no reports on lung parenchyma in MPTP-induced PD mice, nor on the effects of *TL* extract in this model. This study aimed to examine the characteristics of lung parenchyma in MPTP-induced mice and those treated with aqueous *TL* leaf extract. Twenty mice were divided into four groups: control, MPTP, MPTP treated with 250 mg *TL*/kg body weight (BW), and MPTP treated with 500 mg *TL*/kg BW. The animals underwent a rotarod test to assess motor behavior. Lung tissues were characterized using Hematoxylin and Eosin (H&E) and Trichrome staining. The results indicated an improvement in motor behavior in both the 250 mg and the 500 mg *TL*/kg BW-treated MPTP groups compared to the MPTP group. Significant pathological changes were evident in the MPTP mice, including alveolar edema, diffuse alveolar collapse, hemorrhage, leukocyte infiltration, and alveolar septal thickening. In contrast, alveolar characteristics significantly improved following *TL* treatments compared to the untreated MPTP group. Notably, pulmonary hemorrhaging and leukocyte infiltration were reduced in the 250 mg/kg *TL*-treated MPTP group, while alveolar collapse and thickening were rarely observed in the *TL*-treated MPTP groups, particularly in the 500 mg *TL*/kg BW-treated group. In conclusion, MPTP induces pulmonary damage, and this study suggests that aqueous *TL* leaf extract can ameliorate lung pathology caused by MPTP.

Keywords *Parkinson's disease, MPTP, Respiratory defect, Thunbergia laurifolia Lindl.*

P-07

Thunbergia Laurifolia Ameliorates Motor Defects and Renal Damage in the Subacute MPTP Induced PD in Mice

Chatchadaporn Jaiyen[1], Kewalee Seeharach[1], Chanida Thongsopha[1], Noppadol Phasukdee[1], Paiwan Sudwan[1], Salin Mingmalairak[2], Ranida Quiggins [1, *]
[1] Department of Anatomy, Faculty of Medicine, Chiangmai University, 110 Intawaroros Road, Si Phum, Muang, Chiang Mai 50200, Thailand
[2] Department of Physiology, Faculty of Medicine, Chiangmai University, 110 Intawaroros Road, Si Phum, Muang, Chiang Mai 50200, Thailand
*Corresponding author, e-mail: ranida.quiggins@cmu.ac.th

Abstract

The compound 1-methyl-4-phenyl-1, 2, 3, 6-tetrahydropyridine (MPTP) is commonly considered to be the toxin that causes dopaminergic neuron degeneration, resulting in Parkinson's disease (PD). MPTP also causes kidney dysfunctions through an inflammation process. *Thunbergia laurifolia* (*TL*) leaf extract has been reported as an effective potent detoxifier, an antioxidant, and an anti-inflammatory agent. We aim to investigate whether post-*TL* treatments in the subacute MPTP- induced PD ameliorate motor behavior deficits and renal damage in a mouse model of PD. Twenty-four male C57BL/6 mice were randomly divided into four groups (six mice per group); Control, PD model, PD+*TL*250, and PD+*TL*500. All groups except the control group received intraperitoneal injections (i.p.) of MPTP at a dose of 30 mg/kg BW for five consecutive days. Three days after the last MPTP administration, PD+*TL*250 and PD+*TL*500 groups received i.p. injections of *TL* extract at a dose of 250 and 500 mg/kg BW, respectively for 14 days. All mice performed the rotarod test and the pole test on days 0, 8, 15, and 22. Then, mice of all groups were sacrificed and kidneys were collected. The kidney sections were stained with hematoxylin-eosin and were examined under a light microscope. We found that the retention time on the rotarod test of PD model was significantly shorter than that of the control, and there was no difference between the PD and PD+*TL* group. The t-turn and t-total of pole test of PD model were significantly longer than that of the control. The t-turn of PD+*TL*500 and t-total of PD+*TL*250 were significantly shorter than that of the PD. The renal cortex of PD demonstrated abnormalities including glomerular widening, cloudy tubular swelling, lumen widening, irregularly shaped epithelial cells of Bowman's capsule, and blurred tubular epithelium. The renal parenchymal cortex of the PD+*TL*250 and PD+*TL*500 were similar to those of the control. In conclusion, the *TL* leaf extract can ameliorate the motor defects and renal damage in the subacute MPTP-induced PD in mice.

Keywords *MPTP, Parkinson's disease, Thunbergia laurifolia, Motor behavior, Kidney*

P-08

Impact of Standardized Extract of *Centella asiatica* (ECa233) on Testicular Histopathology in High-Fat Diet-Induced Dyslipidemic Rats: A Preliminary Investigation

Siriporn Kreungnium[1,2], Kanyakorn Aitsarangkun Na Ayutthaya[1,2], Aubonwan Sitthikhankeaw[1,2], Natthapong Khamaiam[2,3], Suthaphat Kongsak[2,3], Akkarawat Sathong[2,3], Aphinya Chaiklam[2,3], Saowalak Rungruang[2], Chakriya Promsuban[1], Apichaya Niyomchan[4], Hiroki Nakata[5], Wai Chen[6], Mayuree H. Tantisira[7], Patcharada Amatyakul[8], Kroekkiat Chinda[2,9,10], Kannika Adthapanyawanich[1,2,10], Yutthapong Tongpob[1,2,10 *]
[1] Department of Anatomy, Faculty of Medical Science, Naresuan University (NU), Phitsanulok, Thailand 65000
[2] Integrative Cardiovascular Research Unit, Faculty of Medical Science, NU, Phitsanulok, Thailand 65000
[3] Department of Medical Science, Faculty of Medical Science, NU, Phitsanulok, Thailand 65000
[4] Department of Anatomy, Faculty of Medicine Siriraj Hospital, Mahidol University, Bangkok, Thailand 10700
[5] Department of Clinical Engineering, Faculty of Health Sciences, Komatsu University, Japan
[6] Curtin Medical School, and Curtin Enable Institute, Curtin University, Perth, Western Australia, Australia
[7] Faculty of Pharmaceutical Sciences, Burapha University, Chonburi, 20131
[8] Department of Obstetrics and Gynecology, Faculty of Medicine, NU, Phitsanulok, Thailand 65000
[9] Department of Physiology, Faculty of Medical Science, Naresuan University, Phitsanulok, Thailand 65000
[10] Centre of Excellence in Medical Biotechnology (CEMB), Faculty of Medical Science, NU, Phitsanulok, Thailand 65000
*Corresponding author, e-mail: yutthapongt@nu.ac.th

Abstract
Background: Dyslipidemia is associated with male infertility, compromising testicular integrity through mechanisms involving oxidative stress and inflammation. ECa233, a standardized extract of *Centella asiatica*, is rich in triterpenoids, which possess anti-inflammatory, antioxidant, and lipid-lowering properties that may mitigate testicular damage. **Objective:** This study explored the effects of ECa233 on testicular histopathology in high-fat diet-induced dyslipidemic rats. **Methods:** Male Wistar rats 8 weeks (250-310 g) were divided into four groups (n=5/group): regular diet (RD), high-fat diet (HF), HF with ECa233 (30 mg/kg/day), and HF with simvastatin (40 mg/kg/day). Following 12 weeks of oral daily treatment, rats were euthanized, blood was collected for lipid analysis, and testes were examined histopathologically. A blind observer evaluated abnormalities in seminiferous tubules including vacuolization, separation, luminal sloughing, and atrophy across 18 random fields per sample. Data were analyzed using one-way ANOVA with Tukey's post-hoc test. **Results:** Compared with ND rats, HF consumption induced dyslipidemia by significantly elevated levels of total cholesterol, low-density lipoprotein cholesterol (LDL), and triglycerides ($P<0.05$). HF rats also showed significantly decreased testicular weight (0.30±0.03% vs. 0.41±0.03% of body weight, $P<0.001$) and increased histopathological abnormalities in seminiferous tubules (38.42±12.92% abnormal tubules vs. 20.61±9.12% in ND, $P<0.05$). Treatment with ECa233 and simvastatin significantly improved blood lipid profiles, decreasing total cholesterol and LDL levels ($P<0.05$). Interestingly, compared with HF rats, simvastatin demonstrated significantly testicular protective effects (78.08±4.71% normal tubules vs. 61.58±12.92%, $P<0.05$), while ECa233 treatment did not significantly mitigate testicular histopathological alterations. **Conclusions:** While ECa233 effectively improves lipid profiles in HF rats, it does not significantly ameliorate testicular histopathological alterations at the tested dose. This suggests that the ECa233's lipid-lowering effects may not directly translate to testicular protection, possibly due to limited tissue penetration or insufficient dosage. Further studies should explore dose-dependent effects, longer treatment durations, and the mechanisms underlying ECa233 in high-fat diet conditions.

Keywords *Centella asiatica, Testis, Seminiferous tubules, Dyslipidemia, Obesity, Male infertility*

P-09

Alterations of the Structures, Biochemical Components, and SVS4 Expression in Seminal Vesicle of the Depressive-like Behavior Rat Model

Sitthichai Iamsaard* and Sararat Innoi
Department of Anatomy, Faculty of Medicine, Khon Kaen University, Khon Kaen, Thailand.
*Corresponding author, e-mail: sittia@kku.ac.th

Abstract

Chronic stress (CS) is a risk factor to promote depressive-like behaviors and can also cause male infertility. Although its adverse effects of dexamethasone (DEX), used to induce CS, on the seminal plasma reduction were previously reported, the structural and biochemical changes remain unexplored. This study was to investigate the effects of DEX on structural and biochemical alterations in seminal vesicle fluid (SVF) and tissue (SVT). Twenty adult male rats were divided into control and DEX groups (induced with a dose of DEX at 1.5 mg/KgBW for 21 consecutive days). CS with depressive-like behaviors was determined with forced swimming and tail suspension tests. The blood serum and SVF were evaluated for hormones, biochemical components, and malonaldehyde (MDA) level. SVF volume and histomorphometry of SVT were observed. Expressions of apoptotic markers and seminal vesicle secreting protein4 (SVS4) were determined in the SVT. The results showed the reductions size of seminal vesicle and SVF volume in DEX rats. DEX could increase the MDA level in SVF and DNA fragmentation revealed by TUNEL assay. Serum testosterone and levels of magnesium and fructosamine in SVF of DEX group were significantly decreased as compared to control. DEX decreased the epithelial height but increased the muscularis layer of seminal vesicle wall. Significantly, the expression of SVS4 was decreased in SVT induced with DEX. However, no difference of apoptotic marker expressions including Hsp70, pro-caspase3, and pro-caspase9 was observed as compared between groups. It was concluded that CS induced by DEX caused the seminal vesicle changes in histomorphometry and secreting volume. These alterations were associated with increased DNA fragmentation and lipid peroxidation but not via the apoptotic-caspase pathway.

Keywords *Chronic stress, Dexamethasone, Seminal vesicle, Seminal vesicle fluid, SVS4*

P-10

Centella asiatica Extract Inhibits HCT-116 Colorectal Cancer Cell Migration and Invasion through F-Actin

Voramon Upali[1], Chonnapat Naktubtim[1,2], Paween Kunsorn[3], Waritta Sriniang[1], Prasit Suwannalert[1,2*]
[1] Department of Pathobiology, Faculty of Science, Mahidol University, Bangkok 10400, Thailand
[2] Pathobiology Information and Learning Center, Department of Pathobiology, Faculty of Science, Mahidol University, Bangkok 10400, Thailand
[3] Department of Integrative Medicine, Chulabhorn International College of Medicine, Thammasat University, Pathumthani, 12120, Thailand
*Corresponding author, e-mail: prasit.suw@mahidol.ac.th

Abstract

Colorectal cancer (CRC) is a leading cause of cancer-related mortality, with metastasis being a major contributor to poor prognosis. Cell migration and invasion, key processes in cancer progression, are regulated by cytoskeletal components such as F-actin. *Centella asiatica*, a medicinal plant with antioxidant and anti-inflammatory properties, has been studied for its potential anticancer effects. However, its role in CRC cell motility remains unclear. This study aimed to evaluate the effects of *C. asiatica* extract on migration and invasion of HCT-116 CRC cell and its involvement in F-actin modulation. MTT assays, wound healing assays, and Matrigel invasion assays were performed to assess cell viability, migration, and invasion. Immunofluorescence assay analysis was conducted to examine the expression of key protein associated with cytoskeletal remodeling. The results showed that *C. asiatica* extract significantly suppresses HCT-116 cell migration and invasion, correlating with decreased F-actin polymerization. The indication of *C. asiatica* extract suppressing CRC cell motility through F-actin modulation suggests its potential therapeutic role.

Keywords *Colorectal cancer, Centella asiatica, F-actin, Cell migration, Invasion*

Background

Colorectal cancer is one of the leading causes of cancer-related deaths worldwide, with metastasis being a primary factor contributing to poor prognosis [1]. Metastasis involves the migration and invasion of cancer cells into surrounding tissues and distant organs, processes that are heavily dependent on cytoskeletal remodeling, particularly the reorganization of F-actin. Actin cytoskeleton dynamics play a crucial role in colorectal cancer cells (CRC) cell motility, facilitating the formation of protrusive structures such as filopodia and lamellipodia, which aid in migration and invasion [2]. Several regulatory proteins have been implicated in actin filament rearrangement, further promoting CRC progression [3,4]. Given the importance of these pathways, targeting actin cytoskeletal remodeling presents a potential therapeutic approach to limit CRC metastasis.

Centella asiatica, a well-known medicinal plant, has been traditionally used for its wound-healing, neuroprotective, and anti-inflammatory properties [5]. Studies have highlighted its potential anticancer effects, particularly in CRC, through the modulation of key molecular pathways involved in cell proliferation, migration, and invasion [6,7].

Bioactive compounds such as asiatic acid and asiaticoside have been shown to inhibit epithelial-mesenchymal transition (EMT) and suppress signaling pathways responsible for reducing cell viability and motility [8,9].

Given the emerging evidence supporting the role of *C. asiatica* in inhibiting CRC progression, this study aims to investigate the effects of *C. asiatica* extract (CAE) on HCT-116 colorectal carcinoma cell migration and invasion, specifically, its impact on F-actin organization and key regulatory proteins associated with CRC cell motility. HCT-116 is a widely used human

colorectal carcinoma cell line for studying metastatic behavior *in vitro*. Understanding these effects may provide insight into the therapeutic potential of *C. asiatica* extract in mitigating CRC metastasis.

Materials and Methods

Centella asiatica extraction

The dried powder of *C. asiatica* was purchased from an herbal dispensary in Bangkok. 10 grams of dry powder were extracted with 500 ml of 95% ethanol for 3 days and occasionally agitated, filtered, and evaporated until crude extract was obtained.

Cell culture and treatment

The HCT-116 human colorectal carcinoma cell line, originally derived from the colon of a 48-year-old Caucasian male with colorectal cancer, was obtained from ATCC® (CCL-247™, Virginia, USA). The cells are adherent and display epithelial morphology. HCT-116 cells were cultured in McCoy's 5A (Modified) Medium supplemented with 10% heat-inactivated fetal bovine serum (FBS), 1% L-glutamine, 1% penicillin-streptomycin, and non-essential amino acids. The cells were maintained at 37 °C in a humidified 5% CO_2 incubator (Lab-line; USA).

MTT assay

HCT-116 cells were seeded in 96-well plates and incubated for 24 hours. After the CAE application, the MTT solution was added and incubated for 2 hours. Absorbance was measured at 570 nm using an automated microplate reader (1420 Victor 2, Wallac, USA).

Wound healing assay

HCT-116 cells were seeded in 6-well plates and grown to 90% confluence. A wound was created using an SPLScar™ Scratcher (SPL, Korea), followed by treatment with CAE at varying concentrations. Images were taken at 0 and 48 hours using a microscope. The percentage of wound closure was calculated using the formula: [(Initial wound width – Wound width at 48 h) / Initial wound width] × 100. Migration was analyzed with the ImageJ program, and the value was then used to generate the bar graph representing the percentage of migrating cells.

Matrigel invasion assay

Cell culture inserts (Corning, USA, 8.0 µm pores) were coated with ECM gel (Sigma-Aldrich, USA) and seeded with HCT-116 cells in the upper chamber, while 20% FBS in the lower chamber acted as a chemoattractant. After 24 hours, media was replaced with CAE at various concentrations, followed by 72 hours of incubation. Non-invading cells were removed, and the lower membrane was stained with crystal violet. Invading cells were quantified under a microscope and expressed as cells per 10 high-power fields (HPF).

Immunofluorescence assay

HCT-116 cells were permeabilized with Triton X-100 and blocked with serum to prevent nonspecific binding. Cells were incubated with a primary antibody for F-actin, followed by a fluorescently labeled secondary antibody. After washing and nucleus counterstaining with DAPI, slides were mounted. F-actin localization was examined using a fluorescence microscope, assessing its cellular distribution and activation status.

Results

Effects of Centella asiatica extract on HCT-116 colorectal carcinoma cell viability

The viability of HCT-116 colorectal carcinoma cells following treatment with *C. asiatica* extract (CAE) was assessed using the MTT assay to determine non-cytotoxic concentrations. The cells were treated with 50, 100, and 200 µg/mL of CAE. The results indicated that CAE at 200 and 100 µg/mL significantly reduced cell viability compared to the control, whereas 50 µg/mL of CAE showed no significant difference from the control (Fig.1). This concentration was considered safe doses for further analysis of CAE's effects on cell migration, invasion, and actin cytoskeleton remodeling.

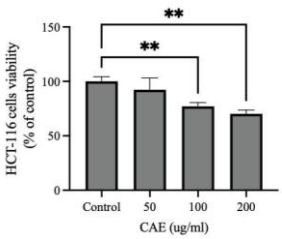

Fig.1 The effect of *CAE* treatment on HCT-116 cell viability at 0, 50, 100, 200 µg/mL. The data are presented as mean ± SD. **P < 0.01.

CAE suppresses migration of HCT-116 cells

The effect of CAE on HCT-116 migration was evaluated using the wound healing assay. Cells treated with 25 and 50 µg/mL CAE exhibited a decrease in migration compared to the control (100%) as migration was significantly reduced in cells treated with 50 µg/mL (Fig.2). The findings indicate that higher concentrations of CAE effectively suppress CRC migration by influencing cytoskeletal organization and motility.

CAE suppresses HCT-116 CRC invasion

The effect of CAE on HCT-116 invasion was assessed using the Matrigel invasion assay. After 72 hours of treatment, cells were treated with 25 and 50 µg/mL CAE, the result showed a reduction in the number of invading cells compared to the control (Fig.3). The decrease in invasion was more pronounced at higher concentrations, with 50 µg/mL CAE demonstrating the most significant reduction (p = 0.045). These findings suggest that CAE effectively inhibits CRC invasion in a dose-dependent manner.

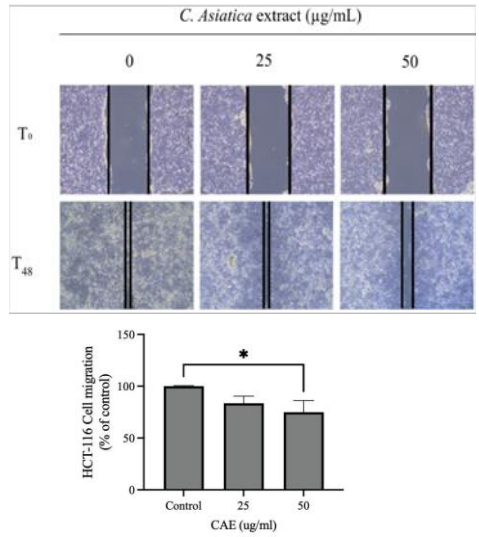

Fig.2 Migration of HCT-116 after 48-hour treatment CAE at 0, 25, 50 µg/mL. Results are presented in a bar graph depicting the percentage of migrating cells. Data are expressed as mean ± SD, with statistical significance set at *P < 0.05.

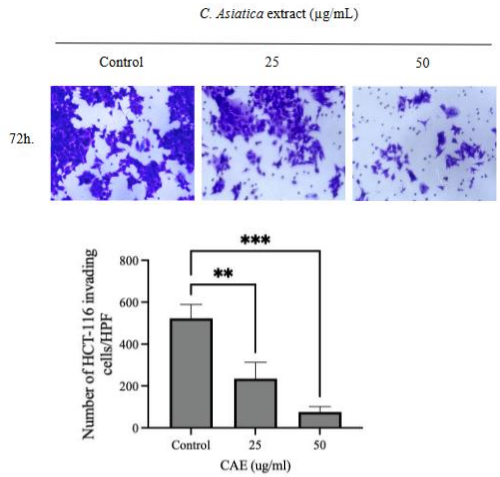

Fig.3 Invasion of HCT-116 cells following 72-hour treatment with CAE at 25 and 50 µg/mL. The data are represented in a bar graph showing the number of invading cells. Results are presented as mean ± SD. **P < 0.01, ***P < 0.001.

CAE immunofluorescence assay on F-Actin

The effects of CAE on the actin cytoskeleton, an immunofluorescence assay was performed to visualize F-actin organization in HCT-116 cells. Fluorescence microscopy revealed distinct cytoskeletal alterations following CAE treatment, suggesting its potential role in modulating F-actin dynamics. Cells treated with CAE exhibited a reduction in F-actin polymerization, correlating with decreased migration and invasion (Fig.4). These findings indicate that CAE may disrupt actin cytoskeleton remodeling, contributing to its inhibitory effects on CRC motility.

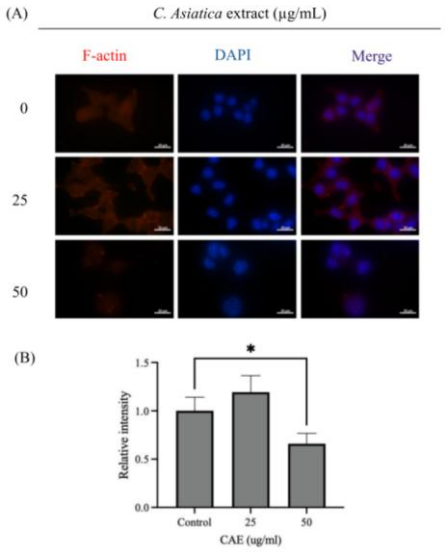

Fig.4 CAE reduces F-actin in CRC. Immunofluorescence analysis of F-actin organization in HCT-116 colorectal carcinoma cells following 48 hours of CAE treatment of 0, 25 and 50 µg/mL. Cells were stained with phalloidin and DAPI (A). Scale bar: 20 µm. Quantification of relative intensity (B). *P < 0.05.

Discussion

Centella asiatica is a medicinal plant known for its wound-healing, anti-inflammatory, and neuroprotective properties. Recently, it has gained attention for its anti-cancer potential, particularly in inhibiting cancer progression. This study investigates *C. asiatica* extract's (CAE) effects on HCT-116 colorectal carcinoma cells (CRC), focusing on cell viability, migration, invasion, and F-actin organization.

Colorectal cancer remains a leading cause of cancer-related deaths worldwide, with metastasis playing a crucial role in disease progression and poor prognosis [1]. A key factor in cancer metastasis is the ability of cancer cells to migrate and invade surrounding tissues. The findings indicate that CAE significantly inhibits CRC cell motility, supporting its potential therapeutic application, heavily relying on F-actin expression and its associated cytoskeletal remodeling. Although F-actin expression did not significantly decrease at 25 µg/ml (p = 0.241), cell migration was still inhibited (Fig.4B). This suggests that the concentration may not be sufficient to suppress overall F-actin expression but may instead affect the organization or structural dynamics of F-actin. Such alterations in F-actin architecture—rather than total expression—could impair the formation of migration-related structures like lamellipodia and filopodia, thereby reducing cell motility [2]. Reclusion of F-actin protrusive structures shown in CAE treatment may serve as an effective approach to suppress cancer progression (Fig.4A).

CAE is known to contain bioactive compounds, including asiatic acid and asiaticoside, which have been reported to suppress CRC cell proliferation and migration by modulating key oncogenic pathways [4,5,7,9]. Asiaticoside has been found to reduce epithelial-mesenchymal transition, a process that promotes cancer invasion and metastasis [8]. Additionally, asiatic acid has been reported to inhibit signaling pathways which plays a crucial role in actin filament polymerization and stress fiber formation [10].

Given these findings, CAE emerges as a promising natural therapeutic agent for targeting CRC migration and invasion by disrupting cytoskeletal remodeling and modulating key oncogenic pathways.

Conclusion

This study demonstrates that CAE effectively inhibits CRC cell migration and invasion by altering F-actin organization and cytoskeletal remodeling. The observed reduction in cell viability, motility, and invasion suggests that CAE may serve as a

potential natural therapeutic agent against CRC metastasis. Future research should explore the molecular pathways involved in CAE-induced cytoskeletal disruption, particularly its interactions with F-actin regulatory proteins and signaling pathways. Further *in vivo* studies and clinical evaluations will be necessary to validate the therapeutic potential of CAE in CRC treatment.

Acknowledgements

The authors sincerely appreciate the Department of Pathobiology, Faculty of Science, Mahidol University, for providing access to their laboratory facilities.

References

1. Siegel RL, Miller KD, Wagle NS, Jemal A. Cancer statistics, 2023. CA Cancer J Clin. 2023;73:17–48.
2. Pollard TD, Cooper JA. Actin, a central player in cell shape and movement. Science. 2009 Nov 27;326(5957):1208–12.
3. Zhou X, Ke C, Lv Y, Ren C, Lin T, Dong F, *et al*. Asiaticoside suppresses cell proliferation by inhibiting the NF-κB signaling pathway in colorectal cancer. Int J Mol Med. 2020;46(4):1525–1537.
4. Manmuan S, Manmuan P, Yoykaew P, Thuetong P, Asipong P, Riantong N, *et al.* Evaluation of standardized extract of *Centella asiatica* on cell viability and repressive cancer migration in metastatic colorectal cancer cells in vitro. Walailak J Sci Technol. 2021;18.
5. Gohil KJ, Patel JA, Gajjar AK. Pharmacological review on *Centella asiatica*: A potential herbal cure-all. Indian J Pharm Sci. 2010;72(5):546–556.
6. Gonçalves BMF, Salvador JAR, Marín S, Cascante M. Synthesis and anticancer activity of novel fluorinated asiatic acid derivatives. Eur J Med Chem. 2016;114:101–17.
7. Hao Y, Huang J, Ma Y, Chen W, Fan Q, Sun X, *et al.* Asiatic acid inhibits proliferation, migration and induces apoptosis by regulating PDCD4 via the PI3K/AKT/mTOR/p70S6K signaling pathway in human colon carcinoma cells. Oncol Lett. 2018;
8. Ma Y, Wen J, Wang J, Wang C, Zhang Y, Zhao L, *et al.* Asiaticoside antagonizes proliferation and chemotherapeutic drug resistance in hepatocellular carcinoma (HCC) cells. Med Sci Monit. 2020;26.
9. Pantia S, Kangsamaksin T, Janvilisri T, Komyod W. Asiatic acid inhibits nasopharyngeal carcinoma cell viability and migration via suppressing STAT3 and claudin-1. Pharmaceuticals. 2023;16:902.
10. Xie L, Huang H, Zheng Z, Yang Q, Wang S, Chen Y, *et al.* Myo1b enhances colorectal cancer metastasis by promoting the F-actin rearrangement and focal adhesion assembly via RhoA/ROCK/FAK signaling. Ann Transl Med. 2021;9:1543.

P-11

The Effect of *Caulerpa racemosa* (CR) on Anti-melanogenesis Through the Upregulation of ERK

Ratchanon Sukprasert[1], Pornpun Vivithanaporn[2], Kant Sangpairoj[3], Nongnuch Luangpon[1], Waranurin Yisarakun[1], Tanapan Siangcham[1]*
1 Faculty of allied health sciences, Burapha university, Chon Buri, Thailand.
2 Chakri Naruebodindra Medical Institute, Faculty of Medicine Ramathibodi Hospital, Mahidol University, Samut Prakan, Thailand.
3 Department of Preclinical Science, Faculty of Medicine, Thammasat University, Pathum Thani, Thailand.
* Corresponding author, e-mail: Tanapan@go.buu.ac.th

Abstract

Caulerpa racemosa (CR) is a macroalgae in the division of Chlorophyta and is well known for its strong antioxidant properties. Notably, high levels of flavonoids and phenols have been identified. It has been reported that the phenol content in CR is higher than that in red algae, which helps inhibit melanin production. Previous studies have reported that CR inhibits melanin production in B16F10 cells. Melanin pigments are products of the melanogenesis process, produced by melanocytes. When alpha-MSH binds to the melanocortin-1 receptor, adenyl cyclase is activated, which in turn activates MAP kinase, leading to increased MITF activity. MITF is phosphorylated by MAPK–ERK signaling, downstream of MC1R activation. We hypothesize that CR inhibit melanin production by upregulation of ERK signaling. We aimed to investigate whether CR potently inhibits melanin production through the upregulation of ERK in SK-MEL-5 human melanocyte cells. We first tested the toxicity of the CR on the viability of SK-MEL-5 cells by MTT assays at 30 mins. Then, the protein expressions of MITF, p-ERK, and t-ERK were measured using Western blot analysis. The band density of the protein was determined and normalized with β-actin as an internal loading control using Image J software (version 5.0). CR did not show the cytotoxic effect on SK-MEL-5 cells. The expression of MITF, a marker of melanogenesis, was inhibited by CR. To clarify the regulation of melanogenesis, CR increased the expression of ERK, an important molecule in the α-MSH–MC1R signaling pathway. Then, co-treatment with U0126 ERK inhibitor we found that co-treatment increased MITF expression and single treatment of U0126 also increases MITF expression. In conclusion, CR inhibits melanogenesis by upregulating ERK cause of MITF degradation. Therefore, CR may be an alternative medicine that can treat diseases related to hyperpigmentation.

Keywords *Caulerpa racemosa*, anti-melanogenesis, *ERK*

P-12

Genetic Association of the *SLC6A4 STin2* Polymorphism with Suicidal Behavior: A Systematic Review and Meta-Analysis

Sulaifan Waehama[1], Nathorn Chaiyakunapruk[2], Ratree Sawangjit[3], Nisalwa Japakeeya[4], Samur Thanoi[5], Gavin P Reynolds[6,7], Sutisa Nudmamud-Thanoi[7,8*]
[1] Medical Science Graduate Program, Faculty of Medical Science, Naresuan University, Phitsanulok, Thailand
[2] Department of Pharmacotherapy, University of Utah College of Pharmacy, South 2000 East, Salt Lake City, USA
[3] Clinical Trials and Evidence-Based Syntheses Research Unit, Mahasarakham University, Maha Sarakham, Thailand
[4] Faculty of Nursing, Prince of Songkla University, Pattani Campus, Charoenpradit Road, Pattani, Thailand
[5] School of Medical Sciences, University of Phayao, Phayao, Thailand
[6] Biomolecular Sciences Research Centre, Sheffield Hallam University, Howard Road, Sheffield, UK
[7] Centre of Excellence in Medical Biotechnology, Faculty of Medical Science, Naresuan University, Phitsanulok, Thailand
[8] Department of Anatomy, Faculty of Medical Science, Naresuan University, Phitsanulok, Thailand
*Corresponding author, e-mail: Sutisat@nu.ac.th

Abstract
Background: The serotonin transporter gene (*SLC6A4*) regulates synaptic serotonin, influencing mood and emotions. The serotonin transporter intron 2 (*STin2*) variable number tandem repeat polymorphism affects *SLC6A4* transcription and transporter function and has been implicated in suicidal behavior (SB), including suicidal ideation (SI), suicide attempts (SA), and suicide completion (SC), suggesting a possible genetic contribution to SB. **Objective**: This systematic review and meta-analysis aimed to assess the association between the STin2 polymorphism and the risk of SB. **Methods**: A systematic search of PubMed, EMBASE, Scopus, and PsycINFO was conducted through July 2024. Case-control studies on the *STin2* polymorphism in SB reporting genotype or allele frequencies and Hardy-Weinberg equilibrium in controls were included. Two reviewers independently extracted data and assessed the study quality. Odds ratios (ORs) with 95% confidence intervals (CIs) were pooled using fixed- or random-effects models based on heterogeneity. The optimal genetic model was identified using Thakkinstian's algorithm and validated by false positive report probability (FPRP). **Results**: From 1,756 records screened, thirteen studies met the inclusion criteria, comprising 1,581 individuals with and 2,971 without SB. Analysis of the *STin2* polymorphism revealed a significant increase in SB risk when comparing the 10 versus 12 alleles (OR = 1.12, 95% CI: 1.00-1.24). In subgroup analyses, the optimal dominant model (FPRP = 0.094) indicated significant associations in mood disorders (OR = 1.93, 95%CI: 1.34-2.79) and major depressive disorder (MDD; OR = 2.23, 95%CI: 1.46-3.40). However, subgroup analyses for SC, SA, SI, or ethnicity (Asian and Caucasian) did not reveal significant associations. **Conclusion**: Carriage of the 10 alleles in the *STin2* polymorphism is associated with an increased risk of SB, with the strongest associations in mood disorders and MDD. This association was not observed across all SB subgroups, suggesting that the genetic influence is more relevant to underlying psychiatric conditions than SB broadly.

Keywords *STin2, Suicidal Behavior, Genetic Polymorphism, SLC6A4, Meta-Analysis*

P-13

Effects of Gamma-oryzanol Mixed with Curcumin on the Testicular Function in a Rat Depression Model

Darunrat Onla-or[1,5], Pornpimon Chuaypen[1,5], Waree Tiyaboonchai[2], Sawanya Charoenlappanit[4], Sittiruk Roytrakul[4], Samur Thanoi[3], Sutisa Nudmamud-Thanoi[1,5], Paweena Kaewman[1,5*]
[1] Department of Anatomy, Faculty of Medical Science, Naresuan University, Phitsanulok, Thailand
[2] Department of Pharmaceutical Technology, Faculty of Pharmaceutical Sciences, Naresuan University Phitsanulok, Thailand
[3] Department of Anatomy, School of Medical Science, University of Phayao, Phayao, Thailand
[4] National Centre for Genetic Engineering and Biotechnology, National Science and Technology Development Agency, Pathum Thani, Thailand
[5] Centre of Excellence in Medical Biotechnology, Naresuan University, Phitsanulok, Thailand
*Corresponding author, e-mail: paweenakae@nu.ac.th

Abstract

Depression has been known to cause dysfunction in various organ systems, including the male reproductive system. Dexamethasone (DEX) is a corticosteroid that induces depression through changes in cortisol levels. One of the well-known changes in cortisol level that affects the function of organs is an increase in cortisol level that leads to impairment of the testis. Changes in spermatogenesis and the seminiferous epithelial cycle are reported to be associated with alterations in the testicular protein profiles, which may serve as biomarkers for testicular dysfunction. Gamma-oryzanol (GO) and Curcumin (Cur) are natural products with anti-inflammatory and antioxidant properties. These compounds might help to rescue and improve spermatogenesis, in which the animals were attenuated by DEX administration. Thus, this study aims to investigate the protective effects of GO mixed with Cur by monitoring the improved seminiferous epithelial cycle and protein profiles in depressive rats induced by DEX. Male Sprague-Dawley rats (6-week-olds) were divided into three groups (n = 3-5 rats per group). Rats in the DEX and DEX-GO+Cur groups were induced into depression by administering DEX at a dose of 1.5 mg/kg daily for 28 days. Additionally, rats in the Control and DEX groups received reverse osmosis (R.O.) water, while those in the DEX-GO+Cur group were administrated with a combination of GO at 10 mg/kg and Cur at 50 mg/kg. At the end of the experiment, the testis was collected and stained with H&E to study the stages of the seminiferous epithelial cycle (stages I – XIV). The results indicated that stage VIII of the epithelial cycle was significantly decreased in the DEX group compared to the Control group while it remained unchanged in the DEX-GO+Cur group. The testicular protein profile was analyzed using proteomics analysis. A total of 325 differentially expressed proteins were identified across all groups, six of which were involved in the p53 signaling pathway. Among these six proteins, Tumor Suppressor P53 (p53) and G1/S-Specific Cyclin-D1 (Cyclin D1) were identified with the 2-fold cut-off value in the DEX group. p53 was down-regulated while Cyclin D1 was up-regulated. In conclusion, GO mixed with Cur shows a protective effect against DEX in the testis, particularly the spermiation process occurring in stage VIII. Moreover, this mixture also rescues testicular proteins that are involved in the mitosis of spermatogonia during spermatogenesis. Therefore, GO mixed with Cur may serve as a potential alternative supplement for enhancing testicular function.

Keywords *Depression, Testis, p53-signaling pathway, Gamma-oryzanol, Curcumin*

P-14

Effect of Crude Mulberry Fruit Extract on Testicular Histopathology in High-fat Diet-fed Rats

Kanyakorn Aitsarangkun Na Ayutthaya[1,2], Siriporn Kreungnium[1,2], Saowalak Rungruang[2], Charkriya Promsuban[1], Apichaya Niyomchan[3], Hiroki Nakata[4], Wai Chen[5], Patcharada Amatyakul[6], Kroekkiat Chinda[2,7,8], Kannika Adthapanyawanich[1,2,8], Yutthapong Tongpob[1,2,8]*

[1] Department of Anatomy, Faculty of Medical Science, Naresuan University, Phitsanulok, Thailand 65000

[2] Integrative Cardiovascular Research Unit, Faculty of Medical Science, Naresuan University, Phitsanulok, Thailand 65000

[3] Department of Anatomy, Faculty of Medicine Siriraj Hospital, Mahidol University, Bangkok, Thailand 10700

[4] Department of Clinical Engineering, Faculty of Health Sciences, Komatsu University, Japan

[5] Curtin Medical School, and Curtin enAble Institute, Curtin University, Perth, Australia

[6] Department of Obstetrics and Gynecology, Faculty of Medicine, Naresuan University, Phitsanulok, Thailand 65000

[7] Department of Physiology, Faculty of Medical Science, Naresuan University, Phitsanulok, Thailand 65000

[8] Centre of Excellence in Medical Biotechnology (CEMB), Faculty of Medical Science, Naresuan University, Phitsanulok, Thailand 65000

*Corresponding author, e-mail: yutthapongt@nu.ac.th

Abstract

Background: High-fat diet (HFD) consumption increases oxidative stress and inflammation, contributing to testicular damage and potential male infertility. Mulberry fruit contains anthocyanins with antioxidants properties that may mitigate HFD-induced testicular damage. **Objective:** To investigate the protective effects of crude mulberry fruit extract (CEM) on testicular histopathological alterations in HFD-fed rats. **Methods:** Sixteen male Wistar rats were divided into four groups (n=4/group): Normal Diet (ND), HFD, HFD+CEM 100 mg/kg/day, and HFD+Atorvastatin (ATV) 10 mg/kg/day. ATV is a cholesterol-synthesis inhibitor, serves as positive control to benchmark CEM's efficacy against a standard pharmacological intervention for lipid-mediated testicular pathology. Following 90 days of oral administration, body and testicular weights were recorded. Blood samples were collected for lipid profile analysis. Testicular tissue was examined histopathologically for epithelial separation, vacuolization, luminal sloughing, irregular morphology, and tubular atrophy using standardized scoring methods. **Results:** No significant differences in the body weight were observed between groups. Testicular weight in the HFD+CEM group was significantly lower than in the HFD group (1.84±0.07 vs 2.16±0.16 g, $p<0.01$), while remaining comparable to the ND group (1.99±0.06 g). HFD rats exhibited significantly increased LDL (34.00±4.97 vs 12.50±3.00 mg/dL, $p<0.001$) and triglyceride levels (22.52±2.38 vs 12.50±3.11 mg/dL, $p<0.01$), compared to ND rats indicating dyslipidemia. CEM administration did not significantly alter serum lipid profiles, while ATV treatment significantly reduced triglyceride level compared to both HFD and HFD+CEM groups ($p<0.05$). Histopathological examination revealed increased epithelial separation in seminiferous tubules in the HFD group compared to ND (separation score: 50.08±13.47 vs 16.67±15.37, $p<0.05$). No significant differences were found between groups for other histological parameters. **Conclusion:** CEM did not significantly modify lipid profiles or improve testicular histopathological damaged caused by HFD-induced dyslipidemia. Future studies should employ standardized (rather than crude) mulberry fruit extracts at various doses to establish optimal therapeutic efficacy and explore potential mechanisms beyond antioxidant activity.

Keywords *Mulberry fruit extract, High-fat diet, Dyslipidemia, Testicular histology, Male reproductive health*

P-15

Mulberry Fruit Extract Ameliorates Dyslipidemia but Fails to Prevent Aortic Wall Thickening in High-Fat Diet-Fed Rats

Aubonwan Sitthikhankeao[1,2], Chalisa Suwannasorn[2], Nutthakamon Seetim[2], Sujira Seesin[2], Wittawat Tajai[1,2], Saowalak Rungruang[2,3], Chakriya Promsuban[1], Piyanee Sriya[4], Apichaya Niyomchan[5], Hiroki Nakata[6], Wai Chen[7], Patcharada Amatyakul[8], Kroekkiat Chinda[2,9,10], Kannika Adthapanyawanich[1,2,10], Yutthapong Tongpob[1,2,10*]

[1] Department of Anatomy, Faculty of Medical Science, Naresuan University, Phitsanulok, Thailand 65000
[2] Integrative Cardiovascular Research Unit, Faculty of Medical Science, Naresuan University, Phitsanulok, Thailand 65000
[3]Department of Medical Sciences, Mahidol University, Amnatcharoen Campus, Amnatcharoen, Thailand 37000
[4] Phramongkutklao College of Medicine: Rachathevi, Bangkok, Thailand 10400
[5] Department of Anatomy, Faculty of Medicine Siriraj Hospital, Mahidol University, Bangkok, Thailand 10700
[6] Department of Clinical Engineering, Faculty of Health Sciences, Komatsu University, Japan
[7] Curtin Medical School, and Curtin Enable Institute, Curtin University, Perth, Western Australia, Australia
[8] Department of Obstetrics and Gynecology, Faculty of Medicine, Naresuan University, Phitsanulok 65000
[9] Department of Physiology, Faculty of Medical Science, Naresuan University, Phitsanulok, Thailand 65000
[10] Centre of Excellence in Medical Biotechnology (CEMB), Faculty of Medical Science, Naresuan University, Phitsanulok, Thailand 65000
*Corresponding author, e-mail: yutthapongt@nu.ac.th

Abstract

Dyslipidemia promotes atherosclerosis through oxidative stress-induced endothelial dysfunction. Mulberry fruits (*Morus alba L.*) are rich in anthocyanins with well-documented antioxidant properties, yet their effects on vascular remodeling and aortic wall integrity remain incompletely understood. This study investigated the impact of mulberry fruit extract on lipid profiles and aortic histopathology in dyslipidemic rats. Twenty male Wistar rats were randomly assigned to four groups (n=5 per group): (1) normal diet (ND), (2) high-fat diet (HFD), (3) HFD with crude extract of mulberry fruit (CEM, 100 mg/kg/day), and (4) HFD-fed with atorvastatin (ATV, 10 mg/kg/day) as a positive control. After 90 days of oral daily treatment, lipid profiles were assessed, and aortic tissues were examined using hematoxylin and eosin and Masson's trichrome staining. The HFD group exhibited increases in total cholesterol (31%), triglycerides (38%), and LDL (263%) compared to the ND group ($p<0.01$). CEM supplementation significantly improved lipid profiles, reducing total cholesterol and LDL (by 12%, and 25%, respectively) compared to the HFD group ($p<0.05$). Histological analysis, however, revealed that CEM supplementation failed to prevent the HFD-induced increases in aortic wall thickness (54.3% in HFD+CEM vs. 56.4% in HFD compared to ND rats), despite improving lipid profiles. In contrast, ATV treatment maintained normal aortic morphology while also improving lipid parameters. Masson's trichrome staining demonstrated collagen deposition increasing in the HFD and HFD+CEM groups compared to both ND and HFD+ATV groups. These findings indicate a dissociation between CEM's effects on lipid metabolism and vascular structure, suggesting that improvement in lipid profiles did not necessarily translate to protection against vascular remodeling associated with dyslipidemia. This dissociation between metabolic improvement and vascular changes indicates that CEM alone may not be sufficient to overcome the vascular detriments of HFD consumption, warranting further investigation into optimizing mulberry extract supplementation in dyslipidemia management.

Keywords *Dyslipidemia, Mulberry fruit (Morus alba L.), Anthocyanin, Aorta, Histopathology*

Background

Cardiovascular diseases (CVDs) remain the leading cause of mortality worldwide, accounting for approximately 18 million deaths annually (1). Dyslipidemia, characterized by elevated total cholesterol, triglycerides and low-density lipoprotein cholesterol (LDL-C), alongside reduced high-density lipoprotein cholesterol (HDL-C) represents a significant modifiable risk factor for CVD development (2). High-fat diets (HFDs) are

well-established dietary factors that induce dyslipidemia by disrupting lipid homeostasis and promoting excessive lipid accumulation in blood vessels (3). This chronic metabolic dysregulation initiates a cascade of pathological events, including increased production of reactive oxygen species, inflammatory cytokine release, and endothelial dysfunction, which collectively accelerate atherosclerosis progression (4). This pathological process involves lipid infiltration into arterial walls, foam cell formation, and extracellular matrix remodeling, ultimately leading to vascular stiffening and reduced blood flow (4).

Currently, HMG-CoA reductase inhibitors (statins) are widely used as a pharmacological treatment for atherosclerosis. Atorvastatin reduces LDL-cholesterol and triglycerides while increasing HDL-cholesterol levels, thereby reducing cardiovascular risk (5). It suppresses cholesterol production in the body, decreasing the amount of cholesterol that may build up on the walls of the arteries and block blood flow to the heart, brain, and other parts of the body. Despite these beneficial effects, statins can have adverse effects such as diarrhea, heartburn, and memory loss (5, 6). Due to the potential side effects of long-term statin usage, there is increasing interest in exploring natural compounds with lipid regulation and vascular-protective properties as alternative or complementary therapies. Natural bioactive compounds, particularly those with antioxidant and anti-inflammatory effects, may offer cardioprotective benefits while minimizing adverse effects associated with conventional lipid-lowering drugs.

Mulberries (*Morus alba L.*) are widely cultivated in the northern and northeastern regions of Thailand. Local people have traditionally used it as medicine (7). Several pharmacological studies have demonstrated that mulberry extracts exhibit beneficial effects in alleviating metabolic disorders such as diabetes, obesity, dyslipidemia, and atherosclerosis (8-10), and more detail of mulberries' properties are availiable in a recent review article (11). Mulberry fruit is rich in anthocyanins, including cyanidin-3-glucoside and cyanidin-3-rutinoside (12). Moreover, it is rich in vitamins, trace elements, and is known for its abundant phenolic compounds, including cyanidin-3-O-glucoside, cyanidin-3-O-rutinoside, rutin, isoquercitrin, resveratrol, and caffeic acid, etc. (11, 12). These phenolic substances give mulberries a variety of biological activities, including antioxidant, antibacterial, anti-inflammatory, hepatoprotective, anti-apoptotic, and immune system enhancing, which have a wide range of applications in food, cosmetic, and pharmaceutical industries (11, 13).

Although the metabolic benefits of mulberry have been demonstrated, its effects on vascular health and remodeling remain inadequately understood. Vascular remodeling, a critical process in atherosclerosis progression, involves structural and functional alterations of the vessel wall in response to pathological stimuli (14). These changes include endothelial dysfunction, smooth muscle cell proliferation, extracellular matrix reorganization, and inflammatory cell infiltration, which ultimately lead to arterial wall thickening and reduced vascular compliance (15). Understanding how mulberry affects these processes is essential for evaluating its potential in cardiovascular disease prevention.

Previous studies investigating mulberry's cardiovascular effects have predominantly focused on lipid profiles, oxidative stress markers, and inflammatory mediators, with limited attention to histopathological alterations in the vascular wall (16, 17). But there is lack of study combining biochemical assessments and histological analyses to elucidate mulberry's impact on vascular structure.

To fill this research gap, this present study investigated the effects of crude mulberry fruit extract on both lipid metabolism and aortic histopathology in high-fat diet-induced dyslipidemic rats, using atorvastatin as a reference standard. We hypothesized that mulberry extract would not only improve lipid profiles but also provide protection against vascular remodeling through its antioxidant and anti-inflammatory properties. This investigation into the relationship between metabolic improvements and vascular structural changes offers important insights into mulberry extract's potential as a comprehensive cardioprotective agent in dyslipidemia.

Materials and Methods

Mulberry preparation

Crude extract of mulberry fruit (CEM) was prepared by the Department of Pharmacy and Natural Products, Scientific Research Institute and Technology of Thailand (TISTR). The extraction process involved maceration of fresh mulberry fruits in 70% ethanol at room temperature for 72 hours, followed by filtration and evaporation under reduced pressure at 40°C. The resulting extract was lyophilized to obtain a dark purple viscous extract, which contains a high concentration of anthocyanins. The anthocyanin content was determined by high-performance liquid chromatography. The extract was stored protected from light at −20°C in airtight containers to maintain stability throughout the experimental period.

Animal model of dyslipidemia

Twenty male Wistar rats (aged 8-week-old and weight between 250-300 g) were obtained from Nomura Siam International Co. Ltd., Bangkok, Thailand. All experiments were approved by Naresuan University Animal Care and Use Committee (NUACUC), Phitsanulok, Thailand, with an ethical protocol number of NU-AE 610730. After 7-day of acclimatization, animals were maintained in a controlled room with a temperature of 22±1 °C, a 12-hour light/dark cycle, and had free access to food and water. The rats were randomly divided into 4 groups, with each group containing 5 rats. Each group was given a different diet for 90 days:

i. Control (ND) group: rats received a vehicle (water) by gavage and were fed a normal diet (protein 28.2%, carbohydrate 52%, total fat 19.8%, energy density 4.2 kcal/g).

ii. Dyslipidemia (HFD) group**:** rats received a vehicle (water) by gavage and were fed a high-fat diet (HFD) supplemented with sugar (protein 26.5%, carbohydrate 14.3%, total fat 59.28%, sodium chloride 0.1% w/w, energy density 5.35 kcal/g, propylene glycol).

iii. HFD+CEM group: rats were fed with HFD and crude extract of mulberry fruit 100 mg/kg/day was administered by gastric tube once daily as an aqueous suspension.

iv. HFD+ATV group: rats were fed with HFD and atorvastatin 10 mg/kg/day was administered by gastric tube once daily as an aqueous suspension.

All groups had ad libitum access to water throughout the 24-week study period. During the 90-day study, the rats were weighed weekly, and behavioral observations were conducted regularly to characterize welfare state. Food intake was monitored every 3 days throughout the study period. Before euthanasia on the 91st day, the rats underwent a fasting period of 6–8 hours to ensure consistent metabolic conditions. Blood samples were collected via inferior vena cava under anesthesia for lipid profile analysis. Following euthanasia by cardiac incision, aortic tissues were harvested for histological examination.

Blood biochemical analysis

Blood samples were collected in tubes containing EDTA and centrifuged at 3,000 rpm for 10 minutes at 4°C to separate plasma. Total cholesterol (TC), triglycerides (TG), high-density lipoprotein cholesterol (HDL-C), and low-density lipoprotein cholesterol (LDL-C) were measured using commercial enzymatic kits (Wako Pure Chemical Industries, Osaka, Japan) according to the manufacturer's instructions. All measurements were performed in duplicate with coefficients of variation less than 5%.

Tissue collection and histological analysis

Rats were deeply anesthetized with thiopental sodium (75 mg/kg, ip), and the thoracic aorta was carefully excised from the aortic arch to the diaphragm and rinsed with cold phosphate-buffered saline to remove residual blood. The aortic tissues were immediately fixed in 10% neutral-buffered formalin for 48 hours at room temperature. Following fixation, the samples were dehydrated through a graded ethanol series (70%, 80%, 90%, and 100%, 2 hours each), cleared in xylene (2 changes, 1 hour each), and embedded in paraffin with the cut surface placed downward in the mold. Serial cross-sections of 5 µm thickness were obtained using a rotary microtome (Leica RM2235, Leica Biosystems, Germany) and mounted on glass slides for histological analysis. A minimum of two sections per animal were prepared for each staining method. For general histological assessment, sections were stained with hematoxylin and eosin (H&E) to evaluate aortic wall thickness and cellular morphology following standard protocols. To assess collagen deposition and extracellular matrix organization, adjacent sections (two sections per animal) were stained with Masson's trichrome, following the manufacturer's instructions (Sigma-Aldrich, St. Louis, MO, USA). All stained slides were examined under a light microscope (Olympus BX53, Tokyo, Japan) equipped with a digital camera (Olympus DP74) at magnifications of 40× and 200×. Images were captured by an investigator blinded to the experimental groups to avoid bias. Quantitative analysis was performed using ImageJ software (National Institutes of Health, Bethesda, MD, USA, version 1.53a).

Aortic morphometric measurements

Aortic structural parameters were measured using histological images following previously established methods (18) by using ImageJ software (Figure 1). Four random fields per section were analyzed at 200× magnification. All measurements were performed by two independent observers blinded to the treatment groups to ensure reliability, with inter-observer variability less than 10%:

i. Aortic internal diameter: The first measurement line was drawn across the widest part of the lumen (A-B, Figure 1). A second perpendicular line was drawn through the center of the first line (C-D, Figure 1), and the two values were averaged.

ii. Aortic external diameter: Using the same measurement lines as the internal diameter, this was measured from outer side of the tunica media (E-F,

Figure 1) to the opposite outer side (G-H, Figure 1) and averaged.

iii. Aortic wall thickness: The aortic wall thickness measurement, from tunica intima to tunica media the lines must be perpendicular to the aortic walls. Meanwhile, the measurement started from the intersection point on the aorta from the internal diameter measurement in 4 corners (A-E, B-F, C-G, and D-H, Figure 1) and averaged.

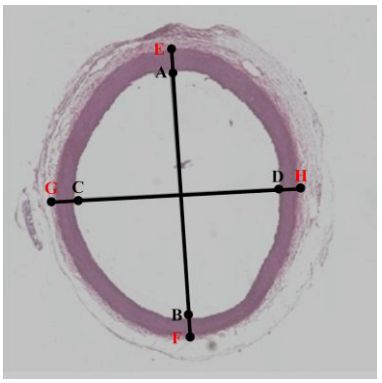

Fig.1 Illustration of H&E staining of aorta demonstrating measurement method of aortic internal diameter, aortic external diameter, and aortic wall thickness assessment.

Statistical analysis

Data analysis was performed using GraphPad Prism software (Version 10.0, GraphPad Software, CA, USA). All results were expressed as mean ± standard deviation (SD). Statistical comparisons between groups were conducted using one-way ANOVA followed by Tukey's post hoc test for multiple comparisons. Pearson's correlation coefficient was calculated to evaluate relationships between lipid parameters and aortic wall thickness. A p-value of less than 0.05 was considered statistically significant.

Results

Anthocyanin content of mulberry extract

The total anthocyanin content of the CEM was quantified and found to be 1,250 mg per 100 g of extract, expressed as cyanidin-3-glucoside equivalents. This high concentration of anthocyanins reflects the bioactive richness of the extract and supports its potential antioxidant and lipid-lowering properties evaluated in this study.

Animal behavior and body weight

All animals exhibited normal behavior throughout the experimental period, with no observable changes in skin, fur, eyes, or mucous membranes. There were no signs of behavioral abnormalities or adverse effects, including tremors, convulsions, salivation, diarrhea, lethargy, coma, or death in any of the groups.

No significant differences in body weight were observed between the four experimental groups after 90 days of treatment (Table 1; $p>0.05$), suggesting that neither the high-fat diet nor the treatments significantly affected body weight gain over the experimental period.

Effects of CEM on lipid profiles

The effects of CEM and atorvastatin on lipid profiles in HFD-induced dyslipidemic rats were presented in Table 1. After 90 days, the HFD group exhibited significant dyslipidemia compared to the ND group, as evidenced by increased total cholesterol (31% increase; $p<0.001$), triglycerides (38% increase; $p<0.01$), and LDL (263% increase, $p<0.001$).

Supplementation with CEM in HFD-fed rats significantly improved these lipid parameters. Compared to the HFD group, total cholesterol decreased by 12% ($p < 0.05$), and LDL by 25% ($p < 0.05$).

Similarly, ATV treatment demonstrated potent lipid-modulating effects, with significant reductions in total cholesterol (20% decrease; $p<0.001$), triglycerides (28% decrease; $p<0.05$), and LDL (26% decrease; $p<0.05$) compared to the HFD group. However, HDL cholesterol levels did not differ significantly among the groups.

Aortic histopathological observations

H&E staining of aortic sections (Figure 2) revealed normal histoarchitecture in the ND group (Figures 2A and B), with a thin, intact endothelium, well-organized elastic laminae, and regularly arranged smooth muscle cells in the media. In contrast, the HFD group (Figures 2C and D) exhibited substantial changes, including intimal thickening, disruption of elastic laminae, and increased smooth muscle cell density in the media.

The HFD+CEM group (Figures 2E and F) showed similar histopathological alterations to the HFD group, with notable medial thickening and disorganization of elastic fibers. In contrast, the HFD+ATV group (Figures 2G and H) maintained near-normal aortic morphology, with minimal changes in the intima and media compared to the ND group.

Table 1 Metabolic parameters data.

Parameters	ND	HFD	HFD+CEM	HFD+ATV
Body weight (g)	527.20±53.42	522.60±43.06	521.50±33.51	525.20±50.23
Total cholesterol (mg/dL)	53.40±3.58	70.00±6.67 ***	61.40±3.51 †	56.00±3.81 †††
Triglyceride (mg/dL)	16.20±3.56	22.40±2.07 *	18.50±3.08	16.00±2.12 †
LDL (mg/dL	10.40±0.55	37.80±9.47 ***	28.20±1.79 ***, †	27.60±3.13 ***, †
HDL (mg/dL)	31.40±2.19	27.80±3.56	28.40±3.91	26.60±2.88

Table 1. The effects of CEM on metabolic parameters in high-fat-diet rats. Mean ± Standard deviation;
* p<0.05 vs ND, *** p<0.001 vs ND, † p<0.05 vs HFD, ††† p<0.001 vs HFD;
One way ANOVA followed by Tukey's post hoc test. (n=5/groups).

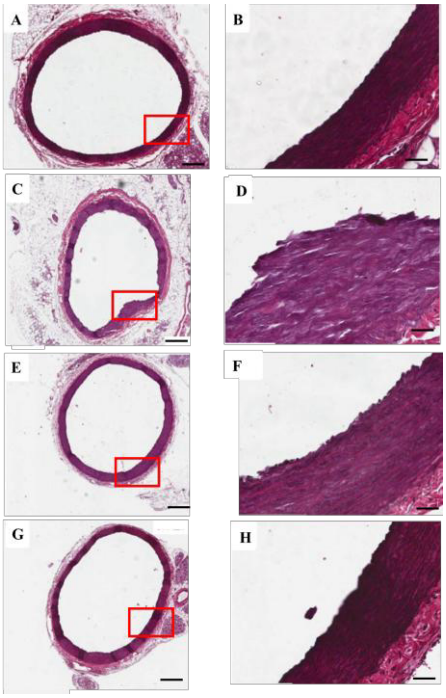

Fig.2 Representative histological images of the aorta from different experimental groups stained with H&E. Panels (A) and (B) show normal diet (ND) rats, (C) and (D) show high-fat diet (HFD) rats, (E) and (F) show HFD rats treated with crude mulberry extract (HFD+CEM), and (G) and (H) show HFD rats treated with atorvastatin (HFD+ATV). 20x and 200x magnification images are shown in (A, C, E, G) and (B, D, F, H), respectively. Scalebar = 500 µm (A, C, E, G) and 50 µm (B, D, F, H).

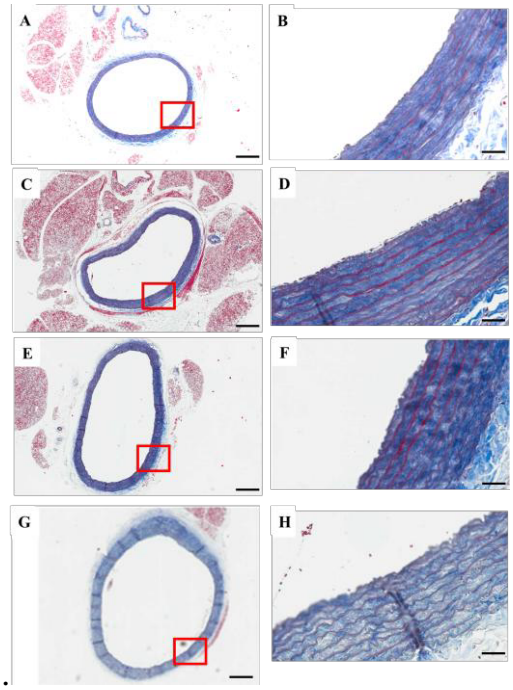

Fig.3 Representative histological images of the aorta from different experimental groups stained with Masson's trichrome. Panels (A) and (B) show normal diet (ND) rats, (C) and (D) show high-fat diet (HFD) rats, (E) and (F) show HFD rats treated with crude mulberry extract (HFD+CEM), and (G) and (H) show HFD rats treated with atorvastatin (HFD+ATV). 20x and 200x magnification images are shown in (A, C, E, G) and (B, D, F, H), respectively. Scalebar = 500 µm (A, C, E, G) and 50 µm (B, D, F, H).

In Masson's trichrome staining for collagen fiber and fibrosis of the aorta (Figure 3), the qualitative investigation by three anatomists shows that the HFD and HFD+CEM groups have more staining of collagen fibers than the ND group. The HFD+ATV group showed similar staining of collagen fibers as the ND group. Also, the aorta sections of all these groups show well-formed elastic fibers that are oriented in a lamellar pattern in their tunica media.

Aortic morphometrical changes

The effects of HFD, CEM, and ATV on aortic morphology are presented in Figure 4. The HFD group (1.60±0.16 mm) exhibited an 11.11% increase in aortic internal diameter compared to the ND group (1.44±0.06 mm), but non-significant ($p > 0.05$). Similar trends were observed in the HFD+CEM (14.58%, 1.65±0.15 mm) and HFD+ATV (13.19%, 1.63±0.20 mm) groups.

Likewise, aortic external diameter measurements revealed no significant differences among the four groups (ND: 1.64±0.07 mm, HFD: 1.86± 0.20 mm, HFD+CEM: 1.95± 0.16 mm, HFD+ATV: 1.88±0.23 mm; $p>0.05$), although a slight increasing trend was observed in the HFD group.

In contrast, aortic wall thickness was significantly higher in both the HFD (0.147±0.029 mm) and HFD+CEM (0.145±0.018 mm) groups compared to the ND group (0.094±0.007 mm; $p<0.01$), representing increases of 56.4% and 54.3%, respectively. Interestingly, treatment with atorvastatin (HFD+ATV: 0.117±0.013 mm) slightly reduced aortic wall thickness to a level comparable to the ND group ($p=0.087$).

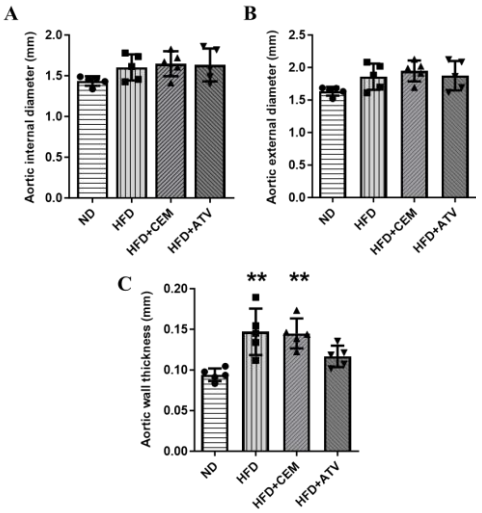

Fig.4 Aortic dimension measurements: (A) aortic internal diameter (mm), (B) aortic external diameter (mm), and (C) aortic wall thickness (mm). Significant differences were observed at **$p \leq 0.01$ vs ND.

Discussion

Our findings indicate that HFD feeding for 90 days induced significant dyslipidemia in rats, characterized by elevated total cholesterol, triglycerides, and LDL level compared to the ND group. Administration of CEM effectively improved these lipid profiles, confirming its potential as a lipid-lowering agent. However, histopathological examination revealed an important dichotomy: despite improved lipid profiles, CEM treatment failed to prevent HFD-induced vascular remodeling, as evidenced by significant increases in aortic wall thickness and collagen deposition comparable to untreated HFD rats. This dissociation between lipid improvement and vascular protection suggests that dyslipidemia and vascular remodeling likely arise through separate mechanisms, with CEM only effectively addressing the former. This finding represents a novel observation with important implications for understanding the differential pathways involved in HFD-induced cardiovascular damage. A previous study by Zhao et al. (19) reported that mulberry fruit extract supplementation lowered serum triglyceride and cholesterol levels in HFD-fed rats, consistent with our observations. However, our histopathological assessment extends these findings by revealing that such metabolic improvements may not translate to vascular protection.

Dyslipidemia is a primary driver of atherosclerosis and cardiovascular disease, often leading to vascular remodeling. Natural compounds like anthocyanins, found in mulberry, have been proposed as potential lipid-lowering agents due to their antioxidant and anti-inflammatory properties (20, 21). Inflammatory mediators (i.e., TNF-α, IL-6, and hsCRP) play crucial roles in vascular remodeling following HFD consumption (22). Prior studies in both human and animal models have shown that atherosclerotic lesions often arise in areas of preexisting intimal hyperplasia, suggesting that structural changes may precede lipid accumulation in the vascular wall (23-26).

Histological assessment of the aorta using H&E staining showed a significant increase in wall thickness in the HFD group, despite no alterations in external or internal diameters. This suggests that vascular remodeling occurred, potentially due to increased extracellular matrix deposition or smooth muscle cell proliferation. This increase in aortic thickness was not prevented by consumption of the CEM.

The persistent aortic wall thickening observed in the CEM-treated group suggests that mechanisms beyond lipid accumulation contribute to vascular remodeling in this context. Several potential explanations warrant consideration. First, anthocyanins and other bioactive compounds in mulberry might not exert direct effects on vascular smooth muscle cell proliferation or extracellular

matrix production (27). Secondly, the dosage used in our study (100mg/kg/day) may have been insufficient to counter established vascular changes, despite being adequate for lipid modulation. Third, the duration of treatment (90 days) may have been too short to reverse structural alterations that had already developed (28).

While anthocyanins have been reported to reduce aortic wall thickening in some contexts (29), our findings indicate that the anthocyanin content or formulation in our mulberry extract may not have provided comparable vascular protection. Notably, atorvastatin administration maintained aortic wall thickness comparable to the ND group, reinforcing its well-established role in vascular protection.

The contrasting effects observed with atorvastatin are particularly informative. Atorvastatin treatment not only improved lipid profiles but also maintained aortic morphology comparable to control animals. This suggests that statins may possess vascular protective mechanisms beyond lipid modulation, including anti-inflammatory and antioxidant properties that directly influence vascular wall homeostasis (30). The differential outcomes between CEM and atorvastatin highlight the complexity of vascular protection and the need for comprehensive evaluation of potential therapeutic agents.

Our findings have important implications for the use of natural compounds in cardiovascular health. While many plant-derived products demonstrate beneficial effects on metabolic parameters, their impact on vascular structure and function may be more nuanced (31). This underscores the necessity of comprehensive evaluation that extends beyond serum biomarkers to include direct assessment of target tissues.

This study has several limitations that should be acknowledged. First, we examined a single dose of mulberry extract; dose-dependent effects may exist but were not captured. Second, while histological examination provides valuable structural information, functional measures of vascular reactivity would offer complementary insights (32). Third, molecular markers of inflammation and oxidative stress were not assessed, limiting mechanistic interpretations. Fourth, our study examined only male rats; sex-specific differences may exist in responses to both HFD and treatments (33). Another is that diet and treatment were commenced at the same time, whether the benefits remain if treatment is commenced after dyslipidemia has set in remains unclear.

Future investigations should address these limitations while investigating additional histological and biochemical markers to better understand the mechanisms underlying vascular changes. Incorporating measurements of inflammatory cytokines, oxidative stress indicators, and direct vascular cell responses would be particularly valuable for elucidating the pathways involved. Additionally, examination of different extraction methods, dosages, and treatment durations could help optimize the potential vascular benefits of mulberry-derived compounds and determine whether higher concentrations or longer interventions might effectively prevent HFD-induced vascular remodeling.

Conclusion

Crude mulberry extract demonstrates significant lipid-lowering properties in HFD-fed rats but is also associated with increased aortic wall thickness, raising concerns about its impact on vascular remodeling. In contrast, atorvastatin effectively maintained normal aortic structure, highlighting differences in their cardiovascular effects. Further investigations are necessary to elucidate the underlying mechanisms and evaluate its safety and therapeutic potential in cardiovascular disease prevention.

Acknowledgements

This research was partially financial supported by Naresuan University (NU), and National Science, Research and Innovation Fund (NSRF) (Grant No. R2566B062), and the Agricultural Research Development Agency (Public Organization) (Grant No. CRP6205031380). This collaboration was also partially supported by Reinventing University Program 2023-2025, The Ministry of Higher Education, Science, Research and Innovation (MHESI), Thailand (Grant No. R2566A043, R2568A026, R2567A147, R2568A037, R2568A033). And the YT and KC was partially funded by Global and Frontier Research University Fund, Naresuan University (Grant No. R2567C003, and R2566C053, respectively). The authors would like to thank the Faculty of Medical Sciences, Naresuan University, and the ICRU's members for their support throughout this research. We would also like to express our gratitude to Peter J Mark and Caitlin Wyrwoll (University for Western Australia), for their support and assistance, particularly with manuscript writing.

References

1. (WHO). WHO. Cardiovascular diseases (CVDs) 2022 [Available from: https://www.who.int/news-room/fact-sheets/detail/cardiovascular-diseases-(cvds).

2. Arvanitis M, Lowenstein CJ. Dyslipidemia. Annals of Internal Medicine. 2023;176(6):Itc81-itc96.
3. Garg R, Aggarwal S, Kumar R, Sharma G. Association of atherosclerosis with dyslipidemia and co-morbid conditions: A descriptive study. Journal of Natural Science, Biology and Medicine. 2015;6(1):163-8.
4. Burtenshaw D, Kitching M, Redmond EM, Megson IL, Cahill PA. Reactive Oxygen Species (ROS), Intimal Thickening, and Subclinical Atherosclerotic Disease. Frontiers in Cardiovascular Medicine. 2019;6:89.
5. Lennernäs H. Clinical pharmacokinetics of atorvastatin. Clinical Pharmacokinetics. 2003;42(13):1141-60.
6. García-Campa M, Flores-Ramírez R, Rojo-Garza S, Carrizales-Sepúlveda EF, Regalado-Ceballos D, Reyes-Araiza R, et al. Atorvastatin before percutaneous coronary intervention: A systematic review and meta-analysis. PLoS One. 2024;19(1):e0293404.
7. Yuan Q, Zhao L. The Mulberry (Morus alba L.) Fruit-A Review of Characteristic Components and Health Benefits. Journal of Agricultural and Food Chemistry. 2017;65(48):10383-94.
8. Chen C-C, Liu L-K, Hsu J-D, Huang H-P, Yang M-Y, Wang C-J. Mulberry extract inhibits the development of atherosclerosis in cholesterol-fed rabbits. Food Chemistry. 2005;91:601-7.
9. Jiang T, Liu Y, Meng Q, Lv X, Yue Z, Ding W, et al. Hydrogen sulfide attenuates lung ischemia-reperfusion injury through SIRT3-dependent regulation of mitochondrial function in type 2 diabetic rats. Surgery. 2019;165(5):1014-26.
10. Zhang H, Ma ZF, Luo X, Li X. Effects of Mulberry Fruit (Morus alba L.) Consumption on Health Outcomes: A Mini-Review. Antioxidants (Basel). 2018;7(5).
11. Adthapanyawanich K, Aitsarangkun Na Ayutthaya K, Kreungnium S, Mark PJ, Nakata H, Chen W, et al. Molecular Mechanisms and Therapeutic Potential of Mulberry Fruit Extract in High-Fat Diet-Induced Male Reproductive Dysfunction: A Comprehensive Review. Nutrients. 2025;17(2):273.
12. Khoo HE, Azlan A, Tang ST, Lim SM. Anthocyanidins and anthocyanins: colored pigments as food, pharmaceutical ingredients, and the potential health benefits. Food and Nutrition Research. 2017;61(1):1361779.
13. Xu L, Cheng J-R, Liu X-M, Zhu M-J. Effect of microencapsulated process on stability of mulberry polyphenol and oxidation property of dried minced pork slices during heat processing and storage. LWT. 2019;100:62-8.
14. Natić MM, Dabić D, Papetti A, Fotirić Akšić MM, Ognjanov V, Ljubojević M, Tešić Ž. Analysis and characterisation of phytochemicals in mulberry (Morus alba L.) fruits grown in Vojvodina, North Serbia. Food Chemistry. 2015;171:128-36.
15. Renna NF, de Las Heras N, Miatello RM. Pathophysiology of vascular remodeling in hypertension. International Journal of Hypertension. 2013;2013:808353.
16. Smeriglio A, Galati EM, Monforte MT, Lanuzza F, D'Angelo V, Circosta C. Polyphenolic Compounds and Antioxidant Activity of Cold-Pressed Seed Oil from Finola Cultivar of Cannabis sativa L. Phytotherapy Research. 2016;30(8):1298-307.
17. Mulvany MJ. Small artery remodelling in hypertension. Basic & Clinical Pharmacology & Toxicology. 2012;110(1):49-55.
18. Chivchibashi-Pavlova D, Stoyanov GS, Bratoeva K. Effects of Melatonin Supplementation on the Aortic Wall in a Diet-Induced Obesity Rat Model. Cureus. 2023;15(1):e33333.
19. Zhao X, Zhu J, Wang L, Li Y, Zhao T, Chen X, et al. U. diffracta extract mitigates high fat diet and VD3-induced atherosclerosis and biochemical changes in the serum liver and aorta of rats. Biomedicine & Pharmacotherapy. 2019;120:109446.
20. Matute-Bello G, Downey G, Moore BB, Groshong SD, Matthay MA, Slutsky AS, Kuebler WM. An official American Thoracic Society workshop report: features and measurements of experimental acute lung injury in animals. American Journal of Respiratory Cell and Molecular Biology. 2011;44(5):725-38.
21. Donno D, Turrini F. Plant Foods and Underutilized Fruits as Source of Functional Food Ingredients: Chemical Composition, Quality Traits, and Biological Properties. Foods [Internet]. 2020; 9(10).
22. Yang Y, Andrews MC, Hu Y, Wang D, Qin Y, Zhu Y, et al. Anthocyanin extract from black rice significantly ameliorates platelet hyperactivity and hypertriglyceridemia in dyslipidemic rats induced by high fat diets. Journal of Agricultural and Food Chemistry. 2011;59(12):6759-64.
23. Kim DN, Schmee J, Lee KT, Thomas WA. Atherosclerotic lesions in the coronary arteries of hyperlipidemic swine. Part 1. Cell increases,

divisions, losses and cells of origin in first 90 days on diet. Atherosclerosis. 1987;64(2-3):231-42.
24. Schwartz SM, deBlois D, O'Brien ER. The intima. Soil for atherosclerosis and restenosis. Circulation Research. 1995;77(3):445-65.
25. Shatoor AS, Al Humayed S, Alkhateeb MA, Shatoor KA, Aldera H, Alassiri M, Shati AA. Crataegus Aronia protects and reverses vascular inflammation in a high fat diet rat model by an antioxidant mechanism and modulating serum levels of oxidized low-density lipoprotein. Pharmaceutical Biology. 2019;57(1):38-48.
26. Stary HC, Blankenhorn DH, Chandler AB, Glagov S, Insull W, Jr., Richardson M, et al. A definition of the intima of human arteries and of its atherosclerosis-prone regions. A report from the Committee on Vascular Lesions of the Council on Arteriosclerosis, American Heart Association. Circulation. 1992;85(1):391-405.
27. Loizzo MR, Tundis R. Plant Antioxidant for Application in Food and Nutraceutical Industries. Antioxidants [Internet]. 2019; 8(10).
28. Qin Y, Xia M, Ma J, Hao Y, Liu J, Mou H, et al. Anthocyanin supplementation improves serum LDL- and HDL-cholesterol concentrations associated with the inhibition of cholesteryl ester transfer protein in dyslipidemic subjects. American Journal of Clinical Nutrition. 2009;90(3):485-92.
29. Virmani R, Kolodgie FD, Burke AP, Farb A, Schwartz SM. Lessons from sudden coronary death: a comprehensive morphological classification scheme for atherosclerotic lesions. Arteriosclerosis, Thrombosis, and Vascular Biology. 2000;20(5):1262-75.
30. Jennings A, Welch AA, Fairweather-Tait SJ, Kay C, Minihane AM, Chowienczyk P, et al. Higher anthocyanin intake is associated with lower arterial stiffness and central blood pressure in women. American Journal of Clinical Nutrition. 2012;96(4):781-8.
31. Oesterle A, Laufs U, Liao JK. Pleiotropic Effects of Statins on the Cardiovascular System. Circulation Research. 2017;120(1):229-43.
32. Giglio RV, Patti AM, Cicero AFG, Lippi G, Rizzo M, Toth PP, Banach M. Polyphenols: Potential Use in the Prevention and Treatment of Cardiovascular Diseases. Current Pharmaceutical Design. 2018;24(2):239-58.
33. Parsons C, Agasthi P, Mookadam F, Arsanjani R. Reversal of coronary atherosclerosis: Role of life style and medical management. Trends in Cardiovascular Medicine. 2018;28(8):524-31.

P-16

Ameliorate Potential of Astragaloside IV Against Atrazine-Induced Male Reproductive Toxicity: Evidence through *in vivo* and *in silico* Approaches

Isehaq Al-Huseini[1], Mohamed Al Mushaiqri[2], Firas Al-Majrafi[2], Nadia Al- Abri[3], Selvaraj Jayaraman[4], Srinivasa Rao Sirasanagandla[2*]
[1]Department of Physiology, College of Medicine and Health Sciences, Sultan Qaboos University, Muscat-123, Oman.
[2]Department of Human and Clinical Anatomy, College of Medicine and Health Sciences, Sultan Qaboos University, Muscat-123, Oman.
[3]Department of Pathology, College of Medicine and Health Sciences, Sultan Qaboos University, Muscat-123, Oman.
[4]Centre of Molecular Medicine and Diagnostics, Department of Biochemistry, Saveetha Dental College & Hospital, Saveetha Institute of Medical Technical Sciences, Chennai-600 077, India.
*Corresponding author, e-mail: srinivasa@squ.edu.om

Abstract
Background: Atrazine is the commonly used herbicide worldwide. It's a well-established endocrine-disrupting chemical that affects various systems of the body, including the male reproductive system. Astragaloside IV is a natural compound with substantial health benefits against various ailments. It is known to possess antioxidant and anti-inflammatory activities. However, its potential effects against the atrazine exposure-induced male reproductive toxicity have not been explored. This study aimed to explore the protective effects of astragaloside IV against atrazine -induced testicular toxicity in mice. **Methods:** After one week of acclimatization, eight-week-old CD-1 mice were randomly divided into four groups (n=10 in each group): vehicle control, atrazine, astragaloside IV, and atrazine + astragaloside IV. The mice were treated with two compounds, atrazine and astragaloside IV, at doses of 100 mg/kg/day and 40 mg/kg/day through the oral route for 21 days. At the end of the experiment, all mice were sacrificed to collect the plasma and tests for biochemical analysis and histopathological examination. Data was analyzed using one-way ANOVA followed by Bonferroni's multiple comparison test. Molecular docking studies were also performed to assess the interactions of atrazine and astragaloside IV with oxidative stress and inflammation-related proteins (glutathione, GPx, SOD, Nrf2, NF-κB, IL-1β, IL-6, TNF-α, cullin-3, and Keap-1). **Results:** Oxidative stress markers, including reduced glutathione, superoxide dismutase, and glutathione peroxidase activity, while malondialdehyde levels were elevated ($p<0.05$) in atrazine-exposed mice. Astragaloside IV supplementation significantly improved these markers ($p<0.05$). Atrazine exposure also decreased testosterone and androgen binding protein (ABP) levels ($p<0.05$), while astragaloside IV supplementation significantly increased these markers ($p<0.05$). Histopathology analysis showed damaged seminiferous epithelium in atrazine-exposed mice, which was mitigated by astragaloside IV supplementation. Molecular docking showed moderate interactions between atrazine and oxidative stress/inflammation-related proteins, with the strongest binding to glutathione (-5.5 kcal/mol). Astragaloside IV exhibited significant binding affinities for glutathione (-9.2 kcal/mol), cullin-3 (-9.1 kcal/mol), and Keap-1 (-8.9 kcal/mol). **Conclusion:** Our study concludes that astragaloside IV could serve as a promising natural compound in ameliorating the atrazine exposure-induced male reproductive toxicity. Further studies are needed to evaluate the molecular mechanisms underlying AS-IV supplementation associated beneficial effects.

Keywords *Atrazine, Astragaloside IV, Toxicity, Natural compound, Herbicide, Reproduction*

P-17

Localization of Diacylglycerol Lipase β in the Nuages Comprising Balbiani bodies of Primary Oocytes in Postnatal Mice

Anussara Kamnate[1], Wiphawi Hipkaeo[2]*
[1]Department of Anatomy, Faculty of Medicine, Princess of Naradhiwas University, Narathiwat, Thailand
[2]Division of Anatomy, Faculty of Medicine, Khon Kaen University, Khon Kaen, Thailand
*Corresponding author, e-mail: wiphawi@kku.ac.th

Abstract

Since endocannabinoids (eCBs) affect various reproductive events from the oogenesis and oocyte maturation to fertilization and from the implantation of the embryo to the final outcome of pregnancy, it is important to clarify intra-ovarian working sites of the eCB-receptor signal for maintenance of normal pregnancy. Diacylglycerol lipase (DGL) β is involved in the synthesis of an eCB 2-arachidonoylglycerol (2-AG). Using immuno-light and electron microscopy, DGLβ and cannabinoid receptor 1 (CB1), a receptor for 2-AG, have been shown to be localized in the primary oocytes of postnatal mice. As a result, DGLβ-immunoreactivity was specifically localized to the nuage of Balbiani bodies and small nuage-derivative structures, in which both amorphous materials and vesicle membranes were regarded as responsible for this localization. Nuage is a membrane-less electron-dense organelle and a major component of Balbiani body. It is involved in the regulation of gonad-specific RNAs. In contrast to the DGLβ-immunoreactivity, weak immunoreactivity for CB1 was detected throughout the ooplasm, where intracellular membranes of vesicles forming tiny scattered aggregates were responsible for its distribution; however, CB1 was not found in the Balbiani nuage. These two distinct localization patterns suggest two potential routes for the functional exertion of an eCB 2-AG synthesized by DGLs: first, 2-AG synthesized at all the DGL sites is released from oocytes and exerts paracrine or autocrine effects on adjacent intra-ovarian cells as well as on the oocytes themselves; and second, where 2AG synthesized within the nuage modulates the post-transcriptional processing of oocytes. However, due to the failure in detection of CB1 in the Balbiani nuage, the validity of the latter possibility remains to be clarified.

Keywords *Primary oocyte, Nuages, Endocannabinoid, Postnatal mice*

P-18

Development and Evaluation of 3D Anatomical Models from Thiel-Embalmed Cadavers Using Photogrammetry

Pattita Kanjanapisan[1], Tawanrat Paensukyen[1], Napawan Taradolpisut[1], Nutmethee Kruepunga[3], Kavin Tangmanpakdeepong[4], Athikhun Suwannakhan[2*]
[1] Biomedical Science Program, Faculty of Science, Mahidol University, Rama VI Road, Bangkok, Thailand
[2] Department of Anatomy, Faculty of Science, Mahidol University, Rama VI Road, Bangkok, Thailand
[3] Department of Anatomy, Faculty of Medicine, Kasetsart University, Bangkok, Thailand
[4] Mahidol University International College, Salaya, Nakhon Pathom, Thailand
*Corresponding author, e-mail: athikhun.suw@mahidol.ac.th

Abstract

Three-dimensional (3D) anatomical models are essential in medical education, providing an interactive and detailed approach to studying human structures. This research aims to improve anatomical education by creating high-resolution and easily accessible 3D models of the human arm using photogrammetry. The objective is to generate detailed 3D anatomical arm models from layer-by-layer dissections of two upper limbs of a Thiel-embalmed cadaver. The methodology involves dissecting the arm in sequential layers, capturing multi-angle photographs at each stage, and processing the images using Adobe Substance 3D sampler to construct 3D models. The models underwent further modification using Meshlab, and were uploaded to Sketchfab for viewing. To assess the educational value and clarity of the model, a questionnaire was distributed to undergraduate students. In this study, 15 models were created to illustrate the multi-layered dissection of the shoulder, axilla, arm, forearm, and hand regions. Overall, the questionnaire results indicated that students were generally satisfied with the 3D anatomical models generated, able to identify relevant anatomical structures similar to the actual cadaveric specimens, and these models are more realistic compared with those from formalin cadavers. These findings suggest that 3D models generated through photogrammetry hold significant educational value and could serve as alternatives to cadaveric specimens in certain educational settings. This research presents a cost-effective and innovative approach to anatomical education, enhancing accessibility, particularly in environments with limited access to cadaveric specimens.

Keywords *Three-dimensional models; Thiel cadavers; Photogrammetry; Medical education*

P-19

Previously Unrecognized Foramina of the Temporal Bone: An Anatomical Study

Tawanrat Paensukyen[1], Pattita Kanjanapisan[1], Napawan Taradolpisut[1], Laphatrada Yurasakpong[2], Nutmethee Kruepunga[3], Athikhun Suwannakhan[2*]
[1] Biomedical Science Program, Faculty of Science, Mahidol University, Rama VI Road, Bangkok, Thailand
[2] Department of Anatomy, Faculty of Science, Mahidol University, Rama VI Road, Bangkok, Thailand
[3] Department of Anatomy, Faculty of Medicine, Kasetsart University, Bangkok, Thailand
*Corresponding author, e-mail: athikhun.suw@mahidol.ac.th

Abstract

The external surface of the temporal bone is traditionally regarded as one of the most consistent anatomical regions of the human body. The only recognized variation is the postglenoid foramen, a rare emissary foramen located posterior to the glenoid fossa. From our observation, additional foramina are, however, present anterior or superior to the postglenoid process, which do not correspond to the postglenoid foramen or any other foramina previously described in anatomical literature. This suggests that the anatomy of the squamous part of the temporal bone requires reexamination to accurately account for these previously unrecognized foramina. This study aims to investigate the prevalence of these foramina and propose a novel classification system to better define their anatomical distribution. A total of 117 donor, 234 sides (97 dried skulls and 20 Thiel-embalmed cadavers) at Mahidol University, Faculty of Science, were examined. Foramina of the squamous part of the temporal bone were identified on 67 sides (28.6%), of which 61 were single and 6 were double. These foramina were classified into four types according to their locations, including preglenoid (56 cases = 23.9%), supra-arcuate (12 cases = 5.2%), postglenoid (4 cases = 1.7%), and glenoid (1 case = 0.4%). In three out of 67 cases (4.5%), the foramen was found communicating with the middle cranial fossa. The preglenoid foramen (n = 56) was located, on average, 1.3 ± 0.3 cm anterior to the postglenoid process and 0.4 ± 0.2 cm above the zygomatic arch of the temporal bone. The supra-arcuate foramen (n = 12) was positioned, on average, 1.5 ± 0.4 cm anterior to the postglenoid process along the suprameatal crest. The postglenoid foramen (n = 3) was found approximately 0.3 ± 0.1 cm posterior to the postglenoid process and 0.5 ± 0.1 cm above the suprameatal line. In summary, the present study provides, for the first time, details of anatomical description of foramina in the squamous part of the temporal bone. Understanding the accurate anatomy of these foramina is vitally important for surgeons and radiologists performing procedures around the ear region. Further studies are needed to investigate the structures passing through these foramina.

Keywords *Temporal bone; Foramen; Anatomical variations; Terminology*

P-20

Whey Protein Isolate Mitigates MPP+-Induced Neurotoxicity in SH-SY5Y Cells via Nrf2 Pathway Activation

Veerawat Sansri[1], Panlekha Rungruang[2,3], Morakot Sroyraya[4*]
[1] Department of Basic Medical Science, Faculty of Medicine Vajira Hospital, Navamindradhiraj University, Bangkok 10300, Thailand
[2] Molecular Medicine Program, Multidisciplinary Unit, Faculty of Science, Mahidol University, Bangkok 10400, Thailand
[3] Center of Excellence for Dental Stem Cell Biology, Faculty of Dentistry, Chulalongkorn University, Bangkok 10330, Thailand
[4] Department of Anatomy, Faculty of Science, Mahidol University, Bangkok 10400, Thailand
*Corresponding author e-mail: morakot.sry@mahidol.ac.th

Abstract

The pathogenesis of Parkinson's disease (PD) is associated with apoptosis of dopaminergic neurons in the substantia nigra pars compacta (SNpc) due to oxidative stress. The present study aimed to assess the antioxidant activity of whey protein isolate in Parkinson's disease models using neurotoxin exposed SH-SY5Y cells which were differentiated into dopaminergic like neurons. Our research indicates that whey protein isolate at concentrations of 5 to 1000 µg/ml is nontoxic to the differentiated SH-SY5Y cells. Interestingly, the lowest concentration of HMS90 (5 µg/ml) reduced the level of intracellular ROS in these cells when co-treated with 1-methyl-4-phenylpyridinium (MPP+) for 24 h. The antioxidant function of whey protein isolate was also established by the increased expression of HO1 and GPx antioxidant enzymes, the Nrf2 downstream targets, by RT-PCR. Also, Nrf2 nuclear translocation in the differentiated SH-SY5Y cells was increased when the cells were treated with 5 µg/ml whey protein isolate together with MPP+. This whey protein isolate may serve as a promising dietary supplement for neuroprotection in PD.

Keywords *Parkinson's disease, Whey protein isolate, MPP+, Nrf2, Antioxidant*

P-21

Anti-Oxidative Stress Effects of Simvastatin in Pancreatic Cells of High-Fat Diet-Fed Induced Obese Rats

Ratchadaporn Yoonakorn[1], Worarat Rojanaverawong[2], Pannita Holasut[2], Phisit Khemawoot[3], Pornpun Vivithanaporn[3], Pakakrong Kwankhao[4], Wachiraporn Thong-on[5], Chutima S. Vaddhanaphuti[2], Manussabhorn Phatsara[1]
[1] Department of Anatomy, Faculty of Medicine, Chiang Mai University, Thailand
[2] Department of Physiology, Faculty of Medicine, Chiang Mai University, Thailand
[3] Faculty of Medicine Ramathibodi Hospital, Mahidol University, Thailand
[4] Chao Phya Abhaibhubejhr Hospital, Prachinburi, 25000, Thailand
[5] Chao Phya Abhaibhubejhr Hospital Foundation, Prachinburi, 25000, Thailand
*Corresponding author, e-mail: manussabhorn.p@cmu.ac.th

Abstract

Nowadays, high-fat diet consumption is increasing worldwide and could lead to obesity and its complications. Excess free fatty acids concomitantly stimulate insulin secretions along with glucose levels and are associated with mitochondrial dysfunction, which subsequently induces the over-production of reactive oxygen species. SOD1 is a well-known antioxidant enzyme against reactive oxygen species. Thus, modulation of SOD1 expression and/or function could restore cellular oxidative stress. This study aimed to examine the effects of simvastatin, the primary drug used for anti-hyperlipidemia, on pancreatic cells in high-fat diet-induced obese rats. Male Wistar rats were randomly divided into a normal diet-fed group (n=3) and a high-fat diet-fed group (n = 6), fed for 12 weeks. At the 12th week, the high-fat diet group was randomly divided into two groups: high-fat diet and high-fat diet treated with simvastatin drugs. The experiment continued for 12 weeks. The animals were sacrificed after fasting for 6-8 hours. A blood-tailed vein was collected to measure the triglyceride level by using a colorimetric enzyme kit. Pancreatic tissues were collected and immersed in 4% paraformaldehyde. Pancreatic sections were stained with hematoxylin and eosin for histopathological study and immunohistochemistry staining (anti-SOD1 antibody) for oxidative stress. The result showed a lowering of triglyceride circulation level and a positive effect on islet morphology in the high-fat diet treated with the simvastatin group compared to the high-fat diet group. Furthermore, the high-fat diet treated with the simvastatin group showed a higher intensity of positive signal and gene expression of SOD1. These findings suggest that simvastatin might reduce triglyceride levels in the bloodstream, enhance pancreatic islet morphology, and may reduce oxidative stress by increasing SOD1 in pancreatic beta cells.

Keywords *Obesity; Oxidative stress; Simvastatin; Superoxide dismutase (SOD1)*

Background

Obesity has been a significant public health concern for decades. Obesity is characterized by a BMI over 30, according to the World Health Organization (1). Obesity is associated with type 2 diabetes (2), non-alcoholic fatty liver disease (3), cardiovascular disease (4), and chronic kidney disease(5). A prolonged high-fat diet and/or glucose consumption is a key factor that initiates overweight and then leads to obesity (1). Insulin resistance is closely related to obesity and type 2 diabetes. Insulin resistance is when cells do not respond to insulin, while increased free fatty acids and glucose in the blood circulation. Then, pancreatic β-cells over-secrete insulin to help glucose enter the cells. Overloading β-cell function subsequently induces these cells' hyperplasia, dysfunction, and apoptosis (6, 7). Elevating free fatty acids (FFAs) together with glucose also induces glucolipotoxicity, mitochondrial dysfunction, and reactive oxygen species (ROS) (8, 9). Superoxide dismutase (Cu/ZnSOD; SOD1) is an antioxidant enzyme found in the cytosol. SOD1 activates superoxide radicals ($O_2\cdot -$) to transform into oxygen (O_2) and hydrogen peroxide (H_2O_2) (10). SOD1 overexpression reduces ROS and apoptosis in maternal diabetic-mellitus-induced embryonic mice (11). Simvastatin is an oral HMG-CoA reductase inhibitor that primarily acts on lowering cholesterol and low-density lipoprotein and reducing dyslipidemia (12). Simvastatin also has anti-inflammatory, antioxidant, and angiogenic effects in streptozotocin (STZ)-

treated Wistar albino rats (13). Nonetheless, the role of simvastatin on pancreatic cell function is limited. Therefore, this study aimed to examine the antioxidant effects of simvastatin on pancreatic cells in high-fat diet-induced obese rats.

Materials and Methods

Animal model

Male Wistar rats (170-190 g) were purchased from Nomura Siam International. All rats were housed in an individual cage in a controlled temperature room with a 12-hour light/dark cycle and food and water *ad libitum* for one week. After acclimatization, 9 rats were randomly divided into two groups. Three rats for the normal diet fed-group (C.P. Mice Feed Food no. 082, Bangkok, Thailand), which consists of 49.5% carbohydrate, 8.3% fat, 26.9% protein, 6.5% vitamins, and 3.4% fiber. 6 rats for the high-fat diet-fed group, which consists of 36.5% powdered normal diet (C.P. Mice Feed Food no. 082, Bangkok, Thailand), 31% lard, 25% casein, 1% cholesterol, 6% vitamin and mineral mixture, 3% DL-methionine, 0.1% yeast powder, and 0.1% sodium chloride (modified from the previous study (14)). The rats were fed for another 12 weeks.

Experimental design

In the 12th week of the experiment, the rats were divided into 3 subgroups: a normal diet-fed group (ND), a high-fat diet-fed group (HFD), and a high-fat diet treated with simvastatin at the dose of 40 mg/kg BW group (HFSim). At the 24th week of the experiment, all rats were injected with sodium thiopental after fasting for 6-8 hours. The blood was collected from the blood-tailed vein.

Triglyceride measurement

The sera were collected and kept at -80 °C. The triglyceride levels were measured by the enzymatic colorimetric assay (BLT00059, Erba Lachema s.r.o., Czech Republic). The absorbance was measured at 500 nm by BioTek Synergy 4 Hybrid microplate reader and Gen 5 1.11 software (Agilent, USA).

Hematoxylin and eosin staining

The pancreatic tissues were fixed in 4% paraformaldehyde and then embedded in a paraffin block. Sections were cut at 5 µm, deparaffinized, and rehydrated in a graded ethanol series, and then stained with hematoxylin and eosin. Seven islets were randomly selected from each non-consecutive pancreatic section. Each islet was measured 3 times for the islet area. The average of the region of interest (ROI) was analyzed for morphological analysis (modified from the previous study (15)). All sections were captured and analyzed using an Eclipse E200 Nikon microscope and ImageJ software (ImageJ 1.54 g, National Institutes of Health, USA).

Immunohistochemistry staining

The pancreatic sections were deparaffinized and rehydrated, incubated with 1X PBS, antigen retrieval in citrate buffer, and endogenous peroxidase was blocked through 3% H_2O_2, incubated with 3% normal goat serum for non-specific blocking. Then, sections were incubated with polyclonal rabbit anti-superoxide dismutase 1 (SOD1) primary antibody (1:40) (ab13498, Abcam, USA) for 1 hour at room temperature and overnight in 4 °C. After washing with PBS, biotin goat anti-rabbit IgG secondary antibody (1:200) (B-2770, Invitrogen, USA) was performed following by avidin-biotin complex kit (1:100) (Vector Laboratories, USA). 3 3'-diaminobenzidine tetrahydrochloride (DAB) was used to detect the reaction. The sections were then counterstained with hematoxylin. All sections were captured and analyzed by a Nikon microscope (Eclipse E200) and ImageJ software (ImageJ 1.54 g, National Institutes of Health, USA), respectively.

Real-time PCR (qPCR)

Total RNA was extracted from 0.1 g of pancreatic tissues, and then cDNA synthesis was performed. Two µL of each cDNA was used. β-actin was presented as an internal reference gene. Specific primer sequences are presented in Table 1.

Statistical analysis

All data were analyzed by using one-way ANOVA with GraphPad Prism Software. The difference between each group of the experiments was presented as mean ± SD. Probability values less than 0.05 were considered significant.

Results and Discussion

Triglyceride level

In Fig.1, the triglyceride levels are shown for all groups. The HFD group presented significantly higher than the ND group ($p < 0.01$). Interestingly, the HFSim group showed significantly decreased triglyceride levels compared to the HFD group ($p < 0.01$).

Morphological study

The pancreatic tissues in the ND group showed a normal histology. Normal size (39.82 ± 14.85), oval-shaped, and identified border of pale clumps of islets of Langerhans lined by crowed acinar cells were observed (Fig. 2A). In contrast, the HFD group

revealed a larger size of the islets (75.43 ± 36.74) with irregular shape and an unidentifiable border. Fat vacuoles have infiltrated into the pancreatic acinar part as a circle white area (Fig. 2B). Islets area significantly decreased in the HFSim group (49.74 ± 14.62) when compared to the HFD group ($p<0.01$) (Fig. 2D). The islet shape and border of the HFSim group appear similarly to those of the ND group (Fig. 2C). There are fewer fat vacuoles. Mean value ± SD in islet areas from all groups is presented (Fig. 2D).

Immunohistochemistry study

The immunohistochemistry staining using anti-SOD1 antibody to represent anti-oxidative stress effects on the islets of Langerhans. In the HFD group, SOD1 positive signals showed brown staining in the islets was significantly decreased (Fig. 3B) compared to the HFSim group (Fig. 3C) ($p < 0.05$) and the ND group (Fig. 3A) ($p < 0.05$), respectively. SOD1 intensity in islets of Langerhans from all groups are expressed as a mean value ± SD (Fig. 3D).

SOD1 gene expression levels

In Fig.4, the HFSim group revealed that the SOD1 expression level was significantly higher than in the HFD group ($p < 0.01$). Additionally, the SOD1 expression level in HFD was significantly lower than in the ND group ($p < 0.01$).

Table 1 Primer sequences

Gene	Primer sequences
SOD1	F: GCAGAAGGCAAGCGGTGAAC R: TAGCAGGACAGCAGATGAGT
β-actin	F: CCTAAGGCCAACCGTGAAAA R: GGAGCGCGTAACCCTCATAC

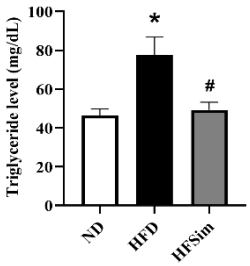

Fig. 1 Triglyceride level in serum. Mean value ± SD of triglyceride level. *$p < 0.01$ compared to the ND group. #$p < 0.01$ compared to the HFD group.

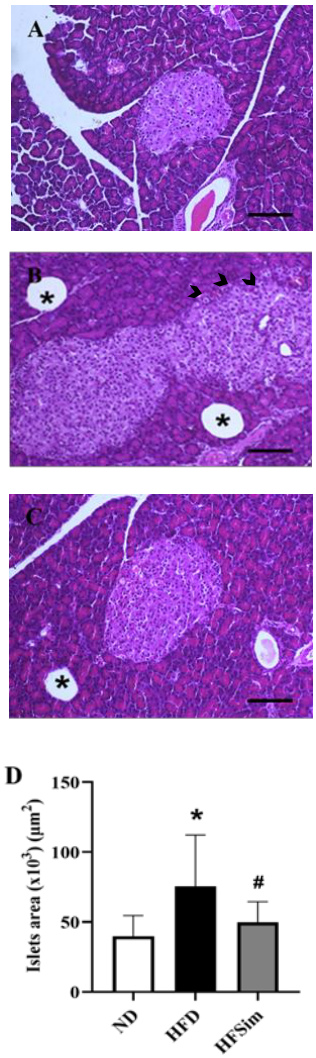

Fig. 2 Hematoxylin and eosin staining. (A) ND group. (B) The HFD group showed a larger islets area. (C) HFSim group showed a significantly decreased islets area when compared to the HFD group. A-C, magnification 20X. Asterisk indicated the fat vacuoles. Arrowhead indicated the zone of an unidentifiable border. Scale bar 100 µm. Mean value ± SD in islet areas from all groups is presented (D). *$p < 0.01$ compared to the ND group. #$p < 0.01$ compared to the HFD group.

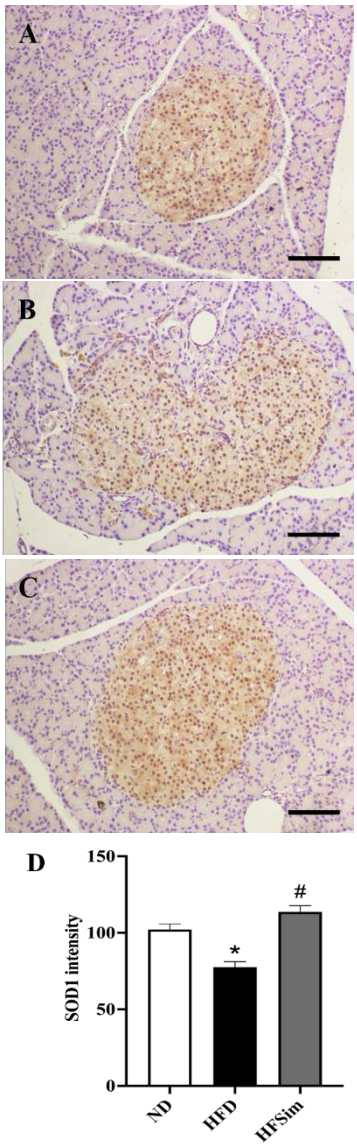

Fig. 3 Immunohistochemistry staining using anti-SOD1 antibody. The positive signals showed brown staining. ND group (A)The positive signals showed a significant increase in the HFSim group (C) when compared to the HFD group (B). A-C, magnification 20X. Scale bar 100 µm. Mean value ± SD of SOD1 intensity in islets of Langerhans from all groups is presented (D). *p < 0.05 compared to the ND group. #p < 0.05 compared to the HFD group.

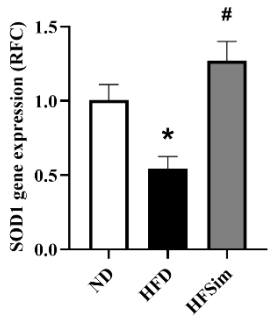

Fig. 4 The expression of the SOD1 gene in pancreatic tissues. Mean value ± SEM of SOD1 gene expression in islets of Langerhans from all groups is presented. *p < 0.01 compared to the ND group. #p < 0.01 compared to the HFD group.

High-fat diet consumption induces an increase in serum triglyceride levels, which may indicate obesity in our experimental rats, which is similar to a previous study. (16). Prolonged high-fat diet consumption can cause damage to pancreatic tissue, which then leads to abnormal histopathology (6). Elevating free fatty acids together with glucose levels stimulates pancreatic β-cells to secrete insulin (17). Excess dietary fat promotes free-fatty acid and also leads to extreme insulin secretion (18). This condition may affect the hypertrophy of islets and overload function (19). In this experiment, high-fat diet rats were used to mimic obese conditions. The HFD group showed an enlargement of pancreatic islets, unidentifiable borders, and fat vacuoles. Even though the fat vacuoles still exist in the HFSim group, the islets size were improved, and a border was identified. Simvastatin is a well-known lipid-lowering drug and hyperlipidemia treatment (12). A previous study has demonstrated increased pancreatic cell proliferation in diabetic rats treated with simvastatin (20). Simvastatin can also decrease triglyceride levels, which is also shown in the HFSim group. Fat accumulation and insulin resistance in obesity may induce ROS production by impaired β-oxidation in mitochondria and decreased antioxidant enzymes. In this study, the HFD group showed a significantly decreased SOD1 gene expression and SOD1 intensity level when compared to the ND and HFSim groups. Simvastatin increases SOD levels in high-fat diet-induced obese rats. Liu et al. (2013) reported that the TgSOD1 rat (SOD1 over-expression rat) fed with a high-fat diet can maintain glucose metabolism and reduce ROS production from mitochondria (21). Interestingly, the HFD group in this study also

presented macrophages migration in the pancreatic acinar part (data not shown). Marikovsky et al. (2003) revealed that macrophages could produce ROS and SOD-1 expression to prevent toxicity and inhibit apoptotic pathway in macrophages (22). Hence, this study suggests that simvastatin not only acts as pancreatic lipid-lowering effect, but it also exerts antioxidant properties by up-regulating SOD1 gene and protein expression. This could subsequently restore pancreatic histopathology in obesity conditions. Nonetheless, the precise mechanisms of antioxidant effect of simvastatin in pancreatic tissues need further investigation.

Conclusion

The administration of Simvastatin mitigates triglyceride circulating levels, improves pancreatic histopathology, and increases superoxide dismutase 1 (SOD1), a major antioxidant enzyme, gene, and protein expression, which may suggest reduced ROS production.

Acknowledgements

This study was partly supported by the Faculty of Medicine Graduate Student Scholarship, Chiang Mai University, and the Chao Phraya Abhaibhubejhr Hospital Foundation. The authors would like to thank Mr. Nobphaphit Saeyang and Miss Lamaiporn Peerapapong for their technical assistance.

References

1. Organization WH. Obesity and overweight 2024 [Available from: https://www.who.int/news-room/fact-sheets/detail/obesity-and-overweight.
2. Ruze R, Liu T, Zou X, Song J, Chen Y, Xu R, et al. Obesity and type 2 diabetes mellitus: connections in epidemiology, pathogenesis, and treatments. Frontiers in Endocrinology. 2023;14.
3. Wondmkun YT. Obesity, Insulin Resistance, and Type 2 Diabetes: Associations and Therapeutic Implications. Diabetes Metab Syndr Obes. 2020;13:3611-6.
4. Perone F, Spadafora L, Pratesi A, Nicolaio G, Pala B, Franco G, et al. Obesity and cardiovascular disease: Risk assessment, physical activity, and management of complications. International Journal of Cardiology Cardiovascular Risk and Prevention. 2024;23:200331.
5. Sharma I, Liao Y, Zheng X, Kanwar YS. New Pandemic: Obesity and Associated Nephropathy. Front Med (Lausanne). 2021;8:673556.
6. Bovolini A, Garcia J, Silva AF, Andrade MA, Duarte JA. Islets of Langerhans phenotype alterations induced by fatty diet and physical activity levels in Wistar rats. Nutrition. 2020;79-80:110838.
7. Cerf ME. Beta cell dysfunction and insulin resistance. Front Endocrinol (Lausanne). 2013;4:37.
8. Dludla PV, Mabhida SE, Ziqubu K, Nkambule BB, Mazibuko-Mbeje SE, Hanser S, et al. Pancreatic β-cell dysfunction in type 2 diabetes: Implications of inflammation and oxidative stress. World J Diabetes. 2023;14(3):130-46.
9. Qatanani M, Lazar MA. Mechanisms of obesity-associated insulin resistance: many choices on the menu. Genes Dev. 2007;21(12):1443-55.
10. Eleutherio ECA, Silva Magalhães RS, de Araújo Brasil A, Monteiro Neto JR, de Holanda Paranhos L. SOD1, more than just an antioxidant. Arch Biochem Biophys. 2021;697:108701.
11. Sato A, Shiraishi Y, Kimura T, Osaki A, Kagami K, Ido Y, et al. Resistance to Obesity in SOD1 Deficient Mice with a High-Fat/High-Sucrose Diet. Antioxidants. 2022;11(7):1403.
12. Talreja O, Kerndt CC, Cassagnol M. Simvastatin. StatPearls. Treasure Island (FL): StatPearls Publishing
Copyright © 2025, StatPearls Publishing LLC.; 2025.
13. Ahmed Yassin MD, Basma Nabil, M.Sc., Fleur Fathy MD, Amany Abdin, M.D. Comparative Study of the Effects of Topically Used Insulin and Simvastatin on Thermal Induced Burn in Diabetic Albino Rats. The Medical Journal of Cairo University. 2018;86(June):1837-45.
14. Kaewmalee J, Ontawong A, Duangjai A, Tansakul C, Rukachaisirikul V, Muanprasat C, et al. High-Efficacy α,β-Dehydromonacolin S Improves Hepatic Steatosis and Suppresses Gluconeogenesis Pathway in High-Fat Diet-Induced Obese Rats. Pharmaceuticals. 2021;14(4):375.
15. Adam SH, Giribabu N, Kassim N, Kumar KE, Brahmayya M, Arya A, et al. Protective effect of aqueous seed extract of Vitis Vinifera against oxidative stress, inflammation and apoptosis in the pancreas of adult male rats with diabetes mellitus. Biomed Pharmacother. 2016;81:439-52.
16. Tessari P, Tiengo A. Metformin treatment of rats with diet-induced overweight and hypertriglyceridemia decreases plasma triglyceride concentrations, while decreasing triglyceride and increasing ketone body output by the isolated perfused liver. Acta Diabetologica. 2008;45(3):143-5.
17. Cen J, Sargsyan E, Bergsten P. Fatty acids stimulate insulin secretion from human pancreatic islets at fasting glucose concentrations via mitochondria-dependent and -independent

mechanisms. Nutrition & Metabolism. 2016;13(1):59.
18. Chueire VB, Muscelli E. Effect of free fatty acids on insulin secretion, insulin sensitivity and incretin effect - a narrative review. Arch Endocrinol Metab. 2021;65(1):24-31.
19. Kahn SE, Hull RL, Utzschneider KM. Mechanisms linking obesity to insulin resistance and type 2 diabetes. Nature. 2006;444(7121):840-6.
20. Stancic A, Korac A, Otasevic V, Jankovic A, Korać B. The effect of simvastatin in pancreas of diabetic rats. Hrana i ishrana. 2018;59:19-25.
21. Liu Y, Qi W, Richardson A, Van Remmen H, Ikeno Y, Salmon AB. Oxidative damage associated with obesity is prevented by overexpression of CuZn- or Mn-superoxide dismutase. Biochem Biophys Res Commun. 2013;438(1):78-83.
22. Makhlouf A-M, Mahmoud A, Ibrahim R, Abdel Aziz Y. Effects of Vitamin D and Simvastatin on Inflammatory and Oxidative Stress Markers of High-Fat Diet-Induced Obese Rats. 2021;2:12.

P-22

Histological Study on the Effect of Rosuvastatin in the Lung Fibrosis Wistar Rat Model

David Pakaya[1*], Rais Trisiyambudi[1], Farid Indra Gunawan[1], Dion Solli Ruruktipa[1], Muhammad Yoland Muliadi[1], Mohammad Fiqri Novian Affandy[1], Mohammad Salman[1], Yuli Fitriana[1], Sarifuddin Anwar[2,3]
[1]Department of Histology, Faculty of Medicine, Tadulako University, Sukarno-Hatta Street Tondo, Palu, Indonesia
[2]Department of Anatomy, Faculty of Medicine, Tadulako University, Sukarno-Hatta Street Tondo, Palu, Indonesia
[3]Department of Pulmonology and Respiratory Medicine, Faculty of Medicine, Tadulako University, Sukarno-Hatta Street Tondo, Palu, Indonesia
*Corresponding author, e-mail: davidpakaya09@gmail.com

Abstract

Amiodarone administration in the long term at high doses can cause toxicity that promote inflammation or scarring and thickening of lung tissue. Rosuvastatin has anti-inflammatory and anti-fibrotic effects that can inhibit the synthesis and accumulation of extracellular matrix and collagenase activity. The aim of this study is to determine the anti-fibrotic effect of rosuvastatin on inter alveolar septum thickness and the percentage of fibrosis area in the pulmonary fibrosis rat model. This is an experimental research with a post test-only control group design. This study used 15 male Wistar rats 12 weeks of age, 200-220 grams of body weight (BW). The rats were divided into three treatment groups; K1: normal control; K2: pulmonary fibrosis rat model (rats received amiodarone 40mg/kg of BW); K3: pulmonary fibrosis rat model treated with 10 mg/kg of BW rosuvastatin. Histology of the inter alveolar septum thickness in the lung was performed using hematoxylin-eosin (H&E) and Sirius Red staining and evaluated in 5 randomly selected and non-overlapping fields of view using an Olympus CX23 light microscope at 400x magnification. The images were quantified using ImageJ software. Data were analyzed with GraphPad Prism 8.0.0 using the non-parametric Kruskal-Wallis test. The interalveolar septum thickness in the lung of the K3 group, which was given rosuvastatin was lower than that of the K2 group, with a significant difference ($p=<0.0001$). The percentage of fibrosis areas showed significant differences ($p=<0.0001$). In the conclusion rosuvastatin provides an anti-fibrotic effect by inhibiting excessive collagen deposition in the interalveolar septum of the rat lung during amiodarone administration.

Keywords *Rosuvastatin, Inflammation, Pulmonary fibrosis*

P-23

Digital PCR-Based Quantification of FRY Methylation as a Noninvasive Biomarker for Pancreatic Ductal Adenocarcinoma Screening

Kanidta Sooklert[1], Amornpun Sereemaspun[1], Nakarin Kitkumthorn[2*]
[1] Department of Anatomy, Faculty of Medicine, Chulalongkorn University, Bangkok, Thailand
[2] Department of Oral Biology, Faculty of Dentistry, Mahidol University, Bangkok, Thailand
*Corresponding author, e-mail: nakarinkit@gmail.com

Abstract

Pancreatic ductal adenocarcinoma (PDAC) is a highly lethal malignancy often diagnosed at advanced stages due to a lack of effective early screening tools. DNA methylation biomarkers in circulating cell-free DNA (cfDNA) offer a promising non-invasive approach for early detection. The FRY gene encodes a protein essential for proper cell division, and its aberrant methylation has been associated with several cancers, including PDAC. Specifically, methylation at cg16941656 has been shown to differentiate PDAC from other adenocarcinomas and benign biliary conditions, supporting its potential as a disease-specific biomarker. This study aims to evaluate the methylation of the FRY gene at cg16941656 in blood samples from PDAC patients using droplet digital PCR (ddPCR) and assess its potential as an early diagnostic biomarker. Blood samples were collected from 20 PDAC patients and 20 healthy individuals. Genomic DNA was extracted and bisulfite-treated, followed by analysis using qRT-PCR and ddPCR. The performance of methylated FRY detection in cfDNA was evaluated by sensitivity, specificity, and area under the curve (AUC) analysis. While qRT-PCR detected FRY methylation in only 2 of 10 PDAC samples, ddPCR demonstrated superior sensitivity, detecting methylation in 100% of PDAC samples and 5% of healthy controls. The ddPCR assay had an AUC of 0.992, with 95% sensitivity and 90% specificity. Methylation levels did not significantly differ by sex or tumor stage, suggesting its potential role in early detection. The ddPCR method also demonstrated a lower limit of detection (0.001 ng/μL) compared to qRT-PCR (0.01 ng/μL). FRY gene methylation detected by ddPCR in plasma cfDNA is a highly sensitive and specific biomarker for PDAC. Its non-invasive nature and ability to detect early-stage disease position it as a promising tool for screening and monitoring at-risk populations. Further large-scale studies are warranted to validate these findings and support clinical implementation.

Keywords *Pancreatic ductal adenocarcinoma, DNA methylation, FRY gene, Droplet digital PCR*

P-24

Cannabidiol Alters Early Neural Tube Formation and Disrupts Forebrain Development

Perawat Garunyapakun[1*], Phitchaporn Tongbai[2], Rungrada Sonpu[2], Nattpawit Kaewnoonual[1], Phetnarin Kobutree[1], Phornyupa Sanguanwong[1], Sirorat Janta[1]
[1] Anatomy unit, Department of Medical Science, Faculty of Science, Rangsit University, Pathum Thani, Thailand
[2] Biomedical Science Program, Faculty of Science, Rangsit University, Pathum Thani, Thailand
[*] Corresponding author, e-mail: perawat.g@rsu.ac.th

Abstract

The increasing use of cannabidiol (CBD) during pregnancy has raised concerns about its potential neurodevelopmental effects, particularly given the high expression of cannabinoid receptors in the developing nervous system. This study investigates the effects of CBD exposure on early neural tube formation and forebrain development using an *in ovo* chicken embryo model, which allows observation of early neural development stages in a vertebrate system with accessibility and clarity. At DAY 3, CBD exposure significantly reduced embryonic survival, suggesting early-stage embryotoxicity. However, histological analysis revealed that CBD-treated embryos exhibited accelerated neural tube differentiation, with distinct ependymal, mantle, and marginal zones forming earlier than in controls. This was accompanied by an increase in Sonic Hedgehog (SHH) protein expression, suggesting that CBD may influence early neural patterning through SHH signaling upregulation. At DAY 13, forebrain analysis revealed disruptions in cortical organization, including a narrowed ependymal zone, increased presence of mesenchymal cells, and reduced neurite outgrowth in CBD-treated embryos. These structural abnormalities suggest that while CBD may initially promote early neural tube maturation — potentially via stimulation of SHH pathways — it may subsequently interfere with the coordinated organization and differentiation of forebrain neurons. These findings raise concerns about the dual-phase effects of CBD on neural development and highlight the need for further investigation in mammalian models to determine its safety during pregnancy. A clearer understanding of CBD's impact on early neurodevelopment is essential for guiding public health policies and recommendations regarding cannabis use during gestation.

Keywords *Cannabidiol, Neural Tube Development, Forebrain Organization, In Ovo Model, Neurodevelopmental Disruption*

P-25

The Protective Role of *Moringa oleifera* extract Mitigates Methotrexate-Induced Neurotoxicity in the Dentate Gyrus of Rodent Models

Khlood Mohammed Mehdar*
Department of anatomy, Faculty of medicine, Najran University, Najran, Kingdom of Saudi Arabia
*Corresponding author, e-mail:

Abstract
Introduction: Methotrexate (MTX), an anticancer medication, is known to cause neurotoxicity, which limits its therapeutic use. The *Moringa oleifera leaf* extract (MLE) possesses antioxidant and anti-inflammatory properties, but its potential role in mitigating MTX-induced neurotoxicity has not been widely studied. **Objective:** This study aimed to investigate the protective effects of MLE against MTX-induced damage in the dentate gyrus (DG). **Material and Method:** Rats were administered MLE orally at a dose of 300 mg/kg body weight twice weekly for four weeks, with or without an intraperitoneal injection of 0.5 mg/kg MTX, also given twice weekly for the same duration. **Results:** MTX administration induced oxidative stress, as indicated by increased malondialdehyde levels and decreased superoxide dismutase (SOD) activity. It also altered dentate gyrus histopathology and triggered inflammation by elevated Toll-like receptor 4 (TLR4) expression. The TLR4 signalling cascade significantly increased Nucleotide-binding oligomerization domain (NOD)-like receptor family pyrin domain containing 3 (NLRP3) inflammasome expression and caspase-1. Notably, co-administration of MLE with MTX significantly reduced inflammation and oxidative stress, improving dentate gyrus structure. **Conclusion:** MLE exhibits antioxidant and anti-inflammatory effects that can alleviate MTX-induced neurotoxicity by down-regulating the brain's TLR4/NLRP3/caspase-1 pathway.

Keywords *Methotrexate, Moringa oleifera leaf extract, Neurotoxicity, Oxidative stress, Toll-like receptor 4, Methotrexate.*

P-26

Clausena Harmandiana Root Extract Improves Cognitive Impairments and Neuroinflammation Induced by Amyloid-β in Rats

Nutchareeporn Nillert[3], Chantana Boonyarat[2], Jariya Umka Welbat[1], Wanassanun Pannangrong[1]*
[1]Department of Anatomy, Faculty of Medicine, KhonKaen University, Mitaparb Road, KhonKaen 40002, Thailand
[2]Department of Pharmaceuticals, Faculty of Pharmaceutical Sciences, Khon Kaen University, Khon Kaen 40002, Thailand
[3]College of Oriental Medicine, Rangsit University, Phahon Yothin Road, Pathum Tani 12000, Thailand
*Corresponding author, e-mail:wankun@kku.ac.th

Abstract

Neuroinflammation caused by amyloid-β (Aβ) is associated with Alzheimer's disease (AD) pathogenesis. In AD, increased microglial activation followed by the release of pro-inflammatory cytokines, including interleukin-1β (IL-1β) and tumor necrosis factor-α (TNFα), results in cognitive impairments. *Clausena harmandiana* root extract (CHRE) exhibits various anti-inflammatory and pharmacological activities. This study aimed to investigate the effects of CHRE on $A\beta_{1-42}$-induced cognitive impairments and neuroinflammation. Adult male rats were randomly divided into 6 groups (n=8) of the sham control, V+Aβ, CB+Aβ, CHRE125+Aβ, CHRE250+Aβ, and CHRE500+Aβ. Sodium carboxymethylcellulose, Celebrex (10 mg/kg BW), and CHRE (125, 250, and 500 mg/kg BW) were given orally for 35 days. Rats were given CHRE (125, 250, and 500 mg/kg BW) by oral gavage for 35 days. On day 21, the rats were injected with $A\beta_{1-42}$ peptide into both lateral ventricles. Ten days later, their recognition memory was assessed using the novel object recognition test. All rats were then euthanized to observe the expression of $A\beta_{1-42}$ and inflammatory markers in the hippocampus. The expression of CD11b-positive microglia was examined by immunohistochemistry, and the western blot investigated two major pro-inflammatory cytokines (IL-1β and TNFα). The results indicated that pretreatment with CHRE at all doses attenuated short- and long-term recognition memory impairment. In addition, CHRE significantly decreased the expression of $A\beta_{1-42}$ and all inflammatory markers in the brain tissue, compared with the sham control group. This suggests that CHRE has a potential therapeutic effect against cognitive impairments and neuroinflammation induced by $A\beta_{1-42}$.

Keywords *Clausena harmandiana*, *Alzheimer's disease, Amyloid-β, Neuroinflammation, Recognition memory*

P-27

Effects of Curcumin Solid Dispersion on Neuronal Changes in Dexamethasone-induced Depression Model

Ponthip Cheenkhwan[1,6], Suchiwa Pan-on[2], Waree Tiyaboonchai[3,6], Samur Thanoi[4], Sawanya Charoenlappanit[5], Sittiruk Roytrakul[5], Sutisa Nudmamud-Thanoi[1,6], Jureepon Roboon[1,6*]
[1] Department of Anatomy, Faculty of Medical science, Naresuan University, Phitsanulok, Thailand
[2] Department of Cosmetic Science and Technology, Faculty of Pharmaceutical Sciences, Burapha University, Chonburi, Thailand
[3] Department of Pharmaceutical, Faculty of Pharmaceutical Sciences, Naresuan University, Phitsanulok, Thailand
[4] Department of Anatomy, School of Medical sciences, University of Phayao, Phayao, Thailand
[5] National Centre for Genetic Engineering and Biotechnology, National Science and Technology Development Agency, Pathum Thani, Thailand
[6] Centre of excellence in Medical Biotechnology, Naresuan University, Phitsanulok, Thailand
*Corresponding author, e-mail: jureeponr@nu.ac.th

Abstract

Depression is a prevalent mental disorder affecting millions worldwide. Curcumin, a polyphenolic compound from turmeric (Curcuma longa), is well known for its pharmacological properties, including anti-inflammatory, antioxidant, and neuroprotective effects. However, its therapeutic potential is limited by poor brain permeability and rapid systemic elimination, which reduces its effectiveness. To address these challenges, this study investigates the development of a curcumin solid dispersion (CSD) to enhance its absorption and bioavailability in the brain, thereby maximizing its therapeutic potential for depression treatment. This study aims to evaluate the neuroprotective effects of CSD and its impact on protein expression in a dexamethasone-induced depression model. Six-week-old male Sprague-Dawley rats were divided into five groups: a control group, a CSD-treated group, a DEX-induced group, "a DEX + CSD group and a DEX + Fluoxetine" group. Histological evaluation of the CA1 and CA3 hippocampal regions was conducted using hematoxylin and eosin (H&E) staining. Additionally, proteomic analysis was performed to examine protein expression within the TNF signaling pathway. Results indicated no significant difference in the number of normal neurons in the CA1 and CA3 regions among the groups. However, the DEX-induced group showed a trend toward decreased neuronal cell numbers compared to the control group, while the DEX + CSD group exhibited a trend toward increased neuronal cell numbers compared to the DEX-induced group. Furthermore, proteomic analysis of the DEX + CSD group showed decreased expression of proteins associated with the TNF signaling pathway compared to the DEX-induced group. These findings suggest that CSD exerts neuroprotective effects, as evidenced by an enhanced number of normal neuronal cells in the hippocampus and reduced protein expression in the TNF signaling pathway. Consequently, CSD may help mitigate neuronal damage associated with dexamethasone-induced depression, highlighting its potential as a therapeutic intervention for neurodegenerative and mood disorders.

Keywords *Depression, Hippocampus, Curcumin solid dispersion, Neuroprotective effects, Proteomics*

P-28

Effect of Melatonin on Pancreatic Beta Cell Regeneration in Streptozotocin-Induced Type 1 Diabetic Rats

Napat Sillapee[1], Pattanapong Boonprom[2], Ratchadaporn Pramong[2], Janyaruk Suriyut[2*]
[1] Medical Degree Program, Faculty of Medicine, Srinakharinwirot University, Sukhumvit 23, Bangkok, Thailand
[2] Department of Anatomy, Faculty of Medicine, Srinakharinwirot University, Sukhumvit 23, Bangkok, Thailand
*Corresponding author, e-mail: janyaruk@g.swu.ac.th

Abstract

Diabetes (Diabetes Mellitus) is a chronic, non-communicable disease resulting from an imbalance of insulin hormones produced by the beta cells of the pancreas, leading to a reduced ability of cells to utilize sugar. Melatonin, a hormone known for its strong antioxidant properties, can regulate insulin output. The plasma concentrations of melatonin were lower in diabetic than healthy rats and humans. This study investigates the effects of melatonin on pancreatic beta cell regeneration in streptozotocin-induced type 1 diabetic rats. Male Wistar rats were randomly divided into four groups (n=3, each); control, diabetes (DM), diabetes supplemented with 10 mg/kg of melatonin (DM+MEL), and melatonin-treated (10 mg/kg) (MEL) groups. The pancreas was collected after eight weeks. Immunohistochemical analysis revealed that diabetic rats exhibited reduced pancreatic islet size and NKX6.1 expression, indicating beta cell damage. In contrast, melatonin treatment significantly restored islet architecture and increased NKX6.1 expression, suggesting enhanced beta cell preservation and potential regenerative capacity. These findings suggest that melatonin may have a protective and regenerative effect on pancreatic beta cells in diabetic conditions. Further research is necessary to elucidate the precise molecular mechanisms underlying these effects.

Acknowledgement: This study was supported by a research grant from HRH Princess Mahachakri Sirindhorn Medical Center, Faculty of Medicine, Srinakharinwirot University (Contract No. 157/2566).

Keywords *Melatonin, Type 1 diabetes, Pancreatic beta cell, NKX6.1*

P-29

Protective Effect of Melatonin Against Type 1 Diabetes-Induced Myelin Abnormalities in Rat Cerebral Cortex

Na-tat Wajanaponsan[1], Pariwat Wisetwonsa[2], Pattanapong Boonprom[2], Ratchadaporn Pramong[2*]
[1]Medical Degree Program, Faculty of Medicine, Srinakharinwirot University, Sukhumvit 23, Bangkok, Thailand
[2]Department of Anatomy, Faculty of Medicine, Srinakharinwirot University, Sukhumvit 23, Bangkok, Thailand
*Corresponding author, e-mail: ratchadapornpr@g.swu.ac.th

Abstract

Diabetes Mellitus, particularly Type 1 diabetes is a prevalent chronic non-communicable disease. Type 1 diabetes leads to insufficient insulin production and persistent hyperglycemia, which can precipitate a range of debilitating symptoms and severe long-term complications. Among these complications, neurodegenerative changes, particularly in the central nervous system, are of critical concern. Chronic hyperglycemia is associated with oxidative stress, inflammation, and microvascular abnormalities, which together contribute to the deterioration of neural architecture and cognitive function. Interestingly, melatonin, a hormone with potent antioxidant properties, can positively affect the structure of neural connections and stimulate remyelination processes in animal models of demyelinating diseases. Furthermore, melatonin has shown efficacy in enhancing synaptic formation and cognitive function in diabetic models. Therefore, this study aims to elucidate the neuroprotective effects of melatonin on abnormalities in the cerebral cortex of streptozotocin-induced type 1 diabetic rats. Male Wistar rats were randomly divided into four groups; control, diabetes (DM), diabetes supplemented with 10 mg/kg of melatonin (DM+MEL), and melatonin-treated (10 mg/kg) (MEL) groups. The brains were collected after eight weeks. The morphology and the existence of myelin was determined by methylene blue staining and Luxol Fast Blue staining. The results demonstrated that diabetic rats exhibited significant histopathological alterations, including demyelination, axonal degradation, and a pronounced loss of neuronal cells, indicative of severe neurodegenerative changes. In contrast, melatonin treatment was associated with a marked preservation of neuronal architecture, increased neuronal counts, and improved myelin morphology, suggesting a protective effect against diabetes-induced oxidative damage. These findings underscore the potential of melatonin as a therapeutic agent for mitigating the neurodegenerative consequences of chronic hyperglycemia.

Acknowledgement: This study was supported by a research grant from HRH Princess Mahachakri Sirindhorn Medical Center, Faculty of Medicine, Srinakharinwirot University (Contract No. 156/2566).

Keywords *Melatonin, Type 1 diabetes, Myelin, Cerebral cortex*

P-30

Effect of Melatonin on Morphology of Axons in the Cerebral Cortex of Streptozocin-induced Type 1 Diabetic Rats

Bhatrabhorn Nidhinarangkoon[1], Pongsak Khanpetch[2], Cheng Nilbu-nga[2], Ratchadaporn Pramong[2*]
[1]Medical Degree Program, Faculty of Medicine, Srinakharinwirot University, Sukhumvit 23, Bangkok, Thailand
[2] Department of Anatomy, Faculty of Medicine, Srinakharinwirot University, Sukhumvit 23, Bangkok, Thailand
*Corresponding author, e-mail: ratchadapornpr@g.swu.ac.th

Abstract

Diabetes mellitus is a chronic disease characterized by an imbalance of the insulin hormone, leading to elevated blood sugar levels and significant health complications worldwide. Chronic hyperglycemia is associated with oxidative stress, inflammation, and microvascular abnormalities. Diabetes-induced brain injury is a serious complication of diabetes, and it is associated with oxidative stress and neuronal injury. This study investigates the effects of melatonin, a hormone with antioxidant properties, on morphological changes and axonal integrity in the cerebral cortex of type 1 diabetic rats induced by streptozotocin. Male Wistar rats were randomly divided into four groups; control, diabetes (DM), diabetes supplemented with 10 mg/kg of melatonin (DM+MEL), and melatonin-treated (10 mg/kg) (MEL) groups. The brains were collected after eight weeks. The morphology and integrity of axons in the cerebral cortex was determined by hematoxylin and eosin staining and Bielschowsky's sliver staining. The results demonstrated that diabetic rats exhibited significant histopathological changes, including a pronounced loss of neuronal cells and fibers as well as alterations in morphology of pyramidal neurons, and the integrity of axons in cerebral cortex. In contrast, melatonin significantly increased neuron numbers and improved morphology of pyramidal neurons and axonal integrity compared to the diabetic group. These findings suggest that melatonin can protect morphology and the integrity of axons in cerebral cortex from diabetes-induced brain injury. Further research is warranted to optimize its clinical application in diabetic conditions.

Acknowledgement: This study was supported by a research grant from HRH Princess Mahachakri Sirindhorn Medical Center, Faculty of Medicine, Srinakharinwirot University (Contract No. 155/2566).

Keywords *Melatonin, Diabetes, Neutrophil, Axon integrity, Cerebral cortex*

P-31

Hippocampal Proteomic Analysis Reveals Activation of NF-κB Signalling Pathways in a Rat Model of Chronic Unpredictable Mild Stress-induced Anxiety

Plaiyfah Janthueng[1,7], Wanfrutkon Waehama[1,7], Sawanya Charoenlappanit[2], Sittiruk Roytrakul[2], Prapapan Temkitthawon[3,4], Paweena Kaewman[5,7], Jureeporn roboon[5,7], Samur Thanoi[6], Sutisa Nudmamud-Thanoi[2,7,*]
[1] Medical Science Graduate Program, Faculty of Medical Science, Naresuan University, Phitsanulok, Thailand
[2] National Center for Genetic Engineering and Biotechnology (BIOTEC), National Science and Technology Development Agency, Pathumthani, Thailand
[3] Faculty of Pharmaceutical Sciences, Naresuan University, Phitsanulok, Thailand
[4] Center of Excellence in Cannabis Research, Faculty of Pharmaceutical Sciences and Center of Excellence for Innovation in Chemistry, Naresuan University, Phitsanulok
[5] Department of Anatomy, Faculty of Medical Science, Naresuan University, Phitsanulok, Thailand
[6] School of Medical Sciences, University of Phayao, Phayao, Thailand
[7] Centre of Excellence in Medical Biotechnology, Naresuan University, Phitsanulok, Thailand
*Corresponding author, e-mail: sutisat@nu.ac.th

Abstract

Anxiety disorders have frequently been associated with chronic stress and are the most common class of mental disorders. Stress-induced immune system changes lead to neuroinflammation and subsequent alterations in the brain. Among the various signalling pathways implicated in neuroinflammation, the nuclear factor kappa B (NF-κB) pathway is a crucial mediator for inflammation in anxiety disorder. However, the molecular mechanisms underlying the role of NF-κB in stress-induced anxiety disorders are poorly understood. We aimed to investigate the NF-κB signalling protein profile in rat hippocampus under chronic unpredictable mild stress (CUMS). Male Sprague-Dawley rats were divided into 2 groups of control and chronic unpredictable mild stress (CUMS) (N= 5-6); the rats were subjected to a continuous 2-week regimen of CUMS. All rats were measured the locomotion and anxiety-like behaviors on the last day of CUMS, using an open field test (OFT). The proteins in rat hippocampus were investigated by proteomics technique (LC-MS/MS). The analyzed MS/MS data were sent to identify by Mascot MS/MS ions search using the NCBI protein database. The identified and quantified proteins were then analyzed using the JVenn, MEV, and David 6.8. The CUMS group exhibited an increase in total distance travelled and vertical locomotor activity. Anxiety-like behavior in CUMS group was indicated by a higher number of entries into the corner area. Additionally, the proteomic analysis identified 14,096 quantified proteins. A total of 29 differentially expressed proteins were found in CUMS-exposed rats compared to the control group, and these proteins were associated with NF-κB signalling pathways. Among these, 10 proteins were upregulated, 4 proteins were downregulated, and 3 proteins showed no significant changes. Furthermore, two main pathways leading to the activation of NF-κB were identified in response to CUMS-induced anxiety: TNF-α and TLR4 activation. These pathways involved the upregulation of key proteins, including Tnfrsf1a, Ripk1, Lbp, Tlr4, Ticam1, Nfkb2, and Cxcr2. In summary, animals exhibit anxiety-like behavior and hyperlocomotion after 2 weeks of CUMS, accompanied by inflammatory responses by NF-κB responding. Overall, these results provide a better understanding of biological mechanisms underlying neuroinflammation in CUMS-induced anxiety and may help identify potential targets for novel drug treatment.

Keywords *Proteomics, NF-κB signalling, CUMS, Anxiety, Hippocampus*

P-32

Association of *GAD1* and *GAD2* Genes Polymorphisms with Major Depressive Disorder in a Thai Population

Siripaporn Kesyou[1], Benjamard Thaweethee-Sukjai[2], Sirijit Suttajit[3], Samur Thanoi[4], Gavin P Reynolds[5], Sutisa Nudmamud-Thanoi[6,7*]
[1] Medical Science Graduate Program, Faculty of Medical Science, Naresuan University, Phitsanulok, Thailand
[2] School of Medicine, Mae Fah Luang University, Chiang Rai, Thailand
[3] Department of Psychiatry, Faculty of Medicine, Chiang Mai University, Chiang Mai, 50200, Thailand
[4]School of Medical Sciences, University of Phayao, Phayao, Thailand
[5] Biomolecular Sciences Research Centre, Sheffield Hallam University, Sheffield, UK.
[6] Department of Anatomy, Faculty of Medical Science, Naresuan University, Phitsanulok, Thailand
[7] Centre of Excellence in Medical Biotechnology, Naresuan University, Phitsanulok, Thailand
*Corresponding author, e-mail: sutisat@nu.ac.th

Abstract

Major depressive disorder or MDD is a serious health issue which increases the economic burden of many countries globally. MDD involves disruptions in multiple neurotransmitter systems, including gamma-aminobutyric acid (GABA), the major inhibitory neurotransmitter in the central nervous system (CNS). GABAergic signaling plays a crucial role in modulating the release of other neurotransmitters, resulting in being a key target for understanding the pathology of MDD. Glutamic acid decarboxylase (GAD) is an important enzyme in GABA synthesis and has been suggested to be a marker for GABAergic neurons. Given its role in GABA production, genetic variations in *GAD1* and *GAD2* may contribute to MDD susceptibility. Therefore, this study aims to investigate the association between three single nucleotide polymorphisms (SNPs): *GAD1* rs769404, *GAD1* rs701492, and *GAD2* rs2236418 and MDD in a Thai population. The TaqMan SNP genotyping real-time PCR technique was performed to identify the SNPs of *GAD1* rs769404, rs701492 and *GAD2* rs2236418 in 100 MDD patients and 100 healthy controls. MDD patients were diagnosed strictly following the psychiatrist based on criteria in the Diagnostic and Statistical Manual of Mental Disorders-fifth Edition (DSM-V) and the Hamilton Depression Rating Scale (17-items); Thai version (Thai HDRS-17). The result revealed that the rs701492 genotype in *GAD1* gene showed a significant difference between MDD patients and controls. Additionally, the frequencies of the T allele in *GAD1* rs701492 and rs769404 were significantly higher in patients with MDD compared to control. Interestingly, the T allele carrier frequency was significantly higher in MDD patients than in controls. However, there were no significant in single genotype associations of *GAD1* rs469404 and *GAD2* rs2236418 polymorphisms in MDD. These findings suggest that genetic variations in *GAD1* may contribute to MDD susceptibility in the Thai population, supporting the role of the GABAergic system in MDD pathophysiology.

Keywords *Major depressive disorder, GABA, Glutamic acid decarboxylase, Single nucleotide polymorphisms*

P-33

Anxiolytic and Memory-Enhancing Effects of CBD-Enriched Hemp Extract and CBD Isolate in Stress-Induced Anxiety Rats

Wanfrutkon Waehama[1,5], Jureeporn Roboon[2], Prapapan Temkitthawon[3,6], Samur Thanoi[4], Sutisa Nudmamud-Thanoi[2,5*]
[1]Medical Science Graduate Program, Faculty of Medical Science, Naresuan University, Phitsanulok, Thailand
[2]Department of Anatomy, Faculty of Medical Science, Naresuan University, Phitsanulok, Thailand
[3]Faculty of Pharmaceutical Sciences, Naresuan University, Phitsanulok, Thailand
[4]School of Medical Sciences, University of Phayao, Phayao, Thailand
[5]Center of Excellence in Medical Biotechnology, Naresuan University, Phitsanulok, Thailand
[6]Center of Excellence for Natural Health Product Innovation, Faculty of Pharmaceutical Sciences, Naresuan University, Phitsanulok, Thailand
* Corresponding author. email: sutisat@nu.ac.th

Abstract

Anxiety disorder is one of the most common psychiatric conditions, often resulting from the accumulation of stress. Cannabidiol (CBD) has been reported to reduce anxiety-like behaviors and improve recognition memory in mice. This study aimed to investigate the effects of CBD-enriched hemp extract (CBD-E) and CBD isolate (CBD-I) on anxiety and recognition memory in stress-induced anxiety rats by chronic unpredictable mild stress (CUMS). Male Sprague-Dawley rats were orally given either CBD-E or CBD-I, while anxiety-like behaviors were induced by CUMS, in which the rats were exposed to different stressors daily for 14 days. A total of 72 rats were divided into six groups; control, CUMS, CUMS administered with CBD-E (2.5&5 mg/kg) and CBD-I (2.5&5 mg/kg). All rats were behaviorally tested on the last day of the stress induction period including open field test (OFT), elevated plus maze test (EPM) and novel objective recognition test (NOR). The rats in CUMS group showed an increase in the number of closed-arm entries in EPM compared to the control group ($p < 0.05$), indicating anxiety-like behavior. The CUMS administered with CBD-I at 2.5 mg/kg ($p < 0.01$) and 5 mg/kg ($p < 0.05$) showed a significant decrease in the number of closed-arm entries compared to the CUMS group, indicating an anxiolytic effect. Additionally, The CUMS administered with CBD-E at 2.5 mg/kg ($p < 0.05$) and CBD-I at 5 mg/kg ($p < 0.01$) showed a significant increase in the recognition index in NOR compared to the CUMS group, indicating CBD-I and CBD-E demonstrate enhancing memory. This study provides evidence supporting that CBD-I attenuates anxiety-like behaviors and that CBD-I and CBD-E both improve recognition memory in rats subjected to CUMS.

Keywords: *Anxiety, Cannabidiol, Hemp, Behavioral test, Chronic unpredictable mild stress*

P-34

Perception of Body Donation Among Medical Students in A Health Science Academy of Nepal

Anup Pandeya[1*], Navindra Phuyal[1], Niraj Pandey[1]
[1] Department of Anatomy, Rapti Academy of Health Sciences, Ghorahi Dang, Nepal
*Corresponding author, e-mail: anup.pan@student.mahidol.ac.th

Abstract

Body donation is crucial for medical education and research purposes. Medical students learn human anatomy and dissection techniques using preserved dead bodies (cadavers). Acquiring knowledge through the real human body is far more effective than studying textbooks or using digital simulators. Thus, this research aims to identify medical students' perceptions of body donation for medical education. The study was conducted through a questionnaire among 100 medical students. Most participants, 94% heard about the body donation through social media, family or friends, and medical school curriculum. However, 91% of respondents don't know the process and legal guidelines related to body donation in their home country. Further, 48% of the respondents feel positive, 36% respondents feel neutral and 16% feel strongly positive towards the idea of body donation for medical purposes. In addition, 92% of respondents agree that cultural and religious beliefs affect people's willingness to donate their bodies. Other barriers include lack of awareness, fear of disrespect to the body, family disapproval, and legal concerns associated with body donation. Participants suggest that the motivating factors for body donation include public awareness, financial incentives, and clear legal guidelines that should be imposed to donate their bodies. Further, the participants suggest that providing education about the importance of body donation in the field of medical education and research should be highlighted. Similarly, the proper legal guidelines with easy procedures should be implemented for donors. Thus, this study concludes that many medical students are aware of body donation, however, cultural and religious beliefs along with unclear legal guidelines affect the process of body donation in Nepal.

Keywords *Body donation, Medical students, Nepal*

P-35

Morphometric Study into the Celiac Trunk, Superior Mesenteric Artery, and Inferior Mesenteric Artery: A Vascular Dissection for Optimized Abdominal Surgery

Sani Baimai[1*], Tanpichcha Suttithavinkul[2], Sirinush Sricharoenvej[1]
[1]Department of Anatomy, Faculty of Medicine Siriraj Hospital, Mahidol University, Bangkok, Thailand. [2]Medical Intern of Department of Anatomy, Faculty of Medicine Siriraj Hospital, Mahidol University, Bangkok, Thailand
*Corresponding author, e-mail: sanibaimai@gmail.com

Abstract

Understanding abdominal arterial anatomy is crucial for optimizing surgical and interventional procedures, especially gastrointestinal, vascular, and transplant surgeries. CT angiography provides valuable insights but may not fully capture anatomical variations and vessel relationships. Conventional cadaveric dissection is the gold standard for precise morphometric analysis, but region-specific data for the mid-region of the Thai population remains scarce. Knowledge of the celiac trunk (CT), superior mesenteric artery (SMA), and inferior mesenteric artery (IMA) variations is essential to reduce intraoperative complications. The study aims to measure the vertical and horizontal diameters of CT, SMA, and IMA, assess the vertebral-level variability of IMA origins, and evaluate the distance ratios between CT-SMA and SMA-IMA. The mean age of the 30 embalmed cadavers (19 males: M, 11 females: F) was 74.8 years in males and 83 years in females. The mean horizontal (h) and vertical (v) diameters (mm.) were as follows: CT (M: h 6.43, v 6.98; F: h 5.77, v 6.31), SMA (M: h 6.79, v 7.46; F: h 6.41, v 6.60), and IMA (M: h 2.99, v 3.26; F: h 3.15, v 3.24). The vertical-to-horizontal (v/h) ratio was 1.10 for CT (both M and F), 1.11 (M) and 1.03 (F) for SMA, and 1.11 (M) and 1.04 (F) for IMA. The most common IMA origin was at the lower third of L3 (30%), followed by L3-L4 (23.3%). The study offers detailed morphometric data on the major abdominal arteries in the central region of the Thai population, providing a crucial reference for abdominal and vascular surgery. These findings provide critical data for surgical applications, particularly in minimizing iatrogenic ischemia, optimizing arterial ligation techniques, and improving vascular reconstructions and reconstructive surgery. The positional insights gained will enhance preoperative planning, improve surgical precision, and reduce the risk of vascular complications, especially in oncologic resections, aneurysm repair, and endovascular procedures.

Keywords *Abdominal arterial anatomy, Celiac trunk variations, Superior mesenteric artery, Inferior mesenteric artery*

P-36

Anatomical and Computed Tomography-Based Investigations of the Renal Vasculatures and Its Potential Clinical Implications in a Thai Population

Thirawass Phumyoo[1,2], Salinee Naewla[1+], Benrita Jitaree[3], Veerawat Sansri[1], Benjamart Pratoomthai[1],Waraporn Sakaew[4], Tawut Rudtanatip[4], Arnon Pudgerd[5], Pasuk Mahhakanukrauh[6], Chirapat Inchai[6], Boonyakorn Boonsri[7], Choowadee Pariwatthanakun[8], Torpong Claimon[9], Wasu Tanasoontrarat[9],Nichapha Chandee[10], Sirirak Mukem[11], Kulwadee Karnjana[11+], Nontawat Benjakul[12*,2]
[1] Division in Anatomy, Department of Basic Medical Science, Faculty of Medicine Vajira Hospital, Navamindradhiraj University, Bangkok, Thailand.
[2] Vajira Pathology-Clinical-Correlation Target Research Interest Group, Faculty of Medicine Vajira Hospital, Navamindradhiraj University, Bangkok, Thailand.
[3] Ramathibodi medical school, Chakri Naruebodindra Medical Institute, Faculty of Medicine Ramathibodi Hospital, Mahidol University, Samut Prakan, Thailand.
[4] Department of Anatomy, Faculty of Medicine, Khon Kaen University, Khon Kaen, Thailand.
[5] Division of Anatomy, School of Medical Sciences, University of Phayao, Phayao, Thailand
[6] Department of Anatomy, Faculty of Medicine, Chiang Mai University, Chiang Mai, Thailand.
[7] Division of Health and Applied Sciences, Faculty of Science, Prince of Songkla University, Songkhla, Thailand.
[8] Faculty of Medicine, Mahasarakham University, Mahasarakham Thailand.
[9] Department of Radiology, Faculty of Medicine Vajira Hospital, Navamindradhiraj University, Bangkok, Thailand.
[10] Faculty of Integrative Medicine, Rajamangala University of Technology Thanyaburi, Pathumthani, Thailand.
[11] School of Medicine, Walailak University, Nakhon Si Thammarat, Thailand.
[12] Department of Anatomical Pathology, Faculty of Medicine Vajira Hospital, Navamindradhiraj University, Bangkok, Thailand.
[+]These authors contributed equally as essential authors.
*Corresponding author, e-mail: phumyoobenjakul@gmail.com

Abstract

The prevalence of kidney disease is rising and has become a significant public health and urban medicine concern in Thailand, especially renal cysts. The partial nephrectomy has been required for the patients with renal cysts. Nevertheless, there are few studies of thorough renal vasculature knowledge that are important for surgical planning to minimize complications. Consequently, the purpose of this study was to explore the renal vasculature variation in the Thai population with renal cysts. This study was performed on the abdominal region using cadaveric investigation in twenty-seven embalmed cadavers and a CT scan investigation in twelve patients with renal cysts on both renal sides. This study found a single renal artery in 43 of 54 sides (79.6%) and a single accessory renal artery in 11 sides (20.4%). Furthermore, all cases with renal cysts had early (pre-hilar) branching patterns. The distance between the branching point of renal artery division and the mid-renal hilum was 20.65 ± 10.12 mm. During partial nephrectomy, there is enough wide space to perform selective ligation or clamping on each segmental artery. In conclusion, the present study provides preliminary results of an essential knowledge of renal vasculature in the Thai population of the central region of Thailand for the surgical planning of partial nephrectomy using both investigations.

Keywords *Main renal and segmental vasculatures, Computed tomography imaging, Partial nephrectomy*

Background

The prevalence of kidney disease is rising and has become a significant public health and urban medicine concern in Southeast Asian countries such as Thailand, for example, diabetic nephropathy, hypertensive nephropathy, glomerulonephritis, etc. Renal cysts are also a kidney disease common to up to 35% of people. The characteristics of renal cysts are fluid-filled sacs that form on or in the kidneys, and they could be classified into simple cysts and

complex cysts.[1] This renal disease is often benign and asymptomatic but can cause complications or be associated with underlying conditions like the increased risk of hypertension.

With a rising number of patients with renal cysts, they have required renal surgical therapy like partial nephrectomy to extend their quality of life before reaching end-stage kidney disease (ESKD). Partial nephrectomy, or kidney-sparing surgery, is a procedure to remove a diseased tissue while preserving as much healthy kidney tissue as possible, and it can be used in cases involving renal cysts, especially those classified as complex or high-risk.[2] However, there are few studies of thorough renal vasculature knowledge that are essential for planning partial nephrectomy, intrarenal surgery, and renal transplantation to minimize peri-operative and post-operative complications.[2, 3]

The previous literature revealed that renal vascular anatomy could be wildly variable, with accessory renal arteries and veins in up to 15%. In particular, main renal arteries divide into two divisions, including anterior and posterior divisions, with early (pre-hilar) branching or hilar branching to provide numerous segmental arteries supplying each renal segment.[4-10] Although the variations of renal vasculature have been reported worldwide, there might be differences in genetic characteristics between different populations, and there are few studies of renal vasculature in the Thai population with renal cysts,

Therefore, the aim of this study was to examine the renal vasculature variation in the Thai population with renal cysts using conventional cadaveric dissection and computed tomography investigation to provide its potential clinical implications for planning further renal surgery.

Materials and Methods

The research procedures of the present study were approved by the Institutional Review Board of the Faculty of Medicine Vajira Hospital (Study code: 107/66E, COA: 111/2566) and performed in accordance with the Declaration of Helsinki of the World Medical Association (WMA). The research protocols comprise the cadaveric investigation of legally donated bodies and the CT scan investigation of the patients.[11]

Cadaveric investigation

This investigation was performed on the abdominal region of adult embalmed cadavers who legally donated the body by giving their written informed consent prior to death for medical research and education to the Faculty of Medicine Vajira Hospital, Navamindrahiraj University, Bangkok, Thailand, and the Faculty of Medicine Ramathibodi Hospital, Mahidol University, Samut Prakan, Thailand. Eighty-one embalmed cadavers were dissected during the routine abdominal dissection of medical undergraduate students, but only twenty-seven embalmed cadavers with renal cysts on both renal sides (16 males and 11 females; age range of 44 to 94 years) were recruited in this study to examine the morphological variation of renal vasculature include:

- *Data collection: Observation*

1. Branching pattern of renal artery division (Early (pre-hilar) branching / Hilar branching pattern)

2. Pattern of renal artery (Single main renal artery / Accessory renal artery (single or double arteries))

- *Data collection: Measurement*

1. Diameters of main renal artery and vein at its origin

2. Horizontal distances from the origin of main renal artery and vein to the branching point of renal artery division

3. Horizontal distances from the branching point of renal artery and vein division to mid renal hilum

CT scan investigation

A preliminary investigation was conducted by reviewing retrospectives from the DICOM medical records of twelve patients with renal cysts (6 males and 6 females age range of 21 to 94 years). All patients underwent CT renal or abdominal angiogram in GE systems (CT Revolution Apex), 256 slices multidetector CT scanner in the Diagnostic Radiology Center, Department of Radiology, Faculty of Medicine Vajira Hospital, Navamindradhiraj University, Bangkok, Thailand. The scanning parameters were 120 kV, 240 mAs, and slice thickness of 0.625 mm. The DICOM viewer software was utilized to examine the renal segmental artery's morphological and number variations.

To eliminate the data collection error of both investigations, only a single investigator was able to conduct the data observations and parameter measurements. For cadaveric investigation, all measurements were performed for three times in millimeters (mm) using digital Vernier caliper.

Statistical analysis

Descriptive statistics were analyzed as mean, standard deviation, and percentage using IBM SPSS statistics software version 26. If the data were in a normal distribution, the student's *t-test* and the paired-samples *t-test* were utilized to compare the

difference between the sexes and sides, respectively. In addition, if the data were abnormal distribution, Mann-Whitney U test and Wilcoxon signed rank were employed to compare the difference between sexes and sides, respectively. The criterion of significance was assigned as 0.05 (two-tail).

Results and Discussion

The results of this study were summarized in three tables based on investigation methods.

Regarding the cadaveric investigation, this study found twenty-seven embalmed cadavers with renal cysts (33.33%) among eighty-one embalmed cadavers. The single renal artery was found in 43 of 54 sides (79.6%), and the accessory renal artery was found in 11 sides (20.4%) with a single accessory renal artery (Fig.1) (Table 1). Accessory renal arteries were found in male more than female (4 Males on both renal sides VS 3 females on left renal side) However, double accessory renal arteries were not found in this study. After tracing the course of accessory renal arteries, most of them originate above or near the main renal arteries, and then they often terminate at the apical or inferior renal segments.

According to the branching pattern of renal artery division, this study found that all 54 sides with renal cysts were an early (pre-hilar) branching pattern (100%) (Fig. 2) (Table 1). The main renal artery arose from the abdominal aorta with an average diameter of 7.27 ± 1.35 mm and traveled at a horizontal distance of 34.85 ± 15.31 mm before branching as the anterior and posterior division (Table 2). However, there was a statistical difference between the sides (p = 0.011). The distances of left and right sides were 29.84 ± 12.93 mm and 40.10 ± 16.24 mm, respectively. Afterward, each renal artery division is divided into segmental arteries to supply each renal segment. The distance between the branching point of renal artery division and the mid-renal hilum was 20.65 ± 10.12 mm. There was no statistical difference between sexes and sides. This study shows that if the surgeon would like to perform main renal artery ligation or clamping[10] during partial nephrectomy[2] using laparoscopic surgery or robotic-assisted nephrectomy, the recommended clamping sites are approximately 29 mm for the left side and 40 mm for the right side. However, this study also reveals that if the surgeon would like to conduct selective clamping on each segmental artery, it could be performed easily because there is enough wide space, about 20 to 30 mm, at the renal hilum.

Table 1 Pattern of renal vasculature using cadaveric investigation

Pattern	N	%
Branching pattern of renal division on renal artery		
• Early branching	54	100
• Hilar branching	0	0
Pattern of renal artery		
• Single main renal artery	**43**	**79.6**
• *Male*	**24**	**44.4**
• Left side	12	22.2
• Right side	12	22.2
• *Female*	**19**	**35.2**
• Left side	8	14.8
• Right side	11	20.4
• Accessory renal artery	**11**	**20.4**
• Single artery	**11**	**100**
• *Male*	**8**	**72.8**
• Left side	4	36.4
• Right side	4	36.4
• *Female*	**3**	**27.2**
• Left side	3	27.2
• Right side	0	0
• Double arteries	**0**	**0**

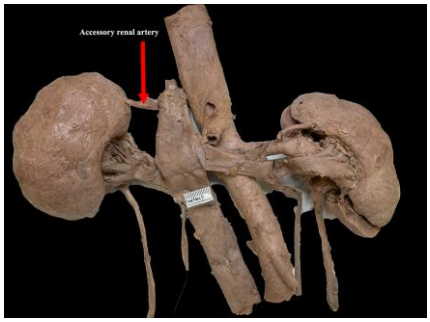

Fig.1 Single accessory renal artery originates from lateral side of abdominal aorta and terminates at apical renal segment.

Fig.2 Early (pre-hilar) branching pattern of renal artery division. MRA – Main renal artery, AntDi – Anterior division, PostDi – Posterior division.

Aristotle et al. (2013)[5] dissected the 30 Indian kidneys from 15 preserved cadavers, and they found that the normal pattern of blood supply to the kidneys was observed in 86.6% cases. Accessory renal artery could be traced in 4 specimens (13.4%) and all these 4 arteries arose from the abdomen aorta. During kidney development (metanephros), the kidneys initially form in the pelvic cavity and ascend to their final position in the abdomen, receiving blood supply from successively higher branches of the aorta. If the lower, original arteries fail to regress, they can persist as accessory renal arteries.[12]

Regarding the main renal vein, it drained to the inferior vena cava with an average diameter of 13.35 ± 3.15 mm. However, there was a statistically significant difference between the sides ($p = 0.000$) (Table 2). The diameters of the left and right sides were 14.73 ± 2.85 mm and 11.47 ± 2.86 mm, respectively. Moreover, the distance from the origin of the main renal vein to the branching point also had significant differences between sides ($p = 0.000$). There were 59.64 ± 12.11 mm for the left side and 20.69 ± 7.75 mm for the right side. Nevertheless, there was no statistical difference between sexes and sides of the distance from the branching point of the renal vein to the mid-renal hilum, and there was 14.21 ± 6.51 mm. This study exposes that the selective clamping on each branch of the renal vein at the renal hilum during partial nephrectomy might be a difficult procedure due to its narrow space. The recommended venous ligation locations were approximately 59 mm for the left and 20 mm for the right.

This study summarized the number of segmental arteries that supplied each renal segment in Table 3 regarding CT scan investigation (Fig.3). The number of segmental arteries could be found in up to three branches at the apical, anterosuperior, and posterior segments. Nevertheless, no segmental artery could be found in up to four renal segments except the posterior segment. The number segmental arteries were no statistical between male and female. However, there was only a preliminary result of the CT investigation. A larger population are required to support the accurate results, and there are few studies of renal vasculature using CT angiography, in particularly, the segmental arteries.[6-7, 9] The present study exposed that the CT scan is the superior imaging modality for accurately characterizing renal segmental arteries that supply blood to each renal segment, and the number of segmental arteries were also associated with the selective segmental arterial ligation at each segment during partial nephrectomy.

Table 2 Parameter measurement of renal vasculature using cadaveric investigation

Parameter	Mean (mm)	SD (mm)
Diameter of main renal artery	7.27	1.35
Diameter of main renal vein*	13.35	3.15
Distance from origin of main renal artery to branching point of renal artery division*	34.85	15.31
Distance from branching point of renal artery division to mid renal hilum	20.65	10.12
Distance from origin of main renal vein to branching point*	40.93	21.97
Distance from branching point of renal vein to mid renal hilum	14.21	6.51

Notes: * Statistical difference between sides ($p < 0.05$)

Fig.3 CT scan investigation. Above picture revealed a small left accessory renal artery originates near the main renal artery and terminates at inferior segment, and below picture showed segmental arteries that supply each renal segment.

Table 3 Number of segmental arteries per each renal segment using CT scan investigation

Renal segment	N	%
Apical segment	**24**	**100**
• Single segmental artery	12	50.0
• Double segmental arteries	2	8.3
• Triple segmental arteries	1	4.2
• No segmental artery	9	37.5
Anterosuperior segment	**24**	**100**
• Single segmental artery	7	29.2
• Double segmental arteries	8	33.3
• Triple segmental arteries	2	8.3
• No segmental artery	7	29.2
Anteroinferior segment	**24**	**100**
• Single segmental artery	12	50.0
• Double segmental arteries	6	25.0
• Triple segmental arteries	0	0.0
• No segmental artery	6	25.0
Inferior segment	**24**	**100**
• Single segmental artery	16	66.7
• Double segmental arteries	0	0.0
• Triple segmental arteries	0	0.0
• No segmental artery	8	33.3
Posterior segment	**24**	**100**
• Single segmental artery	17	70.8
• Double segmental arteries	6	25.0
• Triple segmental arteries	1	4.2
• No segmental artery	0	0.0

Limitation

The present study reveals only the incidence of variation in renal vasculature in the Thai population with renal cysts in the central region of Thailand, and both investigations have a small sample size. Therefore, future research will investigate a large population and analyze the data to further support accurate results.

Conclusion

The present study reveals preliminary results of renal vasculature from cadaveric and CT scan investigations that are necessary knowledge for the surgical planning of partial nephrectomy.

Acknowledgements

This research project is supported by Thailand Science Research and Innovation (TSRI). Contract No. FRB680097/0468.

References

1. Milan AS, Dilip CM. Appearance of Renal Cysts in Adult Human Cadavers. International Journal of Anatomy Radiology and Surgery: JCDR Research and Publications Pvt. Ltd.; 2018.
2. Bouzouita A, Saadi A, Hermi A, Chakroun M, Bouchiba N, Allouche M, et al. Cadaveric study of arterial renal anatomy and its surgical implications in partial nephrectomy. Surgical & Radiologic Anatomy. 2021; 43: 1449-59.
3. Neerja R, Seema S, Pushpa D, Rani K. Surgical Importance of Arterial Segments of Human Kidneys: An Angiography and Corrosion Cast Study. Journal of Clinical and Diagnostic Research: JCDR Research and Publications Private Limited; 2014. 1-3.
4. Khamanarong K, Prachaney P, Utraravichien A, Tong-Un T, Sripaoraya K. Anatomy of renal arterial supply. Clin Anat. 2004; 17: 334-6.
5. Aristotle S, Sundarapandian, Felicia C. Anatomical Study of Variations in the Blood Supply of Kidneys. Journal of Clinical & Diagnostic Research. 2013; 7: 1555-7.
6. Tardo DT, Ahern G, Pitman A, Sinha S, Briggs C. Anatomical variations of the renal arterial vasculature: An Australian perspective. Journal of Medical Imaging and Radiation Oncology. 2017; 61: 643-9.
7. Mohiuddin M, Sundus S, Raza I, Kamran M, Kumar H, Mubeen S. Anatomical Variants of Renal Vasculature: A Study in Adults on Multidetector Computerized Tomography Angiography Scan. Professional Medical Journal. 2020; 27: 185-90.
8. Mishra GP, Bhatnagar S, Singh B. Anatomical Variations of Upper Segmental Renal Artery and Clinical Significance. Journal of Clinical & Diagnostic Research. 2015; 9: 1-3.
9. Krishna Patibandla BM, Bharali MD, Galeti EH, Shahab S. Evaluation of renal vasculature and its variants by CT angiography. Asian Journal of Medical Sciences. 2022; 13: 208-15.
10. Deb AA, Agag A, Naushad N, Serag H. Surgical and Functional Outcomes of Artery Only Versus Artery and Vein Clamping in Patients Undergoing Partial Nephrectomy: A Systematic Review and Meta-Analysis. Turkish Journal of Urology. 2022; 48: 180-95.
11. Iwanaga J, Singh V, Ohtsuka A, Hwang Y, Kim HJ, Morys J, et al. Acknowledging the use of

human cadaveric tissues in research papers: Recommendations from anatomical journal editors. Clin Anat. 2021;34(1):2-4.

12. Rehman S, Ahmed D. Embryology, Kidney, Bladder, and Ureter. StatPearls. Treasure Island (FL) ineligible companies. 2025.

P-37

Study of Nutrient Foramen Position in Thoracic Vertebrae for Posterior Thoracic Pedicle Screw Placement in a Northeast Thai Population

Supatsapa Unsri[1], Chanasorn Poodendaen[2], Narawadee Chompoo[2], Poonikha Namwongsakool[2], Natthiya Sakulsak[3], Thas Phisonkunkasem[4], Suthat Duangchit[4], Kaemisa Srisen[2*]

[1] Graduate student, Department of Anatomy, Faculty of Medical Science, Naresuan University, Phitsanulok, Thailand

[2] Department of Anatomy, Faculty of Medical Science, Naresuan University, Phitsanulok, Thailand

[3] Faculty of medicine, Praboromarajchanok Institute, Nonthaburi, Thailand

[4] Department of Physiology, Faculty of Medical Science, Naresuan University, Phitsanulok, Thailand

*Corresponding author, e-mail: kaemisas@nu.ac.th

Abstract

Thoracic vertebral deformities, including scoliosis and kyphosis, whether traumatic or degenerative in origin, often require surgical intervention through pedicle screw fixation. Accurate screw placement is crucial to avoid spinal cord injury, necessitating reliable anatomical landmarks. The study aimed to investigate the incidence and precise location of nutrient foramina in the posterior thoracic lamina as potential anatomical landmarks for safe pedicle screw placement in the Northeast Thai population. A total of 1,200 dry thoracic vertebrae (T1-T12, 100 specimens each) from 100 adult skeletons (50 males, 50 females) were examined at the Unit of Human Bone Warehouse for Research: UHBWR, Department of Anatomy, Faculty of Medicine, Khon Kaen University, Thailand. The location and characteristics of nutrient foramina were measured relative to three anatomical landmarks: Distance from the inferior border of the superior articular facet (A), Distance from the lateral border of the laminae (B), and Distance from the midline of the spinous process (C). The data were analyzed using SPSS version 23.0. The results indicated that the highest incidence of nutrient foramina was observed at T1 (84.5%). Significant gender-specific differences ($P<0.05$) were found in all measured parameters at T1 and T3 levels. No significant bilateral asymmetry was observed between left and right sides across all thoracic levels. Overall, males had greater distances across all three parameters, with the most pronounced differences in T1-T4. This study provides detailed morphometric data on nutrient foramina distribution in thoracic vertebrae, offering surgeons valuable reference points for pedicle screw placement in the Northeast Thai population. Furthermore, the gender-specific variations at T1 and T3 levels warrant consideration during surgical planning.

Keywords *Thoracic vertebrae, Spinal cord, Nutrient foramen, Pedicle screw, Surgical anatomy, Thai population*

P-38

A Morphometric Examination of the Zygomaticofacial Foramen in Dry Skulls and Formaldehyde-fixed Cadavers from a Thai Population

Gunnakrit Chanchur[1], Srunchai Boonsirirutchok[1], Somjai Apisawetakan[1], Monsicha Somrit[2], Atthaboon Watthammawut[1*]
[1] Department of Anatomy, Faculty of Medicine, Srinakharinwirot University, Sukhumvit 23, Bangkok 10110, Thailand
[2] Department of Anatomy, Faculty of Science, Mahidol University, Rama VI Road, Bangkok 10400, Thailand
*Corresponding author, e-mail: atthaboon@g.swu.ac.th

Abstract

Accurate localization and awareness of the zygomaticofacial foramen (ZFF) are important in orthognathic surgery, such as zygomatic implants, cosmetic procedures, and filler injections, to minimize complications, for example, nerve damage, numbness, or inadvertent vascular injury. Anatomical variations of the ZFF for size, number, and position have been reported across diverse populations. Still, the varying choices of landmarks used to identify and the specific characteristics of the specimens used have led to differing standards in determining the general location. Therefore, this research aims to bridge this knowledge gap by comparatively analyzing the morphometric characteristics of the ZFF among Thai samples, including dry skulls and formaldehyde-fixed cadavers (FFCs). Precise measurements were obtained by measuring the distance of the ZFFs found in the specimens from the origin of reference to localize a yet high-fidelity Frankfurt plane intersecting at a right angle with the post-zygomaticofrontal suture. The exact position of the ZFF and the intersecting lines were projected to superimpose on the skulls and cadavers by crossline laser technology and measures of the distance using highly accurate digital calipers. About 40 skulls and 30 FFCs first underwent sexing using standard anthropomorphic/forensic standards, and the number and location of the ZFFs were determined and classified according to sex and preservation methods. The results showed that in measured skulls, female skulls had a higher number of ZFFs on both the left and right aspects of the skulls (~1.5 foramina vs. ~0.9 foramina in males), whereas the numbers were more comparable in FFCs (~1.2 lt./1.5 rt. foramina in females vs. ~0.9 lt./1.5 rt. foramina in males). Interestingly, the location of the foramina in both males and females was similar in position from the intersecting reference lines. Still, there was a significant difference in the measurements obtained from the dry skulls (~6 to 8.5 mm. α, ~-1.0 to -3.0 mm. β, ~2.0 mm. γ) when compared to the FFCs (~8 mm. α, ~1.5 mm. β, ~4.5 mm. γ). This was suggested that data obtained from dry skulls or FFCs must be taken with great consideration. Further data and analysis must be conducted to get a more accurate general zone of safety to avoid the ZFF and associated structures. Findings from the present study, specific to the Thai population's anatomical understanding, facilitate individualized surgical planning and support further forensic applications to a better degree for Thai patients.

Keywords *Zygomaticofacial foramen, Facial landmarks, Frankfurt plane, Morphometric studies, Thai population*

P-39

Sex and Stature Estimation from the Humerus in the Northeastern Thai Population and Application in Forensic Anthropology

Phetcharat Phetnui[1], Suthat Duangchit[2], Kitinat Rodthongdee[2], Rachanee Chanasong[3], Phongpitak Putiwat[4], Kaemisa Srisen[4]*
[1] Graduate student, Department of Anatomy, Faculty of Medical Science, Naresuan University, Phitsanulok, Thailand
[2] Department of Physiology, Faculty of Medical Science, Naresuan University, Phitsanulok, Thailand
[3] Faculty of medicine, Praboromarajchanok Institute, Nonthaburi, Thailand
[4] Department of Anatomy, Faculty of Medical Science, Naresuan University, Phitsanulok, Thailand
*Corresponding author, e-mail: kaemisas@nu.ac.th

Abstract

The study of physical differences between males and females, including the estimation of stature from skeletal remains found at crime scenes was crucial in forensic anthropology, particularly in human identification. The humerus served as a valuable skeletal element for this purpose, due to its frequent recovery from forensic and archaeological contexts. Additionally, it was highly durable, resistant to decomposition, and provided essential biological information, such as age, ancestry, stature, and sex. This study aimed to investigate the morphology of the humerus to develop a logistic regression equation for sex estimation and a linear regression equation for stature estimation in the Northeastern Thai population. A total of 200 dry humeri were examined, consisting of 100 male and 100 female specimens. Five parameters were measured: Maximum Length of Humerus (MaxH), Midshaft Circumference of Humerus (MCH), Epicondylar Breadth of Humerus (EBH), Superior Inferior Diameter of Head of Humerus (SIDH), and Weight of Humerus (WH). The collected data were analyzed using SPSS statistical software to create sex estimation and stature estimation equations. The results indicated that the multivariate logistic regression equation for sex estimation achieved an accuracy of 93.5%. For stature estimation, the multivariate regression model produced the lowest standard error of estimate (SEE), with values of 4.233 cm for males, 5.391 cm for females, and 4.862 cm for the overall group. These findings demonstrated that the humerus could be effectively utilized for sex estimation and stature estimation from skeletal remains. Furthermore, this study contributed to the advancement of human identification techniques in forensic anthropology, enhancing the accuracy and reliability of forensic investigations.

Keywords *Forensic anthropology, Sex estimation, Stature estimation, Humerus, Northeastern Thai population*

Background

Human identification was a crucial process in forensic science, particularly when examining skeletal remains found in various situations such as criminal scenes, accidents, or catastrophes [1]. This process based on the principles of forensic anthropology, a field dedicated to studying the physical characteristics of humans through skeletal analysis to determine age, ancestry, stature, and sex when other identification methods were unavailable. Sex estimation was a fundamental step in narrowing down potential identities, therefore increasing the accuracy of human identification. One of the commonly used methods involved calculating the Sexual Dimorphism Index (SDI), a measure of physical differences between males and females. The most reliable bones for sex estimation were those that exhibited distinct sexual dimorphism, such as the pelvis [2] and the skull [3]. Additionally, long bones such as the femur and humerus also exhibited sexual dimorphism and were utilized for sex estimation [4]. Stature estimation was the essential process of human identification, as an individual's stature was closely related to the size of bones. In previous studies on stature estimation from upper limb bones in the Iranian population demonstrated that the derived equations were applicable in forensic pathology and forensic anthropology [5]. Similarly, research on stature estimation from long bones in the Northern Thai

population indicated that the long bones provided high accuracy in stature estimation [6]. However, skeletal morphology varied across different populations due to genetic factors, environmental when applying stature estimation formulas developed for other populations. Therefore, this study aimed to investigate the morphology of the humerus to develop a logistic regression equation for sex estimation and a linear regression equation for stature estimation in the Northeastern Thai population. The results of this study will facilitate the application in forensic anthropology.

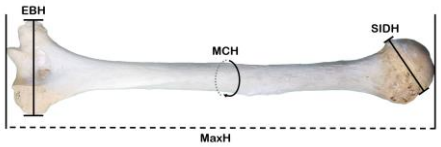

Fig. 1 Showed measurement of 4 parameters on the dry humerus.

Materials and Methods

A total of 200 dry humeri were collected, consisting of 100 male and 100 female specimens in well-preserved condition. Each specimen included recorded information on age, sex, and stature, with all individuals being at least 20 years old. The samples were obtained from the Unit of Human Bone Warehouse for Research: UHBWR, Department of Anatomy, Faculty of Medicine, Khon Kaen University. The humeri were measured according to five parameters (Fig. 1) including influences, and daily activities [7]. For the Northeastern Thai population, distinct physical characteristics influenced by environmental and lifestyle differences could lead to discrepancies Maximum Length of Humerus (MaxH), Midshaft Circumference of Humerus (MCH), Epicondylar Breadth of Humerus (EBH), Superior Inferior Diameter of Head of Humerus (SIDH), and Weight of Humerus (WH). The data collected were analyzed using SPSS V.23.0 statistical software. Descriptive statistics and independent t-tests were performed to assess mean differences between male and female populations. Logistic regression analysis was conducted to develop a multivariate regression equation for sex estimation, followed by multiple linear regression to create linear regression equations for stature estimation in males, females, and the overall group.

Results

The results of this study showed that all parameters had higher mean values in males than in females (Table 1), with statistically significant differences ($p<0.05$).

The multiple regression equation used for sex estimation (Table 2) demonstrated the highest accuracy, with an accuracy rate of 93.5%. The method for using the equation was as follows: after substituting the values into the equation, if the result was greater than 0, the skeleton was classified as male, whereas if the result was less than 0, the skeleton was classified as female.

Table 1 Descriptive statistics and independent t-test statistics for sex differences in dry humerus measurements.

Parameter	Total (N=200)	Male (N=100)	Female (N=100)	t-score	p-value
MaxH (cm)	30.26 ± 1.85	31.46 ± 1.38	29.07 ± 1.45	98.11	<01.0
MCH (cm)	6.02 ± 0.59	6.49 ± 0.34	5.55 ± 0.37	66.18	<01.0
EBH (mm)	58.56 ± 4.83	62.25 ± 2.82	54.87 ± 3.36	82.16	<01.0
SIDH (mm)	42.14 ± 3.67	45.07 ± 2.06	39.20 ± 2.34	84.18	<01.0
WH (g)	96.64 ± 30.84	119.42 ± 23.19	73.86 ± 18.04	51.15	<0.01

Table 2 Multivariate logistic regression models and sex determination accuracy rate.

Logistic regression equation	Accuracy rate (%)
Sex = 3.140(MCH) + 0.400(SIDH) + 0.048(WH) – 40.479	93.5

When the sex estimation equation was tested for probability to assess the distribution of predictions (Fig. 2) was found that the equation exhibited a high accuracy in sex estimation, with only minor errors. The prediction rate for females was higher than for males, as indicated by the predicted probability values. A predicted probability between 0.00 to 0.50 classified the skeleton as female, whereas a predicted probability between 0.51 to 1.00 classified the skeleton as male.

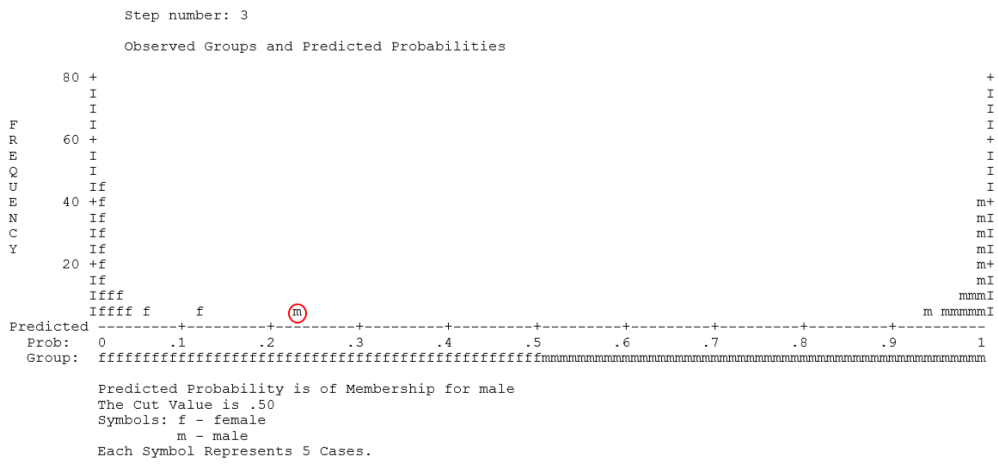

Fig. 2 Observed groups and predicted probabilities based on five parameters measured from dry humerus.

For the study of the linear regression equation for stature estimation was found the multiple regression equation for males had a standard error of estimate (SEE) of 4.233 and coefficient of determination (R^2) of 0.567, while for females, the SEE was 5.391 and the R^2 was 0.328. For the combined population, the SEE was 4.862 and the R^2 was 0.657 (Table 3). In summary the linear regression equation for the overall group had a lower margin of error compared to the male and female groups, and provided a more accurate estimation of stature.

Table 3 Linear regression equations for stature estimation in humerus measurements.

Sample	Linear regression equation	SEE	R^2
Male	4.125(MCH) + 0.630(SIDH) + 2.232(MaxH) + 39.510	4.233	0.567
Female	4.365(MCH) + 1.217(MaxH) + 0.630(SIDH)	5.391	0.328
Overall	0.487(SIDH) + 1.640(MaxH) + 4.341(MCH) + 63.412	4.862	0.657

Discussion and Conclusion

This study found that all measured parameters were higher in males than in females. This difference was attributed to the primary male hormone testosterone, which enhanced periosteal formation. As a result, the epiphyseal plate in males closed later than in females, leading to stronger and larger bones in males compared to females [8][9]. In contrast, the primary hormone in females was estrogen, which inhibited periosteal formation. Consequently, the epiphyseal plate closed earlier in females than in males, resulting in smaller and thinner bones in females compared to males [10]. This study found that the multivariate logistic regression equation for sex estimation from the humerus provided an accuracy of 93.5%, which was higher than that of previous studies in Chinese, Japanese, and Thai populations. The sex estimation

equation for the Chinese population showed an accuracy of 86.8%, while in the Japanese population had an accuracy of 92.4%, and in the Thai population highest accuracy was 97.1%. These results indicate that the accuracy in this study is comparable of the previous research [11]. A study conducted on the Finnish population found that the humerus and femur could be used to determine sex with an accuracy of 92.0%, which is similar to the findings of this study. Regarding the stature estimation equation from the humerus in this study, the standard error of estimate (SEE) for males was 4.233, for females 5.391, and for the combined sexes 4.862. These values are comparable to previous studies on the Northern Thai population the SEE for males was 4.89 and for females was 5.21 [6]. A study conducted on the South Indian population found that the humerus could be used for stature estimation with a margin of error of 2.0 centimeters from the actual stature [12]. The results obtained in different populations varied due to factors such as genetic diversity, daily activities, nutrition, and environmental conditions [13]. Therefore, the effectiveness of the sex estimation equations and stature estimation in this study was likely most appropriate for the Northeastern Thai population. Additionally, this study did not consider age-related changes in bone structure. As individuals age bone mass and composition change with aging, including a decrease in bone mineral content, particularly after menopause in women [14]. To enhance the accuracy, future studies should comprehensively explore age-related variations in bone structure across different age groups.

Acknowledgements

The authors would like to gratefully acknowledge of the Unit of Human Bone Warehouse for Research: UHBWR, Department of Anatomy, Faculty of Medicine, Khon Kaen University for the support and allow the collection of skeletal data, which was essential for the success of this study.

References

1. Keereewan W, Monum T, Prasitwattanaseree S, Mahakkanukrauh P. Stature estimation using the sacrum in a Thai population. Anat Cell Biol. 2023;56(2):259-67.
2. Mohd Ali SH, Omar N, Shafie MS, Nik Ismail NA, Hadi H, Nor FM. Sex estimation using subpubic angle from reconstructed three-dimensional computed tomography pelvic model in a contemporary Malaysian population. Anat Cell Biol. 2020;53(1):27-35.
3. Dayal MR, Billings BK, Brits D, Abdallah A, Spocter MA, Bidmos MA. Sex estimation from dimensions of the base of the skull in Black South Africans. Anthropol Anz. 2022;79(4):411-21.
4. Kate BR, Mujumdar RD. Stature estimation from femur and humerus by regression and autometry. Acta Anat (Basel). 1976;94(2):311-20.
5. Akhlaghi M, Hajibeygi M, Zamani N, Moradi B. Estimation of stature from upper limb anthropometry in Iranian population. J Forensic Leg Med. 2012;19(5):280-4.
6. Mahakkanukrauh P, Khanpetch P, Prasitwattanseree S, Vichairat K, Troy Case D. Stature estimation from long bone lengths in a Thai population. Forensic Sci Int. 2011;210(1-3); 279.e1-7.
7. Stulp G, Barrett L. Evolutionary perspectives on human height variation. Biol Rev Camb Philos Soc. 2016;91(1):206-34.
8. Vanderschueren D, Laurent MR, Claessens F, Gielen E, Lagerquist MK, Vandenput L, et al. Sex Steroid Actions in Male Bone. Endocrine Reviews. 2014;35(6):906-60.
9. Seeman E. Sexual Dimorphism in Skeletal Size, Density, and Strength. The Journal of Clinical Endocrinology & Metabolism. 2001;86(10):4576-84.
10. Khosla S, Oursler MJ, Monroe DG. Estrogen and the skeleton. Trends in Endocrinology & Metabolism. 2012;23(11):576-81.
11. Işcan MY, Loth SR, King CA, Shihai D, Yoshino M. Sexual dimorphism in the humerus: a comparative analysis of Chinese, Japanese and Thais. Forensic Sci Int. 1998;98(1-2):17-29.
12. Singhal S, Rao V. Estimation of total length of humerus from its segments. Med Sci Law. 2011;51(1):18-20.
13. Lai C-Q. Adaptive Genetic Variation and Population Differences. In: Bouchard C, Ordovas JM, editors. Progress in Molecular Biology and Translational Science. 108: Academic Press; 2012. p. 461-89.
14. Kiebzak GM. Age-related bone changes. Experimental Gerontology. 1991;26(2):171-87.

P-40

Optimizing Wetting Fluid for Improved Cadaver Preservation with a Safer and Cost-Effective Approach

Mayurachat Sa-ardrit[1], Sirinad Tankruad[1], Napawan Taradolpisut[1], Sawat Sowapun[1], Jirawat Panprasert[1], Athikhun Suwannakhan[1*]
[1] Department of Anatomy, Faculty of Science, Mahidol University, Rama VI Road, Bangkok, Thailand
*Corresponding author, e-mail: athikhun.suw@mahidol.ac.th

Abstract

Maintaining cadaver condition after dissection is crucial in anatomical education, particularly through the use of wetting fluid, which extends their usability for prolonged storage and teaching. The traditional formula used in our department contains a high concentration of glycerin, along with formalin and phenol. However, excessive glycerin makes specimens greasy and difficult to handle, while also causing tissue darkening, which compromises teaching effectiveness. Additionally, formalin and phenol are toxic substances, and prolonged exposure poses health risks to both staff and students. Moreover, the high cost of glycerin and phenol significantly increases the overall expense of the wetting fluid when used long-term. Therefore, an adjustment to the formula is necessary to minimize toxicity, improve cadaver usability, and reduce operational costs. This study compared the external tissue appearance of 16 cadavers over one year; eight were treated with the traditional wetting fluid, while eight received an improved formula. The improved formula consists of 5.3% glycerin, less than 0.1% formalin, and no phenol, reducing toxicity compared to the traditional formula. The fluids were applied topically after each teaching session or weekly when not regularly used. After one year, cadavers treated with the improved formula were far less oily, exhibited a lighter color, which enhanced handling and anatomical structure identification. No fungal growth was observed in either group. Furthermore, the improved formula would lead to an estimated 70% reduction in chemical costs over one academic year. In conclusion, the improved wetting fluid formula demonstrated superior tissue preservation, improved specimen quality, and enhanced safety while significantly lowering costs. Future work will focus on assessments of the cadavers by staff and students, as well as the study of bacterial growth to determine the appropriate frequency of fluid application for further cost reduction.

Keywords *Embalming, Wetting fluid, Cadaver preservation, Safety*

P-41

Integrating Anatomical Dissection and Digital Learning: Enhancing Medical Education through Gastroepiploic Vascular Anastomosis Variants

Lue.kasamakamin Bhumithadadech[1], Sani Baimai[2*], Sirinush Srichareonvej[2], Papon Cholvisudhi[1]
[1]Medical student of Faculty of Medicine Siriraj Hospital, Mahidol University, Bangkok, Thailand
[2]Department of Anatomy, Faculty of Medicine Siriraj Hospital, Mahidol University, Bangkok, Thailand
*Corresponding author, e-mail: sanibaimai@gmail.com

Abstract

The gastroepiploic artery (GEA) plays a vital role in gastrointestinal and cardiovascular surgeries, particularly in gastrectomy and coronary artery bypass grafting. Anatomical variations in the GEA can affect surgical outcomes, yet they remain understudied in Thai cadavers from the central region. This study aimed to classify GEA variations and evaluate the impact of integrating digital learning with traditional anatomy education.

A total of 36 formaldehyde-preserved stomach specimens were examined at the Department of Anatomy, Faculty of Medicine Siriraj Hospital, Mahidol University. Dissection techniques identified and classified GEA variations using Koskas and Gayet's system. A video demonstration of GEA variation models was created and integrated into the Canvas Learning Management System, supplemented with interactive exercises. This educational approach incorporated Cognitive Load Theory to optimize learning, Multimodal Learning Theory to accommodate different learning styles, and Constructivist Learning Theory to enhance clinical relevance. Four major GEA variations were identified. The most common were Type I (end-to-end anastomosis between right and left GEA) and Type III (a slender anastomosis between two separate vascular networks), each occurring in 36.1% of cases. Type II (no observed anastomosis) was found in 22.2%, while Type IV (end-to-end anastomosis located more than 4 cm away from the greater curvature or occurring between two epiploic arcades) was the least common (5.5%). Among the 90 students using Canvas-based learning materials, the mean accuracy rate on clinical anatomy assessments was 80.2%, with a standard deviation (SD) of ±6.5%. Survey responses indicated that most students found these resources valuable for reinforcing knowledge, improving arterial anastomosis comprehension, and increasing motivation as future physicians. This study highlights significant GEA variations and demonstrates that integrating digital learning into anatomical education may enhance engagement and comprehension. Combining cadaveric dissection with digital tools supports multimodal learning, improves cognitive efficiency, and fosters active learning, providing a scalable model for modern medical education.

Keywords *Gastroepiploic artery, Gastric surgery, Coronary artery bypass grafting, Vascular anastomosis, Scalable model for multimodal learning*

P-42

Portal Vein and Biliary Duct Mapping: Unraveling Branching Patterns, Lengths, and Diameters for Safer Hepatobiliary Surgery

Chutikan Kaensa[1], Sirinush Sricheroenvej[2], Sani Baimai [2*]
[1] Master Student of Anatomy, Department of Anatomy, Faculty of Medicine Siriraj Hospital, Mahidol University, Bangkok, Thailand
[2] Department of Anatomy, Faculty of Medicine Siriraj Hospital, Mahidol University, Bangkok, Thailand
*Corresponding author, e-mail: sanibaimai@gmail.com

Abstract

The liver receives a dual blood supply from the hepatic artery (25%-30%) and portal vein (70–75%), with the latter playing a key role in hepatic perfusion. The anatomical relationship between the portal vein and biliary duct is crucial in hepatobiliary surgery, particularly liver transplant. Understanding variations in portal vein branching patterns, length, and diameters, as well as their correlation with biliary duct anatomy, is essential for optimizing surgical outcomes and reducing complications such as thrombosis, biliary leakage, and ischemic strictures. This study examined 30 formalin-fixed cadaveric livers (15 females, 15 males) with well-preserved intrahepatic vasculobiliary systems. Portal vein and biliary duct branching patterns were documented, and the lengths and diameters of the portal vein were measured. Statistical analysis included descriptive statistics, independent t-test, and Chi-square test to assess sex-based differences. Results showed conventional portal vein bifurcation occurred in 80% of cases. The left portal vein had an average length of 2.14 ± 0.57 cm and a diameter of 1.41 ± 0.67 cm, while the right portal vein measured 1.98 ± 0.45 cm in length and 1.28 ± 0.28 cm in diameter. The left biliary duct variations included Type A (73.33%), Type B (10%), and Type C (16.67%). The right posterior biliary duct exhibited supraportal (70%), intraportal (10%), and combined (20%) types. An association was observed between the right posterior sectoral duct variations and males ($p = 0.049$), which may reflect male-specific morphogenetic timing during intrahepatic duct formation. Although a statistically significant sex-related difference was observed, the underlying embryological basis remains unclear and warrants further investigation. These findings provide a refined anatomical reference for identifying patient-specific anatomical variations using preoperative imaging modalities such as magnetic resonance cholangiopancreatography and computed tomography angiography. This can enhance donor-recipient matching, and the choice of anastomotic techniques in complex hepatobiliary surgeries to minimize postoperative complications.

Keywords *Vasculobiliary systems, Liver transplantation, Hepatobiliary surgery, Vascular and biliary mapping*

Background

The liver plays a vital role in metabolism, detoxification, and bile production. It receives dual blood supply from the portal vein (PV) (70–75%) and hepatic artery (HA) (25-30%), both crucial for segmental liver perfusion (1). The PV and intrahepatic biliary ducts (BD) develop in close anatomical association, influencing hepatobiliary surgeries, particularly liver transplantation (LT) and segmental hepatectomy. Unrecognized anatomical variations can lead to complications such as PV thrombosis, biliary leakage, and ischemic biliary strictures, affecting surgical outcomes (2, 3). This study aims to analyze PV branching patterns, lengths, and diameters and their correlation with BD anatomy, while also assessing sex-based differences. A detailed anatomical reference supports surgical precision by enabling accurate interpretation of preoperative imaging, allowing better selection of transection planes, and reducing the risk of vascular and biliary injury during donor hepatectomy or reconstruction procedures. Identifying these variations can enhance intraoperative decision-making and minimize postoperative complications in LT and hepatobiliary procedures. Furthermore, understanding the developmental factors influencing PV and BD variability may provide deeper insights into structural differences that impact surgical approaches. This study contributes to improving hepatobiliary surgical outcomes and patient safety

by bridging the gap between anatomical research and clinical applications.

Methodology

This descriptive and comparative study analyzed 30 formalin-fixed cadaveric livers (15 females, 15 males) with intact intrahepatic vasculobiliary structures. Specimens with hepatic pathologies, such as cirrhosis or prior surgical alterations, were excluded. The dissection process involved identifying and classifying PV branching patterns, measuring the right and left PV lengths and diameters using digital vernier calipers, and categorizing BD patterns into three types based on their confluence. Statistical analysis included calculating mean values, standard deviations, and percentages. Comparative analyses were performed between male and female specimens using independent t-tests and Chi-square tests to assess sex-based differences. Additionally, interobserver reliability was evaluated using Cohen's Kappa (for categorical data (κ= 1.00) and intra-class correlation coefficients for continuous variables (ICC = 0.95, 95% CI [0.89, 0.98], p = 0.001) to ensure measurement consistency. This study adhered to ethical guidelines and was approved by the Siriraj Institutional Review Board (694/exemption).

Results and Discussion

The majority of PV anatomy exhibited a conventional bifurcation pattern (80%), consistent with findings by Cheng et al. (1997) and Sureka et al. (2015) who reported a similar prevalence in their anatomical study (4, 5) (Fig. 1). Trifurcation was observed in 10%, while other rare variations accounted for the remaining 10% (Fig. 2). The left PV had a mean length of 2.14 ± 0.57 cm and a diameter of 1.41 ± 0.67 cm, while the right PV was 1.98 ± 0.45 cm in length with a diameter of 1.28 ± 0.28 cm. However, these results contradict findings by Tutkuviene et al. (2024) (6), where the right PV had a larger diameter than the left, suggesting potential population-specific or methodological differences in measurement techniques. These variations highlight the need for precise preoperative imaging to identify patient-specific anatomical differences that may influence surgical decision-making (Fig. 3).

Fig. 1 Conventional branching pattern of the portal vein. LPV: left portal vein, RPV: right portal vein, RP-AB: right portal vein anterior branch, RP-PB: right portal vein posterior branch, MPV: main portal vein.

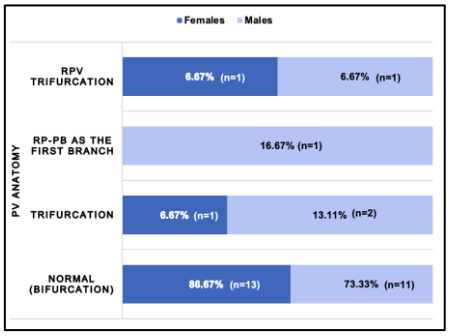

Fig. 2 Variations of portal veins. RPV: right portal vein, RP-PB: right portal vein posterior branch.

During the embryonic development, the intrahepatic BD is developed in close contact with the PV mesenchyme (5). Therefore, in addition to PV variations, the study identified relation of intrahepatic BD variability. The left BD was categorized into three types: Type A (73.33%), Type B (10%), and Type C (16.67%). The right posterior sectoral duct (RPSD) exhibited three confluence patterns: supraportal (70%), infraportal (10%), and

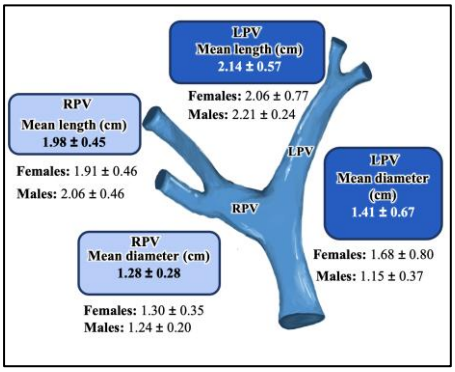

Fig. 3 Parameters of the portal vein. LPV: left portal vein, RPV: right portal vein.

combined (20%). Findings of this study suggest that variations of the RPSD are more frequently associated with PV variations than conventional PV [2/6 (33.33%) vs. 7/24 (29.17%)]. Previous studies, including those by Cheng et al. (1997) and Watanabe et al. (2017) (7), have reported similar

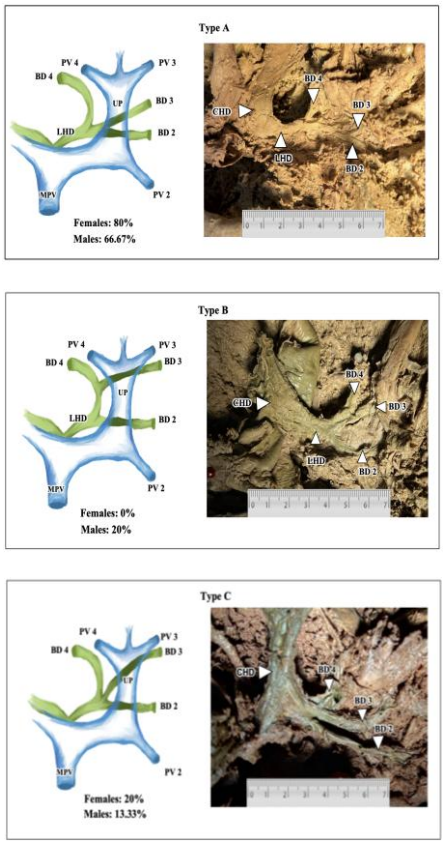

Figs. 4 Variations of the left biliary duct (types A-C). MPV: main portal vein, UP: umbilical portion, CHD: common hepatic duct, LHD: left hepatic duct, BD 2-4: segmental II-IV bile ducts, PV 2-4: segmental II-IV portal vein branches.

findings, reinforcing the importance of understanding these anatomical variations in hepatobiliary surgery (Figs. 4 and 5). Moreover, statistical analysis indicated a weak association between RPSD variations and males ($p = 0.049$).

From a clinical perspective, PV variations significantly impact surgical strategies in LT and segmental hepatectomy. In PV embolization (PVE), trifurcation may increase the complexity of catheter positioning and embolization techniques, requiring careful preoperative planning (5). The identification of PV variations through preoperative imaging, such as magnetic resonance cholangiopancreatography (MRCP) and CT angiography, is crucial in donor selection and anastomotic planning to minimize postoperative complications like thrombosis, biliary leakage, and ischemic strictures (1-3). Similarly, BD configurations influence anastomotic strategies in biliary-enteric reconstruction, particularly for Type B and C variants, which may require modified surgical approaches to prevent postoperative strictures. While most PV and BD parameters were consistent across sexes, variations in the RPSD may have implications for biliary anastomotic planning in male donors.

The findings of this study align with prior research conducted by Reichert et al. (2003) (8), which analyzed BD variations relative to the umbilical fissure in split LT. The predominance of Type A configuration (73.33%) in our study is consistent with previous reports by Cho et al. (2003) (59%) and Kitami et al. (2006) (69%) (2, 9). This suggests that using conventional transection plane of left lateral split LT approaches may be applicable in most cases, variations in BD patterns necessitate individualized surgical modifications to ensure optimal outcomes. Furthermore, the weak statistical correlation between RPSD variations and males, despite being significant ($p = 0.049$), suggests that further investigation is required with larger sample sizes to determine the true impact of sex-related anatomical differences.

Future research should include a larger sample size and apply advanced imaging and molecular techniques to explore genetic and embryological influences on PV and BD variations. Broader demographic studies may also reveal ethnic or environmental factors affecting these patterns, supporting more precise surgical planning.

Conclusion

This study is the first to present detailed vasculobiliary mapping based on Thai cadaveric livers, thus providing population-specific anatomical data relevant to regional surgical practices. The findings suggest that sex-based anatomical differences are minimal, but specific BD configurations require tailored surgical approaches.

Acknowledgments

This research was supported by Chalermphrakiat Grant, Faculty of Medicine Siriraj Hospital, Mahidol University, Thailand.

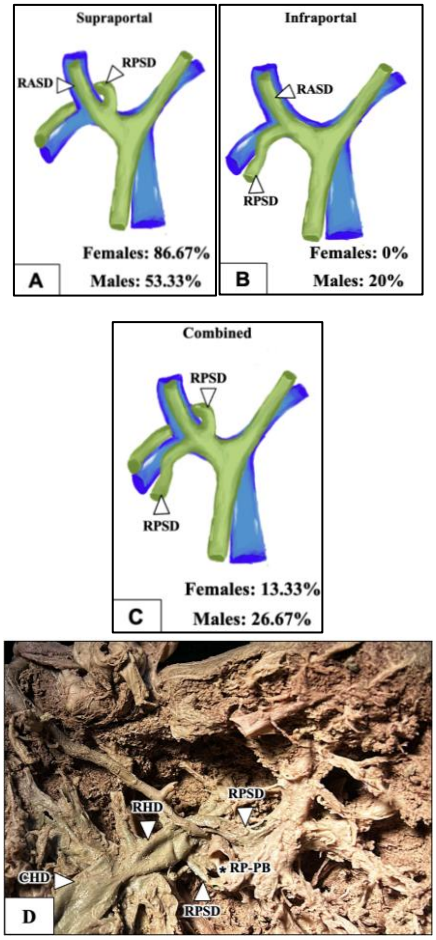

Figs. 5A-C Anterior view of the right posterior sectoral bile duct confluence patterns.

Fig. 5D Posterior view of the combined biliary branching pattern**.** Depicting the supraportal and infraportal branches. RASD: right anterior sectoral duct, RPSD: right posterior sectoral duct. Asterisk: RP-PB, RP-PB: right portal vein posterior branch.

References

Sambath P, Padmanaban E, Amirthalingam U, Anand AM, Sudhakar P, Dhinadhayalan R, George R, Danassegarane R. Hepatic Artery and Portal Vein Variations using Contrast Enhanced Computed Tomography Abdominal Angiography. artery. 2022;15:4-2.

Kitami M, Takase K, Murakami G, Ko S, Tsuboi M, Saito H, Higano S, Nakajima Y, Takahashi S. Types and frequencies of biliary tract variations associated with a major portal venous anomaly: analysis with multi–detector row CT cholangiography. Radiology. 2006 Jan;238(1):156-66

Rodriguez-Davalos MI, Arvelakis A, Umman V, Tanjavur V, Yoo PS, Kulkarni S, Luczycki SM, Schilsky M, Emre S. Segmental grafts in adult and pediatric liver transplantation: improving outcomes by minimizing vascular complications. JAMA surgery. 2014 Jan 1;149(1):63-70.

Cheng YF, Huang TL, Chen CL, Sheen-Chen SM, Lui CC, Chen TY, Lee TY. Anatomic dissociation between the intrahepatic bile duct and portal vein: risk factors for left hepatectomy. World journal of surgery. 1997 Mar;21:297-300.

Sureka B, Patidar Y, Bansal K, Rajesh S, Agrawal N, Arora A. Portal vein variations in 1000 patients: surgical and radiological importance. The British journal of radiology. 2015 Nov 1;88(1055):20150326.

Tutkuviene J, Navakauskaite A, Narutyte R, Brazaitis A, Barkus A, Tamosiunas A. Hepatic portal vein branching patterns according to different liver assessment methods and classifications of branching type. Annals of Anatomy-Anatomischer Anzeiger. 2024 Feb 1;252:152204.

Watanabe N, Ebata T, Yokoyama Y, Igami T, Sugawara G, Mizuno T, Yamaguchi J, Nagino M. Anatomic features of independent right posterior portal vein variants: Implications for left hepatic trisectionectomy. Surgery. 2017 Feb;161(2):347-354. doi: 10.1016/j.surg.2016.08.024.

Reichert PR, Renz JF, Luiz AD, Rosenthal P, Lim RC, Roberts JP, Ascher NL, Emond JC. Surgical anatomy of the left lateral segment as applied to living-donor and split-liver transplantation: a clinicopathologic study. Annals of surgery. 2000 Nov 1;232(5):658-64.

Cho A, Okazumi S, Yoshinaga Y, Ishikawa Y, Ryu M, Ochiai T. Relationship between left biliary duct system and left portal vein: evaluation with three-dimensional portocholangiography. Radiology. 2003 Jul;228(1):246-50

P-43

Pancreas Divisum is a Risk Factor of Pancreatic Diseases: A Systematic Review and Meta-Analysis

Napawan Taradolpisut[1], Athikhun Suwannakhan[1], Thanyaporn Senarai[2], Worawit Suphamungmee[1*]
[1] Department of Anatomy, Faculty of Science, Mahidol University, Rama VI Road, Bangkok, Thailand
[2] Department of Anatomy, Faculty of Medicine, Khon Kaen University, Thailand
*Corresponding author, e-mail: worawit.sup@mahidol.ac.th

Abstract

Pancreas divisum (PD) is the most common congenital anomaly of the pancreatic ductal system, with reported prevalence rates ranging from 0.2% to 47%. Contribution of PD in the development of pancreatic diseases is controversial. The PD, although not considered a disease, is believed to be associated with certain pancreatic conditions or diseases in some cases. This systematic review and meta-analysis aimed to estimate the global prevalence of PD and assess its association with pancreatic diseases. A comprehensive search of Google Scholar, Scopus, and PubMed was conducted. A total of 100 studies involving 174,062 subjects were included. The pooled prevalence of PD was 10.2% (95% CI: 6.9%–13.5%). Subgroup analysis revealed a higher prevalence in patients with known or suspected pancreatic disease (17.8%, 95% CI: 9.9%–25.8%), compared to consecutive patients (4.7%, 95% CI: 3.7%–5.7%). Geographical differences were significant, with the highest prevalence observed in North America (14.6%), followed by Europe (10.7%) and Asia (2.5%), which may indicate genetics as one of the possible underlying factors for the presence of PD. Egger's test demonstrated significant publication bias ($p<0.01$). In conclusion, the PD was four times more common among patients with pancreatic diseases, confirming its role in pancreatic diseases. Although further studies are needed, one proposed theory suggests PD opens through a relatively narrower and ventral duct papilla, which might not effectively drain pancreatic secretions, causing blockages in the flow.

Keywords *Pancreas divisum, Pancreatisis, Systematic review, Meta-analysis*

P-44

Antimalarial Effect of *Tabernaemontana pandacaqui* Leaves from Acid-base Extraction

Jiraporn Sangpratum[1], Pruet Boonsing[1], Gamolthip Niramolyanun[1], Chonnipa Praikongkatham[1], Prakaipet Pankeaw[1] and Niwat Kangwanrangsan[1*]
[1]Department of Pathobiology, Faculty of Science, Mahidol University, 272 Rama VI Road, Bangkok, Thailand
*Corresponding author, niwat.kan@mahidol.ac.th

Abstract

The increasing prevalence of antimalarial drug resistance poses a serious threat to effective malaria treatment and control, emphasizing the urgent need for alternative therapeutic strategies. Herbal medicines have emerged as promising candidates due to their accessibility and cost-effectiveness. *Tabernaemontana pandacaqui*, a medicinal plant widely distributed in tropical regions, was recognized for its rich phytochemical profile and diverse biological activities. This study aims to investigate the phytochemical constituents of *T. pandacaqui* through acid-base extraction, examine the cytotoxicity of its extracts on red blood cells (RBCs), and evaluate their anti-plasmodial activity against asexual blood stages of *Plasmodium falciparum*. Crude extraction using methanol (fraction 1) was obtained, followed by acid-base separation into three fractions: phenol/terpene (fraction 2), quaternary alkaloids and N-oxides (fraction 3), and total alkaloids (fraction 4). Various concentrations (0.1, 1, 10, 100, and 1,000 µg/mL) of all extracts were tested for their cytotoxicity by hemolysis assay at 0, 24, 48, and 72 hr before evaluating their killing activity against *P. falciparum* strain NF54 at the equivalent dose and incubation time points. Parasitemia and morphological changes were analyzed through Giemsa-stained blood smears under the light microscope. Results indicated that all extracts were non-cytotoxic to the human RBCs at all concentrations and incubation time points. The crude methanolic extract and phenol/terpene fraction significantly reduced parasitemia at 1,000 µg/mL. However, the highest concentration of alkaloid fractions caused a moderate reduction of parasitemia when compared to the no-treat control. *T. pandacaqui* treated parasites shared a common morphological damage by the character of pyknotic cell death. In conclusion, *T. pandacaqui* extracts demonstrated selective anti-plasmodial activity with safety toward host red blood cells by *in vitro* investigation. Phytochemicals, particularly polyphenols and terpenes, from *T. pandacaqui* specifically exhibited antimalarial action, which could be suitable for further study as a natural product-based malaria therapy.

Keywords: *Malaria, Tabernaemontana pandacaqui, Phytochemicals, Acid-base extraction, Phenol/Terpene*

Background

Plasmodium falciparum remains the most virulent species of human malaria, responsible for severe complications resulting from its invasion of red blood cells (RBCs). This process leads to anemia, endothelial dysfunction, and microvascular obstruction, contributing to the disease's high morbidity and mortality [1]. Although artemisinin-based combination therapies (ACTs) are the cornerstone of current malaria treatment, the increasing emergence of drug-resistant *P. falciparum* strains—particularly in Southeast Asia [2]—poses a significant threat to the long-term efficacy of these therapies. While malaria vaccines have shown encouraging preliminary results, their widespread deployment and sustained effectiveness are still under evaluation [3]. Considering the growing challenge of drug resistance, there is an urgent need to discover new antimalarial agents that are effective, affordable, and accessible. Medicinal plants have historically served as valuable sources of bioactive compounds with therapeutic potential [4]. Notable examples include quinine from *Cinchona* species and artemisinin from *Artemisia annua*, both of which have been successfully used in malaria treatment [5]. The Apocynaceae family is known for its production of alkaloid-rich species with diverse pharmacological activities. Within this family, the genus *Tabernaemontana* has gained attention for its potential as a source of antimalarial agents [6]. *Tabernaemontana pandacaqui*, a species widely used in traditional medicine, is of particular interest due to its alkaloid content and reported

biological activities [7]. This study aims to evaluate the antimalarial activity of *T. pandacaqui* extracts, with a focus on their phytochemical composition and their efficacy against the asexual blood stage of *P. falciparum.*

Materials and Methods

Plant Materials

Plant specimens were collected from Nakhon Pathom in January 2023. A total of five individual trees from each plant species were sampled. The collected plants were washed thoroughly and separated to determine the wet weight. The samples were then dried in the shade at room temperature. Plant identification and authentication were conducted by the Sireerukachart Herbarium, Faculty of Pharmacy, Mahidol University (PBM, Thailand). After drying, the samples were weighed to determine the dry weight, pulverized into a fine powder, and passed through a British Standard Sieve (BSS No. 10). The powdered samples were stored in airtight containers at room temperature, protected from light, until extraction.

Extraction and Fractionation

Dried leaf samples (15 g each) were extracted using 50 mL of methanol (AR grade, QRec) as the solvent. The mixture was placed in an incubating shaker (LABOAO, LH-100F) at 180 rpm for 24 hr at a temperature below 25°C. After incubation, the mixture was filtered using Whatman No. 1 filter paper. The filtrate was concentrated to 1/10 of its original volume using a rotary evaporator (BUCHI, Rotavapor R200). Aliquots were transferred into Eppendorf tubes and further dried using a speed vacuum concentrator (SAVANT SC210A, Thermo) until crystal formation was observed. The yield of crude methanol extract was calculated based on the dry weight. To examine the phytochemical contents of different fractions, crude methanol extracts were subjected to acid-base extraction. Briefly, the methanol extract was acidified to pH 4 using 1 M hydrochloric acid (AR grade, QRec) to convert alkaloids into their salt forms. The aqueous phase was extracted with 50 mL of chloroform using a separatory funnel. The remaining aqueous layer was then basified to pH 9 using 1 M ammonia solution (AR grade, QRec) and re-extracted with another 50 mL of chloroform (AR grade, ACI Labscan) using a separatory funnel. The alkaloid-rich chloroform layer was collected and concentrated using a rotary evaporator [8]. Finally, drying was performed using a speed vacuum concentrator until crystal formation occurred. The percentage yields were then calculated based on the final dry weight. Compound profiling was conducted using Direct Analysis in Real Time mass spectrometry (DART-MS), and the data were analyzed using the Human Metabolome Database (HMDB)."

Hemolysis Test

T. pandacaqui extract fractions were initially dissolved in dimethyl sulfoxide (DMSO) and subsequently diluted to final concentrations of 0.1, 1, 10, 100, and 1,000 µg/mL using 1X phosphate-buffered saline (PBS). For controls, 1% Triton X-100 was used as the positive control, while 1X PBS with 0.1% DMSO served as the negative control. The assay was conducted in a 96-well plate with duplicate wells for each condition. A volume of 180 µL of each crude extract solution was added to the wells, followed by 20 µL of washed blood adjusted to 50% hematocrit (Hct). The mixtures were gently mixed and incubated at 37°C for 0, 24, 48, and 72 hr. After incubation, 200 µL of the mixture from each well was transferred into a 1.5 mL microcentrifuge tube and centrifuged. A volume of 170 µL of the resulting supernatant was transferred into a new 96-well plate for absorbance measurement. Hemolysis was assessed by measuring the absorbance at 540 nm using a microplate reader (TECAN SPARK 10M). The percentage of hemolysis was calculated based on the absorbance values obtained.

***Plasmodium falciparum* inhibition assay**

Different fraction extracts from *T. pandacaqui* were tested at concentrations of 0.1, 1, 10, 100, and 1,000 nM. Artesunate (ART) at concentrations of 10 and 100 nM was used as a positive control. A 0.1% DMSO solution and culture medium (CM) were used as negative controls. The assay was conducted in 96-well plates. Each well received 180 µL of the designated plant extract concentration and 20 µL of *P. falciparum* culture at 0.3% parasitemia in 50% hematocrit (Hct), primarily in the ring stage. The cultures were incubated at 37°C for 24, 48, and 72 hr. At each time point, samples were harvested into 1.5 mL microcentrifuge tubes and centrifuged to remove the supernatant. The pellets were resuspended and adjusted to 50% Hct. Thin blood smears were prepared, air-dried, and stained with Giemsa to assess the percentage of growth inhibition and observe morphological changes of the parasites under light microscopy. The culture

medium and drug treatments were refreshed every 24 hr throughout the incubation period.

Statistical Analysis

Data were analyzed using GraphPad Prism version 9.0 (GraphPad Software, California, USA). Results are presented as mean ± standard deviation (SD). Comparisons between groups were performed using the Student's *t*-test. Simple linear regression and correlation analyses were also conducted. A *p*-value of ≤ 0.05 was considered statistically significant.

48, and 72 hr. Data were analyzed using ANOVA ($p \leq 0.05$). The results demonstrated that the 1,000 µg/mL concentration induced a higher percentage of hemolysis in fraction 1 and fraction 3, approximately below 30%, whereas Fraction 2 and fraction 4 exhibited minimal toxicity. At concentrations of 0.1, 1, 10, and 100 µg/mL, no significant hemolytic activity was observed, with hemolysis remaining below 5% in all four fractions.

Anti-plasmodial activity

P. falciparum cultures were treated with crude extracts and analyzed for parasitemia at various time points using light microscopy (Fig. 1). Treatment

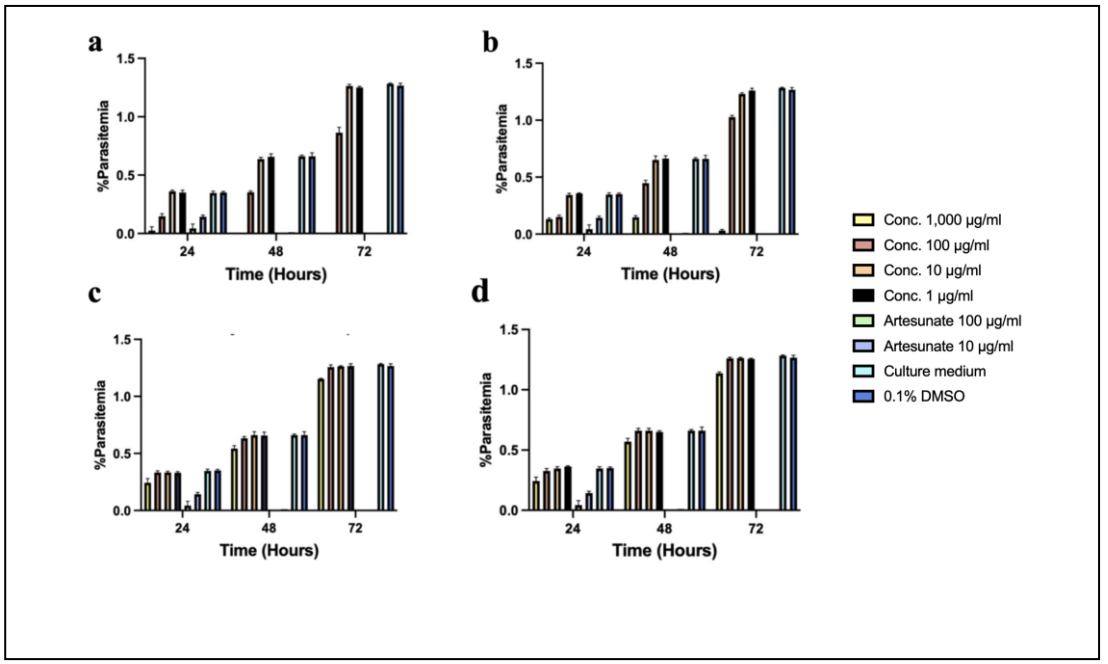

Results

The fractions were obtained using the acid-base extraction method. Each fraction was dried prior to use, and the concentrations were adjusted for testing with red blood cells to determine the percentage of hemolysis. The highest yield was observed in fraction 2 (crude terpenes and polyphenols extract), at approximately 16.08%, followed by fraction 1 (crude methanol extract) at 11.20%, fraction 3 (crude quaternary alkaloids and N-oxides) at 3.51%, and fraction 4 (total alkaloids) at 3.48%, respectively.

The crude extracts were evaluated for hemolytic activity at concentrations of 0.1, 1, 10, 100, and 1,000 µg/mL using a microplate reader at 540 nm, with measurements taken at time intervals of 0, 24,

with 1,000 µg/mL of fraction 1 (Fig. 1a) demonstrated high efficacy, reducing parasitemia to below 0.1% at 24 hr, with further suppression observed at 48 and 72 hr. Similarly, fraction 2 (Fig. 1b) reduced parasitemia to below 0.2% at 24 hr and continued to inhibit parasite growth and replication over the 48- and 72-hr intervals. These results were comparable to the effect observed with 100 nM artesunate. In contrast, fraction 3 (Fig. 1c) and fraction 4 (Fig. 1d) showed higher parasitemia levels, approximately 0.3%, similar to those

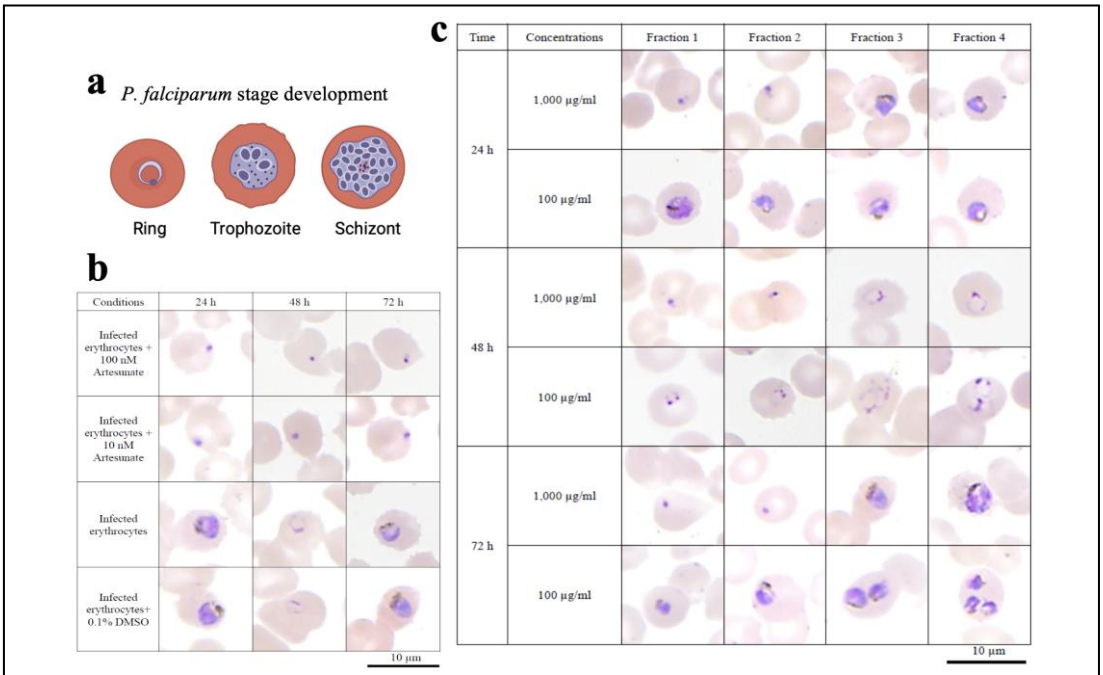

Fig. 2 Inhibition of *Plasmodium falciparum* (NF54) with *T. pandacaqui* leaf extract obtained through acid-base extraction. (a) The developmental stages of *P. falciparum* begin with the ring stage (0–26 h), followed by the trophozoite stage (26–38 h), and then the schizont stage (38–48 h). After the schizont stage, the parasite ruptures to release merozoites, which infect new red blood cells (RBCs) and initiate a new cycle. (b) Parasite growth and morphological changes were observed at 24, 48, and 72 hr. A medium containing 0.1% DMSO and culture medium served as negative controls, while 100 nM and 10 nM artesunate were used as positive controls. (c) Each fraction was tested at concentrations of 100 µg/mL and 1,000 µg/mL over 24, 48, and 72 hr.

observed with 100 µg/mL of fractions 1 and 2. At lower concentrations (100, 10, and 1 µg/mL), fractions 2 and 3 exhibited parasitemia levels nearly equivalent to the untreated control. All fractions tested at 10 and 1 µg/mL showed no significant effect on parasite infection or parasitemia levels.

Morphological Changes

Developmental cycle of *P. falciparum* progresses through the ring stage (0–26 hr), trophozoite stage (26–38 hr), and schizont stage (38–48 hr), followed by rupture of the infected red blood cell and release of merozoites, which invade new red blood cells to initiate the next cycle (Fig. 2a) Treatment with 1,000 µg/mL of fractions 1 and 2 (Fig. 2c) induced morphological changes in *P. falciparum*, characterized by pyknotic death, similar to the effects observed with artesunate (positive control) at 24, 48, and 72 hr. In contrast, fractions 3 and 4 showed a majority of parasites maintaining normal morphology and progressing through the developmental stages—trophozoite at 24 hr, ring stage at 48 hr (indicative of a new cycle), and trophozoite again at 72 hr—suggesting parasite survival.

Discussion

Crude extracts were fractionated using methanol and acid-base extraction. The resulting fractions were evaluated for hemolytic activity at concentrations of 0.1, 1, 10, 100, and 1,000 µg/mL using red blood cell (RBC) lysis assays. Based on established safety criteria, hemolysis values below 10% are considered non-hemolytic [9], reflecting acceptable blood compatibility and low cytotoxicity toward RBCs [9]. In this study, the majority of the fractions demonstrated hemolysis levels below this threshold across all tested concentrations, indicating minimal hemolytic potential. However, at the highest concentration (1,000 µg/mL), fraction 1 and

fraction 3 exhibited hemolysis rates of approximately 30%. Given that hemolysis values exceeding 25% are indicative of potential cytotoxic risk, these two fractions may pose a concern for RBC integrity at elevated concentrations [9].

Crude extracts examination against *P. falciparum* demonstrated the highest inhibitory activity in fraction 1 (Total Phytochemical content) and fraction 2 (rich in terpenes and polyphenols) at a concentration of 1,000 µg/mL. These two fractions were the most effective in reducing parasitemia, However, this concentration represents the highest tested dose, whereas the positive control, artesunate, achieved inhibition at much lower concentrations (100 nM and 10 nM).Although this is a relatively high concentration that might pose cytotoxic risks in humans [9], the study did not observe hemolytic effects on red blood cells (RBCs) at this concentration. Lower concentrations (100 µg/mL) of the same fractions showed partial parasitic inhibition and induced morphological changes in some parasites, although many remained viable. Still, fractions 1 and 2 resulted in significantly lower parasitemia compared to the other fractions, suggesting strong anti-plasmodial potential. The anti-plasmodial activity of crude extracts against *P. falciparum* is generally consistent with findings from various studies. Specifically, methanol extracts—which represent the total phytochemical content—have demonstrated effective anti-plasmodial activity against *P. falciparum*, likely due to the combined effects of various bioactive phytochemicals [10]. Fractions rich in terpenes and polyphenols have demonstrated significant inhibitory effects against *P. falciparum*. The proposed mechanism underlying this activity involves the inhibition of heme biosynthesis and the disruption of hemozoin formation during the trophozoite stage of the parasite's life cycle [11, 12]. In contrast, fractions 3 and 4, which contain alkaloids and N-oxide compounds, are also believed to interfere with hemozoin production [13]. However, in the present study, these alkaloid-containing fractions exhibited relatively limited antiplasmodial effects. A previous study on the stem bark extracts of *T. elegans* evaluated their in vitro antiplasmodial activity against the chloroquine-sensitive *P. falciparum* NF54 strain. The methanol extract exhibited notable activity, with an IC_{50} value of 0.83 µg/mL [14]. Phytochemical separation by acid-base extraction in the *Tabernaemontana* genus has revealed that alkaloid - rich fractions can be effective against *P. falciparum*. Reports have highlighted the antimalarial potential of various *Tabernaemontana* species, emphasizing the roles of indole alkaloids, terpenoids, and polyphenols as key contributors to their activity. For example, *T. divaricata* was reported to produce an alkaloid that showed strong in vitro antimalarial activity against the 3D7 strain of *P. falciparum*, with an IC_{50} value of 1.9 µM. Similarly, *T. macrocarpa* demonstrated activity against the same strain, with an IC_{50} value of 28.8 µM [15]. In contrast, the present study suggests that the observed antiplasmodial effects may be attributed to the terpene and polyphenol content. These previously reported IC_{50} values are substantially lower than the 1,000 µg/mL concentration used in the current study, indicating that effective parasite inhibition can be achieved at much lower doses.

Nevertheless, the efficacy and optimal concentration may vary depending on the specific plant species and the phytochemical composition of the extracts [16]. In terms of cytotoxicity, although some plant extracts have been shown to induce hemolytic effects at high concentrations, others have demonstrated substantial antiplasmodial activity without exhibiting notable toxicity to red blood cells (RBCs) [17]. In the current study, none of the four tested fractions produced a significant reduction in parasitemia at lower concentrations (100, 10, and 1 µg/mL) compared to the negative control. However, treatment with the crude methanol extract and the terpene/polyphenol-rich fraction at 100 µg/mL resulted in a slight decrease in parasitemia, indicating mild antiplasmodial activity at this concentration.

Conclusion

The extracts from *T. pandacaqui* showed no toxicity to red blood cells (RBCs) even at a high concentration (1,000 µg/ml). Phytochemical analysis revealed that polyphenols and terpenes are the major compounds responsible for antimalarial activity, particularly at higher concentrations, where they effectively inhibit *P. falciparum.* Lower concentrations showed only mild effects on the parasites. This study contributes valuable data for the discovery of new traditional medicinal plants with antimalarial potential.

Acknowledgments
This research work was supported by Department of Pathobiology and the CIF and CNI Grant, Faculty of Science, Mahidol University.

References

1. Ashley, E.A., Phyo, A.P., & Woodrow, C., *Malaria.* The lancet, 2018. 391: p. 1608-21.
2. Jagannathan, P., & Kakuru, A., *Malaria in 2022: Increasing challenges, cautions optimism.* Nature communication, 2022. 13: p. 2678.
3. Duffy, P., Gorres, J., Healy, S., & Fried, M., *Malaria vaccines: a new era of prevention and control.* Nature Reviews Microbiology, 2024. 22: p. 756-772.
4. Edoga, H.O., Okuwu, D.E., Mbaebie, B.O., *Phytochemicals constituents of some Nigerian medical plants.* African journal Biotechnology, 2005. 4(7): p. 685-688.
5. Dolabela, M.F., Oliveira, S.G., Peres, J.M., Nascimento, J.M.S., Povoa, M.M., & Oliveeira, A.B., *In vitro antimalarial activity of six Aspirosperma species from the state of Minas Gerais (Brazil).* Annals of the Brazilian Academy of Sciences, 2012. 84(4): p. 899-910.
6. Milliken, W., Walker, B.E., Howes, M.J.R., Forest, F. & Lughadha, EN. , *Plants used traditionally as antimalarials in Latin America: Mining the tree of life for potential new medicines.* Journal of Ethnopharmacology, 2021. 279.
7. Anand, U., Nandy, S., Mundhra, A., Das, N., Pandey, D. K., & Dey, A. , *A review on antimicrobial botanicals, phytochemicals and natural resistance modifying agents from Apocynaceae family: Possible therapeutic approaches against multidrug resistance in pathogenic microorganisms.* Drug Resist, 2020.
8. Sridhar, S.N.C., Sengupta, P., & Paul, A.T., *Development and validation of a new HPTLC method for quantification of conophylline in Tabernaemontana divaricate samples obtained from different seasons and extraction techniques: Insights into variation of pancreatic lipase inhibitory activity.* Industrial Crops & Porducts, 2018. 111: p. 462-470.
9. Amin, K., & Dannenfelser, R., *In vitro hemolysis: Guidance for the pharmaceutical scientist.* Journal of Pharmaceutical Sciences, 2006. 95(6): p. 1173-1176.
10. Ebohon, O., Irabor, F., Erhunse, N., Omagene, A., & Omoregie, E., *In vitro antiplasmodial activity, cytotoxicity, and gas chromatography – flame ionization detector metabolites fingerprint of extracts and fractions from Tetrorchidium didymostemon.* Journal of Ayurveda and Integrative Medicine, 2021. 12(3): p. 480-488.
11. Sun, C., & Zhou, B., *The molecular and cellular action properties of artemisinins: what has yeast told us?* Microbial Cell, 2016. 3(5): p. 196-205.
12. Mamede, L., Ledoux, A., Jansen, O., & Frederich, M., *Natural Phenolic Compounds and Derivatives as Potential Antimalarial Agents.* Plant Medicine, 2020. 86: p. 585-618.
13. Eyal, S., *The Fever Tree: from Malaria to Neurological Diseases.* toxins, 2018. 10(491).
14. Bapela, J., Meyer, M., & Kaiser, M., *In vitro antiplasmodial screening of ethnopharmacologically selected South African plants used for the treatment of malaria.* Journal of Ethnopharmacology, 2014. 155(1): p. 194-198.
15. Hutami, A., Rudyanto, M., & Ekasari, W., *Indole Alkaloids and Antimalarial Activity in the Tabernaemontana Species.* Jurnal Farmasi dan Ilmu Kefarmasian Indonesia, 2023. 10(1): p. 1-15.
16. Venkatesalu, V., Gopalan, N., Pillai, C.R. et al, *In vitro anti-plasmodial activity of some traditionally used medicinal plants against Plasmodium falciparum.* Parasitology Research, 2012. 111: p. 497-501.
17. Phuwajaroanpong, A., Chaniad, P., Plirat, W., Phoopha, S., Septama, A., Chukaaew., & Punsawad, C., *Antiplasmodial Properties of Aqueous and Ethanolic Extracts of Ten Herbal Traditional Recipes Used in Thailand against Plasmodium falciparum.* Tropical Medicine and Infectious Disease, 2022. 7(12).

Author Index

K

L

M

N

O

P

R

S

T

V

W

Y

Acknowledgments

We would like to acknowledge the following organizations and individuals for their support of the 47th International Conference of the Anatomical Association of Thailand (AAT47)

May 7th - 9th, 2025

Bang Saen Heritage Hotel, Chon Buri, Thailand

ABSOTEC CO., LTD.

APPLICAD PUBLIC CO., LTD.

CMED PRODUCTS CO., LTD.

COAX GROUP CORPORATION CO., LTD.

ELSEVIER (NEW KNOLEDGE INFORMATION CO., LTD.)

EMPIRE SCIENTIFIQUE CO., LTD.

FACULTY OF MEDICINE, THAMMASAT UNIVERSITY

HICARE CLINIC

HOLLYWOOD INTERNATIONAL CO., LTD.

INTER PHARMA PUBLIC CO., LTD.

MEGA WE CARE CO., LTD.

MAISON FLAWLESS SCRUBS

OFFICIAL EQUIPMENT MANUFACTURING CO., LTD.

PATRANGSIT HOSPITAL

PP DEALING GROUP CO., LTD.

PRIME MEDICAL CO., LTD.

PRINCESS WELLNESS CLINIC

Q ADVERTISING CO., LTD.

ROMRAWIN CLINIC

RUSHMORE PRECISION CO., LTD.

SCION ASSOCIATED LIMITED PARTNERSHIP

THAI MEDICALS TRADING CO., LTD.

THANES SCIENCE CO., LTD.

THE SCIENCE AND EDUCATIONAL CO., LTD.

THE SLATE HOTEL PHUKET

UPRIGHT SIMULATION CO., LTD.

WICER ENTERPRISE CO., LTD.

YANHEE HOSPITAL


THAI MEDICALS
TRADING


ABSOTEC
WWW.ABSOTECTHAILAND.COM


Prime Medical
Company Limited


HTT
HOLLYWOOD
INTERNATIONAL


THANESCIENCE
บริษัท เทนส์ไซส์ จำกัด


SCI-ED
THE SCIENCE AND EDUCATIONAL


ROMRAWIN
SKIN | SLIMMING | HAIR | ACNE | LASER


patRangsit
HOSPITAL


COAX


ELSEVIER


AppliCAD
Public Company Limited


PP DEALING
PP DEALING GROUP CO., LTD.


WICER ENTERPRISE
บริษัท ไวเซอร์ เอ็นเตอร์ไพรส์ จำกัด


FLEXLAB
Advanced Laboratory Solution


HiCare


ยันฮี
โรงพยาบาล
สุขภาพและความงาม


MAISON


ASCION SOCIATED
ห้างหุ้นส่วนจำกัดขายน็ออนแอสโซซิเอท


Q-ADs


CMED


PRINCESS
Wellness Center


EMPIRE
Scientifique


UPRIGHT
SIMULATION
COMPANY LIMITED


Wellness
We care
By
MEGA
We care


Interpharma
VALUE YOUR LIFE.


THE SLATE
A PHUKET PEARL RESORT

DIGITAL HUMAN ANATOMY SYSTEM

HD Digihuman Virtual Anatomy Table Pro

"HD Digihuman Virtual Anatomy Table Pro" is a multidisciplinary teaching platform, in which the gross anatomy module is processed by ultra-high-precision human tomography sequence image technology. The main features of the product include high-resolution virtual body, touch screen interactive operation, prone perspective observation, etc.

数字人科技 DIGIHUMAN

Layer thickness: 0.1mm

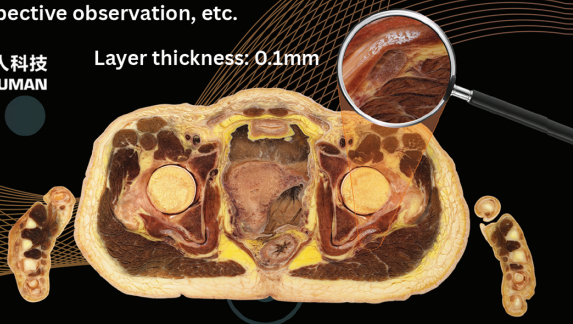

Histology & Pathology

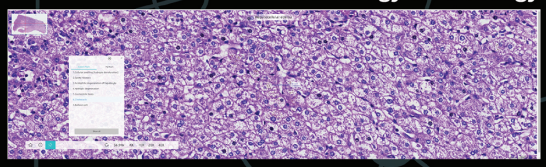

Digihuman 3D Printing Model Series

HD Digihuman Virtual Anatomy Table Mini

Embryology

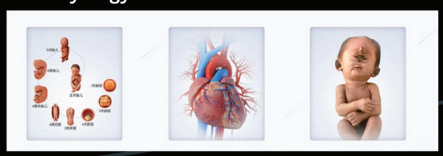

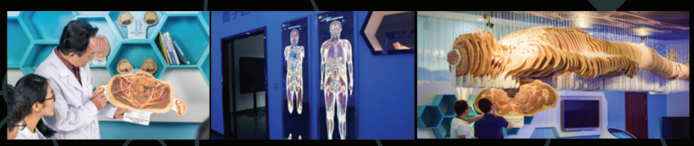

Digihuman HD tomographic 3D printing model

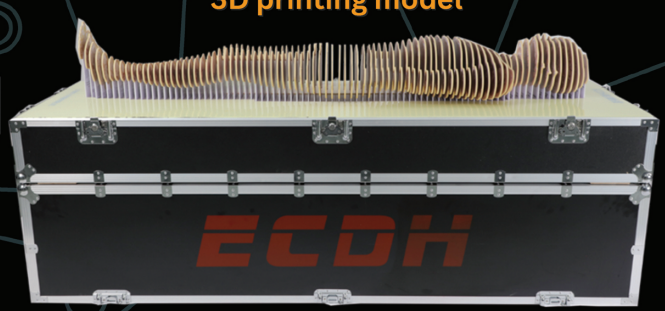

WICER ENTERPRISE
บริษัท ไวเซอร์ เอ็นเตอร์ไพรซ์ จำกัด
ข้อมูลเพิ่มเติม กรุณาติดต่อ
ตัวแทนฝ่ายขาย : วัชราภรณ์ ก่อเกิด (091-6552694) watcharapornkorkerd@gmail.com
Product Specialist : วนพรรณ วุฒิอุดม (089-0018889) wanapan.wicer@gmail.com
41 ซอยอ่อนนุช62 ถนนสุขุมวิท77 แขวงอ่อนนุช เขตสวนหลวง กรุงเทพมหานคร 10250 โทร : 02-3115128 , Email : wicerenterprise939@gmail.com

Organized by

The Anatomy Association of Thailand cooperated with
Faculty of Allied Health Sciences, Burapha University
Faculty of Science, Rangsit University
Faculty of Medicine, Thammasat University
Chulabhorn International College of Medicine, Thammasat University